



The University of
Nottingham

School of Pharmacy

**Polymer-Mediated
Crystallisation of Proteins**

Jing Zhu, MSc

Thesis submitted to the School of Pharmacy,

University of Nottingham for the degree of

Doctor of Philosophy

September 2013

Contents

Abstract	7
Acknowledgments	9
List of Abbreviations	10
List of Figures	14
List of Tables	33
Chapter 1. Introduction	37
1.1 Introduction to chapter	37
1.2 General protein introduction	37
1.2.1 Analysis of protein structure	37
1.2.2 Protein therapeutics	42
1.3 Crystals	46
1.4 Protein crystals	52
1.4.1 Some history of protein crystallisation	53
1.4.2 Principle of protein crystallisation	55
1.4.3 Methods of protein crystallisation.....	56
1.5 Use of additives in protein crystallisation	62
1.5.1 Non polymer methods	62
1.5.1.1 Salts	62
1.5.1.2 Organic solvents.....	64
1.5.1.3 Insoluble surfaces.....	64
1.5.2 Polymer additives.....	68
1.5.2.1 Insoluble polymer surfaces	69
1.5.2.2 Soluble polymer additives.....	72
1.6 Polymers and polymer synthesis methods.....	76
1.6.1 Atom transfer radical polymerisation (ATRP).....	77
1.6.2 Reversible addition-fragmentation chain transfer polymerisation (RAFT).....	80
1.7 Protein targets.....	83

1.7.1 Hen egg-white lysozyme (HEWL).....	84
1.7.2 Concanavalin a (Con A).....	86
1.7.3 Bovine liver catalase (BLC).....	87
1.8 Aims and objectives of the project	89
Chapter 2. Materials, Instrumentation and General Methods	93
2.1 Materials	93
2.2 Instrumentation.....	96
2.3 General methods	101
Chapter 3. Preparation and Characterisation of Monomers and Polymers.....	103
3.1 Introduction	103
3.2 Monomer synthesis.....	105
3.2.1 2-Acrylamidoacetic acid (2-AmAA).....	105
3.2.2 4-Acrylamidobutanoic acid (4-AmBA)	107
3.3 Polymer synthesis.....	110
3.3.1 Atom transfer radical polymerisation (ATRP) method.....	110
3.3.1.1 Polymer conversion calculations.....	110
3.3.1.2 Poly[poly(ethylene glycol) methyl ether methacrylate ₄₇₅] [p(PEGMA ₄₇₅)] (P1).....	111
3.3.1.3 Poly[2-(dimethylamino)ethyl methacrylate] [p(DMAEMA)] (P2).....	116
3.3.1.4 Quaternisation of p(DMAEMA) (P2)	120
3.3.1.5 Poly[2-(dimethylamino)ethyl methacrylate-stat-poly(ethylene glycol) methyl ether methacrylate ₄₇₅] [p(DMAEMA- <i>stat</i> -PEGMA ₄₇₅)] (P3).....	122
3.3.2 Reversible addition-fragmentation chain transfer Polymerisation (RAFT) method.....	125
3.3.2.1 Polymer conversion calculations.....	126
3.3.2.2 Poly[N-(3-(dimethylamido)propyl)methacrylamide] [p(DMAPMAm)] (P4)	126
3.3.2.3 Poly(2-acrylamido-2-methyl-1-propanesulfonic acid) [p(AMPS)] (P5).....	130
3.3.2.4 Poly(2-acrylamidoacetic acid) [p(2-AmAA)] (P6)	133
3.3.2.5 Poly(4-acrylamidobutanoic acid) [p(4-AmBA)] (P7).....	136

3.3.3	Poly[[2-(methacryloyloxy)ethyl]trimethylammonium chloride- <i>co</i> -N-[2-(methacryloyloxy)ethyl]-dimethyl-(2-sulfoethan)aminium hydroxide] [p(METMAC- <i>co</i> -MEDSAH)] (P8).....	138
3.4	General discussion and conclusions	141

Chapter 4. Application of Polymers to Hen Egg-white

Lysozyme (HEWL) Crystallisation 145

4.1	Introduction	145
4.2	Methods	148
4.2.1	Crystallisation technique and plate	148
4.2.2	Preparation of polymer solutions and stock buffer solutions.....	150
4.2.3	Crystallisation protocol for tetragonal HEWL crystals.....	151
4.2.4	Crystal imaging	152
4.2.5	X-ray crystallography.....	153
4.2.6	Dynamic light scattering (DLS) studies	153
4.2.7	Scanning electron microscope (SEM) analysis.....	155
4.3	Results and discussion.....	156
4.3.1	HEWL crystallisation in the presence of neutral polymer in solution: p(PEGMA ₄₇₅) (P1)	156
4.3.2	HEWL crystallisation in the presence of cationic polymers in solution.....	167
4.3.2.1	HEWL crystallisation in the presence of quaternised p(DMAEMA) (P2).....	167
4.3.2.2	HEWL crystallisation in the presence of p(DMAEMA- <i>stat</i> -PEGMA ₄₇₅) (P3).....	195
4.3.2.3	HEWL crystallisation in the presence of a mixture of two polymers: p(PEGMA ₄₇₅) and p(DMAEMA) (P1 & P2) (molar ratio 9:1)	200
4.3.2.4	HEWL crystallisation in the presence of p(DMAPMAm) (P4)	206
4.3.3	HEWL crystallisation in the presence of anionic polymers in solution.....	216
4.3.3.1	HEWL crystallisation in the presence of p(AMPS) (P5) ..	216
4.3.3.2	HEWL crystallisation in the presence of p(2-AmAA) (P6)	225

4.3.3.3 HEWL crystallisation in the presence of p(4-AmBA) (P7)	237
4.3.4 HEWL crystallisation in the presence of cationic/zwitterionic polymer in solution: p(METMAC-co-MEDSAH) (P8)	250
4.4 Conclusions	255

Chapter 5. Application of Polymers to Concanavalin A (Con A)

Crystallisation..... 258

5.1 Introduction	258
5.2 Methods	261
5.2.1 Crystallisation technique and plate	261
5.2.2 Preparation of polymer solutions and stock buffer solutions	261
5.2.3 Crystallisation protocol for Con A crystals	262
5.2.4 Crystal imaging	262
5.2.5 X-ray crystallography	263
5.2.6 DLS studies	263
5.2.7 SEM analysis	263
5.3 Results and discussion	264
5.3.1 Con A crystallisation in the presence of neutral polymer in solution: p(PEGMA ₄₇₅) (P1)	264
5.3.2 Con A crystallisation in the presence of cationic polymer in solution: quaternised p(DMAEMA) (P2) (quaternised ratio: 75 %)	271
5.3.3 Con A crystallisation in the presence of anionic polymer in solution: p(AMPS) (P5)	278
5.4 Conclusions	284

Chapter 6. Application of Polymers to Bovine Liver Catalase

(BLC) Crystallisation..... 286

6.1 Introduction	286
6.2 Methods	289
6.2.1 Crystallisation technique and plate	289
6.2.2 Preparation of polymer solutions and stock buffer solutions	289
6.2.3 Crystallisation protocol for BLC crystals	290
6.2.4 Crystal imaging	290
6.2.5 X-ray crystallography	290

6.2.6 DLS studies	291
6.3 Results and discussion.....	291
6.3.1 BLC crystallisation in the presence of neutral polymer in solution: p(PEGMA ₄₇₅) (P1)	291
6.3.2 BLC crystallisation in the presence of cationic polymers in solution: quaternised p(DMAEMA) (P2) (quaternised ratio: 75 %)...	298
6.3.3 BLC crystallisation in the presence of anionic polymers in solution: p(AMPS) (P5)	303
6.4 Conclusions	309
Chapter 7. Discussion, Conclusions and Future Work	311
7.1 Discussion and conclusions.....	311
7.2 Future work	327
Appendix	330
Supporting spectroscopy graphs.....	330
References	340

Abstract

Proteins are the functional machines of nature and play an essential role in life. Understanding the structure and function of proteins is central to numerous areas of science and technology, including biotechnological, pharmaceutical and chemical industries. Protein crystals are an important objective for many researchers, but even though there are many examples of protein crystals reported, there are still many uncertainties in controlling the crystallisation process. In addition, while protein crystals have mostly been obtained for characterisation purposes, there are other applications where defined assemblies of proteins, either crystals or self-assembled protein nanoparticles, are desirable. These include industrial biocatalysis, therapeutic protein formulations, and even energy-harvesting systems. Accordingly, there remains a high demand for well-defined protein crystals or nanoscale aggregates.

A variety of techniques have been used to produce protein crystals, the typical strategy involves the addition of nucleants surface, or surface-active materials into the crystallisation solution. Solution ‘additives’ of diverse types have proven crucial in the control of protein crystallisation. These additives can act via multiple roles in a crystallisation process, such as by enhancing intermolecular contacts between protein macromolecules, or disrupting unfavourable intermolecular association, or diminishing interactions between protein and solvent. Synthetic polymers are important additives for protein

crystallisation control as there are many possible chemistries which can be introduced into the backbone and side-chains, giving a very wide range of functional behavior. However, because there are so many factors which can affect crystallisation, many of which are still poorly understood, to date only a very few classes of polymers have been studied as additives for protein crystallisation. Moreover, the mechanisms governing their interactions with protein crystals or surrounding solvent are elusive.

In the study presented here, we show that polymers designed with varying degrees of charge, molecular weight and backbone structure influenced the crystallisation of three target proteins: hen-egg white lysozyme (HEWL); concanavalin A (Con A); and bovine liver catalase (BLC). Polymers were prepared as 'additives' into protein solution to influence the proteins crystallisation process, leading to changes in size, habit, morphology and even polymorph of the final crystals. A simple model linking polymer structure and charge to protein isoelectric point (pI) and crystallisation rate is proposed.

Acknowledgements

I would like to thank my supervisors: Professor Cameron Alexander and Dr. Jonathan Burley, for all their guidance, motivation and support during my studies.

I acknowledge Professor Jonas Emsley and Dr. Ingrid Dreveny for lab support in the area of protein crystallisation; and Dr. Stephen Harper for all his help, patience and expertise in X-ray diffraction.

I particularly acknowledge Dr. Francisco Fernandez-Trillo and Dr. Eugene Peter Magennis for all the helpful discussion and support in the area of polymer.

Many thanks go to Mrs. Christy Grainger-Boulby for giving technical aid and assistance with everyday lab issues.

I would like thank Professor Cameron Alexander's and Dr. Jonathan Burley's research groups for their guidance and help, which proved invaluable during this work.

I gratefully thank International Office, University of Nottingham, UK for funding support.

Most importantly I would like to thank my parents and my sister for all their love and support.

List of Abbreviations

2-AmAA – 2-Acrylamidoacetic acid

4-ABA – 4-Aminobutanoic acid

4-AmBA – 4-Acrylamidobutanoic acid

Å – Angstrom

AMPS – 2-Acrylamido-2-methyl-1-propanesulfonic acid

ATRP – Atom transfer radical polymerisation

Bipy – 2,2-Bipyridine

BLC – Bovine liver catalase

CaF₂ – Calcium fluoride

CAT – 2-(Ethylthiocarbonothioylthio)-2-methylpropanoic acid

CDCl₃ – Chloroform-d

CHCl₃ – Chloroform

Con A – Concanavalin A

Cryo – Cryogenic

CTA – Chain transfer agent

DLS – Dynamic light scattering

DMAEMA – 2-(Dimethylamino)ethyl methacrylate

DMAPMAm – N-[3-(dimethylamino)propyl]methacrylamide

DMSO – Dimethyl sulfoxide

DP – Degree of polymerisation

DPBS – Dulbecco’s phosphate buffered saline

E.C. – Enzyme commission (number)

EtOAc – Ethyl acetate

FT-IR – Fourier transform infrared spectroscopy

G-CSF – Granulocyte-colony stimulating factor

GPC – Gel permeation chromatography

HEWL – Hen egg-white lysozyme

[I] – [Initiator]

IR – Infrared spectroscopy

Kcal – Kilocalorie

KDa – Kilodalton

[M] – [Monomer]

MCT – Mercury cadmium telluride

MEDSAH – N-[2-(methacryloyloxy)ethyl]-dimethyl-(2-sulfoethan)aminium
hydroxide

METMAC – [2-(Methacryloyloxy)ethyl]trimethylammonium chloride

MIPs – Molecularly imprinted polymers

M_n – Number average molecular weight

M_w – Molecular weight

MWCO – Molecular weight cut off

NaCl – Sodium chloride

NMR – Nuclear magnetic resonance

P(2-AmAA) – Poly(2-acrylamidoacetic acid)

P(4-AmBA) – Poly(4-acrylamidobutanoic acid)

P(AMPS) – Poly(2-acrylamido-2-methyl-1-propanesulfonic acid)

PBS – Phosphate-buffered saline

PDB – Protein data bank

PDI – Polydispersity index

P(DMAEMA) – Poly[2-(dimethylamino)ethyl methacrylate]

P(DMAPMAm) – Poly[N-(3-(dimethylamido)propyl)methacrylamide]

PEG – Polyethylene glycol

PEGMA₄₇₅ – Poly(ethylene glycol) methyl ether methacrylate $M_w \sim 475$

PEO – Poly(ethylene oxide)

PI – Isoelectric point

PLGA – Poly(lactic-*co*-glycolic acid)

P(PEGMA₄₇₅) – Poly[poly(ethylene glycol) methyl ether methacrylate $M_w \sim 475$]

PVP – Polyvinylpyrrolidone

RAFT – Reversible addition fragmentation chain transfer

RI – Refractive index

Rpm – Revolutions per minute

SEM – Scanning electron microscope

TFA – Trifluoroacetic acid

THF – Tetrahydrofuran

TMS – Tetramethylsilane

Tris – Tris(hydroxymethyl)aminomethane

UVP – UV compatible

V-501 – 4,4'-Azobis(4-cyanovaleric acid)

W/v – Weight/volume

List of Figures

Figure 1-1. Main protein structure levels	39
Figure 1-2. Use of protein crystallography.....	41
Figure 1-3. Encapsulation of therapeutic protein into polymeric particles	44
Figure 1-4. The crystal structure of Fluorite (CaF ₂).....	47
Figure 1-5. Diagram showing the transfer of molecules from solution to crystal according to Gibbs energy change.....	49
Figure 1-6. Thermodynamics of nucleation, according to Gibbs free energy ..	50
Figure 1-7. A view of crystal structure of chymotrypsinogen	53
Figure 1-8. Crystallisation phase diagram of solubility curve showing how the solubility varies with the concentration of crystallising agent	55
Figure 1-9. Micro-batch crystallisation technique.....	59
Figure 1-10. Button dialysis crystallisation technique	60
Figure 1-11. Vapour diffusion techniques: hanging drop, sandwich drop and sitting drop.....	61
Figure 1-12. The solubility curves of a typical protein, enolase, as a function of ionic strength produced by two types of salts.....	63
Figure 1-13. Schematic representation of heterogeneous nucleation facilitate by the insoluble solid surface	65
Figure 1-14. Some example images of protein crystals the nucleated and grew on the mineral substrate surfaces	66

Figure 1-15. Schematic representation of crystal nucleation in a pore, which explains the mechanism of porous substrates induce protein crystallisation.....	67
Figure 1-16. Schematic representation of the molecular imprinting process and selective crystallisation of calcium carbonate	71
Figure 1-17. General ATRP reaction scheme.....	78
Figure 1-18. Structures of PEGMA ₄₇₅ and DMAEMA monomers	80
Figure 1-19. Mechanism of RAFT polymerisation	81
Figure 1-20. Structures of DMAPMAm, AMPS, 2-AmAA and 4-AmBA monomers	83
Figure 1-21. The three-dimensional structure of HEWL, obtained by crystal X-ray diffraction	85
Figure 1-22. Crystallographic structure of a Con A tetramer (from jack bean), obtained by crystal X-ray diffraction.....	87
Figure 1-23. Crystallographic structure of a BLC tetramer.....	88
Figure 1-24. Schematic representation of protein crystallisation utilising polymer additives.....	90
Figure 2-1. Bragg's diffraction	101
Figure 3-1. Structures of polymers, named P1 to P8.....	104
Figure 3-2. Reaction scheme for the synthesis of 2-AmAA.....	105
Figure 3-3. ¹ H-NMR spectra of 2-AmAA	106
Figure 3-4. ¹³ C-NMR spectra of 2-AmAA.....	106

Figure 3-5. Scheme of the mechanism of synthesis of 2-AmAA.....	107
Figure 3-6. Reaction scheme for the synthesis of 4-AmBA.....	107
Figure 3-7. ¹ H-NMR spectra of 4-AmBA	108
Figure 3-8. ¹³ C-NMR spectra of 4-AmBA	109
Figure 3-9. Reaction scheme for the synthesis of p(PEGMA ₄₇₅) homopolymer (P1) via ATRP.....	111
Figure 3-10. ¹ H-NMR spectra for the polymerisation of PEGMA ₄₇₅ to yield p(PEGMA ₄₇₅) (P1).....	113
Figure 3-11. Representative FTIR for p(PEGMA ₄₇₅) (P1).....	113
Figure 3-12. Kinetic plots for the synthesis of p(PEGMA ₄₇₅) (P1) in this study	115
Figure 3-13. Reaction scheme for the synthesis of p(DMAEMA) (P2) via ATRP	116
Figure 3-14. ¹ H-NMR spectra for the polymerisation of DMAEMA to yield p(DMAEMA) (P2).....	117
Figure 3-15. Representative FTIR for p(DMAEMA) (P2).....	117
Figure 3-16. Kinetic plots for the synthesis of p(DMAEMA) (P2) via ATRP method.	119
Figure 3-17. Reaction scheme for quaternisation of p(DMAEMA) (P2).....	120
Figure 3-18. ¹ H-NMR spectra for quaternised p(DMAEMA) (P2).....	121
Figure 3-19. Representative FTIR for quaternised p(DMAEMA) (P2)	122
Figure 3-20. Reaction scheme for the synthesis of a random copolymer:	

p(DMAEMA- <i>stat</i> -PEGMA ₄₇₅) (P3) via ATRP.....	122
Figure 3-21. ¹ H-NMR spectra for the polymerisation of DMAMEA and PEGMA ₄₇₅ to yield p(DMAEMA- <i>stat</i> -PEGMA ₄₇₅) (P3).....	124
Figure 3-22. Reaction schemes for the synthesis of p(DMAPMAM) (P4) via RAFT method and the removal of RAFT end-group	126
Figure 3-23. ¹ H-NMR spectra for the polymerisation of DMAPMAM to yield p(DMAPMAM) (P4).....	128
Figure 3-24. Representative FTIR for p(DMAPMAM) (P4).....	128
Figure 3-25. Reaction schemes for the synthesis of p(AMPS) (P5) via RAFT method and removal of RAFT end-group	130
Figure 3-26. ¹ H-NMR spectra for the polymerisation of AMPS to yield p(AMPS) (P5).....	132
Figure 3-27. Representative FTIR for p(AMPS) (P5).....	132
Figure 3-28. Reaction schemes for the synthesis of p(2-AmAA) (P6) homopolymer via RAFT method and removal of RAFT end-group	133
Figure 3-29. ¹ H-NMR spectra for p(2-AmAA) (P6)	134
Figure 3-30. Representative FTIR for p(2-AmAA) (P6).....	135
Figure 3-31. Reaction schemes for the synthesis of p(4-AmBA) (P7) homopolymer via RAFT method and removal of RAFT end-group	136
Figure 3-32. ¹ H-NMR spectra for p(4-AmBA) (P7)	137

Figure 3-33. Representative FTIR for p(4-AmBA) (P7).....	137
Figure 3-34. Reaction scheme for the synthesis of p(METMAC- <i>co</i> -MEDSAH) (P8) by Dr. E. Peter Magennis	139
Figure 3-35. Representative ¹ H-NMR spectra of p(METMAC- <i>co</i> -MEDSAH) (P8) by Dr. E. Peter Magennis	140
Figure 3-36. Representative FTIR for p(METMAC- <i>co</i> -MEDSAH) (P8).....	140
Figure 4-1. Schematic representation of the interaction of various polymers with cationic HEWL in the protein crystallisation process.	147
Figure 4-2. MRC 2 Well Crystallisation Plate (Swissci), commercially available from Hampton Research.....	148
Figure 4-3. Diagram depicting the sitting drop vapour diffusion technique ..	149
Figure 4-4. The schematic representation of real-time protein concentration changes in the sitting drop	150
Figure 4-5. Schematic representation of protein crystallisation in the DLS quartz cell.....	155
Figure 4-6. Photomicrographs of HEWL crystals, grown in the presence of p(PEGMA ₄₇₅) (P1) at various concentrations.....	159
Figure 4-7. Summary of photomicrograph analysis showing changes in the size of HEWL crystals, grown in the presence of neutral p(PEGMA ₄₇₅) (P1) at various concentrations	160
Figure 4-8. HEWL crystal photomicrographs and X-ray diffraction pattern yielded by the single HEWL crystal in the presence of neutral	

p(PEGMA ₄₇₅) (P1).....	161
Figure 4-9. Summary of DLS data of HEWL crystallisation in the presence of neutral p(PEGMA ₄₇₅) (P1).....	163
Figure 4-10. Variations in the size of HEWL aggregates or crystals in the solution as a function of time during crystallisation experiments induced by neutral p(PEGMA ₄₇₅) (P1).....	164
Figure 4-11. SEM micrographs of HEWL crystals produced under tetragonal conditions, by sitting drop method	165
Figure 4-12. Schematic representation of hypothesis of HEWL crystallisation process without polymer (A); and the interaction of p(PEGMA ₄₇₅) (P1) with HEWL in the protein crystallisation process (B).....	166
Figure 4-13. Photomicrographs showing changes in the size and shape of HEWL crystals, grown under the tetragonal protocol, in the presence of quaternised p(DMAEMA) (P2) ($M_n \sim 46.3$ kDa) (quaternised ratio: 50 %) at various concentrations	170
Figure 4-14a. Photomicrographs of HEWL crystals, grown under the tetragonal protocol, in the presence of p(DMAEMA) ($M_n \sim 17.1$ kDa) (quaternised ratio: 25 %) at various concentrations, with lysozyme concentration: 25 mg/mL.....	173
Figure 4-14b. Photomicrographs of HEWL crystals, grown under the tetragonal protocol, in the presence of p(DMAEMA) ($M_n \sim 17.1$ kDa) (quaternised ratio: 25 %) at various concentrations, with lysozyme	

concentration: 50 mg/mL.....	174
Figure 4-14c. Photomicrographs of HEWL crystals, grown under the tetragonal protocol, in the presence of p(DMAEMA) ($M_n \sim 17.1$ kDa) (quaternised ratio: 25 %) at various concentrations, with lysozyme concentration: 75 mg/mL.....	175
Figure 4-14d. Photomicrographs of HEWL crystals, grown under the tetragonal protocol, in the presence of p(DMAEMA) ($M_n \sim 17.1$ kDa) (quaternised ratio: 25 %) at various concentrations, with lysozyme concentration: 100 mg/mL.....	176
Figure 4-15a. Photomicrographs of HEWL crystals, grown under the tetragonal protocol, in the presence of p(DMAEMA) ($M_n \sim 17.1$ kDa) (quaternised ratio: 50 %) at various concentrations, with lysozyme concentration: 25 mg/mL.....	178
Figure 4-15b. Photomicrographs of HEWL crystals, grown under the tetragonal protocol, in the presence of p(DMAEMA) ($M_n \sim 17.1$ kDa) (quaternised ratio: 50 %) at various concentrations, with lysozyme concentration: 50 mg/mL.....	179
Figure 4-15c. Photomicrographs of HEWL crystals, grown under the tetragonal protocol, in the presence of p(DMAEMA) ($M_n \sim 17.1$ kDa) (quaternised ratio: 50 %) at various concentrations, with lysozyme concentration: 75 mg/mL.....	180
Figure 4-15d. Photomicrographs of HEWL crystals, grown under the tetragonal	

protocol, in the presence of p(DMAEMA) ($M_n \sim 17.1$ kDa) (quaternised ratio: 50 %) at various concentrations, with lysozyme concentration: 100 mg/mL..... 181

Figure 4-16a. Photomicrographs of HEWL crystals, grown under the tetragonal protocol, in the presence of p(DMAEMA) ($M_n \sim 17.1$ kDa) (quaternised ratio: 75 %) at various concentrations, with lysozyme concentration: 25 mg/mL..... 183

Figure 4-16b. Photomicrographs of HEWL crystals, grown under the tetragonal protocol, in the presence of p(DMAEMA) ($M_n \sim 17.1$ kDa) (quaternised ratio: 75 %) at various concentrations, with lysozyme concentration: 50 mg/mL..... 184

Figure 4-16c & d. Photomicrographs showing changes in the size and shape of HEWL crystals, grown under the tetragonal protocol, in the presence of p(DMAEMA) ($M_n \sim 17.1$ kDa) (quaternised ratio: 75 %) at various concentrations, with lysozyme concentration: 75 and 100 mg/mL..... 185

Figure 4-17a. Photomicrographs of HEWL crystals, grown under the tetragonal protocol, in the presence of p(DMAEMA) ($M_n \sim 17.1$ kDa) (quaternised ratio: 100 %) at various concentrations, with lysozyme concentration: 25 mg/mL 187

Figure 4-17b. Photomicrographs of HEWL crystals, grown under the tetragonal protocol, in the presence of p(DMAEMA) ($M_n \sim 17.1$ kDa)

(quaternised ratio: 100 %) at various concentrations, with lysozyme concentration: 50 mg/mL	188
Figure 4-17c & d. Photomicrographs showing changes in the size and shape of HEWL crystals, grown under the tetragonal protocol, in the presence of p(DMAEMA) ($M_n \sim 17.1$ kDa) (quaternised ratio: 100 %) at various concentrations, with HEWL concentration: 75 and 100 mg/mL.....	189
Figure 4-18. Schematic triangle graphs showing the trends of HEWL crystals obtained in the presence of different quaternised ratios of p(DMAEMA) (P2) (25 %, 50 %, 75 % and 100 %) by using different concentrations of HEWL	191
Figure 4-19. Summary of photomicrograph analysis showing changes in the size and number of HEWL crystals, grown in the presence of quaternised p(DMAEMA) (quaternised ratio: 75 %) at various concentrations, with HEWL concentration 50 mg/mL.....	192
Figure 4-20. HEWL crystal photomicrograph and X-ray diffraction patterns yielded by the single HEWL crystal in the presence of cationic quaternised p(DMAEMA) (P2) (quaternised ratio: 75 %)	193
Figure 4-21. Variations of the size of HEWL aggregates or crystals in the solution as a function of time during crystallisation experiment induced by cationic quaternised p(DMAEMA) (P2) (quaternised ratio: 75 %)	194

Figure 4-22. SEM micrographs of HEWL needles produced under tetragonal conditions in the presence of quaternised p(DMAEMA).....	195
Figure 4-23. Photomicrographs of HEWL crystals, grown from the tetragonal protocol in the presence of p(DMAEMA- <i>stat</i> -PEGMA ₄₇₅) (P3) (M _n ~52.9 kDa) with various concentrations.....	197
Figure 4-24. Summary of photomicrograph analysis showing changes in the size and number of HEWL crystals, grown in the presence of p(DMAEMA- <i>stat</i> -PEGMA ₄₇₅) (P3) at various concentrations. .	198
Figure 4-25. HEWL crystal photomicrograph and X-ray diffraction patterns yielded by the single HEWL crystal formed in the presence of cationic p(DMAEMA- <i>stat</i> -PEGMA ₄₇₅) (P3).	199
Figure 4-26. Photomicrographs of HEWL crystals, grown in the presence of a mixture of two polymers: p(PEGMA ₄₇₅) and p(DMAEMA) (P1 & P2) (molar ratio 9:1) at various concentrations.....	203
Figure 4-27. Summary of photomicrograph analysis showing changes in the size and number of HEWL crystals, grown in the presence of a mixture of two polymers: p(PEGMA ₄₇₅) and p(DMAEMA) (P1 & P2) at various concentrations.....	204
Figure 4-28. HEWL crystal photomicrograph and X-ray diffraction patterns yielded by the single HEWL crystal in the presence of a mixture of two polymers: p(PEGMA ₄₇₅) and p(DMAEMA) (P1 & P2).....	205
Figure 4-29. Variations of the size of HEWL aggregates or crystals in the	

<p style="text-align: center;">solution as a function of time during crystallisation experiments induced by a mixture of two polymers: p(PEGMA₄₇₅) and p(DMAEMA) (P1 & P2)</p>	206
<p>Figure 4-30a. Photomicrographs of HEWL crystals, grown under tetragonal crystal condition, in the presence of p(DMAPMAM) (P4) (DP 38) at various concentrations</p>	211
<p>Figure 4-30b. Photomicrographs of HEWL crystals, grown under tetragonal crystal condition, in the presence of p(DMAPMAM) (P4) (DP 83) at various concentrations</p>	212
<p>Figure 4-30c. Photomicrographs of HEWL crystals, grown under tetragonal crystal condition, in the presence of p(DMAPMAM) (P4) (DP 150) at various concentrations</p>	213
<p>Figure 4-31. Summary of photomicrograph analysis showing changes in the size and number of HEWL crystals, grown in the presence of p(DMAPMAM) (P4) (DP 83) at various concentrations</p>	214
<p>Figure 4-32. Variations of the size of HEWL aggregates or crystals in the solution as a function of time during crystallisation experiments induced by p(DMAPMAM) (P4)</p>	215
<p>Figure 4-33. Hypothesis of mechanism of cationic polymer mediated HEWL crystallisation</p>	216
<p>Figure 4-34a. Photomicrographs of HEWL crystals, grown under tetragonal crystal condition, in the presence of p(AMPS) (P5) (DP 53) at</p>	

various concentrations	220
Figure 4-34b. Photomicrographs of HEWL crystals, grown under tetragonal crystal condition, in the presence of p(AMPS) (P5) (DP 99) at various concentrations	221
Figure 4-34c. Photomicrographs of HEWL crystals, grown under tetragonal crystal condition, in the presence of p(AMPS) (P5) (DP 200) at various concentrations	222
Figure 4-35. Summary of photomicrograph analysis showing changes in the size and number of HEWL crystals, grown in the presence of p(AMPS) (P5) (DP 99) at various concentrations	223
Figure 4-36. Variations of the size of HEWL aggregates or crystals in the solution as a function of time during crystallisation experiments induced by p(AMPS) (P5) (DP 99).	224
Figure 4-37. SEM micrograph of HEWL crystal produced under tetragonal conditions in the presence of p(AMPS) (P5), -- x 500 magnification; the scale bar was 50 μ m	225
Figure 4-38a. Photomicrographs of HEWL crystals, grown under tetragonal crystal condition, in the presence of p(2-AmAA) (P6) (DP 18) at various concentrations	231
Figure 4-38b. Photomicrographs of HEWL crystals, grown under tetragonal crystal condition, in the presence of p(2-AmAA) (P6) (DP 46) at various concentrations	232

Figure 4-38c. Photomicrographs of HEWL crystals, grown under tetragonal crystal condition, in the presence of p(2-AmAA) (P6) (DP 72) at various concentrations	233
Figure 4-38d. Photomicrographs of HEWL crystals, grown under tetragonal crystal condition, in the presence of p(2-AmAA) (P6) DP (150) at various concentrations	234
Figure 4-39. Summary of photomicrograph analysis showing changes in the size and number of HEWL crystals, grown in the presence of p(2-AmAA) (P6) (DP 72) at various concentrations	235
Figure 4-40. HEWL crystal photomicrographs and X-ray diffraction patterns yielded by the single HEWL crystal in the presence of p(2-AmAA) (P6) with DPs 18 and 46.....	236
Figure 4-41. Variations of the size of HEWL aggregates or crystals in the solution as a function of time during crystallisation experiments induced by p(2-AmAA) (P6).....	237
Figure 4-42a. Photomicrographs of HEWL crystals, grown under tetragonal crystal condition, in the presence of p(4-AmBA) (P7) (DP 21) at various concentrations	243
Figure 4-42b. Photomicrographs of HEWL crystals, grown under tetragonal crystal condition, in the presence of p(4-AmBA) (P7) (DP 50) at various concentrations	244
Figure 4-42c. Photomicrographs of HEWL crystals, grown under tetragonal	

crystal condition, in the presence of p(4-AmBA) (P7) (DP 100) at various concentrations	245
Figure 4-42d. Photomicrographs of HEWL crystals, grown under tetragonal crystal condition, in the presence of p(4-AmBA) (P7) (DP 200) at various concentrations	246
Figure 4-43. Summary of photomicrograph analysis showing changes in the size and number of HEWL crystals, grown in the presence of p(4-AmBA) (P7) (DP 100) at various concentrations	247
Figure 4-44. HEWL crystal photomicrograph and X-ray diffraction patterns yielded by the single HEWL crystal in the presence of p(4-AmBA) (P7)	248
Figure 4-45. Variations of the size of HEWL aggregates or crystals in the solution as a function of time during crystallisation experiments induced by p(4-AmBA) (P7)	249
Figure 4-46. Hypothesis of mechanism of anionic polymer mediated HEWL crystallisation.....	250
Figure 4-47. Photomicrographs of HEWL crystals, grown under tetragonal crystal condition, in the presence of p(METMAC-co-MEDSAH) (P8) at various concentrations	252
Figure 4-48. Summary of photomicrograph analysis of HEWL crystals, grown in the presence of p(METMAC-co-MEDSAH) (P8) at various concentrations	253

Figure 4-49. Hypothesis of mechanisms of cationic/zwitterionic polymer mediated HEWL crystallisation.....	254
Figure 5-1. Schematic representation of the interaction of various polymers with anionic concanavalin A (Con A) in the protein crystallisation process	260
Figure 5-2. Selected photomicrographs of Con A crystals, grown in the presence of p(PEGMA ₄₇₅) (P1) at various concentrations	265
Figure 5-3. Summary of photomicrograph analysis of Con A crystals, grown in the presence of p(PEGMA ₄₇₅) (P1) at various concentrations....	266
Figure 5-4. Con A crystals photomicrographs and X-ray diffraction patterns yielded by the single Con A crystal in the presence of neutral p(PEGMA ₄₇₅) (P1).....	267
Figure 5-5. Summary of DLS data of Con A crystallisation under neutral p(PEGMA ₄₇₅) (P1) at time points T ₀ and T _{120min}	268
Figure 5-6. Variations of the size of Con A aggregates or crystals in the solution as a function of time during crystallisation experiments induced by neutral p(PEGMA ₄₇₅) (P1).....	269
Figure 5-7. SEM micrographs of Con A crystals formed by sitting drop method	270
Figure 5-8. Schematic representation of hypothesis of anionic Con A crystallisation process without polymer (A); and the interaction of neutral p(PEGMA ₄₇₅) (P1) with anionic Con A in the protein	

crystallisation process (B).....	271
Figure 5-9. Photomicrographs of Con A crystals, grown in the presence of quaternised p(DMAEMA) (P2) at various concentrations	273
Figure 5-10. Summary of photomicrograph analysis of Con A crystals, grown in the presence of quaternised p(DMAEMA) (P2) at various concentrations	274
Figure 5-11. Summary of DLS data of Con A crystallisation under quaternised p(DMAEMA) (P2) at time points T_0 and $T_{120\text{min}}$	275
Figure 5-12. Variations of the size of Con A aggregates or crystals in the solution as a function of time during crystallisation experiments induced by cationic quaternised p(DMAEMA) (P2).....	276
Figure 5-13. SEM micrographs of Con A crystals formed in the presence of quaternised p(DMAEMA) (P2)	276
Figure 5-14. Hypothesis of mechanism of cationic polymer mediated Con A crystallisation.....	277
Figure 5-15. Photomicrographs of Con A crystals, grown in the presence of p(AMPS) (P5) (DP 99) at various concentrations	279
Figure 5-16. Summary of photomicrograph analysis of Con A crystals, grown in the presence of p(AMPS) (P5) at various concentrations	280
Figure 5-17. Summary of DLS data of Con A crystallisation under anionic p(AMPS) (P5) (DP 99) at time points T_0 and $T_{100\text{min}}$	281
Figure 5-18. Variations of the size of Con A aggregates or crystals in the	

solution as a function of time during crystallisation experiments induced by anionic p(AMPS) (P5)	282
Figure 5-19. SEM micrographs of Con A crystals formed in the presence of p(AMPS) (P5).....	283
Figure 5-20. Hypothesis of mechanism of anionic polymer mediated Con A crystallisation.....	284
Figure 6-1. Schematic representation of the interaction of various polymers with anionic bovine liver catalase (BLC) in the protein crystallisation process.....	288
Figure 6-2. Photomicrographs of BLC crystals, grown in the presence of p(PEGMA ₄₇₅) (P1) at various concentrations.....	293
Figure 6-3. Summary of photomicrograph analysis of BLC crystals, grown in the presence of p(PEGMA ₄₇₅) (P1) at various concentrations....	295
Figure 6-4. Summary of DLS data of BLC crystallisation under neutral p(PEGMA ₄₇₅) (P1) at time points T ₀ and T _{120min}	296
Figure 6-5. Variations of the size of BLC aggregates or crystals in the solution as a function of time during crystallisation experiments induced by neutral p(PEGMA ₄₇₅) (P1).....	297
Figure 6-6. Schematic representation of hypothesis of anionic BLC crystallisation process in the absence of polymer (A); and the interaction of neutral p(PEGMA ₄₇₅) (P1) with anionic BLC in the protein crystallisation process (B)	298

Figure 6-7. Hypothesis of mechanism of anionic polymer mediated Con A crystallisation.....	300
Figure 6-8. Summary of DLS data of BLC crystallisation under cationic quaternised p(DMAEMA) (P2) at time points T_0 and $T_{120\text{min}}$	302
Figure 6-9. Variations of the size of BLC aggregates or crystals in the solution as a function of time during crystallisation experiments induced by cationic quaternised p(DMAEMA) (P2)	302
Figure 6-10. Photomicrographs of BLC crystals formed in the presence of p(AMPS) (P5) at various concentrations.....	304
Figure 6-11. Summary of photomicrograph analysis of BLC crystals, grown in the presence of p(AMPS) (P5) at various concentrations.....	305
Figure 6-12. BLC crystal photomicrograph and X-ray diffraction patterns yielded by the single BLC crystal in the presence of anionic p(AMPS) (P5).....	306
Figure 6-13. Summary of DLS data of BLC crystallisation under anionic p(AMPS) (P5) at time points T_0 and $T_{120\text{min}}$	307
Figure 6-14. Variations of the size of BLC aggregates or crystals in the solution as a function of time during crystallisation experiments induced by anionic p(AMPS) (P5)	308
Figure 6-15. Hypothesis of mechanism of anionic polymer mediated BLC crystallisation.....	309
Figure 7-1. Selected optical photomicrographs of HEWL crystals formed under	

conditions of tetragonal crystal-inducing protocol, in the presence of neutral, cationic, anionic and cationic/zwitterionic polymers as solutes in the crystallisation solutions	315
Figure 7-2. Schematic representation of the interaction of various polymers with cationic HEWL in the protein crystallisation process	319
Figure 7-3. Summary of photomicrograph analysis showing changes in the size of HEWL crystals, grown in the presence of different classes of polymers at various concentrations	321
Figure 7-4. Optical images showing changes of Con A crystals, in the presence of different polymers: neutral p(PEGMA ₄₇₅) (P1), cationic quaternised p(DMAEMA) (P2) and anionic p(AMPS) (P5)	322
Figure 7-5. Summary of photomicrograph analysis showing changes in the size of Con A crystals, grown in the presence of different classes of polymers at various concentrations	323
Figure 7-6. Optical images showing changes of BLC crystals, in the presence of different polymers: neutral p(PEGMA ₄₇₅) (P1), cationic quaternised p(DMAEMA) (P2) and anionic p(AMPS) (P5)	324
Figure 7-7. Predicted growth of HEWL ((i)A) and Con A ((ii)A) particles during crystallisation; and actual variations in the size of HEWL ((i)B-D) and Con A ((ii)B-D) aggregates or crystals in the solution as a function of time during crystallisation experiments induced by different polymers by DLS	325

List of Tables

Table 1-1. Seven crystal lattice systems in three dimensions.....	48
Table 1-2. Types of chain growth polymerisation	77
Table 3-1. Summary of synthesis of p(PEGMA ₄₇₅) (P1) via ATRP	114
Table 3-2. Summary of synthesis of p(DMAEMA) (P2) via ATRP.....	118
Table 3-3. Summary of synthesis of p(DMAEMA- <i>stat</i> -PEGMA ₄₇₅) (P3).....	125
Table 3-4. Summary of synthesis of p(DMAPMAm) (P4) via RAFT	130
Table 3-5. Summary of synthesis of p(AMPS) (P5) via RAFT.....	133
Table 3-6. Summary of synthesis of p(2-AmAA) (P6) via RAFT	135
Table 3-7. Summary of synthesis of p(4-AmBA) (P7) via RAFT.....	138
Table 4-1. Summary of hen egg-white lysozyme (HEWL).....	146
Table 4-2. HEWL crystallisation plate set up: p(PEGMA ₄₇₅)	157
Table 4-3. Unit cell dimensions of HEWL crystals formed in the absence (Control) and presence of neutral p(PEGMA ₄₇₅) (P1).....	161
Table 4-4. HEWL crystallisation plate set up: quaternised p(DMAEMA) (P2) (M _n ~46.3 kDa) (quaternised ratio: 50 %).....	168
Table 4-5. HEWL crystallisation plate set up: quaternised p(DMAEMA) (P2) (M _n ~17.1 kDa) (quaternised ratio: 25 %).....	172
Table 4-6. HEWL crystallisation plate set up: quaternised p(DMAEMA) (P2) (M _n ~17.1 kDa) (quaternised ratio: 50 %).....	177
Table 4-7. HEWL crystallisation plate set up: quaternised p(DMAEMA) (P2)	

(M _n ~17.1 kDa) (quaternised ratio: 75 %).....	182
Table 4-8. HEWL crystallisation plate set up: quaternised p(DMAEMA) (P2)	
(M _n ~17.1 kDa) (quaternised ratio: 100 %).....	186
Table 4-9. Unit cell dimension of HEWL crystal formed in the presence of	
cationic quaternised p(DMAEMA) (P2) (quaternised ratio: 75 %)	
.....	193
Table 4-10. HEWL crystallisation plate: p(DMAEMA- <i>stat</i> -PEGMA ₄₇₅) (P3)	
.....	196
Table 4-11. Unit cell dimension of HEWL crystal in the presence of cationic	
p(DMAEMA- <i>stat</i> -PEGMA ₄₇₅) (P3).....	199
Table 4-12. HEWL crystallisation plate set up: a mixture of two polymers:	
p(PEGMA ₄₇₅) and p(DMAEMA) (P1 & P2).....	201
Table 4-13. Unit cell dimension of HEWL crystal in the presence of a mixture	
of two polymers: p(PEGMA ₄₇₅) and p(DMAEMA) (P1 & P2) .	205
Table 4-14a. HEWL crystallisation plate set up: p(DMAPMAm) (P4) (DP 38)	
.....	207
Table 4-14b. HEWL crystallisation plate set up: p(DMAPMAm) (P4) (DP 83)	
.....	208
Table 4-14c. HEWL crystallisation plate set up: p(DMAPMAm) (P4) (DP 150)	
.....	209
Table 4-15a. HEWL crystallisation plate set up: p(AMPS) (P5) (DP 53).....	217
Table 4-15b. HEWL crystallisation plate set up: p(AMPS) (P5) (DP 99).....	218

Table 4-15c. HEWL crystallisation plate set up: p(AMPS) (P5) (DP 200)....	219
Table 4-16a. HEWL crystallisation plate set up: p(2-AmAA) (P6) (DP 18)..	226
Table 4-16b. HEWL crystallisation plate set up: p(2-AmAA) (P6) (DP 46) .	227
Table 4-16c. HEWL crystallisation plate set up: p(2-AmAA) (P6) (DP 72)..	228
Table 4-16d. HEWL crystallisation plate set up: p(2-AmAA) (P6) (DP 150)	229
Table 4-17. Unit cell dimensions of HEWL crystal in the presence of anionic p(2-AmAA) (P6).....	236
Table 4-18a. HEWL crystallisation plate set up: p(4-AmBA) (P7) (DP 21)..	238
Table 4-18b. HEWL crystallisation plate set up: p(4-AmBA) (P7) (DP 50)..	239
Table 4-18c. HEWL crystallisation plate set up: p(4-AmBA) (P7) (DP 100)	240
Table 4-18d. HEWL crystallisation plate set up: p(4-AmBA) (P7) (DP 200)	241
Table 4-19. Unit cell dimension of HEWL crystal in the presence of anionic p(4-AmBA) (P7).....	248
Table 4-20. HEWL crystallisation plate set up: p(METMAC- <i>co</i> -MEDSAH) (P8)	251
Table 4-21. Summary of polymers applied to HEWL crystallisation	255
Table 5-1. Summary of concanavalin A (Con A).....	259
Table 5-2. Con A crystallisation plate set up: p(PEGMA ₄₇₅).....	264
Table 5-3. Diffraction data collection for Con A crystals formed in the absence (Control) and presence of neutral p(PEGMA ₄₇₅) (P1).....	267
Table 5-4. Con A crystallisation plate set up: quaternised p(DMAEMA) (P2) (quaternised ratio: 75 %)	272

Table 5-5. Con A crystallisation plate set up: p(AMPS) (P5) (DP 99).....	278
Table 6-1. Summary of bovine liver catalase (BLC).....	287
Table 6-2. BLC crystallisation plate set up: p(PEGMA ₄₇₅).....	292
Table 6-3. BLC crystallisation plate set up: quaternised p(DMAEMA) (P2)	299
Table 6-4. BLC crystallisation plate set up: p(AMPS) (P5) (DP 99)	303
Table 6-5. Diffraction data collection for BLC crystal.....	306

CHAPTER 1

1. Introduction

1.1 Introduction to chapter

The overall aim of this project was to generate various polymers with varying degrees of charge, molecular weight and backbone structure, and then to study their roles as solution ‘additives’ in model protein crystallisation process. This chapter will explain why we need protein crystals, the importance of protein crystallisation and will focus on polymer additives in protein crystallisation. It will cover general principles of crystallisation, various crystallisation techniques, research and challenge in the crystallisation of protein so far, and an introduction of synthetic methods of polymers and three different model protein targets: hen egg white lysozyme (HEWL), concanavalin A (Con A) and bovine liver catalase (BLC).

1.2 General protein introduction

1.2.1 Analysis of protein structure

Proteins are a heterogeneous class of biological macromolecules with diameters of 1-100 nm. They are polypeptides made of many amino acids, which linked together via peptide bonds in a linear chain-like arrangement. Natural proteins are formed by up to 20 standard L-alpha amino acids, which also referred to as ‘residues’. Protein differs from one another due to the

difference of their order of the amino acid residues, which is defined by the sequence of their gene. A specific sequence of the amino acid residues in a protein is called 'primary structure'. The 'secondary structure' refers to local sub-structures. Some areas within a protein are folded or coiled to form secondary structure, which are maintained by hydrogen bonding between amino acids in different regions. There are two kinds of secondary structure: alpha-helices or beta-pleated sheets.

The 'tertiary structure' is the final three-dimensional structure of a protein. The alpha-helices or beta-pleated sheets are folded further to form a compact globular structure, which driven by various interactions between atoms and molecules, including van der Waals forces, hydrogen bonding, electronic interactions between charged groups and hydrophobic interactions; and, stabilised by covalent disulphide bonds or salt bridges. Moreover, some proteins, which consist of several protein molecules (so called multi-subunit) as single large proteins have another level of structure: 'quaternary structure'. In this protein, each subunit has its own three-dimensional tertiary structure. All subunits associated with each other to form the final functional protein by the same non-covalent interactions or disulphide bonds as that stabilise the tertiary structure. The level of protein structures is shown in Figure 1-1.

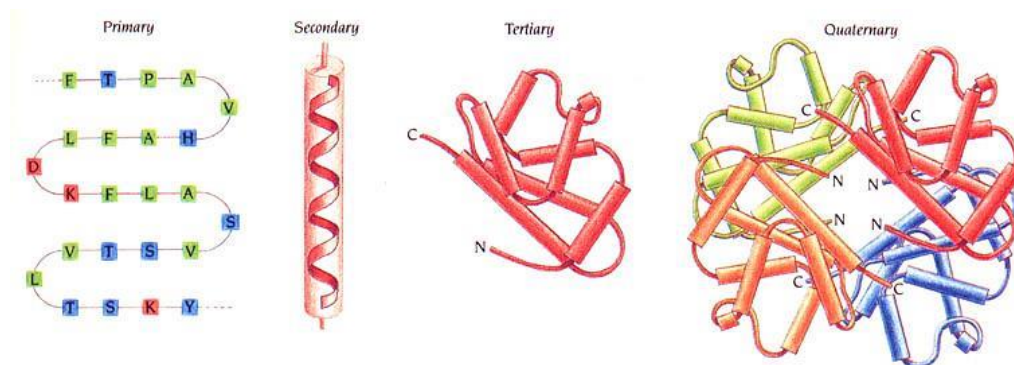


Figure 1-1. Main protein structure levels.¹ The amino acid sequence of a protein's polypeptide chain is called primary structure and F, T, P, A, V etc. represent different amino acids: F represents phenylalanine, T represents threonine, P represents proline, A represents alanine, V represents valine, H represents histidine, L represents leucine, D represents aspartic acid, K represents lysine, S represents serine, Y represents tyrosine. C represents carboxyl group, N represents amino group.

The tertiary or quaternary structure of a protein can play a vital role to understanding the function of protein macromolecules. Currently, two main methods have been employed for determining the three-dimensional structure of a protein: nuclear magnetic resonance (NMR) spectroscopy and X-ray crystallography. Although the NMR method can resolve the atomic structure of many small proteins, there is an upper molecular weight limit of about 25 kDa, or approximately 220 amino acids long for the NMR method. However, the primary tool for determining the three dimensional structure of proteins at the moment is X-ray crystallography, which is much more suitable for determining the structure of larger proteins (> 20 kDa),² but is dependent on the availability

of good quality protein crystals. For the X-ray crystallography method, the target proteins must undergo crystallisation first, in order to provide a high quality single crystal. X-rays can be considered waves of electromagnetic radiation. The regular arrays of atoms in the crystal cause the beams of X-ray to diffract into many directions. By measuring the intensities and angles of these diffracted beams, a three-dimensional picture of electron density within the crystal can be obtained by a crystallographer. Then this three-dimensional image can be used to identify the protein structure. Thus, protein crystallisation serves as a basis for X-ray crystallography.³ By using X-ray method, the studies of the structures of myoglobin in 1950 and hemoglobin in 1955 were awarded the Nobel Prize in Chemistry in 1962. Now, almost 80 % of all protein structures are determined by X-ray crystallography.⁴

The information of tertiary or quaternary structure of the protein is useful in numerous ways. Furthermore, protein crystallographic study is becoming an essential interest in many science and technology areas today, including biotechnological, pharmaceutical and chemical industries, such as drug design and protein engineering (Figure 1-2).⁵

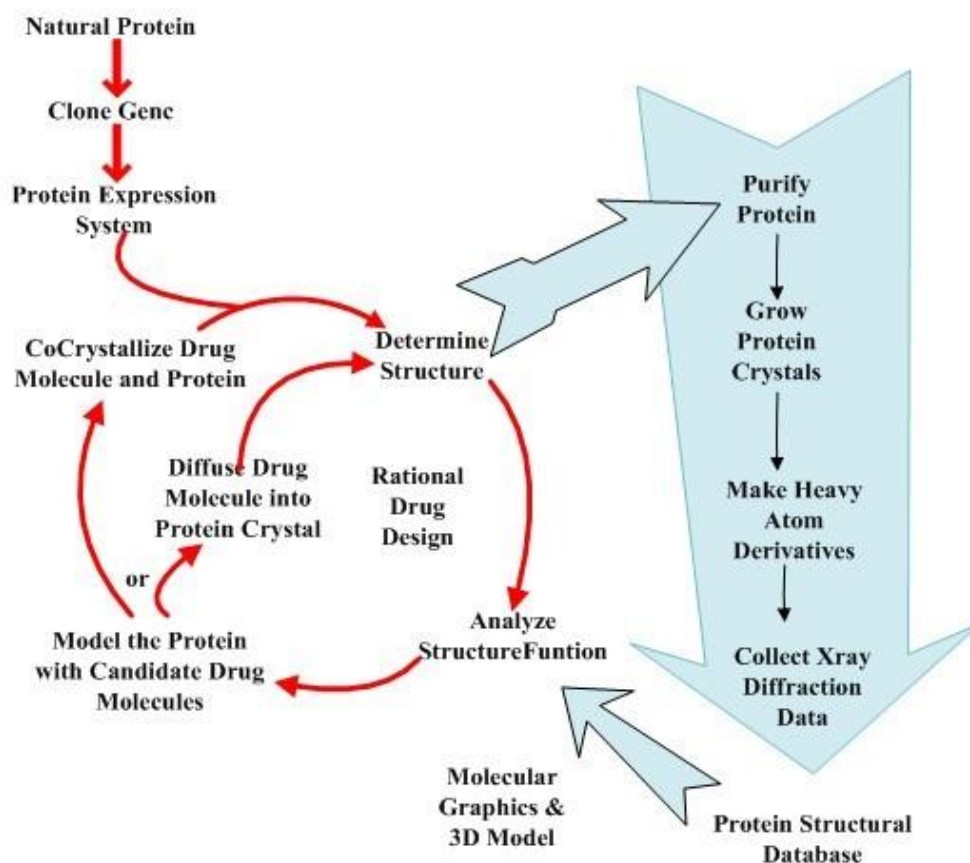


Figure 1-2. Use of protein crystallography.⁵ Diagram showing the application of the crystalline protein in various science areas, by the pathway of combination of X-ray crystallography, computer graphic analysis and synthetic chemistry.

One application of protein crystallography is the rational drug design. Once the tertiary or quaternary structure of the protein is elucidated, it can be used to identify their active sites, possible areas of interactions with other macromolecules, or similarities in structures with other known proteins. For example, in some diseases, such as cancer, some proteins are always considered as drug targets, because they can activate certain biological pathways of the disease. Once the structure of these proteins is known, the

information can be used to guide the design of molecules to fit the active sites of the protein, thereby modifying its function. Typically these designed molecules will be inhibitors of protein function, thus the molecules act as drugs. This kind of method for drug development is known as structure-based design. For example, imatinib, marketed as Glivec or Gleevec, is a tyrosine kinase inhibitor used in the treatment of multiple cancers.⁶

Besides structure and function characterisation purposes, protein crystallography is also important in industrial biocatalysis. The stability of biocatalysts in a reaction environment is a key issue in industrial biocatalysis. One approach to increasing their operational stability is crystallisation.⁷ Cross-linked protein crystals (CLPCs) with high activity and stability have been studied in biocatalytic applications. For instance, xylose isomerase crystals cross-linked with glutaraldehyde and L-lysine have been used as a catalyst for the isomerization of D-glucose to D-fructose.^{8,9}

Aside from the above aspects, the isolation of proteins in crystalline form is essential in many key pharmaceutical areas.⁵ There are other applications where defined assemblies of proteins, either crystals or self-assembled protein nanoparticles, are desirable. These include protein formulations.

1.2.2 Protein therapeutics

Proteins are involved in key cellular functions in the body, which provide the foundations to maintain the homeostasis of the organism. An increased

understanding of the roles of proteins in health and disease is crucial for the identification of new treatment options. Currently, the use of proteins as novel drugs is now well accepted in the treatment of certain diseases. Moreover, recent recombinant DNA techniques allow the production of novel proteins in large quantities.^{10, 11} Protein drugs have several advantages over small drug molecules, such as proteins often have highly specific action, do not interfere with normal biological processes, and therefore, adverse effects are decreased. Moreover, protein therapeutics is more tolerated, because the body produces a lot of proteins naturally. Despite these advantages, the use of protein drugs *in vivo* still has some obstacles, including high molecular weight, structural fragility, short life time and highly sensitive to enzymes.^{12, 13, 14} The oral route of administration for proteins is problematic; generally they have very poor pharmacokinetics. Protein drugs macromolecules are easily degraded and denatured by the enzymes; the high acidity of the stomach could destroy them before they reach the intestine for absorption; and they must cross several biological barriers before reach the site of action.¹⁵ Therefore, improving the stability of protein drugs is very essential for their applications.

One method is encapsulating proteins inside biodegradable polymer shells, which serves to protect the protein from clearing by the body and allow for the sustained and targeted delivery of protein drugs. Poly(lactic-*co*-glycolic acid) (PLGA) polymers have been studied and used for encapsulating of proteins.¹⁶

The encapsulation of the protein is typically via emulsification^{17, 18} or direct

incorporation of solid protein^{19,20} as shown in Figure 1-3.²¹

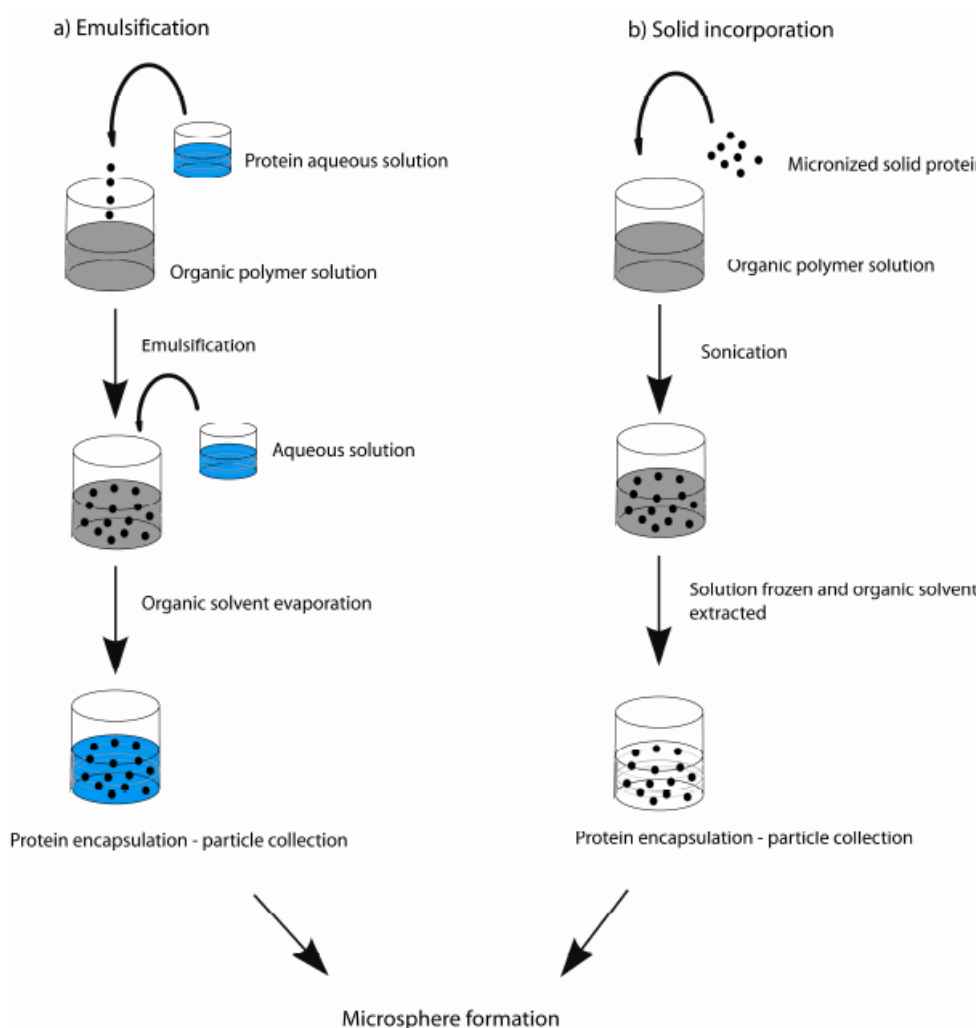


Figure 1-3. Encapsulation of therapeutic protein into polymeric particles by a) emulsification and b) solid incorporation method, taken from Reference.²¹

For the emulsification method, the protein is dissolved in an aqueous solution first and then dispersed in an organic polymer solution to get a protein in polymer solution. After evaporated the organic solvent, PLGA was precipitated around protein macromolecules to form microspheres.^{17, 18} For the direct incorporation of solid protein method, micronised solid protein is directly

suspended in an organic polymer solution via sonication. Then microspheres are obtained after the solution is frozen and organic solvent is extracted.^{19, 20}

This encapsulating protein inside biodegradable polymer shells method does not alter the native properties of the protein. Moreover, it can provide a sustained release of the protein over a few hours or days.²¹

Another method is making the protein more stable by changing some of its amino acids, which can optimize the hydrogen bonding and electrostatic interactions of protein.^{22, 23} For instance, granulocyte-colony stimulating factor (G-CSF) is limited by its low stability, by engineering of its structure, its thermal stability was enhanced of up to 13 °C; the shelf time was improved, and the activity was retained *in vitro*.²³

Moreover, attaching and conjugating the protein to a polymer chain is a successful approach. Polyethylene glycol (PEG) is the most commonly employed polymer. The polymer can alter the solubility of protein and creates a protection barrier on the surface of the protein.²⁴

In addition of all above methods, making protein nanocrystals or nanoaggregates (i.e. particles bigger than an individual protein molecule, but small enough to be colloidally stable) is another essential approach in protein therapeutics. Crystallised protein drug macromolecules remain in active form within the crystal lattice and hence are protected during storage and drug release process.²⁵ Moreover, protein crystals can act as carrier-free delivery systems; have the ability of sustained release for the protein drugs, which

reduces in frequency of intakes, adverse effects and patient compliance.²⁶ Furthermore, subtle changes in protein crystallisation conditions may result in multiple crystal structures from the same crystallising molecules, so called 'polymorphs'. Different polymorphs have different physical properties, for instance crystal habit, melting point and dissolution rate. If produced different polymorphs have different dissolution rate and solubility, they can alter important pharmacokinetic factors, such as absorption rate, drug availability.²⁷ For some unstable protein crystals, if different polymorphs of proteins were produced, which can enhance their stability; this might change the storage shelf life of the proteins similar as small drug molecules.²⁸ Therefore, proteins as drugs, in the form of crystals, can show promise in controlled and sustained delivery and aid in their formulation.

1.3 Crystals

Crystals are physically homogeneous solids, whose atoms, ions, or molecules are in accordance with an ordered pattern extending in all three spatial dimensions. Many of them have a particular well-defined geometrical shape, with regular faces and sharp edges.²⁹ Crystals exist widely in nature; the vast majority of solids are crystals, such as ice, salts and rocks. Figure 1-4 is a model of crystal structure of calcium fluoride.

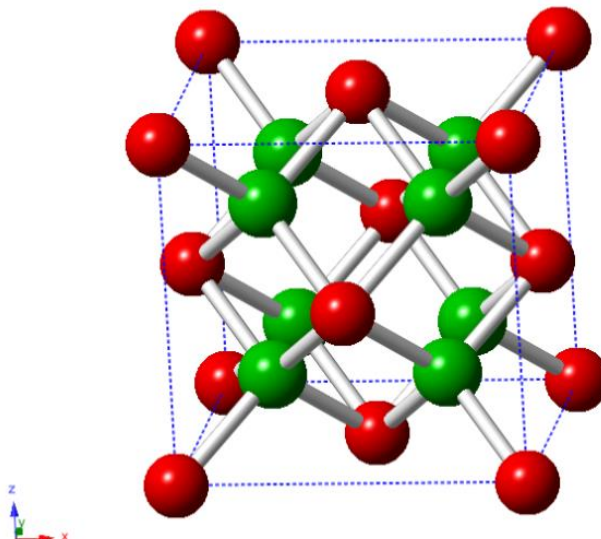


Figure 1-4. The crystal structure of Fluorite (CaF_2). The lattice is a cubic crystal system with unit cell dimensions of $a = b = c = 5.46 \text{ \AA}$, $\alpha = \beta = \gamma = 90^\circ$. Calcium ions (red) reside at the vertices and face centers of a cube, with fluorine ions (green) in the tetrahedral interstices. Calcium ion centers are 8-coordinate, being centered in a ‘box’ for 8 fluorine ions. Fluorine ion center is coordinate to 4 calcium ions.

Crystallisation is the process by which crystals are formed. The crystallisation process of molecules from a solution is a reversible equilibrium phenomenon, driven by the minimization of the free energy of the system.³⁰ For a stable solution, the solute is fully dissolved, and the system is at equilibrium. However, if more solute molecules are added to the solution, and they could not dissolve completely, thus, a new state (the so-called ‘supersaturated state’) will appear. A supersaturated solution represents a chemical system which is not at equilibrium.^{31, 32, 33} The system is thermodynamically driven to a new

equilibrium state with a new minimized free energy. Particular interactions occur between individual solute molecules and they are forced out from the solution and start to form amorphous aggregates. If these interactions are geometrically favorable, these amorphous aggregates will form crystal nuclei. As a result, individual solute molecules align themselves in a repeating series of ‘unit cells’ by adopting a consistent orientation. The crystalline ‘lattice’ then forms together by non-covalent interactions.³⁴

There are seven crystal lattice systems including triclinic, monoclinic, orthorhombic, rhombohedral, tetragonal, hexagonal and cubic as shown in Table 1-1. One type of symmetry used to categorize crystal structures: axis; and the parameters used to give unit cell, which are the lengths of the cell edges (a, b and c) and the angles between them (α , β and γ).

Table 1-1. Seven crystal lattice systems in three dimensions

Lattice System	Axis of Symmetry	Axial Length of Unit Cell	Inter Axial Angles
Triclinic	0 axes	$a \neq b \neq c$	$\alpha \neq \beta \neq \gamma \neq 90^\circ$
Monoclinic	1 two-fold axis	$a \neq b \neq c$	$\alpha = \gamma = 90^\circ, \beta \neq 90^\circ$
Orthorhombic	3 two-fold axes	$a \neq b \neq c$	$\alpha = \beta = \gamma = 90^\circ$
Rhombohedral	1 three-fold axis	$a = b = c$	$\alpha = \beta = \gamma \neq 90^\circ$
Tetragonal	1 four-fold axis	$a = b \neq c$	$\alpha = \beta = \gamma = 90^\circ$
Hexagonal	1 six-fold axis	$a = b \neq c$	$\alpha = \beta = 90^\circ, \gamma = 120^\circ$
Cubic	Minimum of 4 three-fold axes	$a = b = c$	$\alpha = \beta = \gamma = 90^\circ$

There are three stages of crystallisation: nucleation, growth, and cessation of growth. Nucleation is the initial step of the formation of a crystal from a solution. It normally occurs at nucleation sites on surfaces contacting the liquid.

Figure 1-5 shows the process of molecules transfer from solution to crystal. First, individual solute molecules come together at a supersaturated state and produce a stable aggregate. The aggregate must get large enough and first reach a 'critical size', which is defined by the competition of the ratio of the surface area of the aggregate to its volume.^{35, 36} Once the critical size is reached and exceeded, the aggregate becomes a critical nucleus and can grow further. If the size of the aggregate is smaller than the critical nucleus size, it would spontaneously dissolve in the solution.³⁷ This phenomenon is known as Gibbs-Thomson effect; and small free Gibbs energy change is the driven force of molecules transfer from solution to crystal.

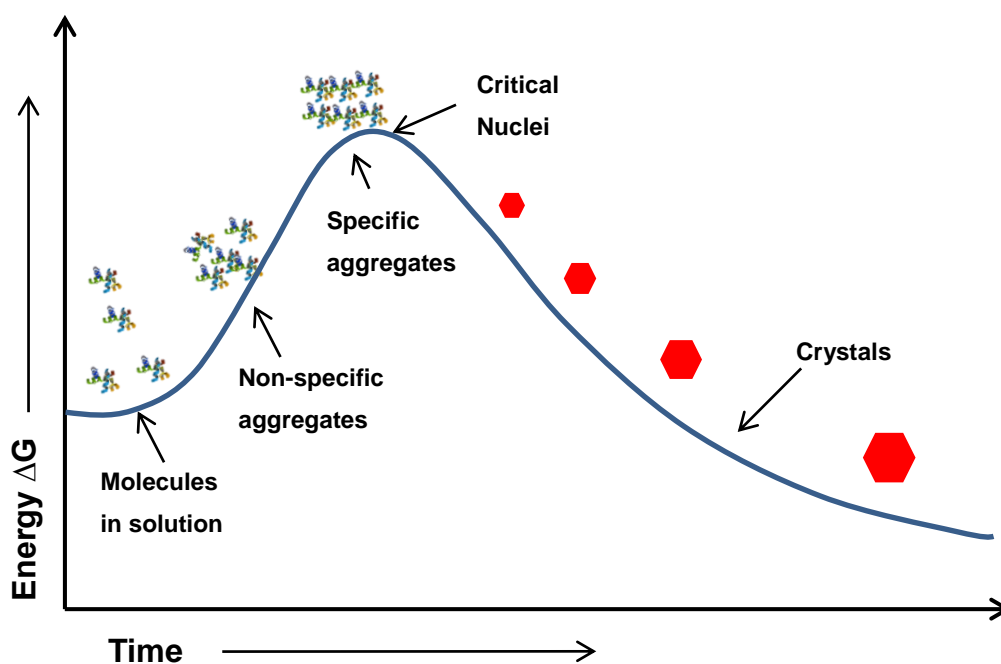


Figure 1-5. Diagram showing the transfer of molecules from solution to crystal according to Gibbs energy change.

For a spherical nucleus with radius r in the classic case:³⁸

$$\Delta G_r = (4/3) \pi r^3 \Delta G_v + 4 \pi r^2 \gamma$$

Where G_v is the Gibbs volume energy and γ is the surface energy. The graph (Figure 1-6) below shows the variation in the Gibbs free energy of nucleation with the increasing size of the radius.

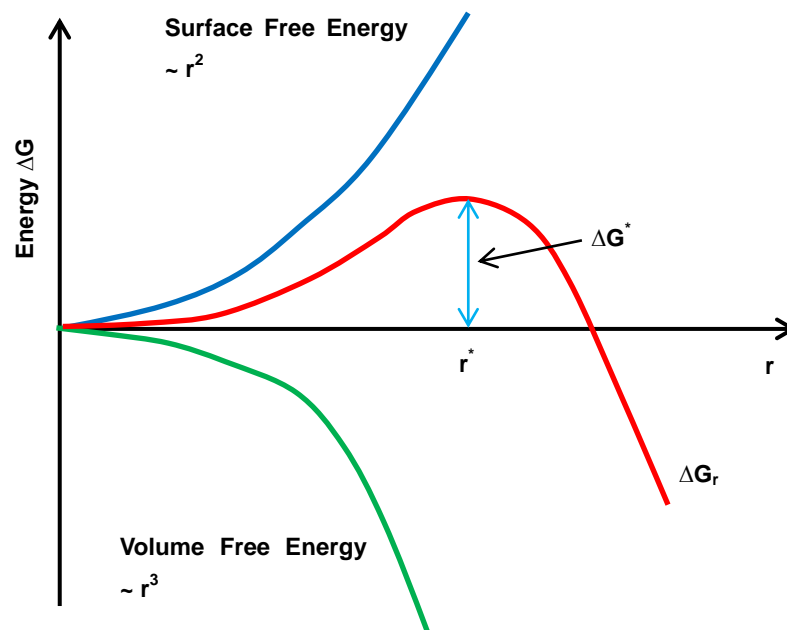


Figure 1-6. Thermodynamics of nucleation, according to Gibbs free energy.

For a spherical nucleus with a radius $r > r^*$, the Gibbs free energy will decrease if the nucleus grows. The r^* is the critical nucleus size; ΔG^* is the nucleation barrier.

Since the degree of occurrence of nucleation and crystal size are determined by the degree of supersaturation of the solution, which is in turn related to the solubility of solute molecules, to some extent by the degree of supersaturation this means that the nucleation can be controlled. The solution with a higher

solubility has many more molecules when at a supersaturated state than the solution with lower solubility, can increase the chance of collisions of diffusing molecules. This leads to an increase in a probability of the formation of stable aggregate. If the number of solute molecules was finite, in this case, it would result in the formation of many small crystals. While, at lower solute concentrations, it is not easy to form individual stable aggregate; thus this condition is much more favoring the formation of single crystals.

Once the critical nuclei are formed, then by adding more atoms, ions and molecules into the characteristic arrangement of the crystalline lattice, crystal growth stage happens. When the solution is supersaturated, nucleation and crystal growth occur simultaneously. They all are driven by the existence of supersaturation. Thus, either of them can be predominant. This means crystal size can in principle be controlled. If the nucleation is predominant over crystal growth, the system tends to produce a large number of small crystals. Otherwise, if the crystal growth is predominant, a small number of large crystals tends to result.

The growth of crystals is strongly affected by diffusion and convection effects. The concentration of solute molecules in the regions near the growing crystal is lower than the rest of the solution, leading to the formation of density gradients in the solution,³⁵ under the effects of gravity convection currents form in these zones.³⁹ These convection currents in turn dominate the diffusion rate.

Finally, crystal growth will be terminated for several reasons. The main reason

is that, as the crystallising solute concentration decreases, the solution system reaches equilibrium, or the crystal has reached a particular size and cannot grow further.⁴⁰ This may be a result of the ‘poisoning’ of the growth surface. For example, some damaged crystallising solute molecules, which are on the growth surface of crystal, could result in the interruption of the crystal lattice growth.

1.4 Protein crystals

Proteins have become particular targets for crystallisation in recent years owing to their growing importance in pharmaceutical applications. Protein crystals contain protein molecules, similar as other materials, but much larger. However, unlike other compound crystals, protein crystals are composed of about 60 %-70 % solvent content.⁴¹ The entire crystal consists of large solvent channels that solvent and other small molecules can diffuse through freely. Thus, their packing in the crystals composes of many holes that are filled with water molecules (ordered or disordered), thus, protein crystals are extremely fragile and instable.⁴² An example of protein crystal lattice structure is shown in Figure 1-7, the structure of chymotrypsinogen crystal, showing the large solvent channels penetrating the unit cell.⁴³

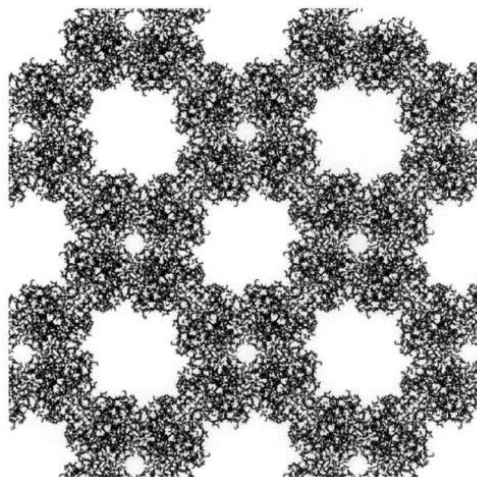


Figure 1-7. A view of the crystal structure of chymotrypsinogen. The molecular packing in the unit cell of chymotrypsinogen crystal consists of several large holes of solvent channels.⁴³

In the protein crystal, the contacts between protein molecules are quite complex, involving a delicate balance of specific and nonspecific flexible interactions,^{44,45} such as hydrogen bonds, salt bridges, electrostatic interactions, van der Waals interactions and hydrophobic interactions. All these interactions together provide for the maintenance of the crystal. In the entire crystal system, the number of these protein-protein interactions is far exceeding the number of crystalline protein molecules, this can explain the differences between protein molecules and small molecules crystals.⁴⁶

1.4.1 Some history of protein crystallisation

Protein crystallisation started at 19th century. The first reported protein crystallisation was by Hünefeld in 1840, even before X-ray was known. The

protein was hemoglobin, which was from the earthworm. Hünefeld pressed the worm's blood between two slides of glass and caused the dehydration of the protein, resulting in flat plate-like hemoglobin crystals.⁴⁷ After that, many researchers focused on studying the crystallisation of hemoglobin from various sources and tried to find a standard procedure in the next several years.^{48, 49} However, there was no general procedure for hemoglobin crystal growth, until in 1851, Fünke found and reported the successful and reproducible methods for the crystallisation of hemoglobin.⁵⁰

Following hemoglobin, other proteins such as plant seed reserve proteins were widely investigated in the last quarter of the 19th century by many researchers such as Osborne.⁵¹ The meaning of these researches for us today is that researchers developed several crystallisation approaches and now still used in common, included slow cooling, dialysis against low concentration of an ionic solution and use of organic solvents such as alcohol as precipitants.

Between 1900 and 1940, researchers started to turn their attention on enzymes, such as urease⁵² and insulin.⁵³ Crystallisation was then considered as an important tool in purifying complex proteins. After the use of X-rays for medical purposes, Laue reported the diffraction of X-rays by crystals for the first time in 1912. Then Ewald and Bragg gave birth to the field of X-ray crystallography, which considered as an important tool for structure analysis of proteins. Today, about 83 % of protein structures deposited in the Protein Data Bank (PDB) was obtained by X-ray crystallography.⁵⁴

1.4.2 Principle of protein crystallisation

In general, protein crystallisation from solution is an extremely complex process. As mentioned in section 1.3, nucleation is the vital step in the crystallisation process and has been well studied in detail.^{55, 56} The crystallisation solution must reach a supersaturation state and overcome the free energy barrier for aggregation first, and then nucleation could occur. There is a classical phase diagram of the solubility curve showing the explanation of crystal nuclei formation and growth,⁵⁷ which illustrate the change of protein molecules concentration against crystallising agent concentration (Figure 1-8).

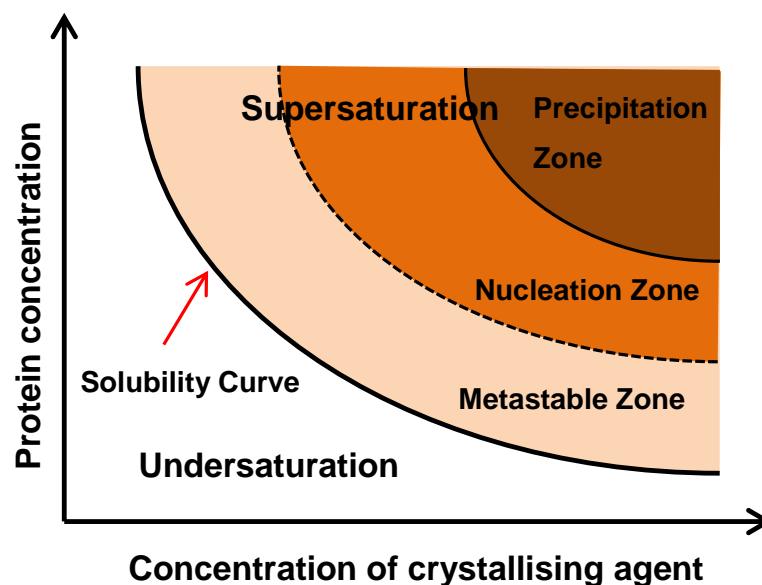


Figure 1-8. Crystallisation phase diagram of solubility curve showing how the solubility varies with the concentration of crystallising agent. The concentration area is divided by the solubility curve into two spaces: undersaturated and supersaturated zone. The supersaturated zone comprises of metastable, nucleation and precipitation zones.⁵⁷

The whole concentration space is divided by the solubility curve into two areas: the undersaturated and supersaturated zones. The area under the solubility curve is undersaturated zone, where the protein concentrations below its solubility limit. In such solution, no crystallisation will takes place. Above the solubility curve is the supersaturation zone, which comprises of three zones: metastable zone, nucleation zone and precipitation zone depending on the level of supersaturation. In the metastable zone, the supersaturation is too small; nucleation does not spontaneously occur. However, if the solution is seeded first, crystals may grow. It is therefore possible to induce nucleation in a selective and deliberate way to control the number of nuclei and the supersaturation point at which they will grow.⁵⁸ In the nucleation zone, the supersaturation is large enough, critical nuclei can form, spontaneous nucleation occurs, and crystals can grow rapidly. In the precipitation zone, the supersaturation is too large, protein aggregates rapidly precipitate from the solution.³²

1.4.3 Methods of protein crystallisation

Protein crystallisation from a solution can be affected by many factors, including biochemical factors, such as protein sample purity, storage and pI; chemical factors, such as sample concentration, precipitant type, precipitant concentration, ionic strength, environment buffer and pH; physical factors, such as temperature, time, viscosity, sample handling and methodology.^{59, 60}

Besides these most well-known factors, there are still many other factors which can in principle influence protein crystallisation, including exactly known ones or not known ones. There are no systematic studies of all these factors on protein crystallisation due to the amount of parameter space to cover.

In order to form high quality crystals, the protein must ideally 100 % pure without any contaminations. Any contamination may lead to poorer crystals, or an amorphous precipitate, or no precipitation at all. Based on the above parameters, many different methods and approaches for creating supersaturation and thus inducing the nucleation process are possible.

One method for protein crystallisation is controlling the solubility of the protein (that is, alter the supersaturation),^{59, 61} which is always very sensitive to temperature and pH as known.^{62, 63} Protein solubility is temperature dependent, due to protonation and deprotonation reaction constants of the amino acid side chains in the protein structure being temperature dependent.⁶⁴ In many cases, temperature maintains constant during crystallisation to obtain fine crystals. Most proteins are crystallised at 4 °C or 18-22 °C. Temperature also affects the kinetic energy of crystallisation, at lower temperatures the protein molecules have lower kinetic energy and can aggregate in an ordered manner more easily. Thus, many earlier proteins crystallisation were induced by slow cooling.⁶⁵ For example, glucagon crystallised by dissolving in solution and cooling from 60 °C to room temperature.⁶⁶

Another method for inducing protein crystallisation is to control the

environment pH. Most proteins tend to share the ability to form crystals and crystallise at biological pH of 6.5-7.5. Different pH can produce different packing orientations of unit cell,⁶⁷ because of that different pH can change the electrostatic character of protein macromolecules. The choice of pH is according to the optimum pH required (does not denature the protein) and also considering the isoelectric point of the protein (pI), because of solubility minimum at its pI.

Besides the control of temperature and pH, chemical precipitating agents are common used methods for achieving supersaturation of proteins and inducing crystallisation. Precipitating agents for protein crystallisation are generally divided into three main categories: salts, such as ammonium sulfate; organic solvents, such as ethanol; and large polymer precipitating agents.⁶⁸

Moreover, various physical techniques have been developed for reaching supersaturation thus inducing protein crystallisation. Among them, three main methods are commonly used: batch and micro-batch; dialysis; and vapour diffusion.

Batch method is a simple and old crystallisation technique. In this method, by mixing the concentrated protein with concentrated precipitating agent, the solution immediately reaches a high supersaturated state and therefore, crystallisation is induced. This method usually needs large volumes of solutions (upward of 1 mL), and typically results in larger crystals. Chayen designed micro-batch method (1992)⁶⁹ as shown in Figure 1-9 and stated an

approach of rapid protein crystallisation by using very small sample droplets as little as 1 μl into an inert oil. The oil can prevent the evaporation of solvent.

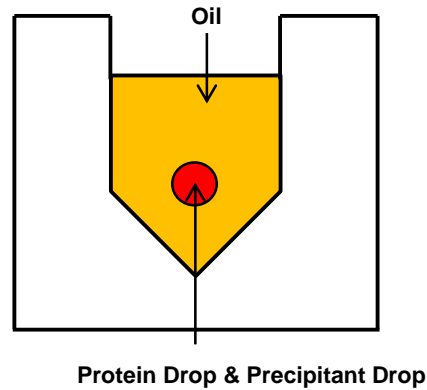


Figure 1-9. Micro-batch crystallisation technique.

There are some disadvantages by using micro-batch method. First, if the precipitant concentration which chosen isn't high enough to obtain supersaturation, crystallisation will never occurs. Furthermore, it is very difficult to manipulate of the crystals from the droplet covered by the oil.

Contrary to batch method, in dialysis method, the solution composition is changed by diffusion of small molecules. In a dialysis crystallisation experiment, the protein solution is contained in a dialysis semipermeable membrane, surrounded by a large volume of precipitant solution. For example, in button dialysis crystallisation (Figure 1-10), a dialysis membrane covers the dialysis button, which allowing the diffusion of solvent into the protein solution through the dialysis membrane. The solute molecules in the protein solution slowly equilibrate against the large volume of precipitant solution, leading to protein crystallisation within the dialysis button.

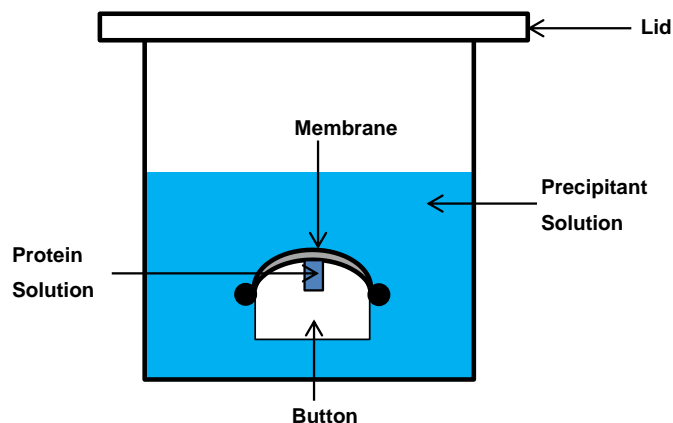


Figure 1-10. Button dialysis crystallisation technique.

However, dialysis method does not work with some precipitant solutions, such as concentrated PEG solutions. Because PEG solutions prefer to draw all the water out of the button faster than dialysis occurs, thus, protein will precipitate rapidly rather than crystallise.

The most popular technique is vapour diffusion method. By using this method, we can screen a large number of crystallisation conditions by varying the composition of each well solution. In the vapour diffusion method, protein solutions achieve supersaturation by the evaporation and diffusion of water between solutions with different concentrations slowly. The technique used during this research was the vapour diffusion method. There are three kinds of vapour diffusion methods: hanging drop, sandwich drop and sitting drop (Figure 1-11).

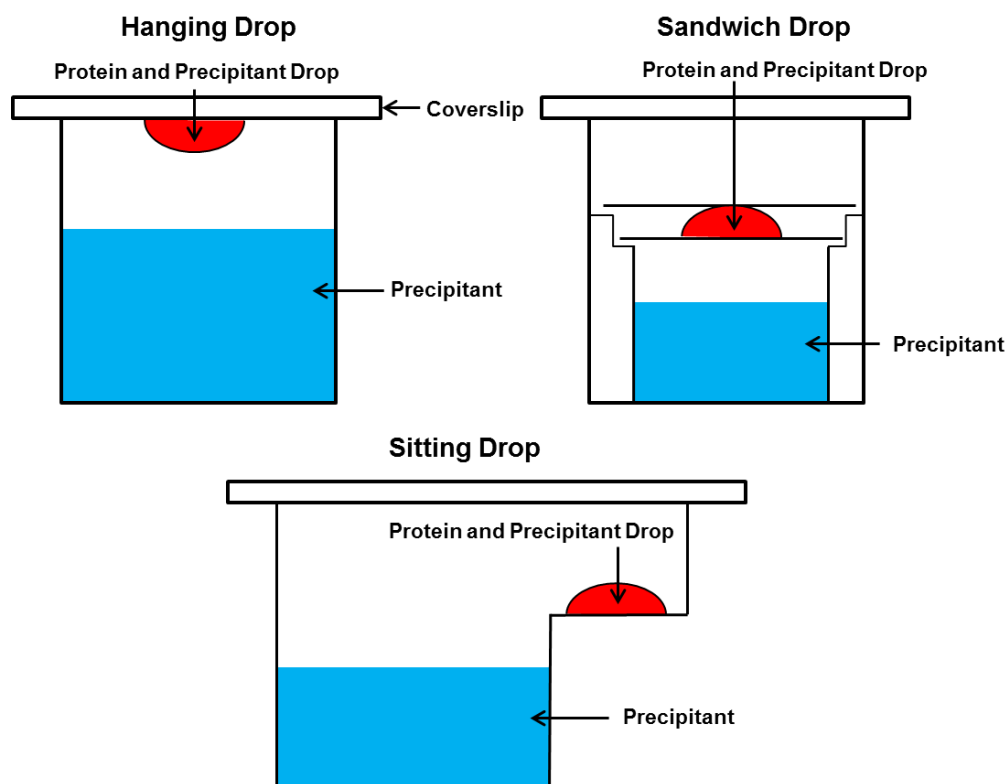


Figure 1-11. Vapour diffusion techniques: hanging drop, sandwich drop and sitting drop.

A drop of 1:1 protein: precipitant solution is normally used in the sample well in the crystallisation experiment. In the hanging drop method, the protein and precipitant solution droplet is suspended from a coverslip. The volume of the droplet is limited; otherwise, it will fall down. In the sandwich drop method, protein and precipitant solution droplet is in contact with both an upper and a lower surface. This method is rarely used due to the two coverslips will reduce the exposure area of the droplet and slow down the rate of water evaporation. In the sitting drop method, protein and precipitant solution droplet is supported by a surface. It is easy to conduct and require very small amount of sample. Using this method, crystallisation takes place when the concentrations of

protein and precipitant increase in the droplet by water vapor from the droplet to the reservoir solution. This process will last until the concentration of precipitant in the droplet equals that of the reservoir solution.

1.5 Use of additives in protein crystallisation

A variety of approaches have been used to aid the production of protein crystals; the most common strategy involves the addition of nucleants, typically surfaces or surface-active materials into the crystallisation solution.⁷⁰

Solution ‘additives’ of many types have proven useful in the control of protein crystallisation.⁷¹ These additives can act via multiple mechanisms,⁷² i.e. they can serve to bridge protein segments, electrostatically, or via hydrogen bonding or hydrophobic interactions.^{5, 72, 73} It is also possible for additives to diminish interactions between protein macromolecules and solvent^{73, 74, 75} to act as solubility-modifying detergents;⁷⁶ or to stabilise intermediate structures/conformations of proteins during the early stages of crystallisation.^{75,}

^{77, 78} There are two principal types of additives, including soluble materials, which added into the crystallisation solution directly, such as precipitants; and non-dissolved solid surfaces, which act as heterogeneous nucleants.

1.5.1 Non polymer methods

1.5.1.1 Salts

Salts act as precipitating agents, according to the ‘salting out’ principle.⁷⁹ The

ionic strength of the solution increases by adding salts, which in turn leads to a decrease in protein solubility. A simple explanation of the salting out effect is that salt ions, principally anions, compete with protein for solvent molecules, i.e. water, thus, salts can dehydrate the protein macromolecules.⁸⁰ When the concentration of salts is sufficiently high and the competition is intense enough, protein molecules are forced to neutralise their surface charges by interacting with one another and then precipitate from the solution, which may result in an ordered arrangement of proteins in the crystalline form. Figure 1-12 shows the typical protein solubility behavior over the entire range of salt concentrations, including ‘salting in’ and ‘salting out’ regions.⁴⁶

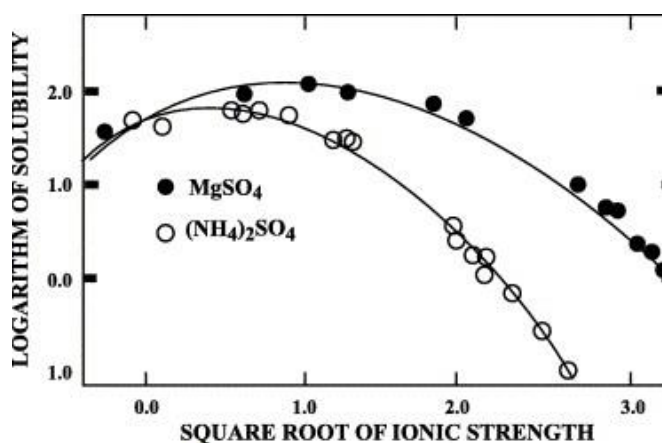


Figure 1-12. The solubility curves of a typical protein, enolase, as a function of ionic strength produced by two types of salts.⁴⁶ The regions of the curves with lower ionic strength where the solubility increases are called ‘salting in’ region; the regions of the curves with higher ionic strength where the solubility decreases are called the ‘salting out’ region.

The ‘Hofmeister series’ shows the order of salting out effect of the ions,⁸¹

$\text{SO}_4^{2-} > \text{HPO}_4^{2-} > \text{CH}_3\text{COO}^- > \text{citrate}^{3-} > \text{tartrate}^{2-} > \text{HCO}_3^- > \text{CrCO}_3^{3-} > \text{Cl}^- > \text{NO}_3^- > \text{ClO}_3^-$ for anionic proteins, while cationic ones are reverse.^{63, 82} The salts commonly used in protein crystallisation involve ammonium or sodium sulfate, ammonium or sodium acetate, sodium or potassium phosphate, sodium or ammonium citrate and sodium chloride.^{59, 60}

1.5.1.2 Organic solvents

Organic solvents can also promote protein crystallisation by a similar competition with protein for water molecules. They can bind to water molecules and alter the interaction between water and protein molecules by H-bonding, thus leading to solvent competition and forcing protein molecules out of the solution. Besides, they may also have ‘excluded volume effects’ by hydrophobic exclusion of protein solutes. Furthermore, they can reduce the dielectric constant of the medium. Coulomb interactions between the individual protein molecules become stronger. Thus, they decrease the capacity of protein molecules and force them out of the solution.^{83, 84} Organic solvents should be added very slowly to mix thoroughly and used at very low temperature or below 0 °C to avoid volatilization.⁵ The common organic solvents are ethanol, acetone and dioxane.⁸⁵

1.5.1.3 Insoluble surfaces

Crystallisation controlled by insoluble solid surfaces is an approach to template

protein crystal growth via heterogeneous nucleation. A number of insoluble solid additives has been studied in protein crystallisation, such as minerals,^{86,87,88} human hair,⁸⁹ hydrophobic self-assembled monolayers,⁹⁰ porous glass and silicon,^{91, 92} silicon-based devices,⁹³ and chemically treated substrate surfaces, i.e. glass⁹⁴ and mica.⁹⁵

Figure 1-13 is an example shows heterogeneous nucleation facilitated by the insoluble solid surface. First, the heterogeneous nucleant attracts and immobilises protein molecules on to its surface through some chemical, electrostatical or structural favor interactions to form protein aggregates. Then these protein aggregates start to form ordered nuclei by adopting a consistent orientation, and are capable of further growth.⁵

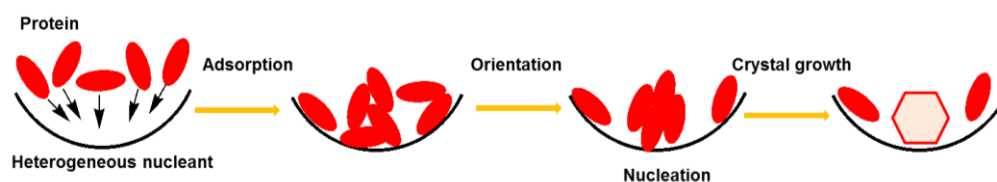


Figure 1-13. Schematic representation of heterogeneous nucleation facilitate by the insoluble solid surface.

The mechanisms by which these insoluble solid surfaces induce heterogeneous nucleation are various. They potentially include: some materials with similar lattice characteristics with protein crystalline lattice that may affect protein crystallisation process,⁸⁷ utilisation of the surface microstructure,^{92, 96} i.e. roughness to promote protein nucleation, or use of surface chemistry properties to afford some specific interactions with protein molecules.⁹⁵

One example of insoluble solid additives is mineral. For instance, McPherson *et al.* tested fifty different mineral samples as heterogeneous nucleants to mediate crystallisation of four common proteins: canavalin, concanavalin B, beef liver catalase and hen egg lysozyme.⁸⁷ Some example images of protein crystals are shown in Figure 1-14. They stated that, by the use of mineral surfaces, nucleation of canavalin and beef liver catalase was promoted at lower critical supersaturation levels, and the crystal habit of each of four proteins was modified. Moreover, the mineral apophyllite with a close lattice match to lysozyme, had a clear influence on the nucleation and crystal growth of protein crystal, which could illustrate the possible mechanism involved a direct lattice match.⁸⁷

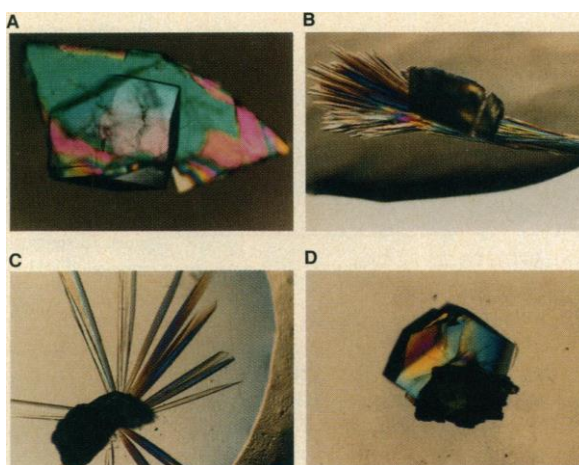


Figure 1-14. Some example images of protein crystals the nucleated and grew on the mineral substrate surfaces.⁸⁷ A and D: Lysozyme crystals on lepidolite and magnetite. B and C: Concanavalin B crystals on gypsum and aragonite.

Another example of insoluble solid additives for enhancing the nucleation of protein crystals is porous substrate, i.e. glass and silicon.^{58, 91, 96} For example,

Chayen *et al.* used porous silicon, which composed of nanoscale crystalline silicon wires and dots surrounded by voids, to enhance nucleation and crystallisation of proteins.⁹² The mechanism they proposed involved local supersaturation of protein molecules associated with the fractality of the porous substrate. The local concentration of protein molecules, which were inside and in the close vicinity of the pores was sufficient for aggregation and possibly induced nucleation (Figure 1-15).

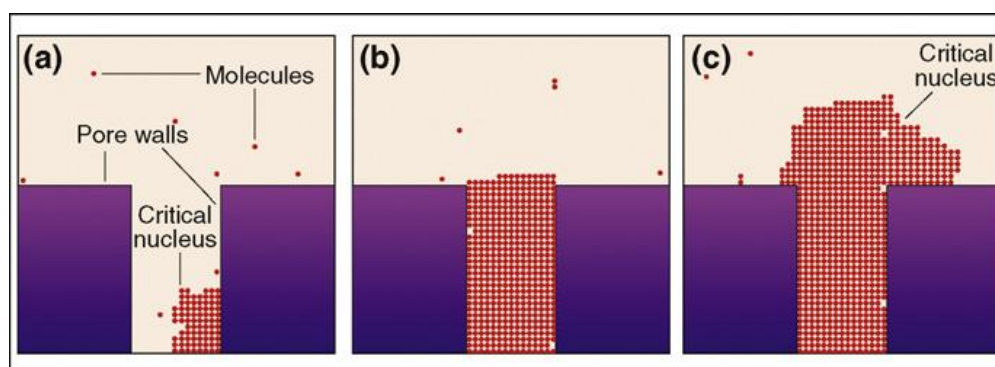


Figure 1-15. Schematic representation of crystal nucleation in a pore, which explains the mechanism of porous substrates induce protein crystallisation.⁹⁷ (a) Protein molecules reside in the corner of the pore and start to aggregate until a critical nucleus forms. (b) The crystal keeps on growing until the entire pore is full of protein molecules. (c) In the close vicinity of the pore, another critical nucleus is then formed, thus protein crystal can breakout from the pore.

Chemically treated substrate surfaces are another type of commonly used insoluble solid additives for facilitating protein crystallisation. For instance, Ripamonti *et al.* prepared chemically modified mica sheets by mixed mica with n-propyltriethoxysilane and 3-aminopropyltriethoxysilane in different ratios to

vary the density of ionisable groups on the mica surfaces; and then tested them as heterogeneous nucleant surfaces for protein crystallisation.⁹⁵ They suggested a possible mechanism may involve that the chemically treated mica sheet surfaces could afford some interactions between the ionisable groups on the mica surfaces and charged residues of the protein, which may facilitate the aggregation and nucleation of protein molecules.

1.5.2 Polymer additives

Although the above additives have effectiveness on enhancing protein crystallisation, however, they still have some disadvantages. For example, some of them require high concentration, meaning that their affinity is low,⁷⁰ such as salts and organic solvents. They must interact with a large number of water molecules to alter the free energy of protein molecules. For non-polymeric insoluble solid surfaces, they are random substances, have no designed specificity for proteins. Moreover, it is not easy to apply a systematic range of non-polymeric insoluble solid surfaces for screening experiments to find an optimized crystallisation condition that would have otherwise been missed.⁹⁸ None of them has been proven as ‘universal’ heteronucleants to enhance the crystallisation for the majority of proteins.⁹⁹

Synthetic polymers are important additives for protein crystallisation control as there are many possible chemistries which can be introduced into the backbone and side-chains, giving a very wide range of functional behaviour.^{5, 100, 101}

Polymers have also been successfully applied as additives in mediating crystallisation of inorganic materials,¹⁰² organic molecules,^{101, 103, 104, 105} as well as some key drugs such as paracetamol.^{106, 107} Proteins^{35, 108} and nucleic acids¹⁰⁹ have become particular targets for polymer-mediated crystallisation in recent years owing to their growing importance in pharmaceutical applications. Polymers provide an ideal approach to control and investigate the majority of protein crystallisations in a reproducible and universal manner; including finding the optimal crystallisation conditions by a systematic screening experiment of altering the chemical characteristics and functionalities. Fundamentally, there are two types of polymers to be distinguished, insoluble polymer surfaces and soluble polymer additives.

1.5.2.1 Insoluble polymer surfaces

Protein crystallisation control by insoluble polymer additives is an approach by which the insoluble polymer surfaces serve as templates, scaffolds or heterogeneous nucleants to promote protein nucleation or template selective polymorphs of protein crystals.^{71, 100}

One application of insoluble polymer surfaces is the use of molecularly imprinted polymers (MIPs) as surfaces for the selective nucleation of crystals via heterogeneous nucleation. Molecular imprinting is a technique by which selective recognition sites can be constructed in polymer matrices, and then used for molecular recognition of memorable template molecules.^{110, 111}

Molecularly imprinted polymers are prepared via molecular imprinting technique. They are formed in the presence of the template molecule, which will be extracted afterwards, resulting in complementary cavities in the polymer with high affinity for the templating species.^{112, 113, 114} Vulfson *et al.* reported that polymers, when imprinted with inorganic material, calcite, were able to induce the nucleation of calcite under conditions favouring the growth of aragonite (Figure 1-16).¹¹⁵ Followed the same principle of MIPs employed in the crystallisation of inorganic small molecules, MIPs was also studied in protein crystallisation. Takeuchi *et al.* demonstrated the effectiveness of different protein-imprinted polymer arrays with acidic or basic functional monomers to classify five tested proteins. They concluded that protein-imprinted polymers could offer a new approach to characterise and profile various proteins in nature.¹¹⁶ Furthermore, Chayen *et al.* found that some MIPs induced crystallisation of proteins and yielded crystals in the conditions that didn't afford crystals otherwise. Moreover, MIPs acted as heterogeneous nucleants and could facilitate the formation of protein crystals in the metastable zone of the crystallisation phase diagram, which would otherwise been missed.¹¹⁴

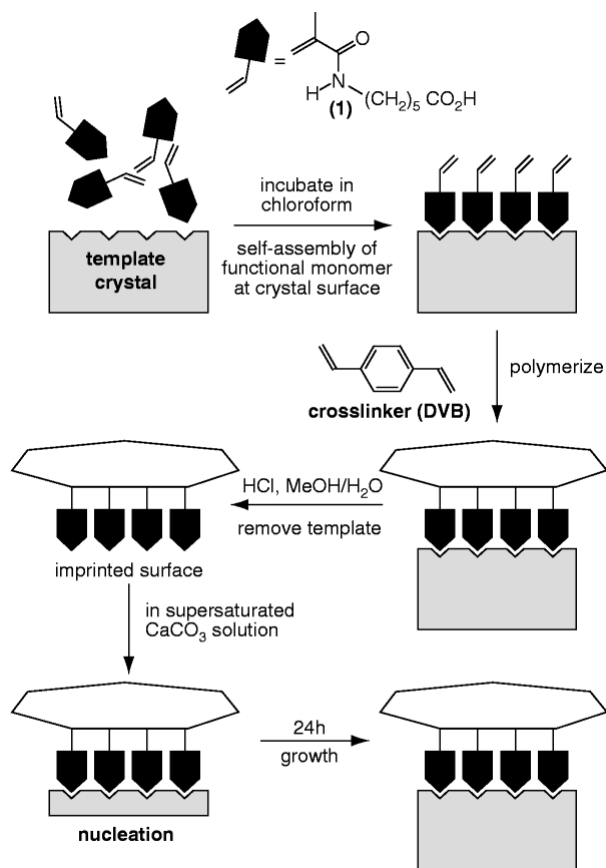


Figure 1-16. Schematic representation of the molecular imprinting process and selective crystallisation of calcium carbonate. Functional monomers adsorbed to a calcite crystal surface, followed by cross-linking to convert monomer self-assemblies into a polymer matrix. Template calcite crystal was removed by washing with acidified aqueous methanol solution to produce imprinted polymer surfaces. Thus, the imprinted polymer surfaces can be used to template selective polymorphs of calcium carbonate crystal.¹¹⁵

In a separate but related approach, a range of insoluble polymer surface libraries has been used to facilitate proteins crystallisation via heterogeneous nucleation. For example, Matzger *et al.* reported a heteronucleant approach by applying polymers as heteronucleant surfaces to achieve functional diversity

and flexibility of crystallisation formats. They applied functionally diverse polymer libraries, such as commercially available polymers and cross-linked copolymers for hen egg-white lysozyme, concanavalin A and bovine liver catalase crystallisation and concluded that the insoluble polymer surface libraries can be successfully applied, such as allowing nucleation rate control of lysozyme, improved lysozyme crystal size, new form access of concanavalin A and formation of high quality bovine liver catalase crystal.⁹⁹

All the above mentioned previous work shows that the use of polymers as solid surfaces is an important and successful approach to mediate protein crystallisation via heterogeneous nucleation. Currently, there is a lack of surface characterisation on polymer surfaces. Moreover, by using this method, there is a great need for the clear understanding of the mechanisms of how these polymers work.

1.5.2.2 Soluble polymer additives

Soluble polymer additives have attracted interest from researchers in polymer-mediated protein crystallisation. Compared to insoluble polymer surfaces that act as templates or heterogeneous nucleants, soluble polymeric additives can influence the biomolecule crystallisation process leading to changes in size, habit and even polymorph of the final crystals.⁷¹ The mechanisms by which polymers act include complexation of electrolytes, thus changing the local ionic strength;⁷¹ the masking or neutralizing of charges on

proteins, which in turn enhances the role of hydrophobic association between protein chains,^{117, 118} or via hydrogen bonding or hydrophobic interactions to diminish the interactions between protein macromolecules and the solvent,^{5,72,73} or by simple viscosity modification which changes the kinetics of crystal growth. Polymeric additives can also stabilise transient protein-protein aggregates by adsorption on their surfaces, leading to faster nucleation and altered crystalline polymorph,^{78, 119, 120} or through attachment to specific crystal faces which then influences the direction of further crystal growth.¹⁰⁰

Cölfen *et al.* used a variety of polymers, such as glycopolymers, low-molar-mass polymers and block copolymers to investigate additives controlled mineral crystallisation, such as barium and calcium carbonate. Compared to insoluble polymer surfaces, different types of soluble polymer additives with diverse functional groups can have big influences on crystallisation of minerals, even can alter the final crystal morphology.^{71,100,121,122}

Crystallisation of proteins would follow the same general principle as that of small molecules.^{109, 123} Some polymers have been studied as additives i.e. nucleants/precipitants for protein crystallisation. They have been pioneered by Polson and co-workers. They used many polymers, such as polyethylene glycol (PEG), dextran, polyvinyl alcohol and polyvinyl pyrrolidone, as precipitants for protein fractionation. They proposed that, among the polymers they had used, PEG 6,000 was appeared to be the most suitable protein precipitant

because its low viscosity, stability and because it did not denature the proteins at room temperature.¹²⁴

Inspired by Polson's results, McPherson *et al.* applied different sizes of PEG: 400, 1,000, 4,000, 6,000 and 20,000 to mediate 22 proteins, such as gene, α -amylase, a protein of unknown function from turkey liver, catalase, abrin, ovalbumin, canavalin and horse albumin. They reported that six proteins were crystallised for the first time by screening of five different molecular weight sizes of PEG; one protein: α -amylase easily afforded crystals when PEG was employed; one other protein that of unknown function from turkey liver yielded excellent quality crystals whereas only poor-quality crystals have been obtained previously. Moreover, they found that the PEGs were active in helping to crystallise a wide range of proteins and exhibited greater applicability than other previously used reagents.¹²⁵ PEG remains in widespread use to aid protein crystallisation because it is stable, neutral, hydrophilic and its solutions are of low viscosity compared to other polymers.^{124, 125}

Based on the previous studies, McPherson *et al.* also screened and assessed various chemicals mixed with PEG 3,350 acting as mixed additives on 81 different proteins. They stated that mixed additives, which composed of polyvalent, charged groups, i.e. di and tri carboxylic acids, diamino compounds, or bearing one or more sulfonyl or phosphate groups were the most promising types of additives to affect protein crystallisation.⁷² They proposed a novel

approach to crystallise proteins by combination of small molecules with simple polymer additives.

More recently, Yao *et al.* used some functional polymers, such as poly(PEGMA), PDMAEMA and some block copolymers to control of lysozyme crystallisation. They showed that only poly(PEGMA) mixed with lysozyme solution could not afford any lysozyme crystals, but PDMAEMA and some block copolymers, which contained high content of the PDMAEMA, such as PDMAEMA-*b*-poly(PEGMA-OH) and PDMAEMA-*b*-PBMA-*b*-poly(PEGMA), had a clear influence on the crystallisation of lysozyme and were able to modulate the shape of crystals but depending on their concentration in protein solution.¹⁰⁸

However, because there are so many factors which can affect crystallisation processes from solution, many of which are still poorly understood, to date only a limited number of polymer additives have been successfully applied in proteins crystallisation, most are PEGs and PEG derivatives. In addition, some of the previous work did not show clear crystal packing information.¹⁰⁸

Moreover, most of the studies are descriptive; the interactions between some of the existing polymer additives and protein macromolecules or surrounding solvent are still unclear, and the mechanisms by which protein crystals form in the presence of these polymers needs to be further investigated.^{100, 108}

1.6 Polymers and polymer synthesis

Polymers are macromolecules, which are composed of a large number of small molecules combined with each other in a repeating order. These small molecules are so called monomers, and the reactions by which they link together are so called polymerisations. There may be hundreds, thousands, tens of thousands, or more monomer molecules in a polymer molecule. There are two common laboratory synthetic methods used to make polymers: stepwise and chain polymerisation.¹²⁶

The first polymerisation method is stepwise polymerisation, which sometimes classified as 'condensation polymerisation'. It is defined that monomers all combine together, thus the molecular weight increases slowly by losing small molecules, such as water. With this method, the molecular weight of polymer increases at a very slow rate at lower conversions, and only at very high conversion (i.e., > 95 %) can reach relatively high molecular weight. Step growth polymerisation is always used to yield branched and networked polymers.¹²⁷

The second one is chain growth polymerisation. It is generally following three steps: chain initiation, chain propagation and termination of the active chain ends. There are several types of synthesis depending on the active site (Table 1-2).

Table 1-2. Types of chain growth polymerisation

Active sites	Synthesis type
Carbanion	Anionic polymerisation
Carbenium ion	Cationic polymerisation
Free radical	Free radical polymerisation

The initiation of anionic polymerisation is usually by strong anions. Theoretically, there is no formal termination for anionic polymerisation method, because of that proton transfer from the solvent or other positive materials rarely take place. The initiation of cationic polymerisation is by strong protic acid. However, this method is extreme sensitive to the reaction conditions, such as solvent types, solvent purity and temperature. Among the above chain growth polymerisations, the most significant method is free radical polymerisation. Atom transfer radical polymerisation (ATRP) and reversible addition-fragmentation chain transfer polymerisation (RAFT) are the most extensively studied synthetic methods.

1.6.1 Atom transfer radical polymerisation (ATRP)

ATRP was first reported by Wang and Matyjaszewski in 1994,¹²⁸ which is one of the most commonly used methods of controlled radical polymerisation. It provides a simple route to many well-defined functional polymers with controlled molecular weight and narrow molecular weight distribution.^{129, 130} A general ATRP reaction usually comprises of a transition metal and ligand based catalyst and alkyl halides act as the initiator.¹²⁹

The ATRP polymerisation as shown in Figure 1-17 starts with the homolytic cleavage of the carbon-halogen bond of the initiator R-X, resulting in a single electron i.e. free radical at the carbon center (R•) and a halogen radical (X•). The halogen radical can bind to metal to change its oxidation state¹³¹ (Figure 1-17A). This process is reversible; the halogen can reunite with the initiator to make it inactive again (Figure 1-17B). Thus, the initiator is only active for a short time before becoming dormant.¹³² When the initiator is active, it can consume monomers and propagate (Figure 1-17C).

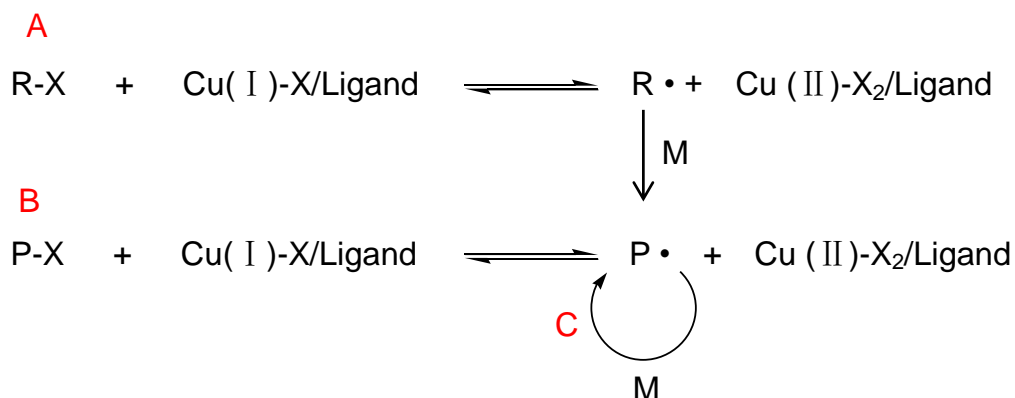


Figure 1-17. General scheme of an ATRP reaction. A: Initiation; B: Dormant species in ATRP; C: Propagation. M represents monomer; P represents a polymer with a number of monomer units.

Several parameters can affect an ATRP reaction. The initiator can affect the initiating efficiency. The faster the initiation, the slower termination and the faster propagation, more monomers are combined together to form a polymer with a narrow molecular weight distribution.¹³³ The catalyst is a very important parameter in an ATRP reaction, because it determines the equilibrium constant

between active and deactivated species. The catalyst system usually contains a transition metal and a ligand. The most commonly studied transition metal in an ATRP reaction is copper, due to its low cost and readily accessible redox character. The ligand must have strong complexation with copper¹³⁴ and can stabilise Cu (II) compared to Cu (I). Besides, the choice of monomers is also very crucial. Monomers that are typically used in ATRP involve various vinyl polymers, which can stabilise the propagating radicals,¹³⁵ such as styrene,^{136, 137} methacrylate,^{137, 138} 2-(dimethylamino)ethyl methacrylate¹³⁹ and acrylonitrile.¹⁴⁰ In addition to initiator, catalyst, ligand and monomer, solvent and temperature can influence the kinetics of ATRP as well.¹³⁵

A wide range of polymers has been created with controlled functionalities and compositions via functionalised initiators.^{141, 142} This approach has been used for the synthesis of methacrylate monomers showing fast ATRP kinetics with low polydispersities by using Cu (I) Br/2,2-bipyridine catalytic system.¹⁴³

Polymers synthesised with ATRP in this project include poly(ethyleneglycol)methyl ether-methacrylate [p(PEGMA₄₇₅)], poly[2-(dimethylamino)ethyl methacrylate] [p(DMAEMA)] and a random copolymer of PEGMA₄₇₅ & DMAEMA (Figure 1-18). From previous researchers' studies, PEG has been found to be an effective additive in promoting the crystallisation of a range of proteins. However, PEG itself has limited chemical functionality, and cannot be derivatised easily to introduce groups which can form specific bonds with protein peptide residues. We thus

dithioesters as the RAFT agents to mediate the polymerisation via a reversible chain-transfer process (Figure 1-19).

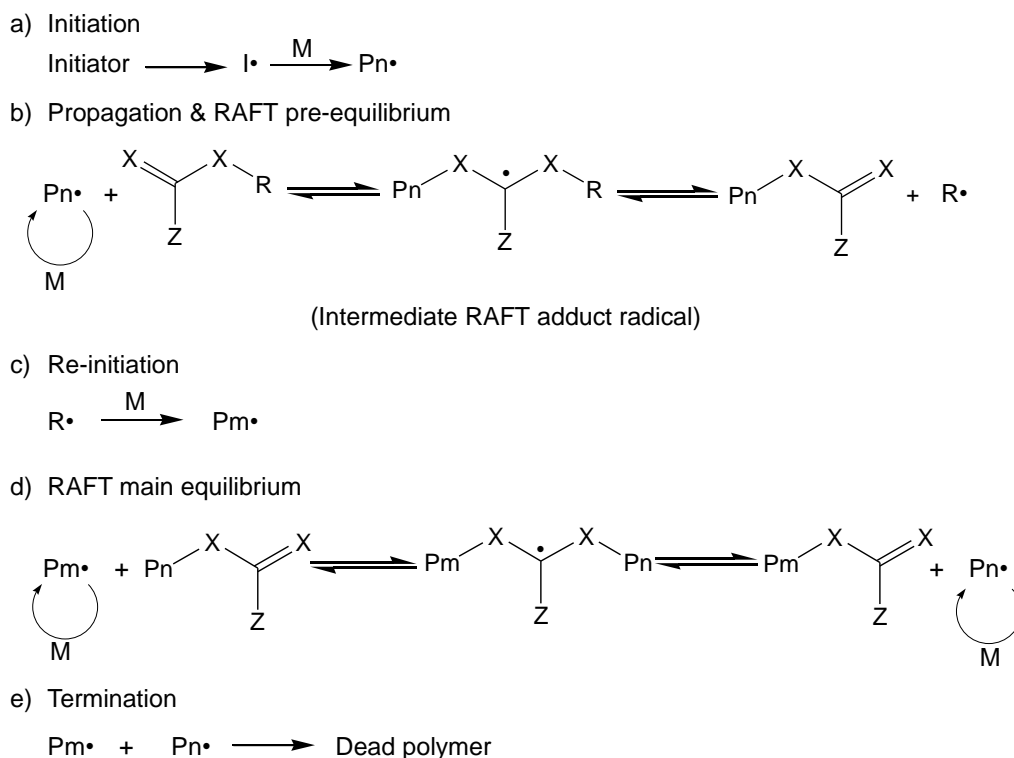


Figure 1-19. Mechanism of an ideal RAFT polymerisation.¹⁴⁷ $\text{Pn}\cdot$ represents a polymeric radical with n monomer units; $\text{Pm}\cdot$ represents a polymeric radical with m monomer units; X normally represents sulfur; the Z group primarily affects the stability and activity of the S=C bond.¹⁴⁵

In an ideal RAFT reaction, initiation is started by an initiator, which decomposes to form two free radicals ($\text{I}\cdot$), these then react with monomer (M) to obtain a chain growth polymeric free radical ($\text{Pn}\cdot$) (Figure 1-19a). Then the chain growth polymeric free radical ($\text{Pn}\cdot$) starts to propagate and reacts with the RAFT agent, to form an intermediate RAFT adduct radical. There is a RAFT pre-equilibrium here between the intermediate RAFT adduct radical and

a polymeric RAFT agent & a leaving group radical ($R\bullet$) (Figure 1-19b). This leaving group radical ($R\bullet$) then reacts with the monomer to form another chain growth polymeric free radical ($Pm\bullet$) (Figure 1-19c). Group R must be a good leaving group and able to react with monomer to aid the fragmentation process. Then the main RAFT equilibrium process takes place, in which all chain growth polymeric free radicals share the radical among them, leading to chain growth (Figure 1-19d).¹⁴⁷ It is very essential that the radicals are shared equally, thus, all the chains have the equal opportunities to propagate, and maintain well defined polymer characteristics. The termination of RAFT polymerisation involves a process called bi-radical termination to form dead polymers (Figure 1-19e).

In comparison to ATRP, a larger variety of monomers can be synthesised via RAFT polymerisation,¹⁴⁸ especially water-soluble polymers,¹⁴⁹ such as vinyl aromatics, acrylates, acrylamides, acrylonitrile, vinyl acetate and vinyl amides.^{150, 151} Polymers synthesised via RAFT in this project include poly[N-(3-(dimethylamido)propyl) methacrylamide] [p(DMAPMAm)], poly(2-acrylamido-2-methyl-1-propanesulfonic acid) [p(AMPS)], poly(2-acrylamidoacetic acid) [p(2-AmAA)] and poly(4-acrylamidobutanoic acid) [p(4-AmBA)]. Similar as DMAEMA, a methacrylamide monomer: DMAPMAm, which has tertiary amines groups, was selected to afford positive charges and form another type of cationic polymer. For the choice of anionic polymers, they were chosen according to the pKa of the polymers, and also

considering the protein crystallisation pH, at which the polymers could provide charged residues. Three acrylamide monomers, including AMPS, 2-AmAA and 4-AmBA, which have ionisable sulfonic acid or carboxyl groups were homopolymerised to generate anionic water soluble homopolymers in this project (Figure 1-20).

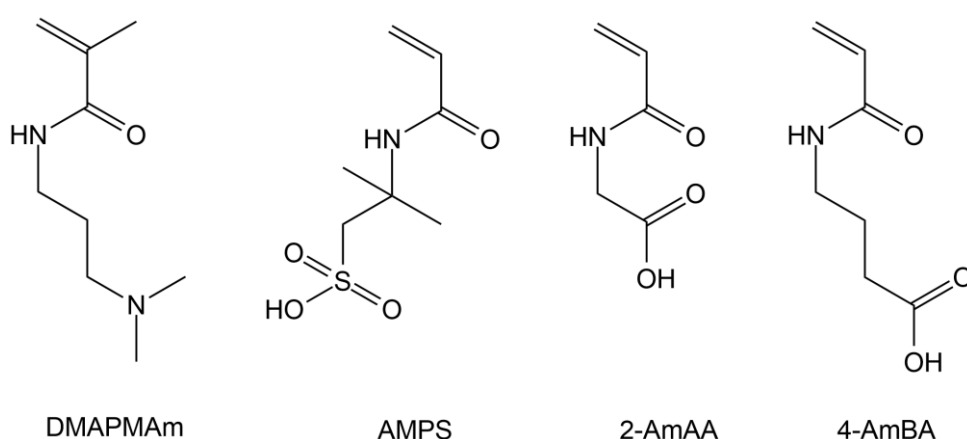


Figure 1-20. Structures of DMAPMAm, AMPS, 2-AmAA and 4-AmBA monomers.

1.7 Protein targets

Hen egg-white lysozyme (HEWL), concanavalin A (Con A) and bovine liver catalase (BLC) were the protein targets used for crystallisation during this research, because of their range of size and charge. The isoelectric point (pI) of HEWL is 11.35, when at its crystallisation pH 4.8, HEWL macromolecules are positively charged, i.e. cationic.¹⁵² The isoelectric point (pI) of Con A is 4.5,¹⁵³ when at crystallisation pH 8.5, Con A macromolecules are anionic. The isoelectric point (pI) of BLC is 5.4,¹⁵⁴ and when at crystallisation pH of 6.8, BLC macromolecules may carry some negative charges, hence being a weekly

anionic protein at this pH.

1.7.1 Hen egg-white lysozyme (HEWL)

Lysozyme is a single chain enzyme and 129 amino acid in length¹⁵⁵ (E.C. 3.2.1.17). It has a molecular weight (Mw) of 14.3 kDa, pI of 11.35, four disulphide bridges, formed by α -helices, and was discovered in 1922 by Fleming.^{156, 157} It is present in tears, saliva, mucus and the egg-white of chickens. Lysozyme protects the body from bacterial infection as a natural antibiotic. It can attack the cell wall of the bacteria by catalysing the hydrolytic cleavage of polysaccharides in the cell walls, leading to bacterial lysis.¹⁵⁸

HEWL has five structurally characterised crystal forms: monoclinic, triclinic, hexagonal, orthorhombic and tetragonal.¹⁵⁹ It has been the most studied crystallisation system for the last 60 years. Alderton and Fevold first reported tetragonal HEWL crystals in 1946.¹⁶⁰ Phillips and Johnson first applied X-ray crystallography to elucidate the three-dimensional structure of HEWL in 1965.^{161, 162} So far there are about 750 lysozyme crystallographic structures which have been obtained and are available in the PDB (Berman *et al.*, 2000). A model of the three-dimensional structure of HEWL is presented in Figure 1-21.

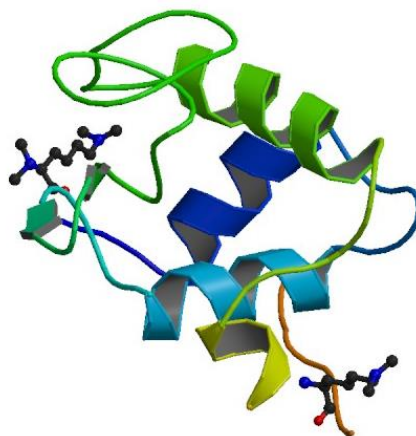


Figure 1-21. The three-dimensional structure of HEWL obtained by crystal X-ray diffraction, at a resolution of 1.8 Å and a crystallographic R factor of 17.3 %. This polymorph is the orthorhombic $P2_12_12_1$, with unit cell dimensions of $a = 30.6$ Å, $b = 56.3$ Å, $c = 73.2$ Å, and one molecule per asymmetric unit. Structure includes Mg^{2+} and SO_4^{2-} ions.¹⁶³

As mentioned in section 1.5.2, Matzger *et al.* applied a series of insoluble polymer surfaces to influence lysozyme crystallisation. They reported that HEWL crystallisation under conditions favouring the tetragonal form resulted in exclusively tetragonal crystals, but the insoluble polymer surfaces could successfully control lysozyme nucleation rate and improve lysozyme crystal size.^{159,99} Moreover, Yao *et al.* used some soluble polymer additives to control lysozyme crystallisation via tetragonal crystal growth as well and stated that some polymers were able to modulate the shape of crystals.¹⁰⁸ With this in mind, we chose HEWL as the first protein target. The main reason for the use of HEWL in this research is that it has become the most preferred crystallisation system for the majority of protein crystallisation studies. This is

because the fact that it is easily purified for commercial use, low cost and widespread. Moreover, from the literature HEWL is relatively straightforward to crystallise in a specific polymorph (the tetragonal form) within one day with little effort.

1.7.2 Concanavalin A (Con A)

Concanavalin A (Con A) is a lectin (carbohydrate-binding protein), which is extracted from the jack-bean. It binds to certain structures that are found in various sugars, glycoproteins, and glycolipids specifically.¹⁶⁴ Like most lectins, Con A is a homotetramer, each sub-unit has a molecular weight of 25.5 kDa, two chains and 235 amino acids. Each monomer of Con A binds two metallic ions: usually Mn^{2+} at site S1 and Ca^{2+} at site S2.¹⁶⁵ Con A was the first lectin which used as commercial basis, and now it is widely applied in biology and biochemistry. For example, Con A can be used to characterise surface structure of glycoproteins and other sugar-containing entities exposed on the membrane of various cells;¹⁶⁶ and some research showed that the cancer cells can be aggregated readily by Con A while other cells cannot.¹⁶⁷

Con A was first crystallised by Sumner and Howell in 1936.^{168, 169} A later investigation of the structure of Con A was conducted by Greer *et al.* in 1970. They studied the X-ray diffraction of Con A crystal and found Con A crystallised in two space groups $I222$ or $I2_12_12_1$.¹⁷⁰ For the last 60 years, Con A has been studied widely and yielded more than 50 X-ray crystal structures,

including the native state of Con A bound to manganese and calcium,^{171, 172} Con A bound with carbohydrates,^{173, 174, 175, 176} metal free Con A,^{177, 178} and Con A bound to other transition metals.^{179, 180} Currently, there are several common structurally characterised crystal forms of Con A, bound to manganese and calcium ions, including triclinic $P1$,¹⁸¹ orthorhombic $I222$,¹⁷¹ orthorhombic $C222_1$ ¹⁷² and orthorhombic $P2_12_12_1$.⁹⁹ A model of crystallographic structure of Con A bound to manganese and calcium ions is presented in Figure 1-22.

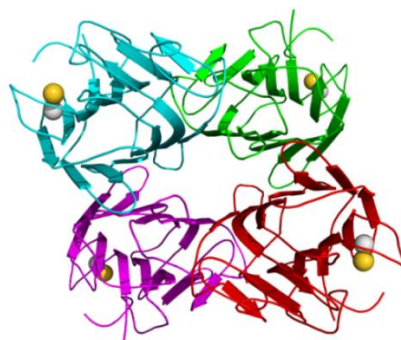


Figure 1-22. Crystallographic structure of a Con A tetramer (from jack bean), obtained by crystal X-ray diffraction, at a resolution of 2.4 Å. The space group $I222$ with unit cell dimensions of $a = 63.15$ Å, $b = 86.91$ Å, $c = 89.25$ Å. Monomers with color cyan, green, red and magenta; Calcium (gold) and manganese cations (grey) are depicted as spheres.¹⁸²

1.7.3 Bovine liver catalase (BLC)

Catalase is a common enzyme in all living organisms. It protects cells against toxic effects of hydrogen peroxide to proteins, lipids, and nucleic acids, by catalysing the reaction of decomposition of hydrogen peroxide to water and oxygen.¹⁸³ Catalase from bovine liver is a tetramer of four equal polypeptide

chains: each subunit is over 500 amino acids long¹⁸⁴ and has a molecular weight of 60 kDa.

Catalase from bovine liver was firstly crystallised by Sumner and Dounce in 1937.¹⁸⁵ After that, McPherson *et al.* introduced PEG 6,000 and 20,000 as additives to mediate catalase from sheep or deer liver crystallisation, and produced large size of sheep liver catalase crystal and deer liver catalase crystal with complex shape.¹²⁵ Like Con A, the crystallisation and structural characterisation of catalase has been studied for almost 60 years. There were two common structurally characterised crystal forms of BLC crystal: trigonal $P3_221$ (form I)¹⁸⁶ and orthorhombic $P2_12_12_1$ (form II)¹⁸⁷. Recently, Matzger *et al.* applied polymer-induced heteronucleant for BLC crystallisation and obtained another orthorhombic form (form III).^{99, 188} A model of crystallographic structure of BLC (form II) is presented in Figure 1-23.

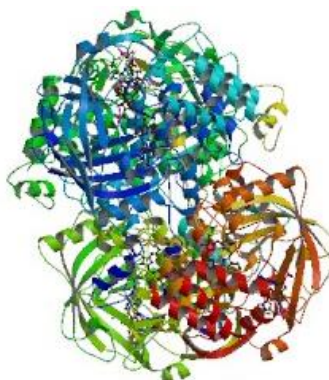


Figure 1-23. Crystallographic structure of a BLC tetramer, at a resolution of 2.69 Å and a crystallographic R factor of 20.5 %. It adopts the space group $P2_12_12_1$ with unit cell dimensions of $a = 68.65$ Å, $b = 173.74$ Å, $c = 186.32$ Å. Monomers with different colors are equal.⁹⁹

1.8 Aims and objectives of the project

In this project, in order to probe some of the factors involved in polymer-mediated protein crystallisation, we set out to prepare different classes of polymers with varying degrees of charge, molecular weight and backbone structure, and then to study their roles as additives in model protein solutions. The guiding hypothesis was that specific functional polymers in solution could alter the rate of protein crystallisation from solutions, and thereby influence the shape, size, and/or polymorph of the resultant crystals.

The aim of this project was threefold. The first two objectives are shown in Figure 1-24. The first aim of this project was to design some key polymers with varying degrees of charge, molecular weight and backbone structure via proper ATRP or RAFT methods (Figure 1-24A). The polymers should be hydrophilic and stable when dissolved in protein crystallisation buffer solutions with different pH. They also need to be compatible with protein structures.

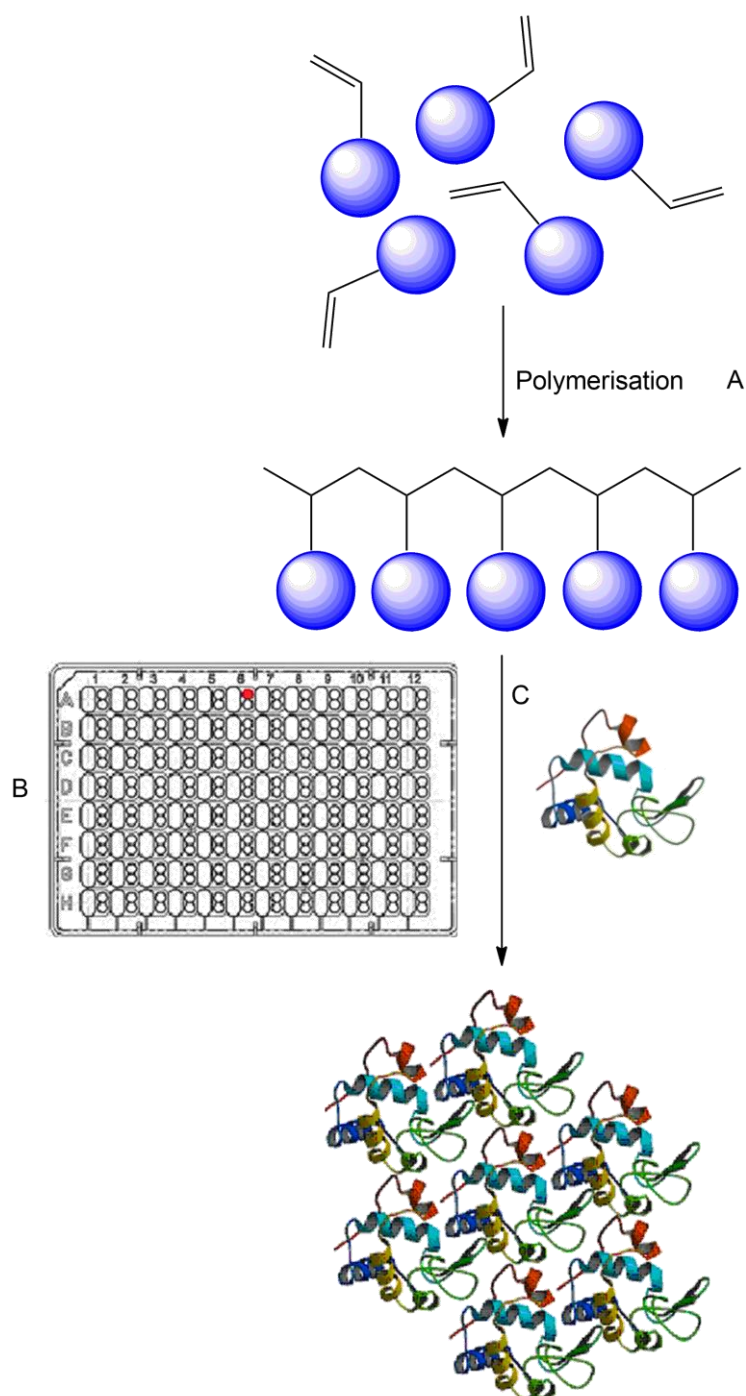


Figure 1-24. Schematic representation of protein crystallisation utilising polymer additives. A) Polymerisation of functional monomers to yield the polymer. B) 96-well crystallisation plate, each sample well (red) composes of protein and polymer additives. C) Polymer acts as ‘additive’ to mediate protein crystallisation.

The second aim was to use these polymers as solution additives to mediate various model proteins crystallisation via sitting drop vapour diffusion techniques (Figure 1-24C). In this research, hen egg white lysozyme (HEWL), concanavalin A (Con A) and bovine liver catalase (BLC) were selected as target proteins for crystallisation experiments. The first model protein was HEWL. HEWL macromolecules are positively charged at tetragonal crystallisation pH of 4.8, i.e. cationic. It is readily available and relatively straightforward to crystallise in the tetragonal form within one day. These facts allow us to develop experimental protocols to investigate the effects of these polymers successfully, such as alter protein crystal size, morphology, even crystal packing motifs, and obtain multiple forms from the same crystallisation condition. Besides the exploration of HEWL, we also aim to evaluate whether these polymers were suitable for other proteins, especially anionic proteins. Con A and BLC were selected as anionic model proteins for further crystallisation.

The final objective was to examine the mechanisms of how these polymers affect protein crystallisation and to develop an understanding of the interactions between polymer and protein macromolecules or the surrounding solvent. Moreover, we hoped to establish structure-function relationships linking the types of polymers used in these experiments and the protein crystal habits produced would generated. These relationships might be used as models to guide a wide range of protein crystallisation experiments in the future.

Accordingly, with the polymer additives, proteins can be nucleated into particles (amorphous or crystalline) and obtain polymer & protein nanoaggregates or nanocrystals, which will be useful in pharmaceutical, biotechnological or chemical applications.

CHAPTER 2

2. Materials, Instrumentation and General Methods

2.1 Materials

4,4'-Azobis(4-cyanovaleric acid) (V-501) was purchased from Fluka®, UK and recrystallised from MeOH by Dr. Francisco Fernandez-Trillo. 2-(Ethylthiocarbonothioylthio)-2-methylpropanoic acid (CAT) was also kindly supplied by Dr. Francisco Fernandez-Trillo. A cationic/zwitterionic copolymer of [2-(methacryloyloxy)ethyl]trimethylammonium chloride and N-[2-(methacryloyloxy)ethyl]-dimethyl-(2-sulfoethan)aminium hydroxide [p(METMAC-*co*-MEDSAH)] was kindly supplied by Dr. E. Peter Magennis. HEWL, Con A and BLC were purchased from Sigma-Aldrich®, UK (L6876, C7275 and C40, respectively). They were all used without further purification. MRC 2 Well Crystallisation Plates (Swissci) (UVP plate, 96 reservoir wells, reservoir volume: 50 to 100 µl, with 2 corresponding sample wells: 5 µl max fill volume) were purchased from Hampton Research, UK. Dulbecco's Phosphate Buffered Saline (DPBS) was purchased from Lonza Group Ltd. All solvents, reagents and proteins, were of analytical or HPLC grade and purchased from Sigma-Aldrich®, Acros® or Fisher Scientific®, UK without further purification unless otherwise.

- 2-(Dimethylamino)ethyl methacrylate (DMAEMA) (98 %) – Fluka
- 2-(Ethylthiocarbonothioylthio)-2-methylpropanoic acid (CTA) –

synthesised by Dr. Francisco Fernandez-Trillo, School of Pharmacy, the University of Nottingham

- 2,2-Bipyridine ($\geq 99\%$) – Sigma Aldrich
- 2-Acrylamido-2-methyl-1-propanesulfonic acid (AMPS) – Sigma Aldrich
- 4,4'-Azobis(4-cyanovaleric acid) (V-501) (recrystallised from MeOH by Dr. Francisco Fernandez-Trillo) – Fluka
- 4-Aminobutanoic acid ($\geq 99\%$) – Acros Organics
- Acrylic chloride (96%) – Alfa Aesar
- Aluminium stubs with carbon tabs – Agar Scientific
- Aluminum oxide - Neutral grade – Sigma Aldrich
- Ammonium sulfate ($\geq 99\%$) – Sigma
- Bovine liver catalase (BLC) (C40, $\geq 10,000$ units/mg protein) – Sigma Aldrich
- Cellulose acetate membrane 0.2 μm – Aldrich
- Chloroform ($\geq 99.5\%$) – Sigma Aldrich
- Chloroform-d – Sigma Aldrich
- Concanavalin A (Con A) from *Canavalia ensiformis* (Jack bean) (C7275) – Sigma Aldrich
- Copper (II) Bromide – (CuBr_2 , 99%) - Alfa Aesar
- Deuterium oxide (D_2O) – Sigma Aldrich
- Dialysis membrane (MWCO 1000, regenerated cellulose) – Spectrapor
- Diethyl ether (anhydrous, $\geq 99\%$) – Sigma Aldrich

- Dimethyl sulfoxide-d6 – Sigma Aldrich
- Dulbecco's phosphate buffered saline (DPBS) – Lonza Group Ltd
- Ethanol (anhydrous, $\geq 99.5\%$) – Sigma Aldrich
- Ethyl acetate (anhydrous, 99.8 %) – Sigma Aldrich
- Ethylene glycol (anhydrous, 99.8 %) – Sigma Aldrich
- Glycerol anhydrous puriss – ($>99.5\%$) - Fluka
- Glycine ($\geq 98.5\%$) – Sigma Aldrich
- Hen egg white lysozyme (HEWL) (L6876, $\geq 100,000$ units/mg protein) – Sigma Aldrich
- Hydrochloric acid (HCl) (ACS reagent, 37 %) – Sigma Aldrich
- Methyl 2-bromopropionate (98 %) – Sigma Aldrich
- Methyl iodide (99 %) – Sigma Aldrich
- MRC 2 Well Crystallisation 96 Plate – Hampton Research
- N-(3-(dimethylamido)propyl)methacrylamide (DMAPMAm) – Sigma Aldrich
- Petroleum ether – Sigma Aldrich
- Poly(ethylene glycol) (PEG 4000) – Sigma Aldrich
- Poly(ethylene glycol) methyl ether methacrylate (PEGMA₄₇₅) – Sigma Aldrich
- Poly(ethylene oxide) (PEO) – Sigma Aldrich
- Polystyrene – Sigma Aldrich
- Polyvinylpyrrolidone – Sigma Aldrich

- Sodium acetate (anhydrous) – Sigma Aldrich
- Sodium chloride (NaCl) – Fisher Scientific
- Sodium phosphate ($\geq 99\%$) – Sigma Aldrich
- Tetrahydrofuran (THF) (anhydrous, $\geq 99.9\%$) – Sigma Aldrich
- Toluene (anhydrous, 99.8 %) – Sigma Aldrich
- Trifluoroacetic acid ($\geq 99\%$) – Sigma Aldrich
- Trizma base ($\geq 99.9\%$) – Sigma

2.2 Instrumentation

Gel permeation chromatography (GPC)

The polydispersity index (PDI) and molecular mass of the polymers were determined using Polymer Laboratories GPC-50 (Varian, Inc.) plus fitted with differential refractometer (RI), capillary viscometer (DP) and dual angle laser light-scattering (15° and 90°) detectors. The flow rate was 1.00 mL/min or 0.5 mL/min and experiments were conducted at room temperature. Organic soluble polymer analysis was carried out on the GPC-50 Plus with Resipore Mixed-D columns (Agilent Tech. Inc.) (eluent-chloroform/5 % Et₃N) calibrated with linear polystyrene standards. Cationic polymer analysis was carried out on the same GPC-50 Plus with CATSEC-300 (250 mm \times 4.5 mm ID) column (eluent-200 mM NaCl with 0.1 % trifluoroacetic acid (v/v)) calibrated with polyvinylpyrrolidone (PVP) standards. Anionic polymer analysis was carried out on the same GPC-50 Plus with Polymer Labs aquagel-OH guard columns

(50 × 7.5 mm, 8 μm, Polymer Labs UK) (eluent-Dulbecco's PBS without Ca²⁺ and Mg²⁺ ions) calibrated with a single, narrow poly(ethylene oxide) (PEO) standard (Polymer Labs, Mp 128 kDa, [η] 1.2968 dL/g) using a dn/dc value of 0.133 g/mL. Samples were prepared at 1-5 mg/mL in the mobile phase and injected 100 μL onto the column. Molecular weight and polydispersity index were calculated using Polymer Labs Cirrus 3.0 Software.

NMR spectroscopy

¹H and ¹³C nuclear magnetic resonance (NMR) spectra were recorded on a Bruker Avance 400 MHz spectrometer. The instrument is fitted with a 5mm switchable quadruple probe for the detection of ¹H, ¹³C, ¹⁹F and ³¹P, and also with z-axis pulsed field gradients for gradient shimming. Chemical shifts were reported at 400 MHz (¹H) and 101 MHz (¹³C) in ppm (δ units) relative to TMS in chloroform-d (CDCl₃), tetramethylsilane (DMSO-d₆), Methanol-d₄, or D₂O solutions.

Infrared spectroscopy (IR)

IR spectra of polymer samples (approximate 5 mg) were recorded on KBR discs on a Bio-rad FTS6000 Fourier Transform Spectrometer instrument. It is a high performance research grade multi-range FT-IR spectrometer, covering the spectral range 11,000-400 cm⁻¹ capable of both rapid scan and step scan operation. Its high quality 60° Michelson air bearing

piezoscan interferometer features piezoelectric-based continuous dynamic alignment (which simultaneously maximizes the spectral throughput and minimizes the noise in the measurements) and a KBr beam splitter for the mid IR. This FTIR instrument employs external reflection, micro-ATR equipped using a silicon crystal. It is interfaced with a Nicolet Avatar 360 spectrometer and uses a liquid nitrogen cooled MCT (HgCdTe) detector. It focuses more than 150 mW of infrared power at the sample, by using a high wattage water-cooled ceramic source rather than air-cooled sources for the mid IR and a two-inch clear aperture through the interferometer. The system was cooled by liquid nitrogen for 10 min before the detection of the polymer sample.

Dynamic light scattering (DLS)

Dynamic Light Scattering (DLS) was measured by using a Viscotek Model 802 instrument (Viscotek Europe Ltd.), equipped with an internal laser (825-832 nm) and a maximum radiation power of 60 mW. From standard auto correlation functions, measured diffusion coefficients were related to particle hydrodynamic radius via the Stokes-Einstein Equation.

$$RH = kT/6\pi\eta D$$

Where RH is the hydrodynamic radius, k is the Boltzmann constant, T is the temperature, and η is the viscosity of the solvent. In addition, it was assumed that particles were spherical and non-interacting.

Measurements quoted are the averages of samples with at least ten readings of

particle size recorded at 19 °C. Data processing was performed with the software program OmniSize 3.0 (Viscotek Europe Ltd.).

Freeze drier

Water was removed by immersing reagent tubes containing the samples in liquid nitrogen, once frozen the samples were placed on an Edwards Modulyo freeze drier equipped with an Edwards high vacuum pump for 3 days at -25 °C and the water was then removed.

Rotary evaporator

Solvents evaporated under reduced pressure on a Buchi Rotavapor R-200 equipped with a B490 heating bath with 4 °C.

Centrifuge

Centrifugation was carried out on an Eppendorf Refrigerated Microcentrifuge. All protein solutions were centrifuged at 13,000 rpm for 5 minutes at 4 °C. Polypropylene micro-centrifuge tubes in size 1.5 mL (Sigma-Aldrich, T3406) with an integral flip cap were used here.

Optical microscopy

Protein crystals in the crystallisation plates were quantitatively observed using a Leica Stereomicroscope (63x magnification) with a Leica CLS1 50X

fan-cooled light source. A Nikon Coolpix 4500 digital camera was connected to image the crystals.

Scanning electron microscope (SEM)

The samples were loaded onto aluminium stubs with carbon tabs pre-fixed. These were then gold coated using an SCD 030 Blazers sputter coater for 5 minutes at 30mA. The coated samples were transferred into a JEOL JSM 6060 LV Scanning electron microscope and imaged at 20-30 kV. Prior to gold coating, protein crystals were taken out from the crystallisation plates, washed with crystallisation buffer solutions.

X-ray crystallography

Protein crystallographic analysis was carried out on a Rigaku micromax 007 microfocus X-ray generator with high-flux Osmic confocal multi-layer optics. X-rays were collimated to a 0.3 mm beam with X-rays from the copper K alpha emission (1.5418 Angstroms). Diffraction patterns were collected on Rigaku R-Axis 4++ image plates. Crystals were maintained at temperatures of -180 °C by an X-stream 2000 nitrogen vapour system.

In X-ray crystallography, X-ray beam is employed to hit the crystal samples. Atoms in the crystal scatter X-ray waves and will produce secondary spherical waves emanating from electrons. Those regular arrays of spherical waves normally in some specific directions, determined by Bragg's law (Figure 2-1):

$$2 d \sin \theta = n \lambda$$

Here, d is the distance between diffracting planes; θ is the incident angle; n is any integer; and λ is the wavelength of the beam.

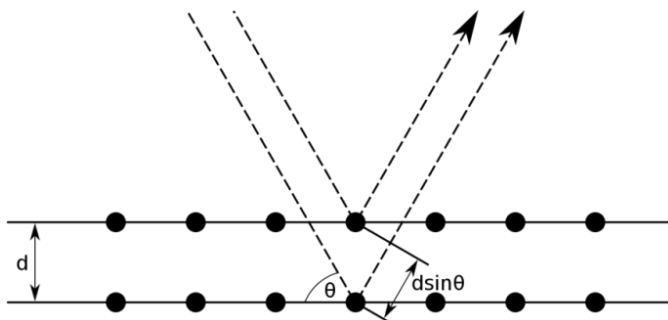


Figure 2-1. Bragg's diffraction. Two incident beams (wavelength λ) scattered off two atoms in the crystalline.

Therefore, X-rays are diffracted resulting in a pattern on the detector. Then the crystallographer can get a three-dimensional image of the density of electrons within the crystal by measuring the angles and intensities of these diffracted patterns. Thus, the mean atom positions, their chemical bonds and other information within the crystals can be determined.

2.3 General methods

General synthetic methods

Poly[poly(ethylene glycol) methyl ether methacrylate₄₇₅] [p(PEGMA₄₇₅)], poly[2-(dimethylamino)ethyl methacrylate] [p(DMAEMA)] and a random copolymer of PEGMA₄₇₅ and DMAEMA [p(DMAEMA-*stat*-PEGMA₄₇₅)] were prepared by a variant of published ATRP route by using

Cu(I)Br/2,2-bipyridine (Bipy) catalytic system and methyl 2-bromopropionate (MBrP) as the initiator. Poly[N-(3-(dimethylamido)propyl)methacrylamide] [p(DMAPMAm)], poly(2-acrylamido-2-methyl-1-propanesulfonic acid) [p(AMPS)], poly(2-acrylamidoacetic acid) [p(2-AmAA)] and poly(4-acrylamidobutanoic acid) [p(4-AmBA)] were synthesised using RAFT methods. The polymerisation employed 2-(ethylthiocarbonothioylthio)-2-methylpropanoic acid (CAT) as the RAFT agent and 4,4'-azobis(4-cyanovaleric acid) (V-501) as the initiator. A hybrid copolymer of [2-(methacryloyloxy)ethyl]trimethylammonium chloride and N-[2-(methacryloyloxy)ethyl]-dimethyl-(2-sulfoethan)aminium hydroxide [p(METMAC-co-MEDSAHH)] was kindly supplied by Dr. Eugene Peter Magennis. For more details see Chapter 3.

General crystallisation method

Crystallisation was performed in 96-well crystallisation plates, using the sitting drop vapour diffusion technique. Specifically, a solution (50 μL) of tested polymer buffer was pipetted in triplicate in the reservoir wells; protein solution, (1 μL) and buffered polymer solution (as described above, 1 μL) were pipetted into sample wells of the crystallisation plate. The plate was then sealed and incubated at 19 $^{\circ}\text{C}$. More details are shown in Chapter 4.

CHAPTER 3

3. Preparation and Characterisation of Monomers and Polymers

3.1 Introduction

As mentioned in 'Chapter 1', although there are many examples of protein crystals reported, successful crystallisation of proteins from solution is still an extremely difficult task. Only a small number of techniques are suitable for helping proteins crystallise; besides, there are many uncertain and poorly understanding factors can affect and govern the crystallisation process from solution.⁵⁹

One essential strategy for protein crystallisation is using polymers as 'additives' into the protein solution.¹⁸⁹ Synthetic polymers are important additives for protein crystallisation control as there are many possible functionalities can be introduced into the backbone and side-chains, giving a very wide range of functional behaviour.^{5, 100, 101} They can influence protein crystallisation process to a large extent in terms of size, habit, morphology and even polymorph of the crystal.⁷¹ Although a number of polymeric additives have been studied to influence protein crystallisation, most of the studies are descriptive; the interactions between some of the existing polymeric additives and protein macromolecules or surrounding solvent are still unclear, and the mechanisms by which protein crystals form in the presence of these polymers needs to be

further studied.^{100, 108}

In order to investigate some of the factors involved in polymer-mediated protein crystallisation, we designed various classes of polymers with varying degrees of charge, molecular weight and backbone structure, and then to study their role as additives in model protein solutions. In this paper, four classes of materials, including neutral, cationic, anionic and cationic/zwitterionic polymers based on methacrylate or (meth)acrylamide monomers were successfully prepared and shown in Figure 3-1.

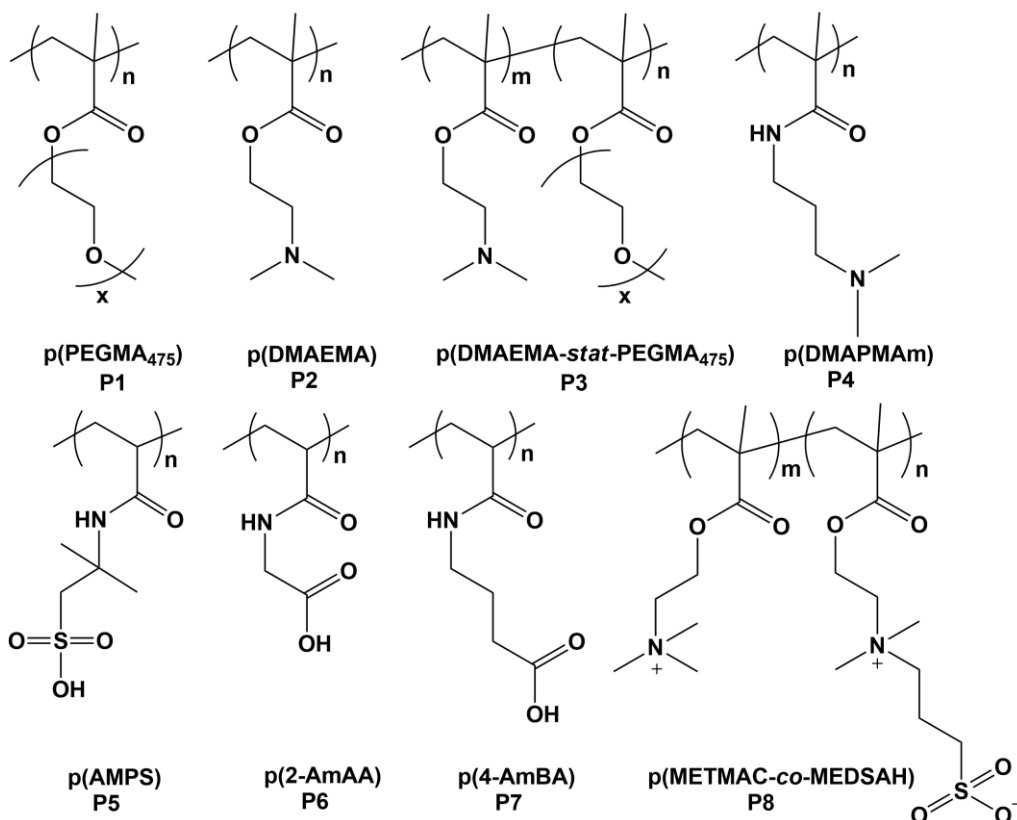


Figure 3-1. Structures of polymers, named P1 to P8. Neutral polymer: P1; cationic polymers: P2-4; anionic polymers: P5-7 and cationic/zwitterionic copolymer: P8.

3.2 Monomer synthesis

3.2.1 2-Acrylamidoacetic acid (2-AmAA)^{190, 191}

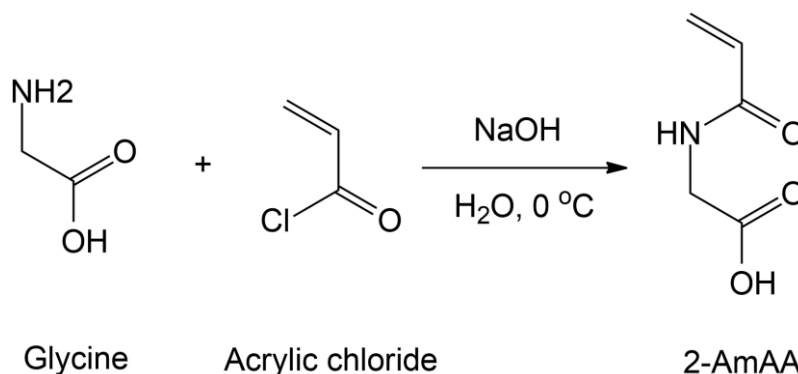
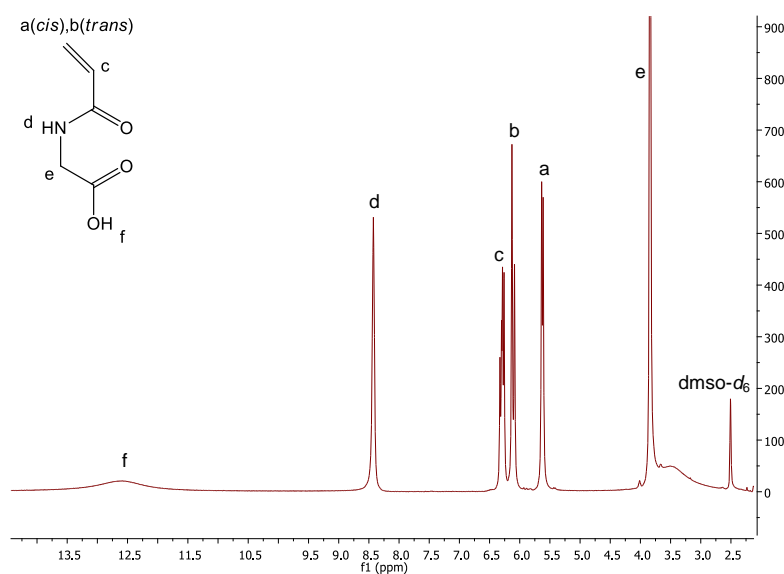
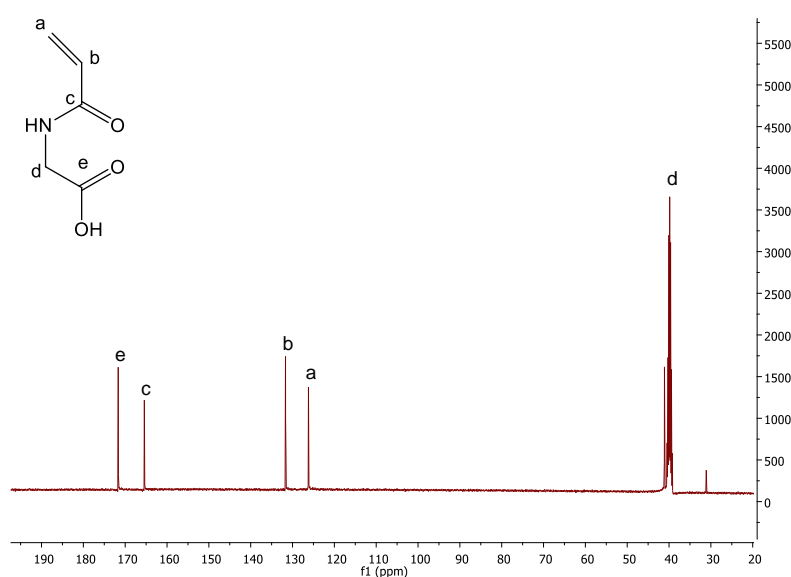


Figure 3-2. Reaction scheme for the synthesis of 2-AmAA.

2-AmAA was prepared in a 500 mL round bottomed flask with a magnetic stirrer, by adding glycine (22 mL, 133 mmol) to NaOH (2M, 264 mL) and cooling to 0 °C by using an ice bath. After glycine dissolved completely, acrylic chloride (24.1 g, 266 mmol) was added dropwise over a period of 30 minutes via an addition funnel. The reaction mixture was stirred for 1 hour. The resulting mixture was acidified to pH 1.0 with HCl (1 M). The crude product was saturated with NaCl and extracted with ethyl acetate (EtOAc) five times from the acidified aqueous solution and then dried over magnesium sulfate. The solution volume was reduced to 25 mL with a rotary evaporator. The obtained solution was diluted with ethyl acetate and cool to 0 °C with vigorous stirring to precipitate a solid. After filtering, then the formed suspension was washed with ethyl acetate/diethyl ether (1:1) (200mL). The solvent was removed with a rotary evaporator. Precipitation was carried out another time, and the final white solid (6.62 g, 39 %) was dried under vacuum

overnight. Characterisation was carried out by $^1\text{H-NMR}$ (Figure 3-3) and $^{13}\text{C-NMR}$ (Figure 3-4). $^1\text{H-NMR}$ (400 MHz, DMSO) δ (ppm) 12.58 (s-board, 1H, COOH), 8.43 (s, 1H, NH), 6.29 (dd, $J = 16.9, 10.2$ Hz, 1H, $\text{CH}=\text{CH}_2$), 6.11 (d, $J = 17.0$ Hz, 1H, $\text{CH}_2=\text{CH}$), 5.62 (d, $J = 9.9$ Hz, 1H, $\text{CH}_2=\text{CH}$), 3.84 (d, $J = 5.3$ Hz, 2H, CH_2). $^{13}\text{C-NMR}$ (101 MHz, DMSO) δ (ppm) 171.66 (COOH), 165.42 (CONH), 131.68 ($-\text{C}=\text{}$), 126.19 ($=\text{CH}_2$), 40.00 (CH_2).

Figure 3-3. $^1\text{H-NMR}$ spectra of 2-AmAA.Figure 3-4. $^{13}\text{C-NMR}$ spectra of 2-AmAA.

2-AmAA monomer was synthesised by using similar conditions according to the reference with modification.¹⁹⁰ The reaction was carried out in sodium hydroxide (2 M) solution using 1:2:4 molar ratio of glycine to acrylic chloride to sodium hydroxide at 0 °C. The mechanism of this acylation reaction is shown in Figure 3-5.

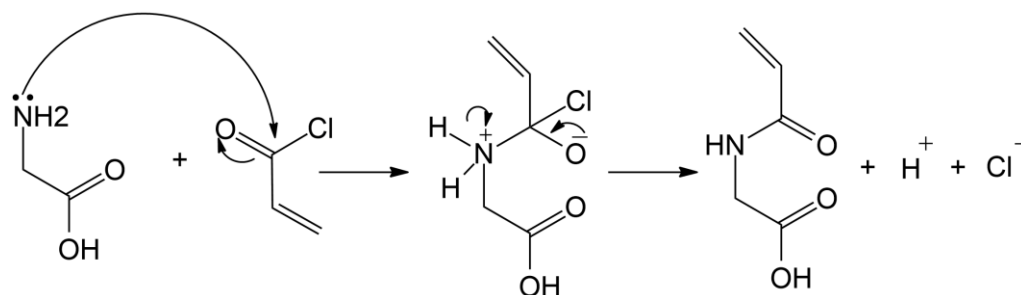


Figure 3-5. Scheme of the mechanism of synthesis of 2-AmAA.

3.2.2 4-Acrylamidobutanoic acid (4-AmBA)^{190, 191}

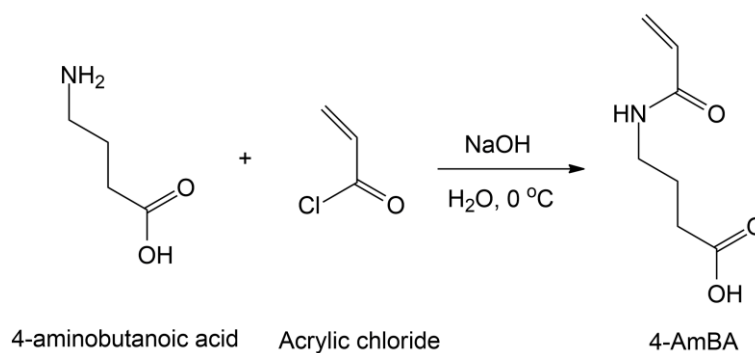
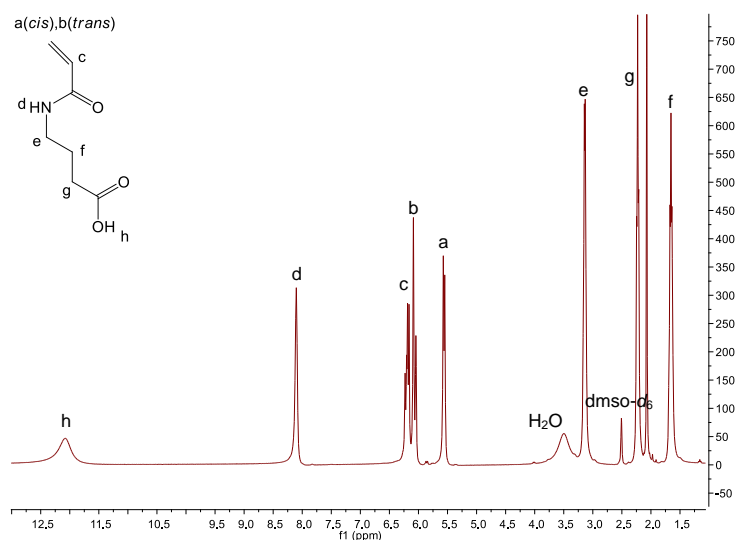
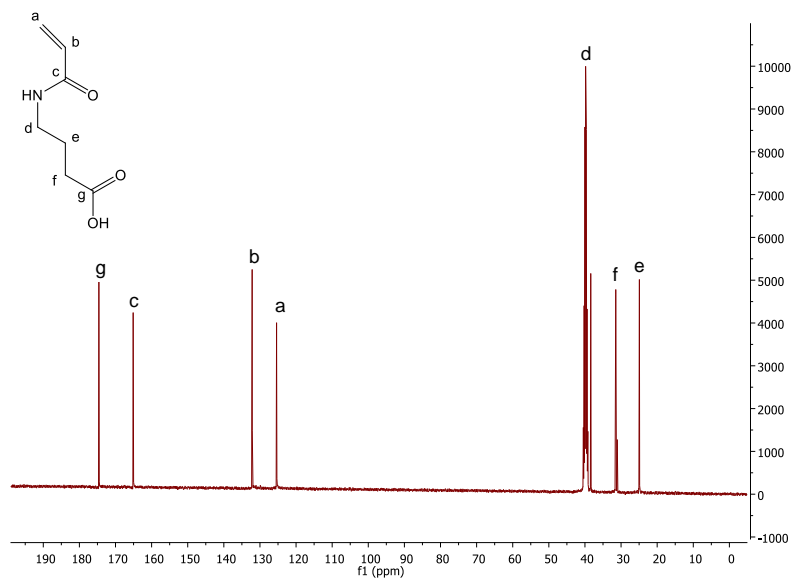


Figure 3-6. Reaction scheme for the synthesis of 4-AmBA.

Similar to 2-AmAA, 4-AmBA synthesis was carried out in a 500 mL round bottomed flask with a magnetic stirrer, by adding 4-aminobutanoic acid (4-ABA) (10 g, 97.0 mmol) to NaOH (2M, 194 mL) and cooling to 0 °C by using an ice bath. After glycine dissolved completely, acrylic chloride (19 mL,

194 mmol) was added dropwise over a period of 30 min via an addition funnel. The reaction mixture was stirred for 1 hour. The pH of the resulting mixture was adjusted to 1.0 using HCl (1 M). The aqueous phase was saturated with NaCl and extracted with EtOAc (5 x), then dried over magnesium sulfate. The solution volume reduced in the rotary evaporator to 25mL. The obtained solution was allowed to precipitate in the freezer overnight, filtered, washed with cold EtOAc and dried under vacuum. The final white solid (7.2 g, 47 %) was yielded. Characterisation was carried out by $^1\text{H-NMR}$ (Figure 3-7) and $^{13}\text{C-NMR}$ (Figure 3-8). $^1\text{H-NMR}$ (400 MHz, DMSO) δ (ppm) 12.08 (s-board, 1H, COOH), 8.10 (s, 1H, NH), 6.20 (dd, $J = 16.8, 10.0$ Hz, 1H, $\text{CH}=\text{CH}_2$), 6.07 (d, $J = 16.8$ Hz, 1H, $\text{CH}_2=\text{CH}$), 5.56 (d, $J = 9.7$ Hz, 1H, $\text{CH}_2=\text{CH}$), 3.14 (d, $J = 5.8$ Hz, 2H, $\text{CH}_2\text{-NH}$), 2.23 (t, $J = 6.9$ Hz, 2H, $\text{CH}_2\text{-COOH}$), 1.70 (dd, $J = 38.8, 32.1$ Hz, 2H, $\text{CH}_2\text{CH}_2\text{CH}_2$). $^{13}\text{C-NMR}$ (101 MHz, DMSO) δ (ppm) 174.60 (COOH), 165.11 (CONH), 132.15 ($-\text{C}=\text{}$), 125.39 ($=\text{CH}_2$), 39.64 (CH_2NH), 31.26 (CH_2COOH), 24.93 ($\text{CH}_2\text{-CH}_2\text{-CH}_2$).

Figure 3-7. $^1\text{H-NMR}$ spectra of 4-AmBA.

Figure 3-8. ¹³C-NMR spectra of 4-AmBA.

As mentioned in the introduction chapter, the effect of polymer on protein crystallisation is likely to depend on the exact polymer functionality. Acrylamide monomers 2-AmAA and 4-AmBA were selected as anionic monomers, due to the presence of ionisable sulfonic groups, which could introduce of some negative charges during the protein crystallisation process. Then those two monomers were used for RAFT polymerisation to form hydrophilic homopolymers. However, the product yield of those monomers were not as high as literature reported (70 %),¹⁹² this may because of the inevitable loss during purification process.

3.3 Polymer synthesis

3.3.1 Atom transfer radical polymerisation (ATRP) method

General protocol for ATRP:¹⁴³

In a typical procedure, Cu(I)Br/2,2-bipyridine (Bipy) was the catalytic system and methyl 2-bromopropionate (MBrP) was the initiator. Polymerisation was conducted in a tube fitted with a two way stopcock and sealed with a septum. The polymerisation solution was degassed by three vacuum-nitrogen cycles and placed into an oil bath at 70 °C. An NMR spectrum was recorded at the beginning of the experiment. The reaction was stopped by removing the septum thus exposing the reaction to oxygen. After reaction, an NMR spectrum was recorded to calculate the degree of conversion. The reaction mixture was passed through aluminum oxide and washed through with chloroform to remove the catalyst. The polymer was precipitated in a 100:1 excess of petroleum ether to remove the un-reacted monomer.

3.3.1.1 Polymer conversion calculations

The overall monomer conversion was calculated by ¹H-NMR spectra by comparing the vinyl proton signals from the monomers (5.6 and 6.1 ppm) to the overall integration from the OCH₂ adjacent to the methacrylate group (4.01-4.48 ppm) for methacrylate-based monomers: PEGMA₄₇₅ and DMAEMA.

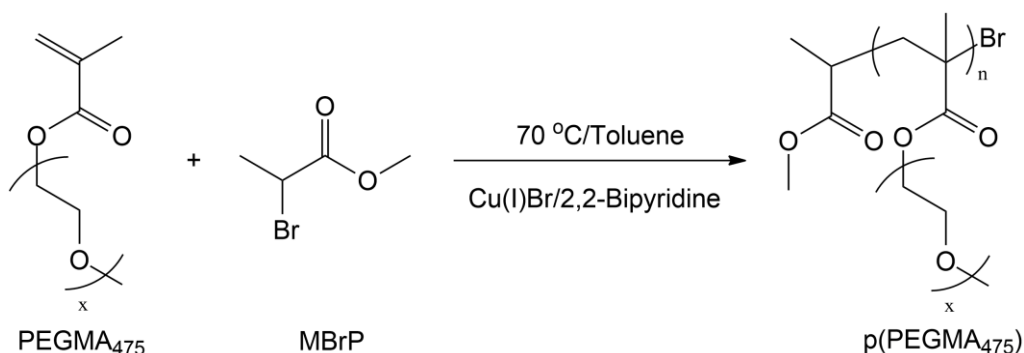
3.3.1.2 Poly[poly(ethylene glycol) methyl ether methacrylate₄₇₅][p(PEGMA₄₇₅)] (P1)^{193, 194}

Figure 3-9. Reaction scheme for the synthesis of p(PEGMA₄₇₅) homopolymer (P1) via ATRP.

In a typical ATRP procedure, 2,2-Bipyridine (0.13 g, 0.84 mmol), PEGMA₄₇₅ (3 g, 6.32 mmol), toluene (3.75 mL) and methyl 2-bromopropionate (MBrP) (0.07 g, 0.42 mmol) were added to a 10 mL tube fitted with a two way stopcock and sealed with a septum. The tube was connected to both a vacuum line and a nitrogen pump. The mixture was degassed by three freeze thaw cycles in liquid nitrogen. The frozen mixture was charged with nitrogen before the addition of Cu(I)Br (0.06 g, 0.42 mmol). The mixture was then degassed by three vacuum-nitrogen cycles and placed into an oil bath at 70 °C for 6 h. An NMR spectrum was recorded at the beginning of the experiment. Samples were taken at specific time points by piercing the septum with a syringe; the septum was resealed using parafilm. Air was removed from the syringe by purging it with nitrogen three times. The reaction was stopped by removing the septum thus exposing the reaction to oxygen. After reaction, NMR spectrum was

recorded to enable calculation of degree of conversion. The reaction mixture was passed through aluminum oxide and washed through with chloroform to remove the catalyst. The mixture was precipitated in a 100:1 excess of petroleum ether to remove the un-reacted monomer, and then yielded the polymer (1.9 g, 63 %). $^1\text{H-NMR}$ (400 MHz, CDCl_3) δ (ppm) 4.28-3.92 (m, 2H, $\text{COO-CH}_2\text{-CH}_2\text{O}$), 3.72-3.52 (m, 2xH, $\text{OCH}_2\text{-(CH}_2\text{)}_x\text{O-CH}_3$), 3.41-3.36 (m, 3H, OCH_3), 2.39-1.56 (m, 2H, $\text{CH}_2\text{-MA backbone}$), 1.18-0.55 (m, 3H, $\text{CH}_3\text{-MA}$). $\text{IR } \nu$ (cm^{-1}) 2849 (C-H), 1721 (C=O), 1464, 1346 (C-H), 1240, 1089 (C-O), 1026, 934, 846 (C-C). The $^1\text{H-NMR}$ and $^{13}\text{C-NMR}$ spectra of monomer PEGMA₄₇₅ are shown in Appendix (Page 330).

Overall monomer conversion was calculated from $^1\text{H-NMR}$ spectra by comparing the vinyl proton signals from the monomers (5.6 and 6.1 ppm, Figure 3-10, signals a and b) to the overall integration from the OCH_2 across the range 3.9 to 4.4 ppm (Figure 3-10, signal d). In the region of 3.9-4.4 ppm two protons of the remaining monomers resonate as well as two protons from the polymer.

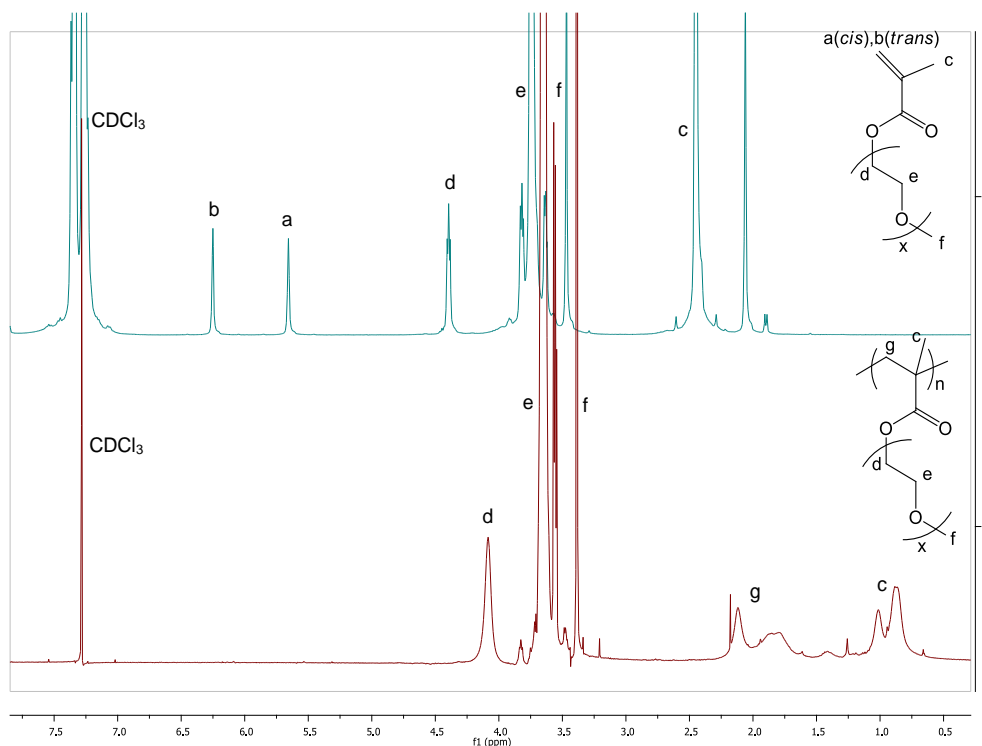


Figure 3-10. $^1\text{H-NMR}$ spectra for the polymerisation of PEGMA_{475} to yield $\text{p(PEGMA}_{475}\text{)}$ (P1). Top: Reaction mixture at the beginning of the polymerisation experiment. Bottom: Purified polymer P1.

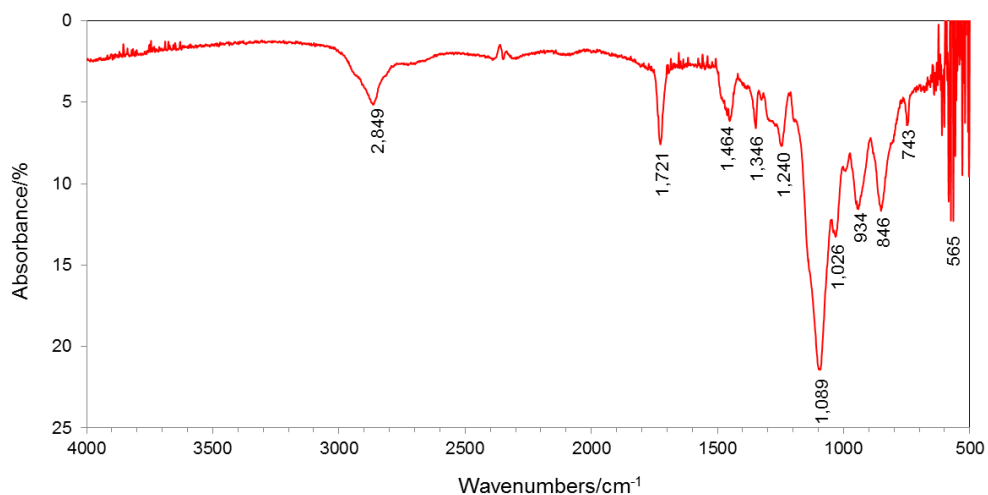


Figure 3-11. Representative FTIR for $\text{p(PEGMA}_{475}\text{)}$ (P1).

$\text{P(PEGMA}_{475}\text{)}$ was synthesised by using the general ATRP method as above shown. The size of the polymer was controlled by the ratio of

[Monomer]:[Initiator]. Several experiments with different [Monomer]:[Initiator] ratios for the synthesis of p(PEGMA₄₇₅) were carried out (Table 3-1).

Table 3-1. Summary of synthesis of p(PEGMA₄₇₅) (P1) via ATRP

No.	[M]:[I] ^c	Conversion (¹ H-NMR)	Time in minutes	M _n (GPC)	M _n (Theoretical)	PDI
1 ^a	50:1	30 %	360	27109	7196	1.15
2 ^b	15:1	60 %	120	30815	4275	1.20
3 ^b	20:1	83 %	180	36388	7885	1.26
4 ^b	100:1	84 %	540	39405	39900	1.23

a) Experimental conditions: 70 °C; Monomer/Toluene=1:2 (w/v); [I]/[CuBr]/[Bipy]=1/1/2. b) Experimental conditions: 70 °C; monomer/toluene=1:1.25 (w/v); [I]/[CuBr]/[Bipy]=1/1/2. c) Molar ratio of [Monomer]:[Initiator]. Theoretical, from monomer/initiator ratio and monomer conversion. GPC analysis (eluent-chloroform, poly(styrene) standards). Polydispersity index (PDI) from GPC.

Table 3-1 shows a summary of p(PEGMA₄₇₅) (P1) synthesised in this study and Figure 3-12 shows their kinetic plots. Generally, a conversion of 60 % was targeted to decrease the possibility of side reactions. Experiment 1 with [Monomer]:[Initiator] = 50:1, the conversion was about 30 % after 6 hours, and the PDI measured by GPC was found about 1.15 (Table 3-1, entry 1). The kinetic plot shows its slow initiation (Figure 3-12, 1). As the conversion of this experiment was relatively low, experiments 2-4 with different [Monomer]:[Initiator] ratios and a smaller amount of toluene were carried out. Generally the conversions were above 60 %, and the PDI measured by GPC were found about 1.20 (Table 3-1, entries 2-4). The polymerisation of p(PEGMA₄₇₅) (P1) exhibited pseudo-first order kinetics and a linear increase of molecular weight with conversion (Figure 3-12) while the polydispersity of the

polymers was narrow throughout the polymerisation. In this way, several materials could be prepared, with different molecular weights.

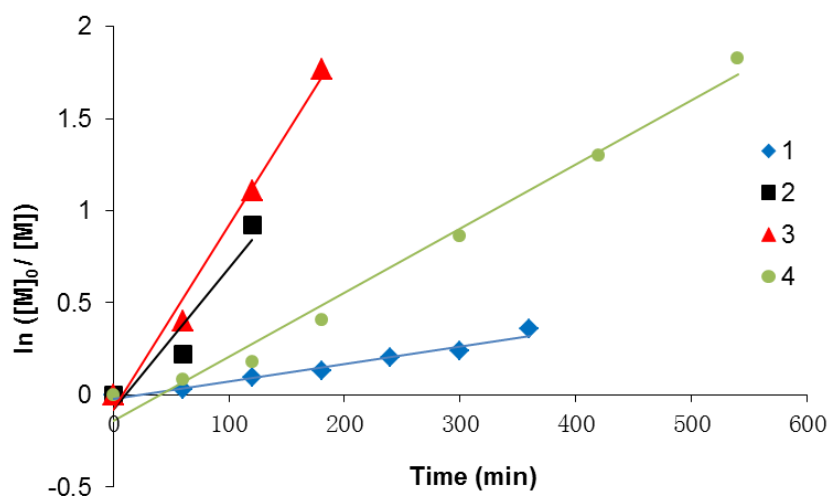


Figure 3-12. Some examples of kinetic plots for the synthesis of p(PEGMA₄₇₅) (P1) in this study.

The GPC used to determine molecular weight data (M_n GPC) for the synthesis of p(PEGMA₄₇₅) showed large discrepancies compared to the theoretical number molecular weight (M_n Theoretical) in some experiments (Table 3-1, entries 1-3). Molar masses determined by GPC in chloroform will depend on how the polymer interacts with the column and how similar the polymer compared to the standards (polystyrene). From previous researchers' study, polymers with macromolecular brushes may provide unusual GPC results;¹⁹⁵ and the PDI may have been influenced by chain branching, thus, some side reactions may take place due to the presence of PEG-bismethacrylates as impurities in the PEGMA₄₇₅ monomer supplied.

3.3.1.3 Poly[2-(dimethylamino)ethyl methacrylate] [p(DMAEMA)]

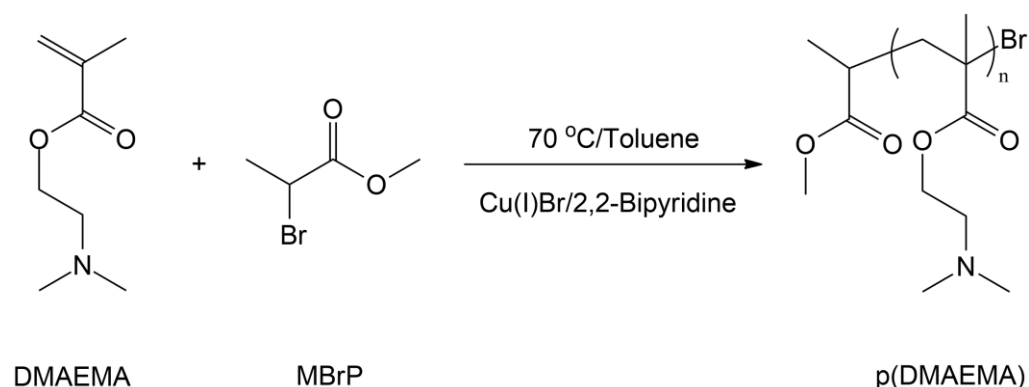
(P2)^{196,197,198}

Figure 3-13. Reaction scheme for the synthesis of p(DMAEMA) (P2) via ATRP.

Typically, the same ATRP procedure as described above (Section 3.3.1.2) was carried out. 2,2-Bipyridine (0.12 g, 0.76 mmol), DMAEMA (6 g, 38.2 mmol), toluene (6 mL), methyl 2-bromopropionate (MBrP) (0.06 g, 0.38 mmol) and Cu(I)Br (0.05 g, 0.38 mmol) were added to a tube fitted with a two way stopcock and sealed with a septum. After being degassed, the reaction mixture was charged with nitrogen and placed into an oil bath at 70 °C overnight. The reaction mixture was passed through aluminum oxide and washed through with chloroform to remove the catalyst. The polymer was precipitated in a 100:1 excess of petroleum ether to remove the un-reacted monomer. Then a yellow compound was obtained (4.7 g, 78 %). ¹H-NMR (400 MHz, CDCl₃) δ (ppm) 4.28-3.90 (m, 2H, OCH₂), 2.73-2.42 (m, 2H, CH₂N), 2.40-2.13 (m, 6H, N(CH₃)₂), 2.08-1.55 (m, 2H, CH₂-MA backbone), 1.17-0.62 (m, 3H, CH₃-MA).

IR ν (cm^{-1}) 2933, 2762 (C-H), 1720 (C=O), 1447, 1384 (C-H), 1262, 1140 (C-O), 1231 (C-N), 1013 (C-C). The ^{13}C -NMR spectra of monomer DMAEMA is shown in Appendix (Page 331).

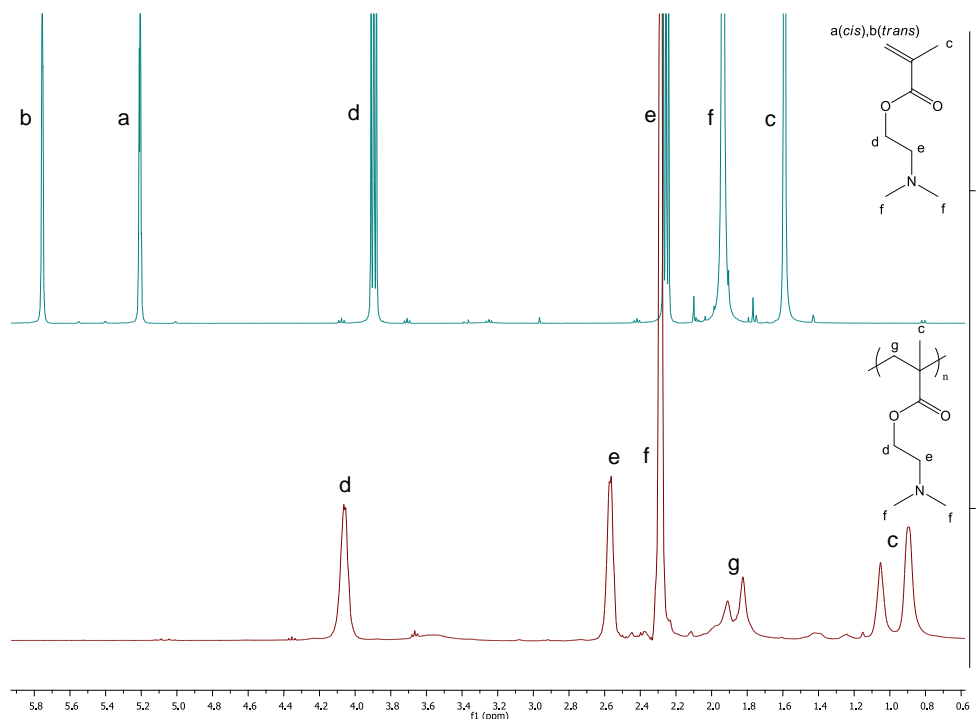


Figure 3-14. ^1H -NMR spectra for the polymerisation of DMAEMA to yield p(DMAEMA) (P2). Top: Monomer DMAEMA. Bottom: Purified polymer p(DMAEMA) (P2).

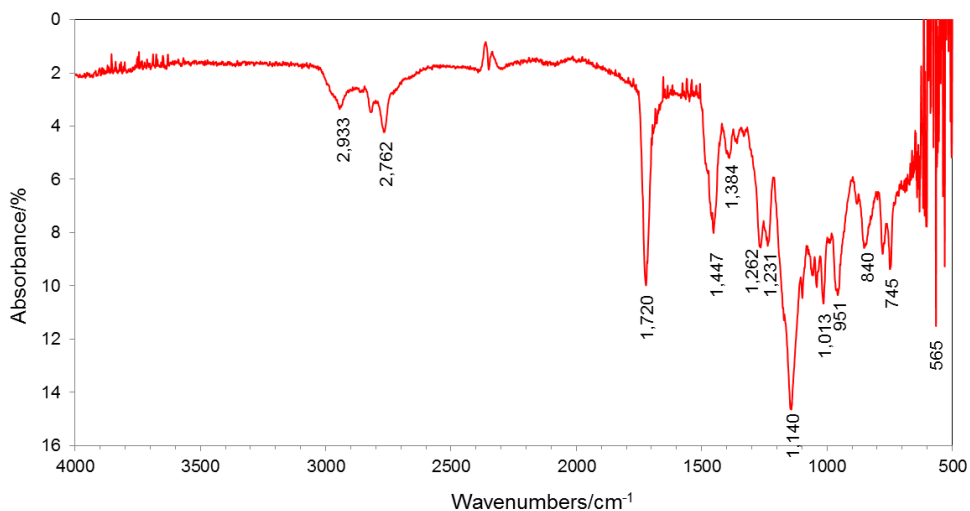


Figure 3-15. Representative FTIR for p(DMAEMA) (P2).

Table 3-2 shows selected properties of p(DMAEMA) (P2) synthesised in this study. The size of the polymer was also controlled by the [Monomer]:[Initiator] ratio. Two repeat experiments with different [Monomer]:[Initiator] ratios were carried out. The PDI was measured by CHCl₃ GPC (polystyrene standard) and found in the range 1.20-1.60. Experiments 1 and 2 with a molar ratio of [Monomer]:[Initiator] = 100:1, generally the conversion was about 28 % based on monomer masses after 6 hours, and the PDI measured by GPC was found about 1.30 (Table 3-2, entries 1 and 2). The conversions of these experiments were relatively low, a common method for resolving this problem is either prolong the reaction time or lower the ratio of [Monomer]:[Initiator]. Then, experiments 3 and 4 with a molar ratio of [Monomer]:[Initiator] = 50:1 were carried out (Table 3-2, entries 3 and 4). The conversion was about 70 % after 6 hours, and the PDI measured by GPC was found about 1.52.

Table 3-2. Summary of synthesis of p(DMAEMA) (P2) via ATRP

No.	[M]:[I] ^b	Conversion	Time (min)	Mn (GPC)	Mn (Theoretical)	PDI
1a	100:1	16 %	210	40816	2562	1.25
2a	100:1	28 %	360	42403	4402	1.30
3a	50:1	70 %	360	44171	5502	1.52
4a	50:1	68 %	360	46299	5345	1.52

a) Experimental conditions: 70 °C; Monomer/Toluene=1:1 (w/v); [I]/[CuBr]/[Bipy]=1/1/2. b) Molar ratio of [Monomer]:[Initiator]. Theoretical, from monomer/initiator ratio and monomer conversion. GPC analysis (chloroform, poly(styrene) standards). Polydispersity index (PDI) from GPC.

Figure 3-16 shows selected kinetic plots for the synthesis of p(DMAEMA) (P2) by ATRP. The polymerisation of p(DMAEMA) (P2) exhibited pseudo-first

order kinetics and a linear increase of molecular weight with conversion. In this way, several materials could be prepared, with different molecular weights.

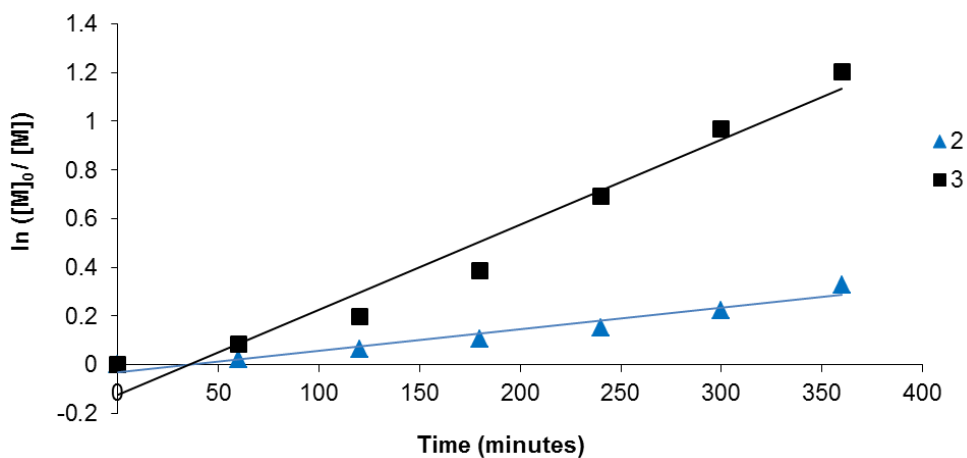


Figure 3-16. Kinetic plots for the synthesis of p(DMAEMA) (P2) via ATRP method. Blue represents experiment 2 (Table 3-2, entry 2). Black represents experiment 3 (Table 3-2, entry 3)

However, the number average molecular weights determined from GPC (M_n GPC) was much higher compared to the theoretical molecular weights (M_n Theoretical) based on monomer conversion (Table 3-2). Also, polymers had slightly broad molecular weight distributions. These results suggested that GPC with polystyrene standard and CHCl_3 as the solvent may not a proper method for characterising this kind of polymer. Further GPC investigation may need by using more closely matched calibration standard rather than polystyrene.

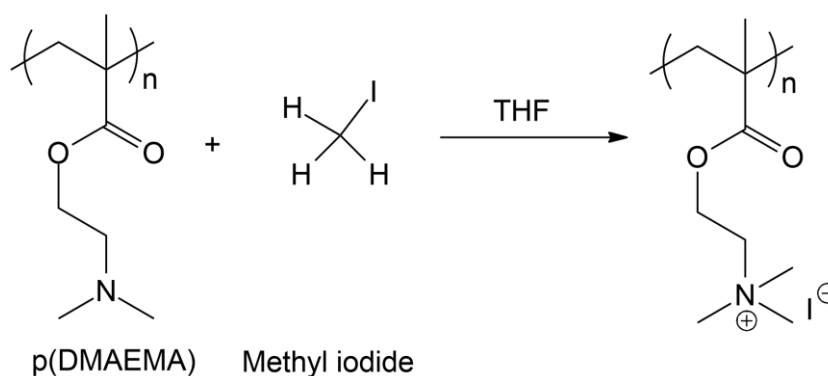
3.3.1.4 Quaternisation of p(DMAEMA) (P2)^{199, 200, 190}

Figure 3-17. Reaction scheme for quaternisation of p(DMAEMA) (P2).

In a round bottom flask with a magnetic stirring bar, p(DMAEMA) homopolymer (3 g) was dissolved in tetrahydrofuran (THF) (90 mL). The flask was sealed with a rubber septum and a molar equivalent of methyl iodide calculated was added via syringe. The mixture was left to react for 48 hours at room temperature. The color of the reaction mixture changed from dark yellow to light yellow. After this time the flask was opened and the solvent was removed under reduced pressure to yield a light yellow solid. Then around 10 mL of deionised water was added and freeze dried to yield the desired polymer.

¹H-NMR (400 MHz, D₂O) δ (ppm) 4.61-4.31 (m, 2H, OCH₂-quaternised DMAEMA), 4.23-4.08 (m, 2H, OCH₂-DMAEMA), 4.00-3.64 (m, 2H, CH₂N(CH₃)₃), 3.41-3.03 (m, 9H, N(CH₃)₃), 2.94-2.80 (m, 2H, CH₂N(CH₃)₂), 2.54-2.33 (m, 6H, N(CH₃)₂), 2.19-1.77 (m, 4H, CH₂-MA backbone), 1.23-0.71 (m, 6H, CH₃-MA). IR ν (cm⁻¹) 3433 (R₄N⁺), 2952 (C-H), 1720 (C=O), 1468 (C-H), 1261, 1141 (C-O), 1226 (C-N), 946 (C-C).

In this study, a modification was carried out on p(DMAEMA) (P2) to introduce

permanent positive charges by the addition of a methyl group to the p(DMAEMA) tertiary amine repeating unit with CH_3I , i.e. quaternisation. The degrees of quaternisation were targeted at 25 %, 50 %, 75 % and 100 %. Characterisation was carried out by $^1\text{H-NMR}$ and IR. An example of $^1\text{H-NMR}$ spectra is shown in Figure 3-18. The experimental level of quaternisation was calculated through $^1\text{H-NMR}$ by comparing relevant peaks in the quaternised (Figure 3-18, signal g) and un-quaternised p(DMAEMA) repeating units (Figure 3-18, signal d).

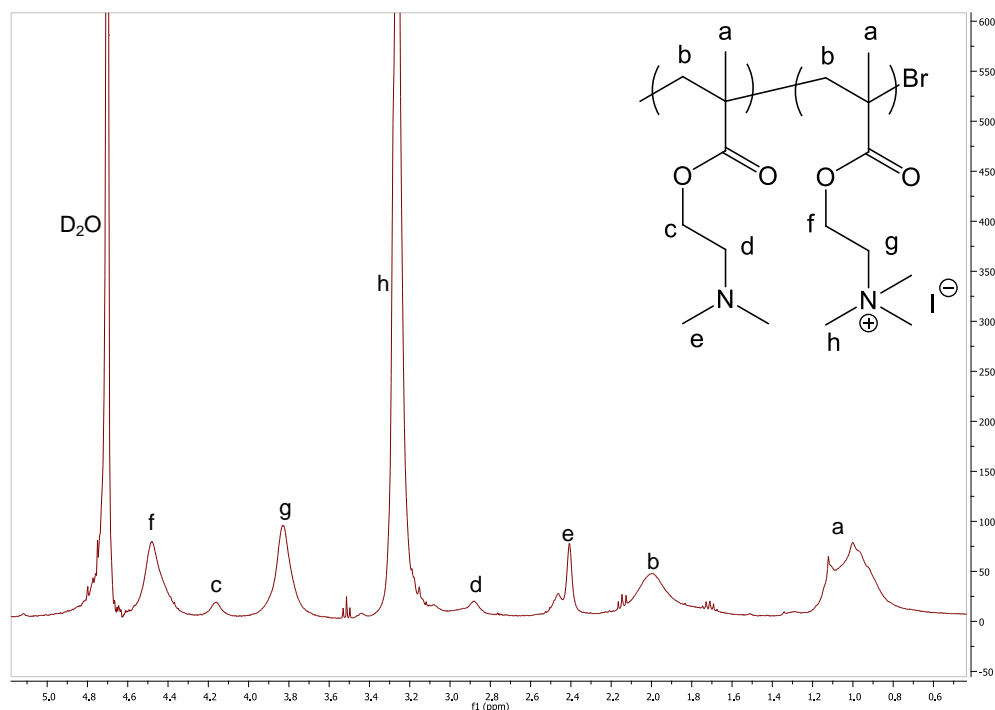


Figure 3-18. $^1\text{H-NMR}$ spectra for quaternised p(DMAEMA) (P2).

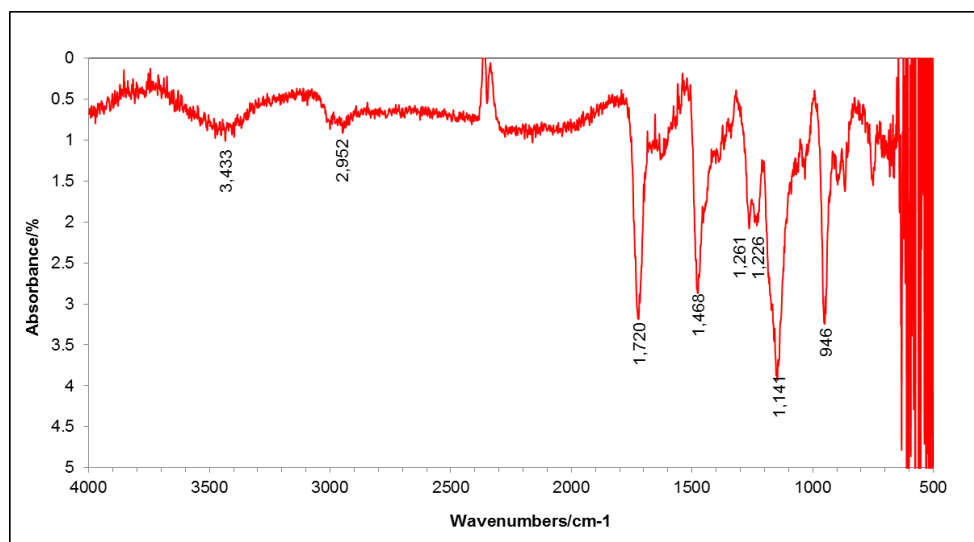


Figure 3-19. Representative FTIR for quaternised p(DMAEMA) (P2).

3.3.1.5 Poly[2-(dimethylamino)ethyl methacrylate-*stat*-poly(ethylene glycol)

methyl ether methacrylate₄₇₅] [p(DMAEMA-*stat*-PEGMA₄₇₅)] (P3)^{190,191,201}

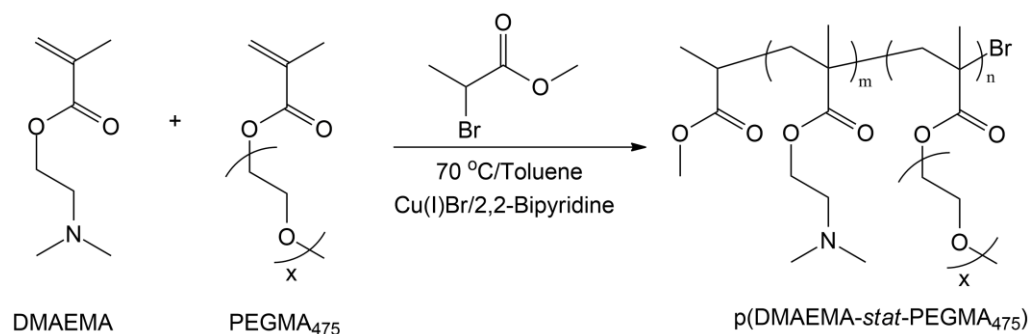


Figure 3-20. Reaction scheme for the synthesis of a random copolymer: p(DMAEMA-*stat*-PEGMA₄₇₅) (P3) via ATRP.

2,2-Bipyridine (0.02 g, 0.14 mmol), DMAEMA (0.11 g, 0.70 mmol), PEGMA₄₇₅ (3.01 g, 6.34 mmol), toluene (3.12 mL), methyl 2-bromopropionate (MBrP) (0.01 g, 0.07 mmol) and Cu(I)Br (0.01 g, 0.07 mmol) were added to a 10 mL tube fitted with a two way stopcock and sealed with a septum and placed into an oil bath at 70 °C for 5 h 50 min. The reaction mixture was

passed through aluminum oxide and washed through with chloroform to remove the catalyst. The polymer was precipitated in a 100:1 excess of petroleum ether to remove the un-reacted monomer. This produced 0.78 g of polymer (25 % yield). $^1\text{H-NMR}$ (400 MHz, CDCl_3) δ (ppm) 4.31-4.05 (m, 4H, CO-OCH_2) (both), 3.92-3.61 (m, 2xH, $\text{CO-OCH}_2\text{-(CH}_2\text{)}_x\text{O-CH}_3$), 3.60-3.51 (m, 3H, OCH_3), 2.52-2.32 (m, 2H, CH_2N), 2.15-1.90 (m, 6H, $\text{N(CH}_3\text{)}_2$), 1.31-0.85 (m, 4H, $\text{CH}_2\text{-MA backbone}$) (Appendix Page 331).

Figure 3-21 shows an example of $^1\text{H-NMR}$ spectra for the polymerisation of DMAMEA and PEGMA₄₇₅ to yield p(DMAEMA-*stat*-PEGMA₄₇₅) (P3). Overall monomer conversion was calculated from $^1\text{H-NMR}$ spectra (Figure 3-21, signals a and b) by comparing the vinyl proton signals from the monomers (5.4-6.4 ppm) to the overall integration across the range 4.1 to 4.6 ppm (Figure 3-21, signals c and f).

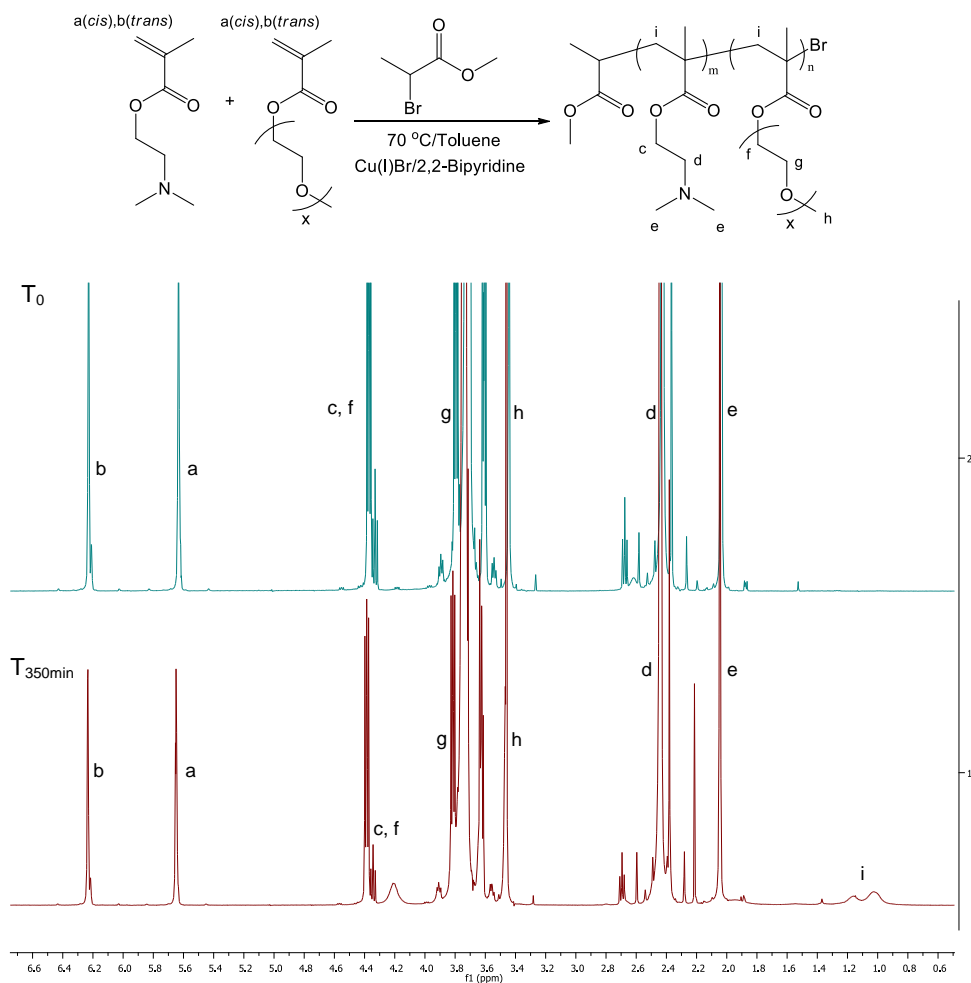


Figure 3-21. $^1\text{H-NMR}$ spectra for the polymerisation of DMAMEA and PEGMA₄₇₅ to yield p(DMAEMA-*stat*-PEGMA₄₇₅) (P3). Top: Reaction mixture at the beginning of the polymerisation (T_0). Bottom: Reaction mixture at 350 min of the polymerisation ($T_{350 \text{ min}}$).

A random copolymer of DMAEMA and PEGMA₄₇₅ was synthesised via ATRP method as above and selected properties are shown in Table 3-3. With the ratio of [DMAEMA]:[PEGMA₄₇₅]:[Initiator] = 10:90:1, the polymerisation of p(DMAEMA-*stat*-PEGMA₄₇₅) (P3) proceeded slowly, only 25 % of conversion was achieved after 6 h, and the PDI measured by GPC was found about 1.29.

Further experiments with a longer reaction time or different [DMAEMA]:[PEGMA₄₇₅]:[Initiator] ratios may need to be carried out.

Table 3-3. Summary of synthesis of p(DMAEMA-*stat*-PEGMA₄₇₅) (P3)

DMAEMA	PEGMA ₄₇₅	Conversion	Time (min)	M _n (GPC)	PDI
10 %	90 %	25 %	350	52915	1.29

Experimental conditions: 70 °C; Monomers/Toluene=1:1 (w/v); [I]/[CuBr]/[Bipy]=1/1/2. GPC analysis (chloroform, poly(styrene) standards). Polydispersity index (PDI) from GPC.

3.3.2 Reversible addition-fragmentation chain transfer polymerisation

(RAFT) method

General protocol for RAFT polymerisation:²⁰²

2-(ethylthiocarbonothioylthio)-2-methylpropanoic acid (CAT) was employed as the RAFT agent, 4,4'-azobis(4-cyanovaleric acid) (V-501) as the initiator.

Polymerisations were conducted in round bottom flasks sealed with a rubber septum and parafilm. An NMR spectrum was recorded at the beginning of the experiment. The polymerisation solutions were degassed using argon for at least 10 min and transferred to an oil bath preheated to 70 °C. After reaction, the solution was quenched by cooling in ice-water and opening to air. Another NMR spectrum was recorded to enable calculation of degree of conversion. The polymer was purified by dialysis in water with dialysis membrane (MWCO 1000). The molar mass of all the polymers made was estimated from the monomer conversion and GPC data. For the removal of a RAFT end-group, the reaction was carried out at 70 °C.

3.3.2.1 Polymer conversion calculations

The overall monomer conversion was calculated by $^1\text{H-NMR}$ spectra by comparing the vinyl proton signals from the monomers (5.6 and 6.1 ppm) to the overall integration from CHCl_3 (around 7.26 ppm) (50 μL was added to each NMR sample as the standard for calculation) in the case of (meth)acrylamide-based monomers, including DMAPMAm, AMPS, 2-AmAA and 4-AmBA.

3.3.2.2 Poly[N-(3-(dimethylamido)propyl)methacrylamide] [p(DMAPMAm)] (P4)

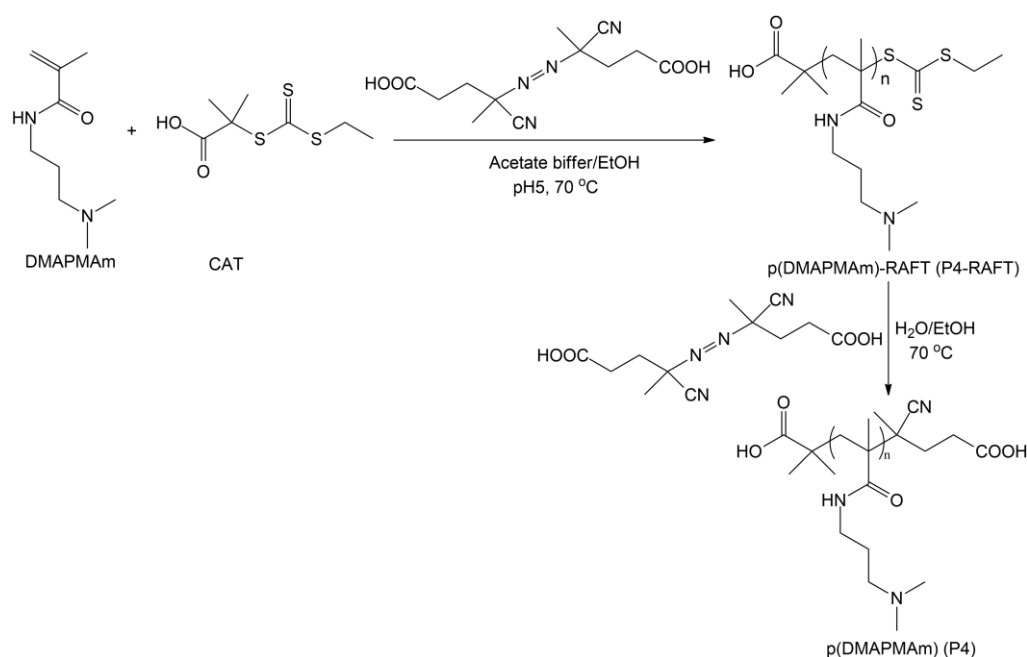


Figure 3-22. Reaction schemes for the synthesis of p(DMAPMAm) (P4) via RAFT method and the removal of RAFT end-group.

In a typical RAFT polymer synthesis experiment, DMAPMAm (1000 mg, 5.874 mmol, 0.75 M) in acetate buffer solution (10 mM, 6.768 mL), 2-(ethylthiocarbonothioylthio)-2-methylpropanoic acid (CAT) (0.059 mmol, 0.24 M) in ethanol (0.245 mL) and V-501 (1.65 mg, 0.006 mmol, 0.03 M) in ethanol (0.196 mL) were prepared separately and then mixed together (to make a final ratio 100:1 of monomer to RAFT agent). The polymerisation was carried out overnight. The p(DMAPMAm)-RAFT was purified by dialysis against water and recovered as a light yellow powder (716.8 mg, 72 %) after freeze-drying from water (3 days). The p(DMAPMAm)-RAFT polymer (428 mg) in water and V-501 (258 mg) in ethanol were prepared separately and then mixed together (to make a final ratio 1:30 of polymer to initiator). In order to remove the RAFT end-group, this mixture was degassed and reacted at 70 °C overnight. The title compound p(DMAPMAm) (P4) was purified by dialysis against water and recovered as a white powder (369 mg, 86 %) after freeze-drying from water (3 days). ¹H-NMR (400 MHz, D₂O) δ (ppm) 3.33-2.95 (m, 4H, NH-CH₂-CH₂-CH₂), 2.96-2.71 (m, 6H, N(CH₃)₂), 2.04-1.48 (m, 2H, NH-CH₂-CH₂), 1.18-0.69 (m, 2H, CH₂-MAm backbone). IR ν (cm⁻¹) 3329 (N-H), 2963, 2687 (C-H), 1618 (C=O), 1522 (N-H), 1462 (C-H), 1202 (C-N). The spectra of ¹³C-NMR of monomer DMAPMAm and GPC of polymer p(DMAPMAm) are shown in Appendix Page 332.

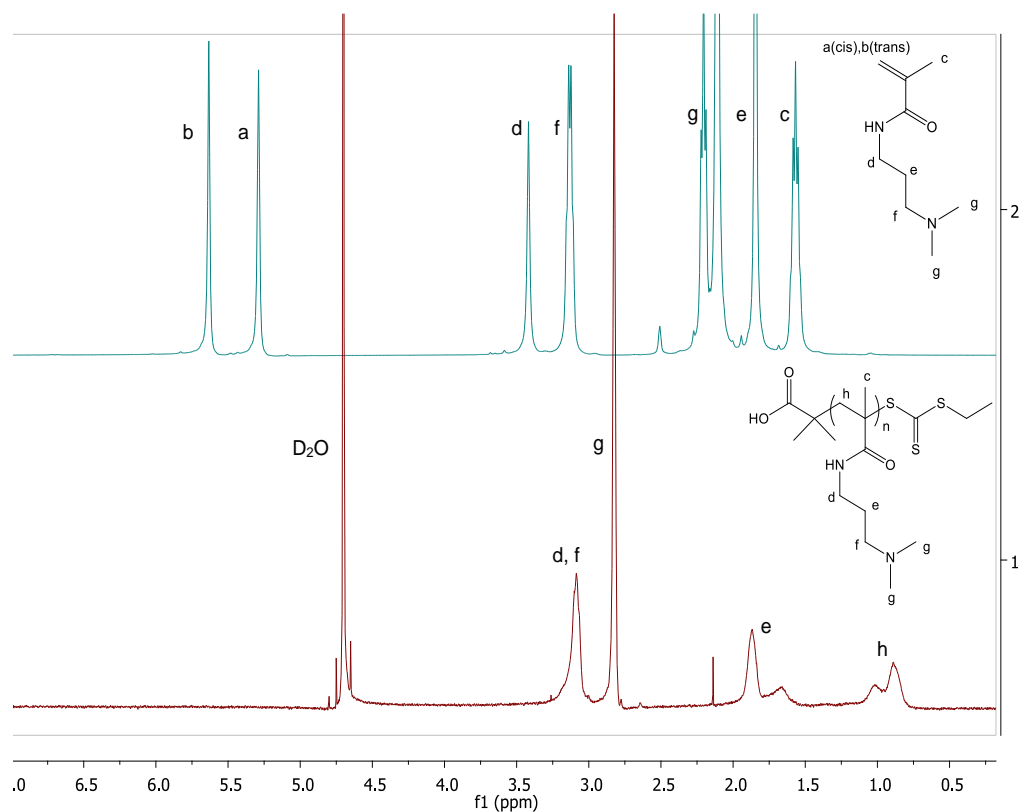


Figure 3-23. $^1\text{H-NMR}$ spectra for the polymerisation of DMAPMam to yield p(DMAPMam) (P4). Top: Monomer DMAPMam. Bottom: Purified polymer p(DMAPMam) (P4).

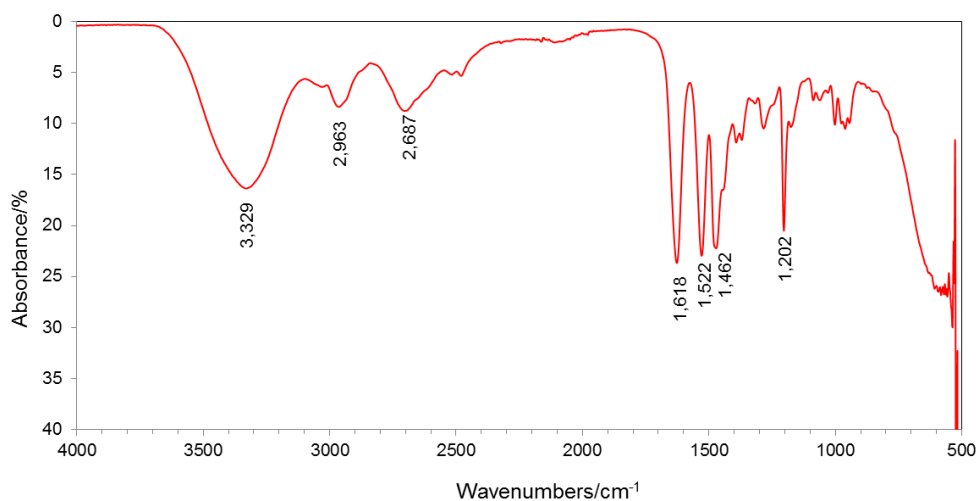


Figure 3-24. Representative FTIR for p(DMAPMam) (P4).

P(DMAPMAM) (P4) homopolymers were synthesised using the general polymerisation procedure as described above. In the reaction conditions, CAT was used as chain transfer agent (CTA) and V-501 was used as a water-soluble initiator. DMAPMAM monomer was initially dissolved in 10 mM acetate buffer solution pH 5.5. CAT and V-501 were dissolved in ethanol to reach the concentration of 0.24 M and 0.03 M respectively as stock solutions. The above three portions were mixed to get a final molar ratio of 100:1:0.1 (monomer:CAT:V-501) and monomer concentration of 0.75 M. Temperature was controlled to be 70 °C all through the reaction. After 16 hours reaction, the mixture was cloudy and hard to dissolve in any solvent. This phenomenon suggested that polymerisation was occurred. In order to obtain polymers with different molecular weights, synthesis of p(DMAPMAM) (P4) with three targeted degrees of polymerisation (DPs) 50, 100 and 200 were carried out. The stock solutions of CAT and initiator were fresh made for each polymerisation. Also, the oxygen-excluding process was checked and carried out very carefully. Cationic aqueous GPC was used to characterise p(DMAPMAM) (P4). A summary of properties for the synthesis of p(DMAPMAM) (P4) is shown in Table 3-4. Generally the conversion was above 70 % after 16 h

Table 3-4. Summary of synthesis of p(DMAPMAm) (P4) via RAFT

No.	[M]:[CAT] ^a	DP ^b	Conversion (¹ H-NMR)	Time (h)	M _n (GPC)	PDI
1a	50	45	91 %	16	-	-
1b		38	77 %	19	5820	1.43
2a	100	27	27 %	2.5	-	-
2b		88	88 %	16	-	-
2c		83	83 %	19	9253	1.50
3a	200	167	84 %	16	-	-
3b		150	75 %	19	15641	1.69

^a Molar ratio of [Monomer]:[Initiator] (targeted DP). ^b The actual degree of polymerisation (DP) in the brackets is the final value calculated from ¹H-NMR. GPC analysis (eluent-200 mM NaCl with 0.1 % trifluoroacetic acid, polyvinylpyrrolidone standards). Polydispersity index (PDI) from GPC.

3.3.2.3 Poly(2-acrylamido-2-methyl-1-propanesulfonic acid) [p(AMPS)]

(P5)

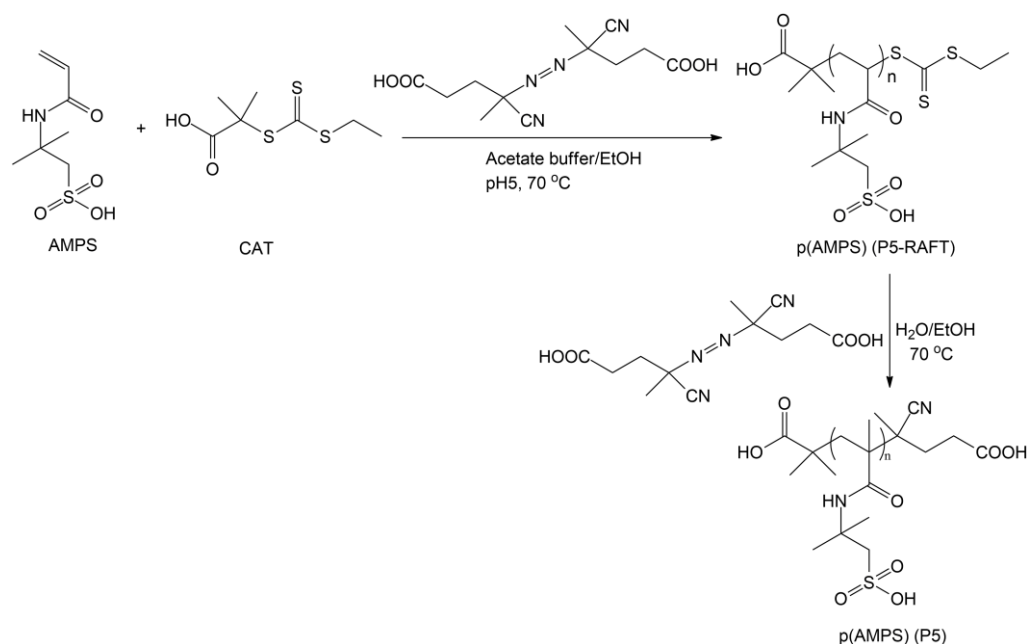


Figure 3-25. Reaction schemes for the synthesis of p(AMPS) (P5) via RAFT method and the removal of RAFT end-group.

Similar RAFT experiment as DMAPMAm was carried out. AMPS (1000 mg, 4.83 mmol, 0.75 M) in acetate buffer solution (10 mM, 6.43 mL), CAT (0.048 mmol, 0.24 M) in ethanol (0.2 mL) and V-501 (1.4 mg, 0.005 mmol, 0.03 M) in ethanol (0.167 mL) were prepared separately and then mixed together (to make a final ratio 100:1 of monomer to RAFT agent). The polymerisation was carried out overnight. The p(AMPS)-RAFT was purified by dialysis against water and recovered as a light yellow powder (869 mg, 87 %) after freeze-drying from water (3 days). The p(AMPS)-RAFT (255 mg) in water and V-501 (200 mg) in ethanol were prepared separately and then mixed together (to make a final ratio 1:30 of polymer to initiator). In order to remove the RAFT end-group, this mixture was degassed and reacted at 70 °C overnight. The title compound p(AMPS) (P5) was purified by dialysis against water and recovered as a white powder (230 mg, 90 %) after freeze-drying from water (3 days). ¹H-NMR (400 MHz, D₂O) δ (ppm) 7.82-7.20 (m, 1H, NH), 3.65-3.02 (m, 2H, CH₂-SO₃H), 2.27-1.84 (m, 1H, CH-Am backbone), 1.61-1.30 (m, 6H, C(CH₃)₂). IR ν (cm⁻¹) 3298 (N-H), 2916 (C-H), 1638 (C=O), 1531 (N-H), 1439 (C-H), 1368 (C-N), 1179, 1040 (SO₂), 621 (S-O). The spectra of ¹³C-NMR of monomer AMPS and GPC of polymer p(AMPS) are shown in Appendix Page 333.

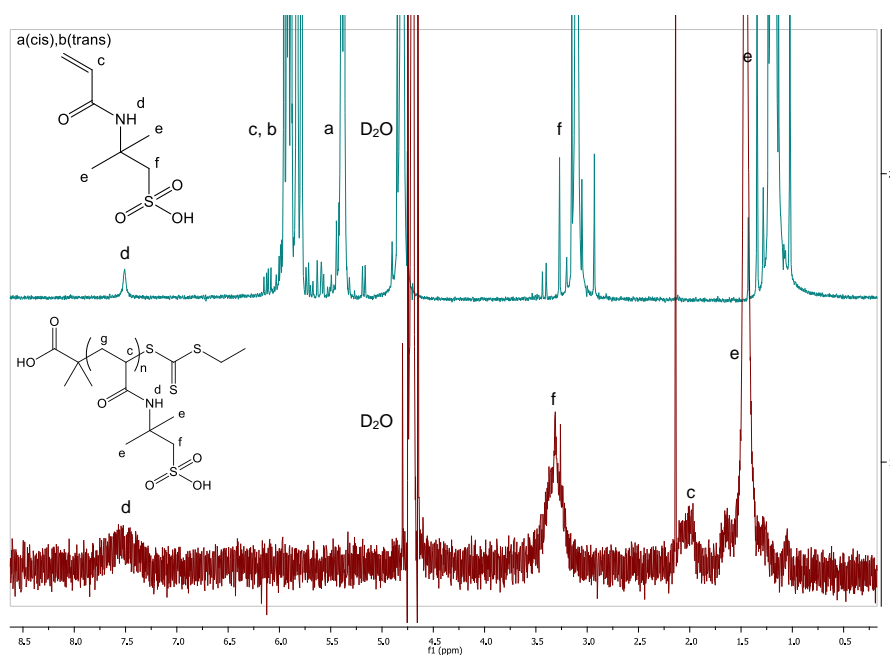


Figure 3-26. $^1\text{H-NMR}$ spectra for the polymerisation of AMPS to yield p(AMPS) (P5). Top: Monomer AMPS. Bottom: Purified polymer p(AMPS) (P5).

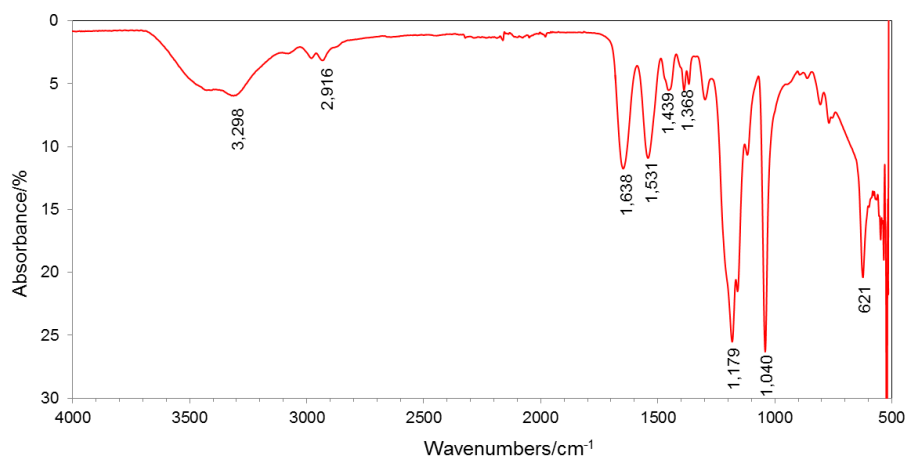


Figure 3-27. Representative FTIR for p(AMPS) (P5).

P(AMPS) (P5) homopolymers were synthesised by using the general polymerisation procedure as described above. After 3 hours reaction, the mixture was cloudy and hard to dissolve in any solvent. This phenomenon suggested that polymerisation was occurred. In order to obtain polymers with

different molecular weights, synthesis of p(AMPS) homopolymer with four targeted degrees of polymerisation (DPs) 40, 70, 100 and 200 were carried out, generally the conversion was above 75 %. Aqueous GPC was used to characterise p(AMPS) (P5). A summary of synthesis of pAMPS (P5) is shown in Table 3-5.

Table 3-5. Summary of synthesis of p(AMPS) (P5) via RAFT

No.	Monomer	DP ^a	Conversion (¹ H-NMR)	Time (h)	M _n (Theoretical)	M _n (GPC)	PDI
1	AMPS	38	96 %	2	8100	-	-
2	AMPS	53	75 %	1	11208	-	-
3	AMPS	99	99 %	3	20120	21787	1.14
4	AMPS	200	100 %	16	41674	47561	1.19

^a The actual degree of polymerisation (DP) in the brackets is the final value calculated from ¹H-NMR. Theoretical, from monomer/initiator ratio and monomer conversion. GPC analysis (eluent-DPBS, poly(ethylene oxide) standards). Polydispersity index (PDI) from GPC.

3.3.2.4 Poly(2-acrylamidoacetic acid) [p(2-AmAA)] (P6)

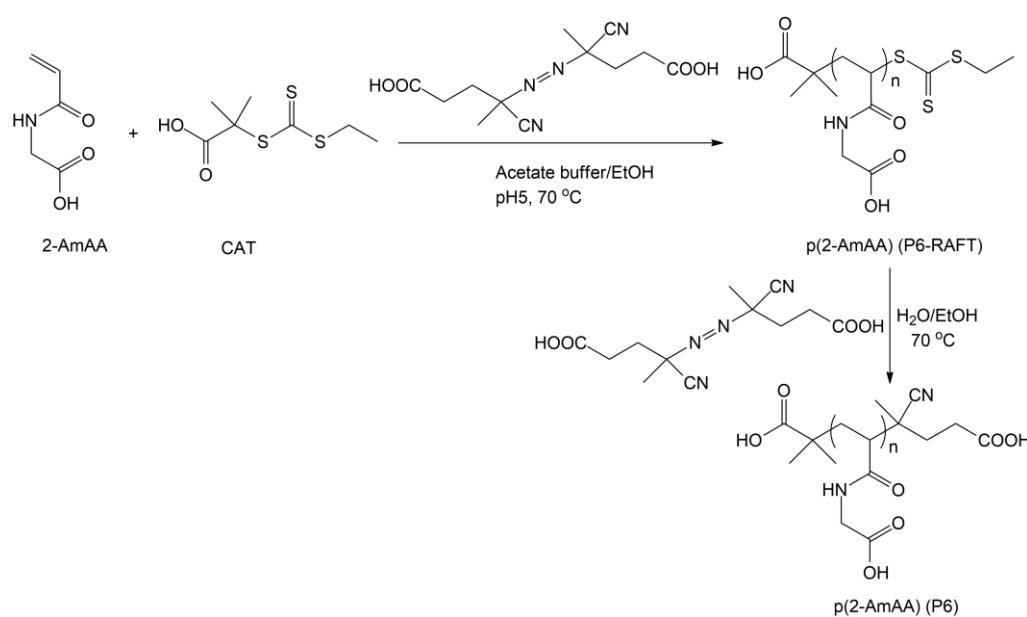


Figure 3-28. Reaction schemes for the synthesis of p(2-AmAA) (P6)

homopolymer via RAFT method and the removal of RAFT end-group.

2-AmAA (1000 mg, 7.75 mmol, 0.75 M) in acetate buffer solution (10 mM, 10.3 mL), CAT (0.077 mmol, 0.24 M) in ethanol (0.322 mL) and V-501 (2.17 mg, 0.008 mmol, 0.03 M) in ethanol (0.226 mL) were prepared separately and then mixed together. The polymerisation was carried out for 3 h. The polymer was purified by dialysis against water and recovered as a light yellow powder (542 mg, 54 %). In order to remove the RAFT end-group, the p(2-AmAA)-RAFT polymer (542 mg) in water and V-501 (150 mg) in ethanol were prepared separately and then mixed together. The title compound p(2-AmAA) was purified by dialysis against water and recovered as a white powder (490.8 mg, 91 %) after freeze-drying from water (3 days). $^1\text{H-NMR}$ (400 MHz, D_2O) δ (ppm) 4.09-3.27 (m, 2H, NH-CH_2), 2.38-1.88 (m, 1H, CH-Am backbone), 1.79-1.17 (m, 2H, CH_2 -Am backbone). IR ν (cm^{-1}) 3250 (N-H), 2932 (C-H), 1549 (N-H), 1383 (C-O), 1233 (O-H), 1018 (C-N). The GPC spectra of polymer p(2-AmAA) are shown in Appendix Page 334.

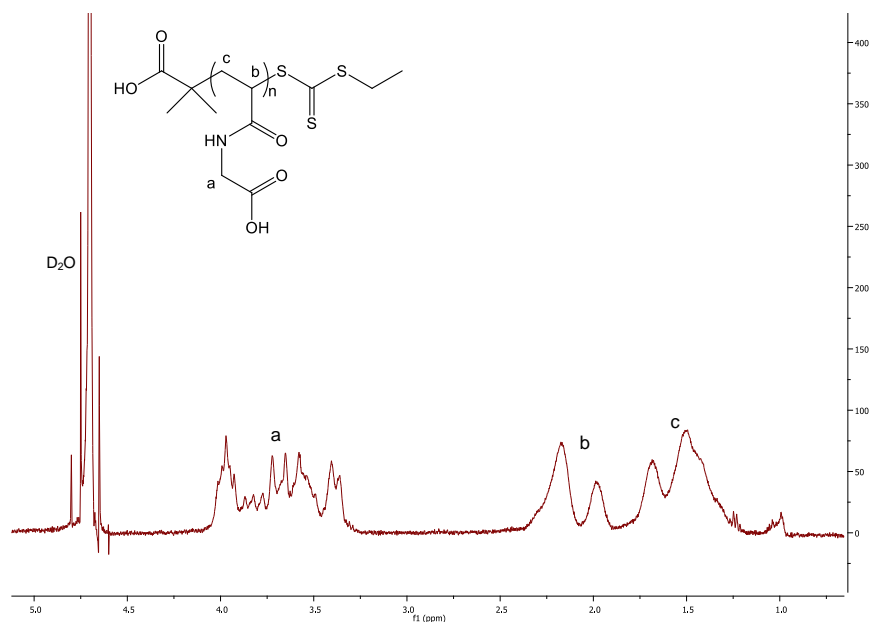


Figure 3-29. $^1\text{H-NMR}$ spectra for p(2-AmAA) (P6).

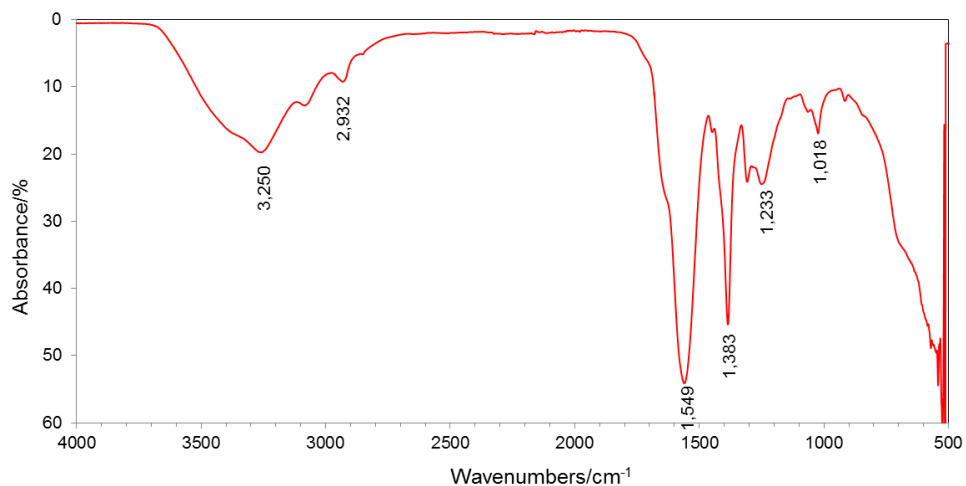


Figure 3-30. Representative FTIR for p(2-AmAA) (P6).

P(2-AmAA) (P6) homopolymers were also prepared by using the above polymerisation procedure similar as described in section 3.3.2.2. Table 3-6 shows some properties of p(2-AmAA) (P6) prepared in this study. Synthesis of p(2-AmAA) homopolymer with several targeted degrees of polymerisation (DPs) 20, 50, 100 and 200 were carried out. Aqueous GPC was used to characterise p(2-AmAA) (P6).

Table 3-6. Summary of synthesis of p(2-AmAA) (P6) via RAFT

No.	Monomer	DP ^a	Conversion (¹ H-NMR)	Time (hours)	M _n (Theoretical)	M _n (GPC)	PDI
1	2-AmAA	18	90 %	3	2322	2501	-
2	2-AmAA	46	80 %	2.5	6158	6153	1.07
3	2-AmAA	72	72 %	2.5	9296	14513	1.05
4	2-AmAA	150	75 %	16	19350	26205	1.09

^a The actual degree of polymerisation (DP) in the brackets is the final value calculated from ¹H-NMR. Theoretical, from monomer/initiator ratio and monomer conversion. GPC analysis (eluent-DPBS, poly(ethylene oxide) standards). Polydispersity Index (PDI) from GPC.

3.3.2.5 Poly(4-acrylamidobutanoic acid) [p(4-AmBA)] (P7)

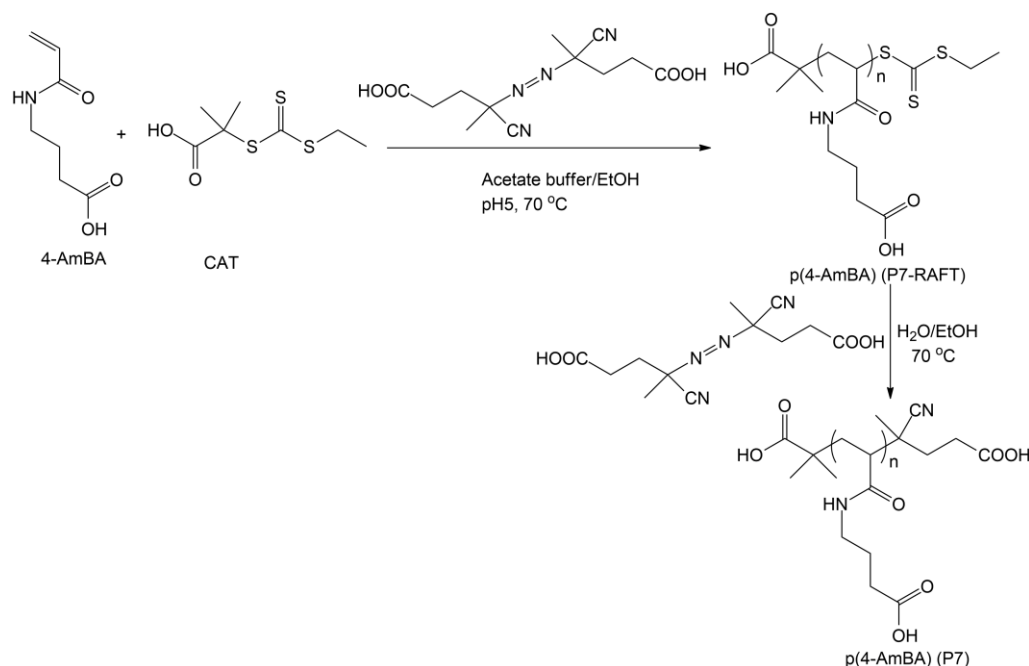


Figure 3-31. Reaction schemes for the synthesis of p(4-AmBA) (P7) homopolymer via RAFT method and the removal of RAFT end-group.

4-AmBA (2000 mg, 12.7 mmol, 0.75 M) in acetate buffer solution (10 mM, 17.0 mL), CAT (0.127 mmol, 0.24 M) in ethanol (0.529 mL) and V-501 (3.57 mg, 0.013 mmol, 0.03 M) in ethanol (0.372 mL) were prepared separately and then mixed together. The polymerisation was carried out overnight. The polymer was purified by dialysis against water and recovered as a light yellow powder (1804 mg, 90 %) after freeze-drying from water (3 days). The p(4-AmBA)-RAFT polymer (200 mg) in water and V-501 (150 mg) in ethanol were prepared separately and then mixed together to remove the RAFT end-group. The title compound p(4-AmBA) was purified by dialysis against water and recovered as a white powder (192.2 mg, 96 %) after freeze-drying

from water (3 days). $^1\text{H-NMR}$ (400 MHz, D_2O) δ (ppm) 3.21-2.92 (m, 2H, NH-CH_2), 2.29-2.14 (m, 2H, $\text{CH}_2\text{-COOH}$), 2.00-1.79 (m, 1H, CH-Am backbone), 1.79-1.57 (m, 2H, $\text{CH}_2\text{-CH}_2\text{-CH}_2$), 1.58-1.25 (m, 2H, $\text{CH}_2\text{-Am backbone}$). IR ν (cm^{-1}) 3240 (N-H), 2916 (C-H), 1636 (C=O), 1535 (N-H), 1395 (C-O), 1175 (O-H), 1042 (C-N). The GPC spectra of polymer p(4-AmBA) are shown in Appendix Page 334.

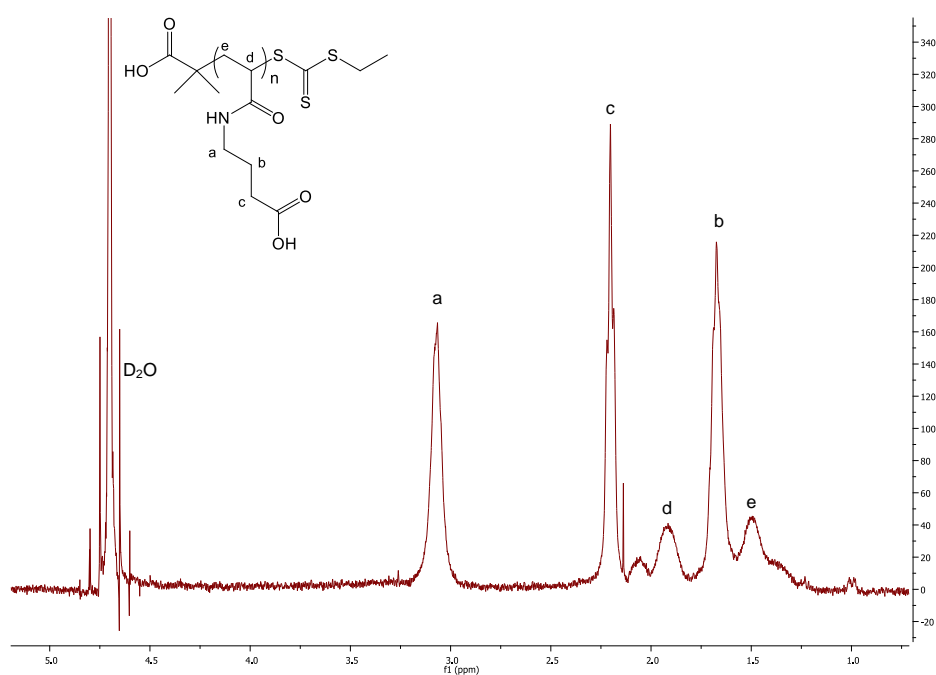


Figure 3-32. $^1\text{H-NMR}$ spectra for p(4-AmBA) (P7).

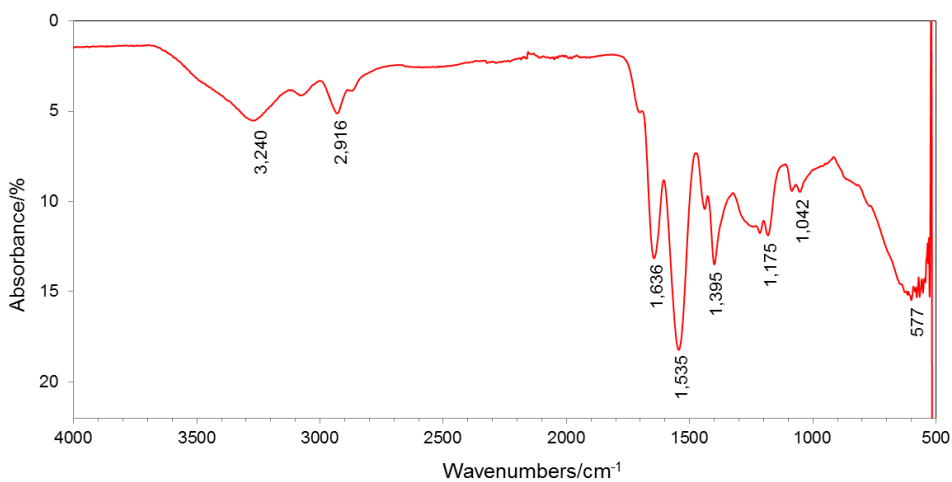


Figure 3-33. Representative FTIR for p(4-AmBA) (P7).

Similar as described in section 3.3.2.2, p(4-AmBA) (P7) homopolymers were synthesised with four targeted (theoretical) DPs 20, 50, 100 and 200. Aqueous GPC was used to characterise p(4-AmBA) (P7). Generally the conversion was around 90 % as shown in Table 3-7.

Table 3-7. Summary of synthesis of p4-AmBA (P7) via RAFT

No.	Monomer	DP ^a	Conversion (¹ H-NMR)	Time (h)	M _n (Theoretical)	M _n (GPC)	PDI
1	4-AmBA	21	92 %	3	3521	3492	1.09
2	4-AmBA	50	100 %	16	8074	10829	1.04
3	4-AmBA	100	100 %	16	15924	16804	1.09
4	4-AmBA	200	100 %	16	31624	31132	1.06

^a The actual degree of polymerisation (DP) in the brackets is the final value calculated from ¹H-NMR. Theoretical, from monomer/initiator ratio and monomer conversion. GPC analysis (eluent-DPBS, poly(ethylene oxide) standards). Polydispersity index (PDI) from GPC.

3.3.3 Poly[[2-(methacryloyloxy)ethyl]trimethylammonium chloride-co-N-[2-(methacryloyloxy)ethyl]-dimethyl-(2-sulfoethan)aminium hydroxide] [p(METMAC-co-MEDSAH)] (P8)

A cationic/zwitterionic copolymer of [2-(methacryloyloxy)ethyl]trimethylammonium chloride and N-[2-(methacryloyloxy)ethyl]-dimethyl-(2-sulfoethan)aminium hydroxide [p(METMAC-co-MEDSAH)] (P8) was synthesised and kindly supplied by Dr. Eugene Peter Magennis. Molar ratio of METMAC: MEDSAH was 1:1.

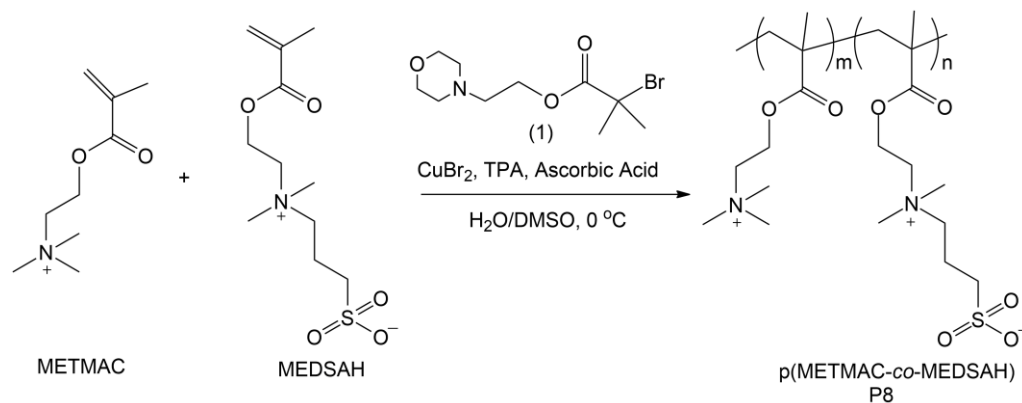


Figure 3-34. Reaction scheme for the synthesis of p(METMAC-co-MEDSAH) (P8) by Dr. Eugene Peter Magennis.

To a reaction flask, 144 mg (0.695 mmol) of METMAC, 194 mg (0.695 mmol) of MEDSAH, 1.554 mg (5.6 μ mol) of 2-(N-Morpholino)ethyl-2-bromobutyrate (1), 200 μ L of a 0.069 M aqueous solution with CuBr₂ and Tris(2-pyridylmethyl)amine (TPA), and 50 μ L of DMSO were added. This mixture was degassed for 30 minutes over ice after which 270 μ L of a degassed 1 mg/mL solution of ascorbic acid were added to begin the polymerisation. The polymerisation was monitored by ¹H-NMR spectroscopy over time and terminated by exposing to air. The polymers were obtained by dialysis against water for 3 days followed by freeze drying to yield a white amorphous solid (P8). ¹H-NMR (D₂O, 400 MHz) δ (ppm) 4.49 (m, 4H, COCH₂) (METMAC and MEDSHA), 3.78 (m, 4H, NCH₂) (METMAC and MEDSAH), 3.60 (m, 2H, N(CH₃)₂CH₂) (MEDSAH), 3.2 (m, 15H, N(CH₃)) (both), 2.98 (m, 2H, CH₂SO₃) (MEDSAH), 2.28 (m, 2H, CH₂CH₂CH₂) (MEDSAH), 2.30-1.75 (m, 4H, CH₂-MA) (METMAC and MEDSAH), 0.99-2.00 (m, 6H, CH₃) (METMAC

and MEDSAH). IR ν (cm^{-1}) 3393 (R_4N^+), 2941 (C-H), 1715 (C=O), 1474 (C-H), 1153, 1032 (SO_2), 946 (C-C), 713 (S-O).

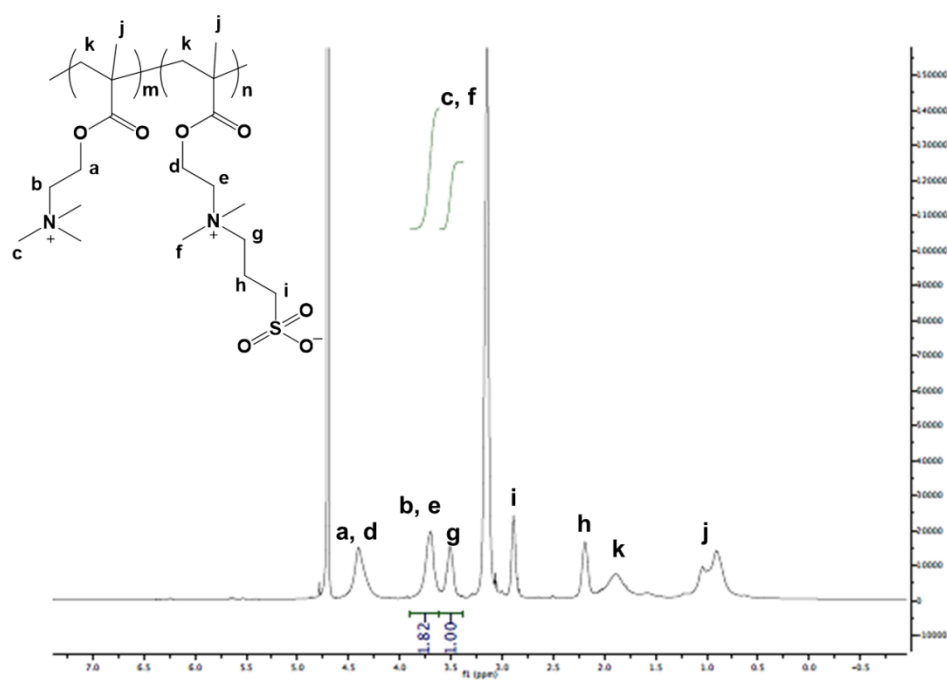


Figure 3-35. Representative ^1H -NMR spectra of p(METMAC-*co*-MEDSAH) (P8) by Dr. E. Peter Magennis.

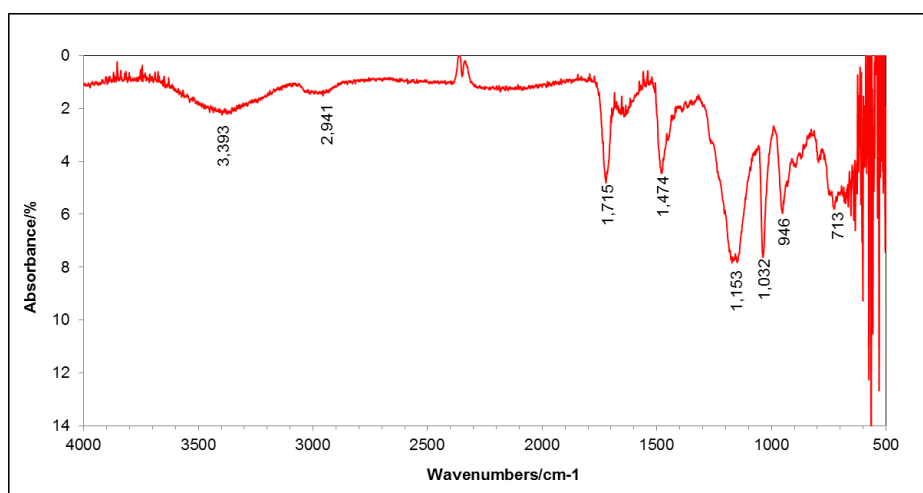


Figure 3-36. Representative FTIR for p(METMAC-*co*-MEDSAH) (P8).

3.4 General discussion and conclusions

As mentioned in Introduction Chapter, the effects of polymers on protein crystallisation are expected to depend strongly on the polymer functionalities. From previous researchers' studies, PEG has been found to be an effective additive in promoting the crystallisation of a range of proteins.^{124, 125} However, the PEG has a high molecular weight limitation of around 40 kDa,²⁰³ because PEG above that molecular weight will no longer be cleared from the kidney.²⁰⁴ Moreover, PEG itself has limited chemical functionality, and cannot be derivatised easily to introduce groups which can form specific bonds with protein peptide residues. We thus chose poly(ethylene glycol) methyl ether methacrylate₄₇₅ (PEGMA₄₇₅), as a neutral methacrylate derivative of PEG to obtain a polymer, p(PEGMA₄₇₅) (P1), analogous to PEG but with hydrophilic side-chain functionality and a hydrophobic main-chain. The PEGMA exhibits a similar biocompatible profile as PEG however since the PEG side chain of the PEGMA is linked by a cleavable ester bond the size limitations for poly(PEGMA) will not be the same as for PEG. Moreover, poly(PEGMA)-based materials have been shown to mediate protein crystallisation in solution.¹⁰⁸

To test the effects of varying degrees of charge on protein crystallisation, monomers containing tertiary amine groups were selected to afford positive charges, including one methacrylate monomer 2-(dimethylamino)ethyl methacrylate (DMAEMA) which was either homopolymerised (P2) and quaternised

or copolymerised with PEGMA₄₇₅ (P3) and one methacrylamide monomer N-(3-(dimethylamido)propyl)methacrylamide (DMAPMAm), which was also homopolymerised (P4) to form cationic polymers. The tertiary amines functionalities were designed to enhance water solubility of the polymers²⁰⁵ and also to provide lone-pair donor or charged residues dependent on pH and degree of protonation or quaternisation.

Anionic polymers were chosen according to the pKa of the polymers, and also by considering the protein crystallisation pH, such that the polymers could provide charged residues under relevant crystallising conditions. We chose three acrylamide-based main chain monomers, including 2-acrylamido-2-methyl-1-propanesulfonic acid (AMPS), 2-acrylamidoacetic acid (2-AmAA) and 4-acrylamidobutanoic acid (4-AmBA), due to the presence of ionisable sulfonic acid or carboxyl groups, which could introduce of some negative charges and generate anionic water soluble homopolymers (P5-7). Moreover, a cationic/zwitterionic copolymer of [2-(methacryloyloxy)ethyl]trimethylammonium chloride (METMAC) and N-[2-(methacryloyloxy)ethyl]-dimethyl-(2-sulfoethan)aminium hydroxide (MEDSAH) with both positive charges and zwitterionic components was prepared in order to span an even wider range of charge-charge interactions (P8).

P(PEGMA₄₇₅) (P1), p(DMAEMA) (P2), and a random copolymer of p(DMAEMA-*stat*-PEGMA₄₇₅) (molar ratio of 1:9) (P3) were prepared by a

variant of published ATRP route, which has been used for the synthesis of methacrylate monomers showing fast ATRP kinetics with low polydispersities by using Cu(I)Br/2,2-bipyridine (Bipy) catalytic system and methyl 2-bromopropionate (MBrP) as the initiator.¹⁴³ N-Methylation of p(DMAEMA) with different degrees of quaternisation was carried out to vary the total permanent cation content by the addition of a methyl group to the tertiary amine repeating unit with CH₃I according to literature procedure.^{199, 200} CHCl₃ was employed for the GPC analysis of those methacrylate polymers. However, those polymers produced had slightly broad PDIs from GPC analysis. Also the M_n differed from that calculated by ¹H-NMR, is explained by the conventional calibration used on the GPC. This broadening suggests that more closely matched calibration standard rather than polystyrene may need in the future studies.

Monomers 2-AmAA and 4-AmBA were prepared in good yields and high purity by modified literature protocols.^{190, 191} P(DMAPMAm) (P4), p(AMPS) (P5), p(2-AmAA) (P6) and p(4-AmBA) (P7) were synthesised using RAFT methods according to protocols described in the literature,²⁰² because RAFT polymerisation is probably the most versatile and suitable for the synthesis of acrylamide based polymers.²⁰⁶ The polymerisation employed 2-(Ethylthiocarbonothioylthio)-2-methylpropanoic acid (CAT) as RAFT agent and 4,4'-azobis(4-cyanovaleric acid) (V-501) as the initiator. Aqueous conditions (eluent-200 mM NaCl with 0.1 % TFA or DPBS) were applied for

the GPC analysis of those (meth)acrylamide polymers. It is known that RAFT agent reacts with a propagating polymer chain and forms a macro-RAFT agent. In order to preclude the influence of dithioester on proteins, we used the same initiator to substitute dithioester on the polymer. A cationic/zwitterionic copolymer of p(METMAC-*co*-MEDSAH) (P8) was kindly supplied by Dr. E. Peter Magennis; METMAC: MEDSAH molar ratio is 1:1.

In these ways, four classes of materials, including neutral, cationic, anionic and cationic/zwitterionic polymers based on methacrylate or (meth)acrylamide monomers with varying degrees of charge, molecular weight and backbone structure were successfully prepared and then investigated for crystallisation studies.

CHAPTER 4

4. Application of Polymers to Hen Egg-white Lysozyme (HEWL) Crystallisation

4.1 Introduction

As 'Chapter 3' mentioned, four classes of materials, including neutral, cationic, anionic and cationic/zwitterionic polymers based on methacrylate or (meth)acrylamide monomers were successfully prepared. In the present chapter their effect as additives in crystallisation of HEWL is investigated.

The first model protein was hen egg-white lysozyme (HEWL), as this protein has become the most preferred crystallisation system for the majority of protein crystallisation studies. It is readily available and relatively straightforward to crystallise in a specific polymorph (the tetragonal form) within one day. We then designed experimental protocols to investigate the effects of polymers on protein crystal size, crystal packing motifs, and polymorphic forms under crystallisation conditions normally favouring the tetragonal HEWL polymorph. The isoelectric point (pI) of HEWL is 11.35, therefore when at its crystallisation pH 4.8, HEWL macromolecules are positively charged, i.e. cationic (Table 4-1).¹⁵²

Table 4-1. Summary of hen egg-white lysozyme (HEWL)

Protein	pI ^a	Mw (kDa)	Crystallisation pH
HEWL 	11.35	14.3	4.8

^a Isoelectric point (pI) is the pH at which a particular molecule or surface carries no net electrical charge.

In order to investigate the effects of polymers on protein crystallisation, such as the use of polymers to help proteins crystallise, or the use of polymers to guide proteins to associate into protein-protein dimer, trimer and higher order complexes, we prepared different classes of polymers with varying degrees of charge, molecular weight and backbone structure, and then studied their role as additives in model protein solutions. The guiding hypothesis was that select functional polymers in the solution could enhance the rate of protein crystallisation from solutions, as well as influence morphology shape, size, habit and polymorph of the crystal. A simple hypothesis linking polymer structure and charge to the effect on protein crystallisation is proposed and shown in Figure 4-1. Details will discuss later. Protein crystallisation experiments were performed on 96-well plates, by using the sitting drop vapour diffusion technique.

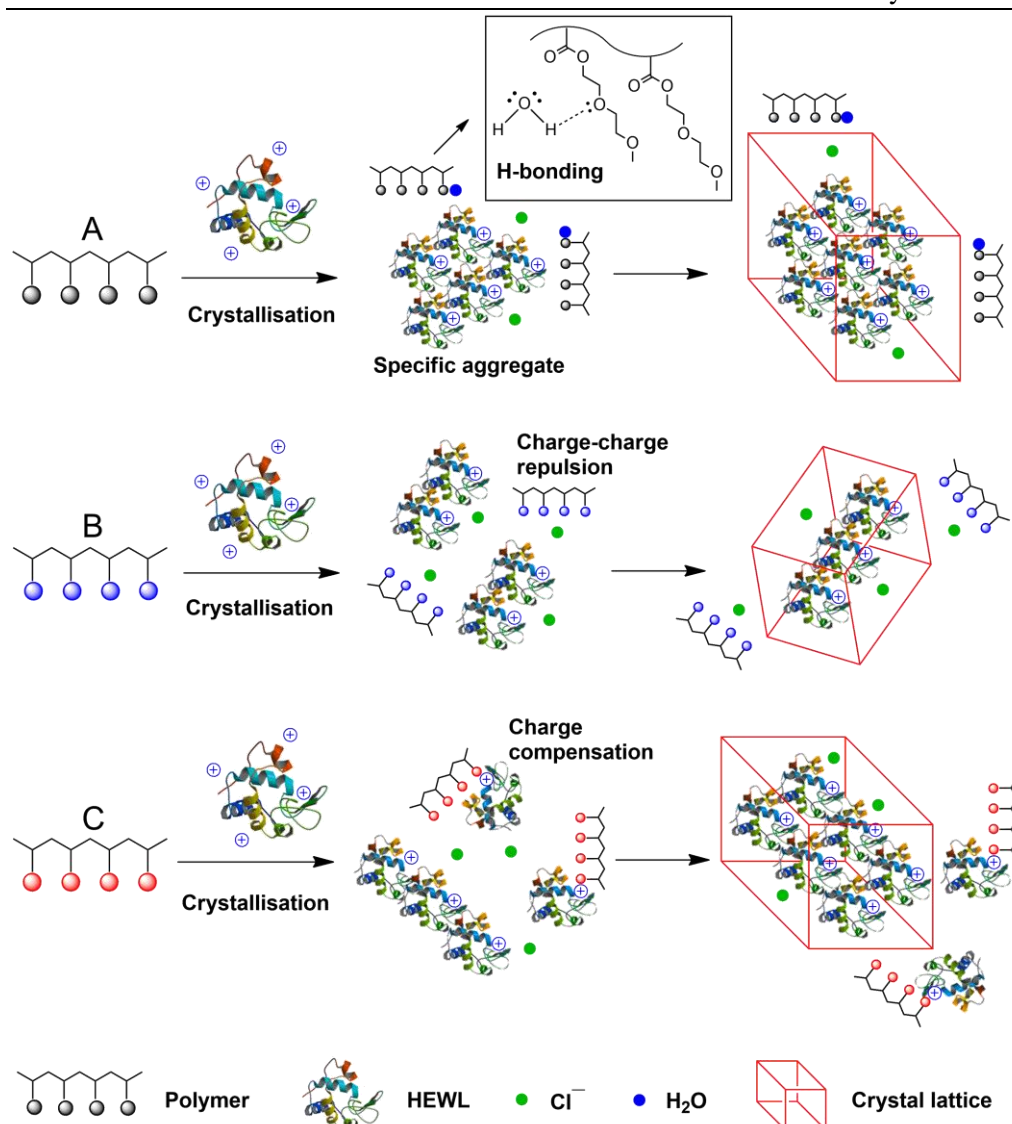


Figure 4-1. Schematic representation of the interaction of various polymers with cationic HEWL in the protein crystallisation process. (A) Neutral polymer: H-bonding with water and thus promoting protein crystallisation via a dehydration mechanism. (B) Cationic polymer: charge-charge repulsions between cationic polymer and cationic HEWL. (C) Anionic polymer: attracting cationic HEWL for charge compensation. HEWL macromolecules are positively charged at tetragonal crystallisation pH of 4.8, i.e. cationic. Cl^- ions are derived from the crystallisation buffer solutions.

4.2 Methods

4.2.1 Crystallisation technique and plate

The technique used for protein crystallisation was the sitting drop vapour diffusion method, which is the most popular, as it can be used to screen a broad range of crystallisation conditions, using small amounts of materials, but can also be scaled up in order to obtain large crystals for X-ray diffraction analysis. MRC 2 Well Crystallisation Plates (Swissci) (UVP plate, 96 reservoir wells, reservoir volume: 50 to 100 μl , with 2 corresponding sample wells: 5 μl max fill volume) were purchased from Hampton Research (Figure 4-2). Specifically, a solution (50 μL) of tested polymer buffer was pipetted in triplicate in the reservoir wells. Protein solution (1 μL) and buffered polymer solution (as described above, 1 μL) were pipetted into sample wells of the crystallisation plate. Generally, a drop of 1:1 protein: polymer solution was usually used here.

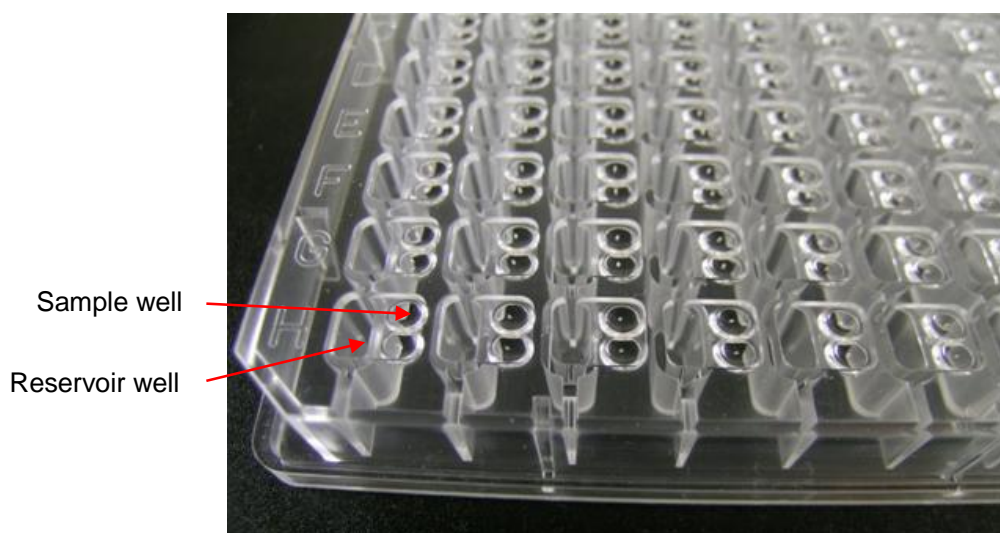


Figure 4-2. MRC 2 Well Crystallisation Plate (Swissci), commercially available from Hampton Research.

The entire crystallisation plate system was sealed using transparent sealing tape (with a chemically inert adhesive). This prevents solvent being lost to the external environment. The differences in polymer and ions concentration between the drop and the reservoir solution causes water to evaporate from the drop, resulting in an increase of the supersaturation level within the sitting drop. This continues until the concentration of the polymer in the drop is the same as in the reservoir well solution. Thus, equilibration takes place through the vapour phase. Over time, protein nucleation will take place (Figure 4-3).

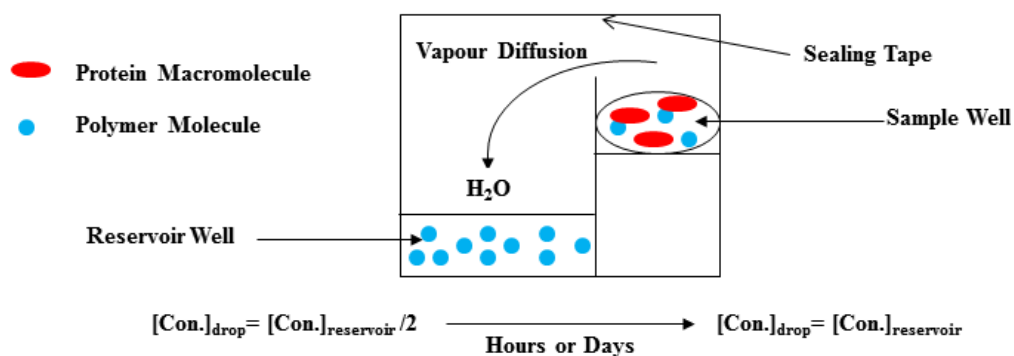


Figure 4-3. Diagram depicting the sitting drop vapour diffusion technique. The reservoir has usually twice the polymer concentration than the sitting drop. Water vapour diffusion takes place in a single well environment.

At the beginning of the experiment, water vapour diffusion from the sitting drop to the reservoir solution causes a reduction in the volume of the sitting drop, which in turn increases the supersaturation level of all the solutes within it. Over time, the rate of supersaturation eventually decreases due to the precipitation of protein or other solutes (Figure 4-4).

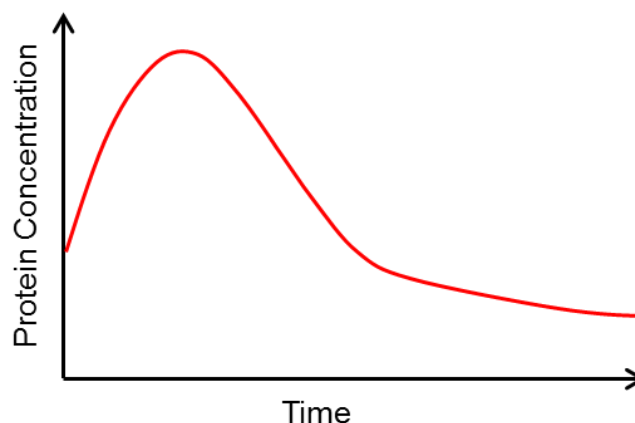


Figure 4-4. The schematic representation of real-time protein concentration changes in the sitting drop.²⁰⁷

4.2.2 Preparation of polymer solutions and stock buffer solutions

Four classes of polymers including neutral, cationic, anionic and cationic/zwitterionic shown below were applied for HEWL crystallisation:

- P(PEGMA₄₇₅) (P1) – Neutral;
- Quaternised p(DMAEMA) (P2):
Degrees of quaternisation: 25 %, 50 %, 75 % and 100 %;
- A random copolymer [p(DMAEMA-*stat*-PEGMA₄₇₅)] (P3);
- P(DMAPMAm) (DPs: 38, 83 and 150) (P4);
- P(AMPS) (DPs: 53, 99 and 200) (P5);
- P(2-AmAA) (DPs: 18, 46, 72 and 150) (P6);
- P(4-AmBA) (DPs: 21, 50, 100 and 200) (P7);
- P(METMAC-*co*-MEDSAH) (P8) – Cationic/zwitterionic.

Cationic

Anionic

The stock polymer solutions in H₂O at a concentration of ~ 40 % (w/v) were prepared. In order to use polymers as part of the reservoir and sample solutions in HEWL crystallisation, it was necessary, to alter the pH to around 4.8,¹⁶⁰ which is chosen from the optimum pH (4.2-4.8) for the tetragonal crystal-inducing protocol of HEWL; and also considering the solubility of polymers. The stock buffer solutions of 0.25 M sodium acetate and 20 % (w/v) NaCl at pH 4.8 and 0.1 M sodium acetate at pH 4.8 were also prepared and filtered using a 0.2 µm cellulose acetate membrane filter.

By using the above mentioned pH-altered polymer solutions and the stock buffer solutions, the following polymer solutions were prepared at a final volume of 2 mL, 1 mL, 500 µL or 250 µL: 0.02 %, 0.2 %, 2 %, 4 %, 6 %, 8 %, 10 %, 12 %, 14 %, 16 %, 18 %, 20 %, 22 % and 24 % (w/v) in 0.25 M sodium acetate and 20 % (w/v) NaCl at pH 4.8. All polymers with various concentrations were completely dissolved in the buffer solutions.

4.2.3 Crystallisation protocol for tetragonal HEWL crystals^{160, 208}

HEWL was purchased from Sigma (catalogue number: L6876, EC: 3.2.1.17, pI: 11.35, lysozyme activity: ~ 50,000 units/mg protein). 0.1 M sodium acetate solution at pH 4.8 was prepared and filtered through a 0.2 µm cellulose acetate membrane filter. This was used to prepare the 50 mg/mL HEWL solution, which was then centrifuged at 13,000 rpm for 5 min at 4 °C.

HEWL crystallisation was performed on a 96-well crystallisation plate, using

the sitting drop vapour diffusion technique, grown under conditions favouring the tetragonal form. All manual pipetting was conducted on an open lab bench. Specifically, 50 μL of polymer buffer solution (0.25 M sodium acetate and 20 % (w/v) NaCl at pH 4.8) was pipetted in triplicate in the reservoir well; 1 μL of protein (50 mg/mL HEWL in 0.1 M sodium acetate solution at pH 4.8) and 1 μL polymer buffer solution taken from each reservoir were pipetted into corresponding sample well of the crystallisation plate. In each sample well, the polymer concentration was half of that in the reservoir well, the final concentration of HEWL in each sample well was 25 mg/mL. For control purposes, some wells contained no polymer in their solutions. The plate was then sealed and incubated at 19 $^{\circ}\text{C}$. Crystals formed within 1-2 days.

4.2.4 Crystal imaging

For optical microscopy, HEWL crystals formed in the crystallisation plate were directly observed by using a Leica Stereomicroscope, with a Leica fan-cooled light source, connected to a Nikon Coolpix 4500 digital camera (4.0 megapixels). 63 x magnifications were used to obtain the image of the whole sample well. Furthermore, in order to compare the effects of those polymers on protein crystallisation, we selected polymers with similar DP across the range of 80-100 for further image analysis by ImageJ.

4.2.5 X-ray crystallography

In this study, HEWL crystals were determined by single crystal X-ray diffraction recorded at room temperature on an X-ray generator with high-flux Osmic confocal multi-layer optics. Crystals first were mounted in a loop, which is made of plastic or nylon and attached to a solid rod. Thus, HEWL crystals for diffraction were cryoprotected with mother liquor containing 30 % glycerol, then protein crystals were maintained at temperatures of -180 °C by an X-stream 2000 nitrogen vapour system.^{209, 99, 210} By this freezing process, the radiation damage of the X-rays and the noise in the Bragg peaks due to thermal motion can be reduced.²¹¹

4.2.6 Dynamic light scattering (DLS) studies

During crystallisation experiments, complex processes take place in the protein solution with an increase of supersaturation. The onset and rate of protein crystallisation in solution depend on the mechanism of how protein macromolecules incorporate with each other.^{118,212,213} This interaction among protein macromolecules can govern them aggregate together to form crystals or amorphous aggregates in a period time.

In the present study, dynamic light scattering (DLS) is a sensitive and widely used method to determine the size and mode of aggregation of proteins and other biomolecules in solution, by detecting variations in size of macromolecules. DLS has already been successfully used to distinguish

between protein solutions leading to crystallisation or to amorphous precipitation.²¹⁴ Moreover, it is a very helpful method to screen for the probability for crystal formation in the protein solution, for example, dispersity analysis to optimize the crystallisation conditions.^{215,216,217,218}

Therefore, in this research, DLS was applied to monitor model protein crystallisation process by determining the particle size directly in the protein crystallisation solution. HEWL was crystallised using batch crystallisation method, where the protein solution, the protein fully dissolved in the buffer, and the precipitant solution (e.g., salts, soluble polymer, and small organic molecules) are directly added together, immediately leading to a supersaturated protein solution.¹⁵⁹ As the time increased, protein aggregates grew in size until the critical nucleus was reached and then capable of further growth. The increase size of aggregates in the crystallisation solution could be easily monitored by DLS.

Selected polymers with similar DP across the range of 80-100 were employed for DLS studies, including p(PEGMA₄₇₅) (P1), quaternised p(DMAEMA) (P2) (quaternised ratio 75 %), a mixture of two polymers: p(PEGMA₄₇₅) and p(DMAEMA) (P1 & P2) (molar ratio 9:1), p(DMAPMAm) (P4) (DP 83), p(AMPS) (P5) (DP 99), p(2-AmAA) (P6) (DP 72) and p(4-AmBA) (P7) (DP 100). For each experiment, 100 µL of 15 mg/mL HEWL in 0.1 M sodium acetate buffer at pH 4.8 was mixed with 100 µL of 1 mg/mL of polymer in 0.25 M sodium acetate and 20 % (w/v) NaCl at pH 4.8 directly in the VISCOTEK

DLS Quartz cell and then monitored by VISCOTEK DLS (Figure 4-5).

Temperature: 19 °C; Crystal Growth time: 7 hours.

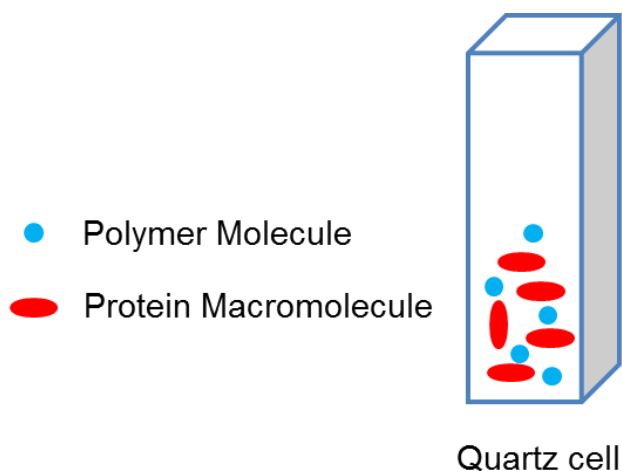


Figure 4-5. Schematic representation of protein crystallisation in the DLS quartz cell.

4.2.7 Scanning electron microscope (SEM) analysis

Scanning electron microscopy (SEM) is a technique that can be used to tackle the limited resolution of optical microscopy. It plays an essential role in the study of biological or pharmaceutical crystals.²¹⁹ The output signals, which make up the SEM images, are reflected from an opaque surface. SEM images are then formed by topographic contrast. Thus, SEM is a very useful method to observe morphological characters of the crystals.

Representative HEWL crystals grown in the presence of three selected polymers from each class, containing neutral p(PEGMA₄₇₅) (P1), cationic quaternised p(DMAEMA) (P2) and anionic p(AMPS) (P5) using sitting drop vapor diffusion method, were subjected to SEM analysis in this project. Prior

to gold coating, protein crystals were taken out from the crystallisation plates, washed with crystallisation buffer solutions (mother liquor). The samples (protein crystals) were loaded onto aluminium stubs with carbon tabs pre-fixed.^{220,221} These were then gold coated using an SCD 030 Blazers sputter coater for 5 min at 30 mA. The coated samples were transferred into a JEOL JSM 6060 LV scanning electron microscope and imaged at 15-30 kV.

4.3 Results and discussion

4.3.1 HEWL crystallisation in the presence of neutral polymer in solution:

p(PEGMA₄₇₅) (P1)

In order to investigate the influence of neutral p(PEGMA₄₇₅) (P1) on HEWL crystallisation, we set out to prepare neutral p(PEGMA₄₇₅) (P1) with a range of concentrations. By using the above mentioned pH-altered stock buffer solution, the following p(PEGMA₄₇₅) (P1) ($M_n \sim 39.4$ kDa) solutions with various concentration were prepared at a final volume of 1 mL, 500 μ L or 250 μ L: 0.02 %, 0.2 %, 2 %, 4 %, 6 %, 8 %, 10 %, 12 %, 14 %, 16 %, 18 %, 20 %, 22 % and 24 % (w/v) in 0.25 M sodium acetate and 20 % (w/v) NaCl at pH 4.8. 50 μ L of polymer buffer solution was pipetted in triplicate in the reservoir well; 1 μ L of protein (50 mg/mL HEWL in 0.1 M sodium acetate solution at pH 4.8) and 1 μ L polymer buffer solution taken from each reservoir were pipetted into corresponding sample well of the crystallisation plate. Some sample wells contained no polymer as the control. Table 4-2 shows HEWL crystallisation

plating method under p(PEGMA₄₇₅) (P1).

Table 4-2. HEWL crystallisation plate set up: p(PEGMA₄₇₅)

	1	2	3	4	5	6	7	8	9	10	11	12
0.25 M Na Acetate, 20 % NaCl	800 µL (0.25 M Na Acetate, 20 % NaCl)	400 µL (0.25 M Na Acetate, 20 % NaCl)	200 µL (0.25 M Na Acetate, 20 % NaCl)									
p(PEGMA ₄₇₅) 40 % H ₂ O	1 µL (0.02 %) 1199 µL	5 µL (0.2 %) 595 µL	25 µL (2 %) 275 µL	50 µL (4 %) 250 µL	75 µL (6 %) 225 µL	100 µL (8 %) 200 µL	125 µL (10 %) 175 µL	150 µL (12 %) 150 µL	175 µL (14 %) 125 µL	200 µL (16 %) 100 µL	225 µL (18 %) 75 µL	250 µL (20 %) 50 µL
pH	4.8	4.8	4.8	4.8	4.8	4.8	4.8	4.8	4.8	4.8	4.8	4.8
0.25 M Na Acetate, 20 % NaCl	↓	↓	↓	↓	↓	↓	↓	↓	↓	↓	↓	↓
p(PEGMA ₄₇₅) 40 % H ₂ O	↓	↓	↓	↓	↓	↓	↓	↓	↓	↓	↓	↓
pH	↓	↓	↓	↓	↓	↓	↓	↓	↓	↓	↓	↓
0.25 M Na Acetate, 20 % NaCl	↓	↓	↓	↓	↓	↓	↓	↓	↓	↓	↓	↓
p(PEGMA ₄₇₅) 40 % H ₂ O	↓	↓	↓	↓	↓	↓	↓	↓	↓	↓	↓	↓
pH	↓	↓	↓	↓	↓	↓	↓	↓	↓	↓	↓	↓
0.25 M Na Acetate, 20 % NaCl	↑	↑	↑	↑	↑	↑	↑	↑	↑	↑	↑	↑
p(PEGMA ₄₇₅) 40 % H ₂ O	↑	↑	↑	↑	↑	↑	↑	↑	↑	↑	↑	↑
pH	↑	↑	↑	↑	↑	↑	↑	↑	↑	↑	↑	↑
0.25 M Na Acetate, 20 % NaCl	200 µL (0.25 M Na Acetate, 20 % NaCl)											
p(PEGMA ₄₇₅) 40 % H ₂ O	0 µL (22 %) 300 µL											
pH	4.8	4.8	4.8	4.8	4.8	4.8	4.8	4.8	4.8	4.8	4.8	4.8
0.25 M Na Acetate, 20 % NaCl	↓	↓	↓	↓	↓	↓	↓	↓	↓	↓	↓	↓
p(PEGMA ₄₇₅) 40 % H ₂ O	↓	↓	↓	↓	↓	↓	↓	↓	↓	↓	↓	↓
pH	↓	↓	↓	↓	↓	↓	↓	↓	↓	↓	↓	↓
0.25 M Na Acetate, 20 % NaCl	↑	↑	↑	↑	↑	↑	↑	↑	↑	↑	↑	↑
p(PEGMA ₄₇₅) 40 % H ₂ O	↑	↑	↑	↑	↑	↑	↑	↑	↑	↑	↑	↑
pH	↑	↑	↑	↑	↑	↑	↑	↑	↑	↑	↑	↑
0.25 M Na Acetate, 20 % NaCl	200 µL (0.25 M Na Acetate, 20 % NaCl)											
p(PEGMA ₄₇₅) 40 % H ₂ O	0 µL (22 %) 300 µL											
pH	4.8	4.8	4.8	4.8	4.8	4.8	4.8	4.8	4.8	4.8	4.8	4.8
0.25 M Na Acetate, 20 % NaCl	↓	↓	↓	↓	↓	↓	↓	↓	↓	↓	↓	↓
p(PEGMA ₄₇₅) 40 % H ₂ O	↓	↓	↓	↓	↓	↓	↓	↓	↓	↓	↓	↓
pH	↓	↓	↓	↓	↓	↓	↓	↓	↓	↓	↓	↓
0.25 M Na Acetate, 20 % NaCl	↑	↑	↑	↑	↑	↑	↑	↑	↑	↑	↑	↑
p(PEGMA ₄₇₅) 40 % H ₂ O	↑	↑	↑	↑	↑	↑	↑	↑	↑	↑	↑	↑
pH	↑	↑	↑	↑	↑	↑	↑	↑	↑	↑	↑	↑

Figure 4-6 shows the photomicrographs of HEWL crystals obtained in the presence of p(PEGMA₄₇₅) (P1) ($M_n \sim 39.4$ kDa) with various concentrations, as solute in the crystallisation solutions. HEWL crystallisation under conditions favouring the tetragonal form resulted in exclusively tetragonal crystals within 1-2 days without any polymer (Figure 4-6, Control). Neutral p(PEGMA₄₇₅) (P1) nucleated a few large crystals, most of the HEWL crystals were readily identified by their distinctive morphology as tetragonal. As the concentration of p(PEGMA₄₇₅) (P1) in solution was increased, a similar increase in size and decrease in number of HEWL crystals were found. Moreover, the shape of crystals was quite different from that obtained in control experiments. Lower concentration of p(PEGMA₄₇₅) (P1) in solution (< 2 %, w/v) resulted in concomitant formation of needles and tetragonal HEWL crystals. However, as the concentration of p(PEGMA₄₇₅) (P1) was increased, only tetragonal crystals were formed. It is reported that HEWL needles have formed in solutions with high salt concentrations,²²² and in the presence of acid-functionalized polymeric surfaces, such as cross-linked acrylic acid and methacrylic acid.¹⁵⁹

p(PEGMA₄₇₅) ($M_n \sim 39.4$ kDa)

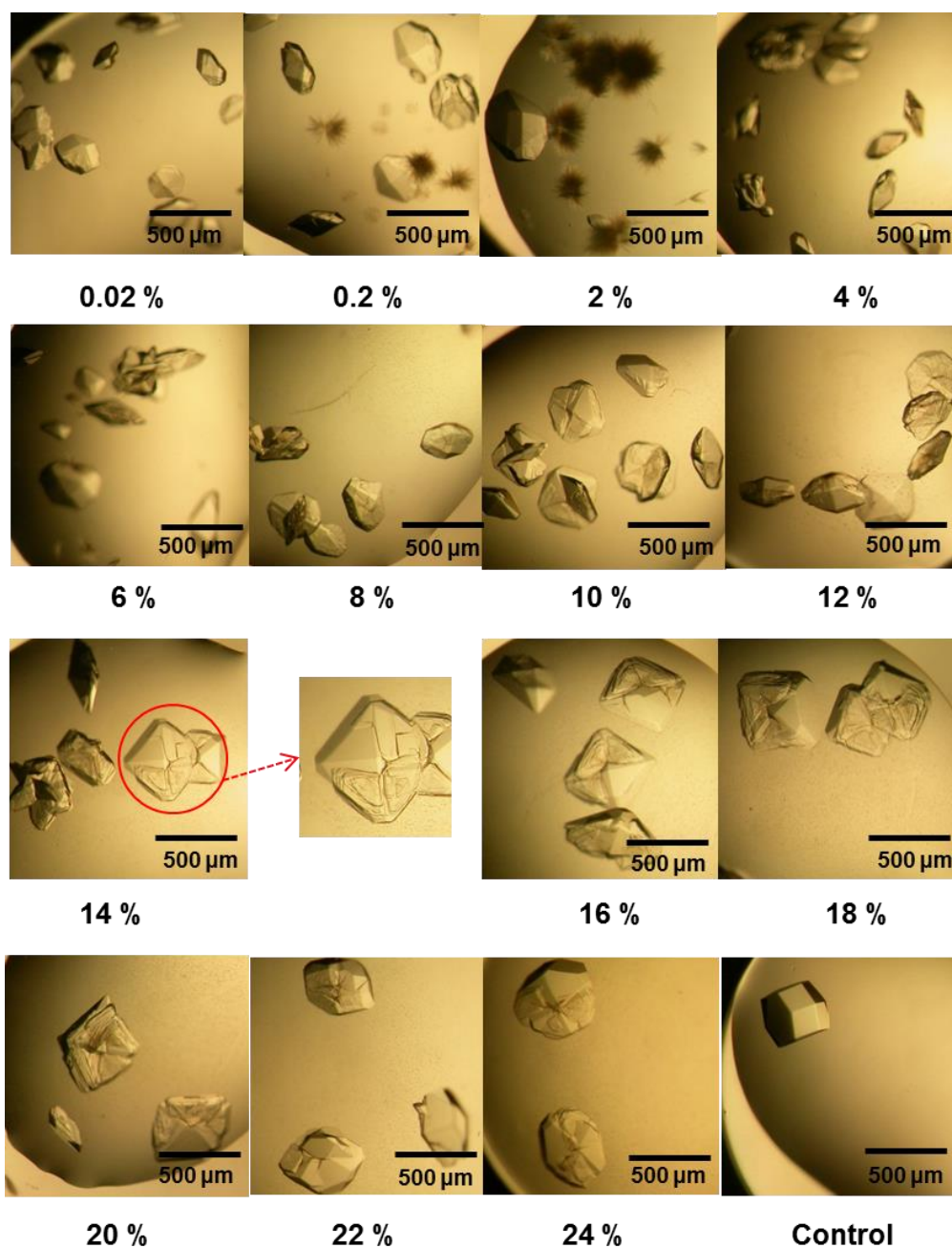


Figure 4-6. Selected photomicrographs of HEWL crystals, grown in the presence of p(PEGMA₄₇₅) (P1) ($M_n \sim 39.4$ kDa) at various concentrations. Image labelled 'Control' represents HEWL crystals grown from sample wells without polymer. The scale bar was 500 μm.

Figure 4-7 presents a summary of HEWL crystal size distribution by measuring the average length (μm) of the largest diameter of each crystal at each polymer concentration and number distribution as well. Image analysis of photomicrograph data was done by using ImageJ software. There was a clear effect on HEWL crystallisation depending on the concentration of neutral p(PEGMA₄₇₅) (P1). For cationic HEWL, as the concentration of neutral p(PEGMA₄₇₅) (P1) in solution was increased, the size of crystals increased and the number decreased very clearly.

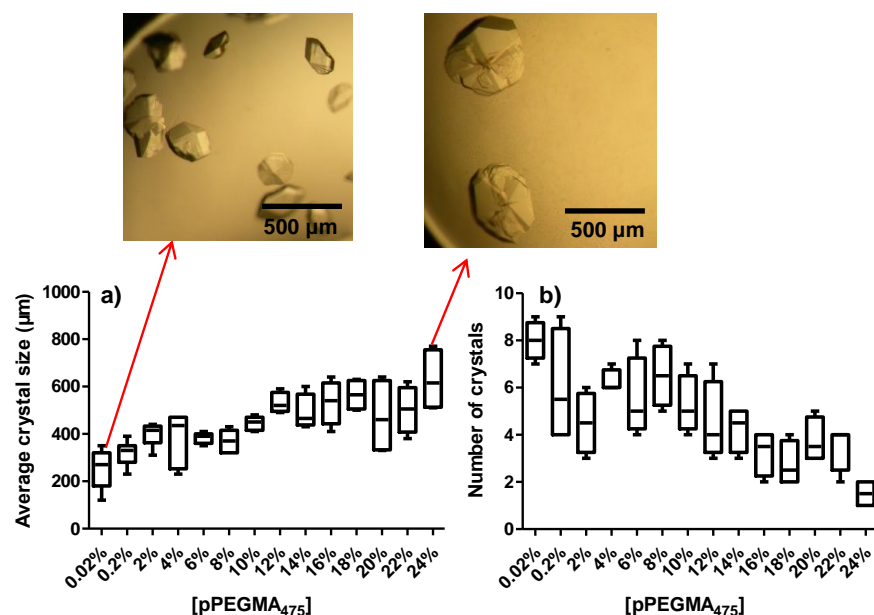


Figure 4-7. Summary of photomicrograph analysis showing changes in the size and number of HEWL crystals, grown in the presence of neutral p(PEGMA₄₇₅) (P1) at various concentrations. a) Average length (μm) of the largest crystal diameter; b) Experiment count for the number of crystals per sample well.

Diffraction data were collected for HEWL crystals using single crystal X-ray diffraction recorded at room temperature. Figure 4-8 illustrates the diffraction

patterns of HEWL crystals obtained by X-ray crystallography and Table 4-3 shows unit cell dimensions of HEWL crystals. Therefore, HEWL crystallisation in the presence of neutral p(PEGMA₄₇₅) (P1) under the tetragonal-inducing protocol, resulted in tetragonal crystals, which were confirmed by single crystal X-ray diffraction.

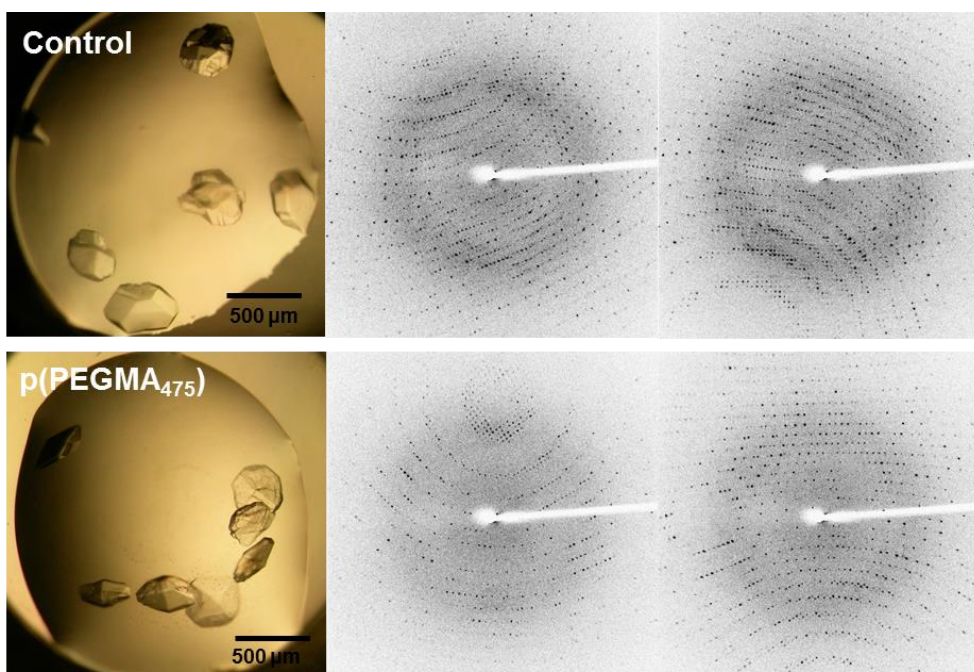


Figure 4-8. HEWL crystal photomicrographs and X-ray diffraction patterns yielded by the single HEWL crystal in the presence of neutral p(PEGMA₄₇₅) (P1). Image labelled ‘Control’ represents HEWL crystals grown from sample wells without p(PEGMA₄₇₅) (P1). Two scattering angles: 0 ± 1 degrees and 90 ± 1 degrees.

Table 4-3. Unit cell dimensions of HEWL crystals formed in the absence (Control) and presence of neutral p(PEGMA₄₇₅) (P1)

	a, b, c (Å)	α, β, γ	Volume	Unit cell lattice
Control	78.64, 78.64, 37.07	$90^\circ, 90^\circ, 90^\circ$	229,289	Tetragonal
p(PEGMA ₄₇₅)	78.42, 78.42, 37.17	$90^\circ, 90^\circ, 90^\circ$	228,638	Tetragonal

Figure 4-9 shows a summary of DLS data of HEWL crystallisation under neutral p(PEGMA₄₇₅) (P1). Figure 4-9a shows autocorrelation functions, which were analysed to obtain the distribution of particle radii, as shown in Figure 4-9b and Figure 4-9c. At the beginning of the experiment (T_0), HEWL macromolecules were non-interacting in the solution. The scattering from rapidly diffusing small individual macromolecules, only remained correlated for very short times and the decay times were short. The average size of the particles in the crystallisation solution was around 200 nm, measured by size distribution. With the addition of p(PEGMA₄₇₅) (P1), HEWL crystallisation initiated and aggregates formed. As the time increased, HEWL aggregates grew in size. Large particles diffused slower than small particles, and the correlation function decayed at a slower rate. After 420 minutes ($T_{420\text{min}}$), the average size of the particles in the crystallisation solution was around 900 nm. The size of pure neutral p(PEGMA₄₇₅) (P1) in the solution was also characterised by DLS and was found at around 7 nm.

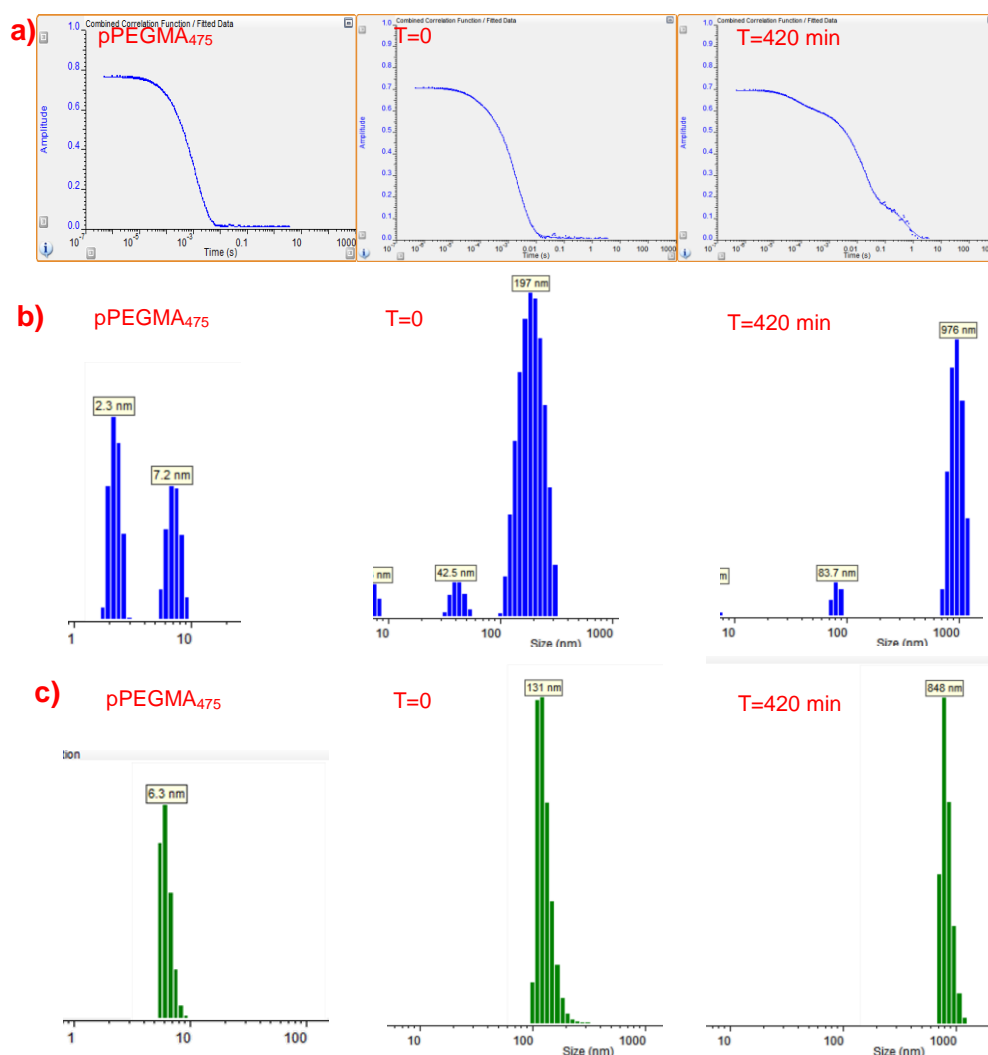


Figure 4-9. Summary of DLS data of HEWL crystallisation in the presence of neutral p(PEGMA₄₇₅) (P1). Pure neutral p(PEGMA₄₇₅) (P1) in the solution was also characterised by DLS. a) representative autocorrelation functions; b) radii distribution by intensity; c) radii distribution by number.

All other DLS data details, including autocorrelation functions and radii distribution by intensity at each time points are shown in the Appendix Pages 335-336. Representative Tukey plots of DLS data show protein aggregates growth in size as a function of time during HEWL crystallisation experiments

with p(PEGMA₄₇₅) (P1) (Figure 4-10). After the addition of neutral p(PEGMA₄₇₅) (P1), a characteristic increase in protein aggregate size can be observed. For control purpose, HEWL crystallisation experiment in the absence of polymer was carried out as well.

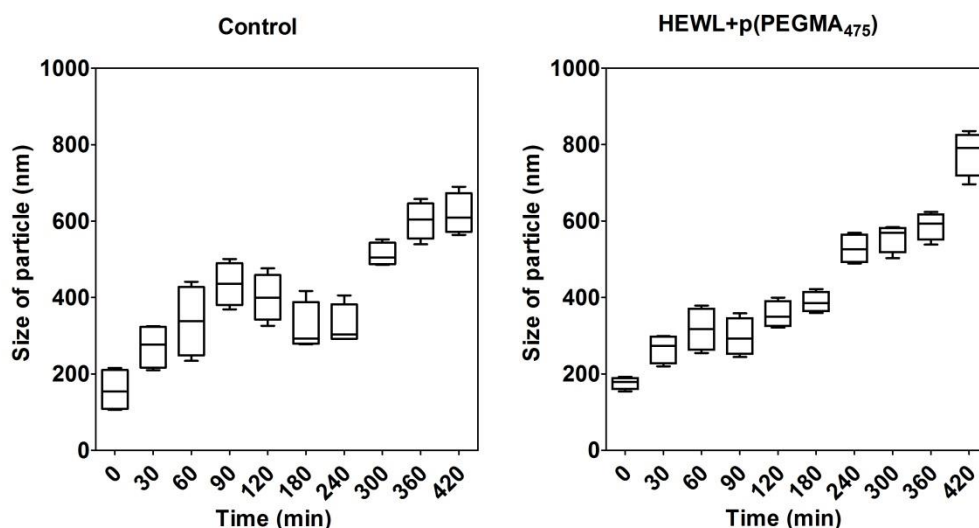


Figure 4-10. Variations in the size of HEWL aggregates or crystals in the solution as a function of time during crystallisation experiments induced by neutral p(PEGMA₄₇₅) (P1). Control experiment contained no polymer.

HEWL crystals, which grown in the presence of neutral p(PEGMA₄₇₅) (P1) using sitting drop vapor diffusion method were then subjected to SEM analysis. The SEM results (Figure 4-11) show that HEWL crystals had not been purified completely, there were still some salts left in the samples. However, all images showed a striking feature of crystals: all HEWL crystals, formed without polymer (Control) or when in the presence of neutral p(PEGMA₄₇₅) (P1) had sharp edges, even though the edges of HEWL crystals with slight etch defects.

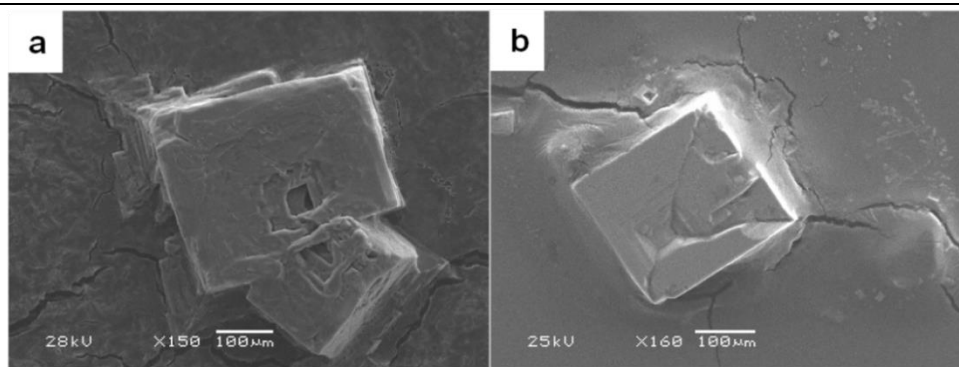


Figure 4-11. SEM micrographs of HEWL crystals produced under tetragonal conditions: a) control, without any polymer. b) in the presence of p(PEGMA₄₇₅) (P1). The scale bar was 100 μm .

Compared with optical microscopy images, which protein crystals have striking features, including the presence of sharp edges and observation of nearly monodisperse crystallites, in SEM the HEWL crystals do not look so well defined. This may be because of poor mechanical properties and stability of protein crystals.²²³ When protein crystals were taken out from the crystallisation plates and washed with crystallisation buffer solution, they were not handled easily and dehydrated slightly. Thus, a treatment for improving the stability of protein crystals may need in future study. There was insufficient time in the thesis period to conclude these experiments, but future work should consider this.

All above results together illustrate that p(PEGMA₄₇₅) (P1) acted as a solution additive and had the ability to influence HEWL crystallisation. We might expect that neutral p(PEGMA₄₇₅), as a neutral methacrylate derivative of PEG, was non-ionic and thus would compete with protein solutes for water and

dehydrated protein macromolecules.¹²⁵ Moreover, p(PEGMA₄₇₅) may have ‘volume-excluded effects’ by hydrophobic exclusion of protein solutes.²²⁴ Neutral polymers of this type could also reduce the dielectric constant of the crystallisation solution, leading to an increase of the effective distance over which protein electrostatic effects would take place,²²⁵ consequently protein aggregation and phase separation was promoted.¹⁰⁸ In turn, HEWL macromolecules may have been more able to associate with each other (Figure 4-12).

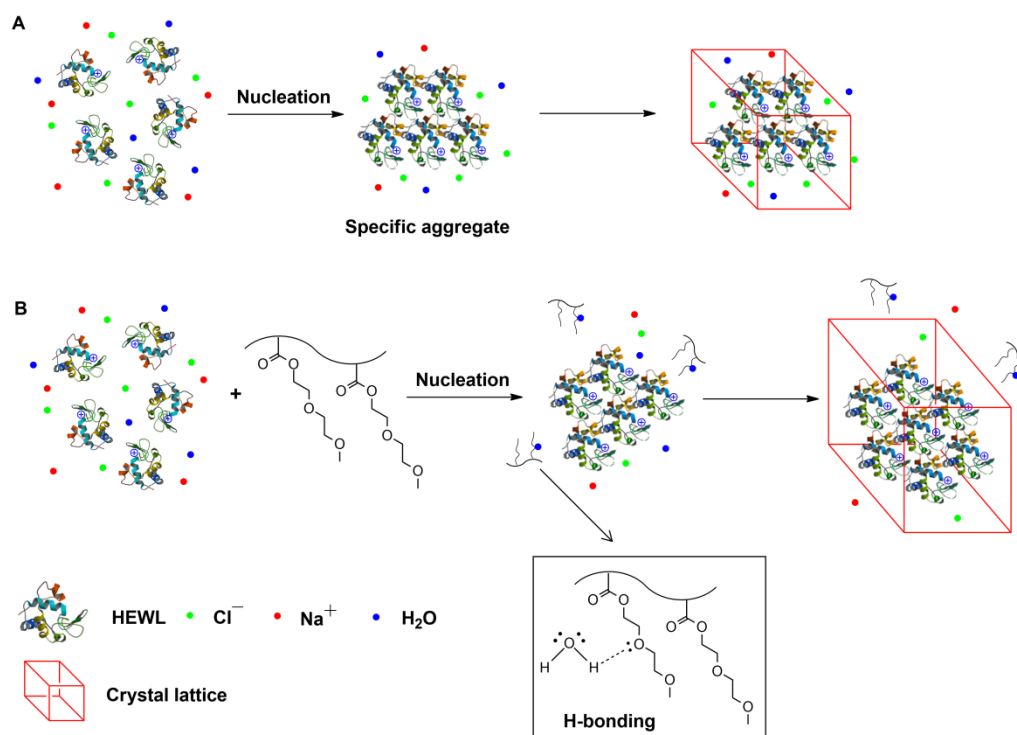


Figure 4-12. Schematic representation of hypothesis of HEWL crystallisation process without any polymer (A); and the interaction of p(PEGMA₄₇₅) (P1) with HEWL in the protein crystallisation process (B). HEWL macromolecules are positively charged at tetragonal crystallisation pH of 4.8, i.e. cationic. Na^+ and Cl^- ions are derived from the crystallisation buffer solutions.

4.3.2 HEWL crystallisation in the presence of cationic polymers in solution

4.3.2.1 HEWL crystallisation in the presence of quaternised p(DMAEMA)

(P2)

Quaternisation was carried out on p(DMAEMA) (P2) to introduce permanent positive charges by an addition of a methyl group to the p(DMAEMA) tertiary amine repeating unit. We used methyl iodide to quaternise two sizes of p(DMAEMA) with different molecular weights. Typically, similar crystallisation procedures as described in Section 4.3.1 were carried out. Five quaternised p(DMAEMA) (P2) with different quaternised ratios were applied for HEWL crystallisation:

- i) Quaternised p(DMAEMA) ($M_n \sim 46.3$ kDa) (quaternised ratio: 50 %);
- ii) Quaternised p(DMAEMA) ($M_n \sim 17.1$ kDa) (quaternised ratio: 25 %);
- iii) Quaternised p(DMAEMA) ($M_n \sim 17.1$ kDa) (quaternised ratio: 50 %);
- iv) Quaternised p(DMAEMA) ($M_n \sim 17.1$ kDa) (quaternised ratio: 75 %);
- v) Quaternised p(DMAEMA) ($M_n \sim 17.1$ kDa) (quaternised ratio: 100 %).

i) Quaternised p(DMAEMA) (P2) ($M_n \sim 46.3$ kDa) (quaternised ratio: 50 %)

The following polymer solutions were prepared by using the above pH-altered buffer solution: quaternised p(DMAEMA) (P2) ($M_n \sim 46.3$ kDa) (quaternised ratio: 50 %) 0.02 %, 0.2 %, 2 %, 4 %, 6 %, 8 %, 10 %, 12 %, 14 %, 16 %, 18 % and 20 % (w/v) (Table 4-4). HEWL concentration: 50 mg/mL.

Table 4-4. HEWL crystallisation plate set up: quaternised p(DMAEMA) (P2)

($M_n \sim 46.3$ kDa) (quaternised ratio: 50 %)

	1	2	3	4	5	6	7	8	9	10	11	12
0.25 M Na Acetate, 20 % NaCl	800 μ L (0.25 M Na Acetate, 20 % NaCl)	400 μ L (0.25 M Na Acetate, 20 % NaCl)	200 μ L (0.25 M Na Acetate, 20 % NaCl)	200 μ L (0.25 M Na Acetate, 20 % NaCl)	200 μ L (0.25 M Na Acetate, 20 % NaCl)	200 μ L (0.25 M Na Acetate, 20 % NaCl)	200 μ L (0.25 M Na Acetate, 20 % NaCl)	200 μ L (0.25 M Na Acetate, 20 % NaCl)	200 μ L (0.25 M Na Acetate, 20 % NaCl)	200 μ L (0.25 M Na Acetate, 20 % NaCl)	200 μ L (0.25 M Na Acetate, 20 % NaCl)	200 μ L (0.25 M Na Acetate, 20 % NaCl)
Quaternised p(DMAEMA) (50 %) 34.81 %	1 μ L (0.02 %)	6 μ L (0.2 %)	29 μ L (2 %)	57 μ L (4 %)	86 μ L (6 %)	115 μ L (8 %)	144 μ L (10 %)	172 μ L (12 %)	201 μ L (14 %)	230 μ L (16 %)	259 μ L (18 %)	287 μ L (20 %)
H ₂ O	1199 μ L	594 μ L	271 μ L	243 μ L	214 μ L	185 μ L	156 μ L	128 μ L	99 μ L	70 μ L	41 μ L	13 μ L
pH	4.8	4.8	4.8	4.8	4.8	4.8	4.8	4.8	4.8	4.8	4.8	4.8
0.25 M Na Acetate, 20 % NaCl	↓	↓	↓	↓	↓	↓	↓	↓	↓	↓	↓	↓
Quaternised p(DMAEMA) (50 %) 34.81 %												
H ₂ O												
pH												
0.25 M Na Acetate, 20 % NaCl	↓	↓	↓	↓	↓	↓	↓	↓	↓	↓	↓	↓
Quaternised p(DMAEMA) (50 %) 34.81 %												
H ₂ O												
pH												
0.25 M Na Acetate, 20 % NaCl	↑	↑	↑	↑	↑	↑	↑	↑	↑	↑	↑	↑
Quaternised p(DMAEMA) (50 %) 34.81 %												
H ₂ O												
pH												
0.25 M Na Acetate, 20 % NaCl	0 μ L	200 μ L (0.25 M Na Acetate, 20 % NaCl)	↑	↑	↑	↑	↑	↑	↑	↑	↑	↑
Quaternised p(DMAEMA) (50 %) 34.81 %												
H ₂ O	300 μ L											
pH	4.8											
0.25 M Na Acetate, 20 % NaCl	200 μ L (0.25 M Na Acetate, 20 % NaCl)	↑	↑	↑	↑	↑	↑	↑	↑	↑	↑	↑
Quaternised p(DMAEMA) (50 %) 34.81 %												
H ₂ O	0 μ L											
pH	4.8											

Figure 4-13 shows HEWL crystals obtained in the presence of quaternised p(DMAEMA) (P2) ($M_n \sim 46.3$ kDa) (quaternised ratio: 50 %) at various concentrations (0.02 % to 20 % (w/v)), as solute in the crystallisation solutions. Each concentration was repeated six times for reproducibility. Cationic quaternised p(DMAEMA) (P2) ($M_n \sim 46.3$ kDa) (quaternised ratio: 50 %) had an increased propensity for nucleating many small crystals. Along with the concentration of quaternised p(DMAEMA) (P2) in solution was increased, the number of HEWL crystals appeared to increase; the size of crystals appeared to decrease. Instead of tetragonal, two other forms of HEWL crystals, including needles and monoclinic crystals were obtained, which was confirmed by single crystal X-ray diffraction results later. As mentioned in Section 4.3.1, HEWL needles can be grown in solutions with high salt concentrations;²²² or in the presence of acid-functionalised polymeric surfaces, such as cross-linked acrylic acid and methacrylic acid.¹⁵⁹ However, HEWL monoclinic crystals have rarely been observed previously under conditions which otherwise promote tetragonal crystal-polymorphs.

Quaternised p(DMAEMA) (P2) ($M_n \sim 46.3$ kDa) (quaternised ratio: 50 %)

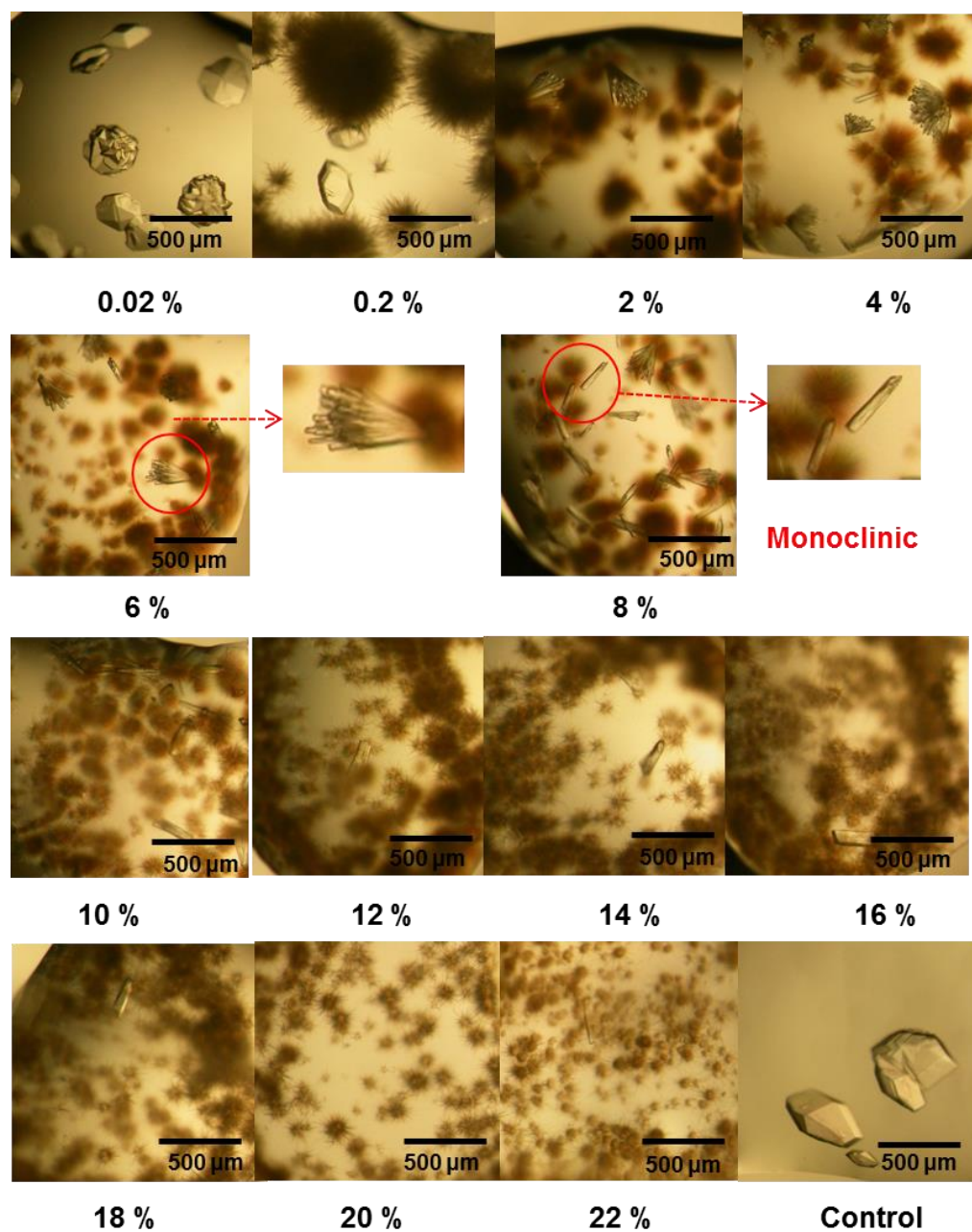


Figure 4-13. Photomicrographs showing changes in the size and shape of HEWL crystals, grown under the tetragonal protocol, in the presence of quaternised p(DMAEMA) (P2) ($M_n \sim 46.3$ kDa) (quaternised ratio: 50 %) at various concentrations. HEWL concentration: 50 mg/mL. Image labelled 'Control' represents crystals grown from sample wells without polymer.

It was immediately clear that quaternised p(DMAEMA) had influenced the results of HEWL crystallisation experiments, especially the crystal morphology and form. For better understanding the mechanism of how quaternised p(DMAEMA) affected HEWL crystallisation, a series of crystallisation experiments in the presence of different quaternised p(DMAEMA) ($M_n \sim 17.1$ kDa) systems (quaternised ratios: 25 %, 50 %, 75 % and 100 %), with various concentrations of HEWL (25, 50, 75 and 100 mg/mL) were carried out (Section ii-v).

ii) Quaternised p(DMAEMA) (P2) ($M_n \sim 17.1$ kDa) (quaternised ratio: 25 %)

The following polymer solutions were prepared by using the above pH-altered buffer solution: quaternised p(DMAEMA) ($M_n \sim 17.1$ kDa) (quaternised ratio: 25 %) 0.02 %, 0.2 %, 2 %, 4 %, 6 %, 8 %, 10 %, 12 %, 14 %, 16 % and 18 % (w/v). Table 4-5 presents the crystallisation plating method and Figures 4-14a-d show images of HEWL crystals obtained in the presence of quaternised p(DMAEMA) ($M_n \sim 17.1$ kDa) (quaternised ratio: 25 %) at various concentrations. HEWL concentrations: 25, 50, 75 and 100 mg/mL.

Table 4-5. HEWL crystallisation plate set up: quaternised p(DMAEMA) (P2)

($M_n \sim 17.1$ kDa) (quaternised ratio: 25 %)

	1	2	3	4	5	6	7	8	9	10	11
0.25 M Na Acetate, 20 % NaCl	800 μ L (0.25 M Na Acetate, 20 % NaCl)	400 μ L (0.25 M Na Acetate, 20 % NaCl)	200 μ L (0.25 M Na Acetate, 20 % NaCl)	200 μ L (0.25 M Na Acetate, 20 % NaCl)	200 μ L (0.25 M Na Acetate, 20 % NaCl)	200 μ L (0.25 M Na Acetate, 20 % NaCl)	200 μ L (0.25 M Na Acetate, 20 % NaCl)	200 μ L (0.25 M Na Acetate, 20 % NaCl)	200 μ L (0.25 M Na Acetate, 20 % NaCl)	200 μ L (0.25 M Na Acetate, 20 % NaCl)	200 μ L (0.25 M Na Acetate, 20 % NaCl)
Quaternised p(DMAEMA) (25 %) 31.84 % H ₂ O	1.3 μ L (0.02 %)	6.3 μ L (0.2 %)	31.4 μ L (2 %)	63 μ L (4 %)	94 μ L (6 %)	126 μ L (8 %)	157 μ L (10 %)	188 μ L (12 %)	220 μ L (14 %)	251 μ L (16 %)	283 μ L (18 %)
pH	1198.7 μ L 4.8	593.7 μ L 4.8	268.6 μ L 4.8	237 μ L 4.8	206 μ L 4.8	174 μ L 4.8	143 μ L 4.8	112 μ L 4.8	80 μ L 4.8	49 μ L 4.8	17 μ L 4.8
0.25 M Na Acetate, 20 % NaCl	↓	↓	↓	↓	↓	↓	↓	↓	↓	↓	↓
Quaternised p(DMAEMA) (25 %) 31.84 % H ₂ O	↓	↓	↓	↓	↓	↓	↓	↓	↓	↓	↓
pH	↓	↓	↓	↓	↓	↓	↓	↓	↓	↓	↓
0.25 M Na Acetate, 20 % NaCl	↑	↑	↑	↑	↑	↑	↑	↑	↑	↑	↑
Quaternised p(DMAEMA) (25 %) 31.84 % H ₂ O	↑	↑	↑	↑	↑	↑	↑	↑	↑	↑	↑
pH	↑	↑	↑	↑	↑	↑	↑	↑	↑	↑	↑
0.25 M Na Acetate, 20 % NaCl	0 μ L	300 μ L 4.8	↑	↑	↑	↑	↑	↑	↑	↑	↑
Quaternised p(DMAEMA) (25 %) 31.84 % H ₂ O	200 μ L (0.25 M Na Acetate, 20 % NaCl)	↑	↑	↑	↑	↑	↑	↑	↑	↑	↑
pH	↑	↑	↑	↑	↑	↑	↑	↑	↑	↑	↑
0.25 M Na Acetate, 20 % NaCl	0 μ L	300 μ L 4.8	↑	↑	↑	↑	↑	↑	↑	↑	↑
Quaternised p(DMAEMA) (25 %) 31.84 % H ₂ O	200 μ L (0.25 M Na Acetate, 20 % NaCl)	↑	↑	↑	↑	↑	↑	↑	↑	↑	↑
pH	↑	↑	↑	↑	↑	↑	↑	↑	↑	↑	↑

Quaternised p(DMAEMA) (P2) ($M_n \sim 17.1$ kDa) (quaternised ratio: 25 %)

a) HEWL concentration: 25 mg/mL

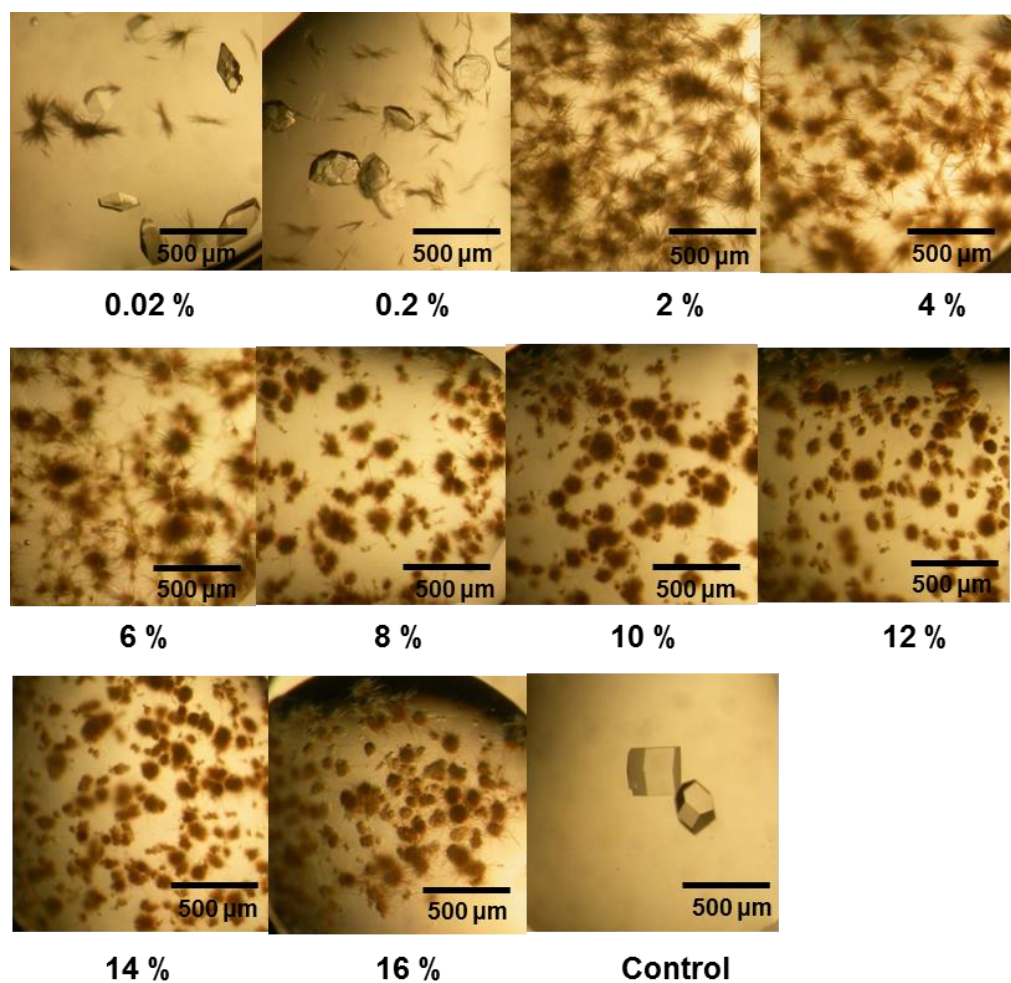


Figure 4-14a. Photomicrographs of HEWL crystals, grown under the tetragonal protocol, in the presence of p(DMAEMA) ($M_n \sim 17.1$ kDa) (quaternised ratio: 25 %) at various concentrations, with HEWL concentration: 25 mg/mL. Image labelled 'Control' represents crystals grown from sample wells without polymer. The scale bar was 500 μm.

Quaternised p(DMAEMA) (P2) ($M_n \sim 17.1$ kDa) (quaternised ratio: 25 %)

b) HEWL concentration: 50 mg/mL

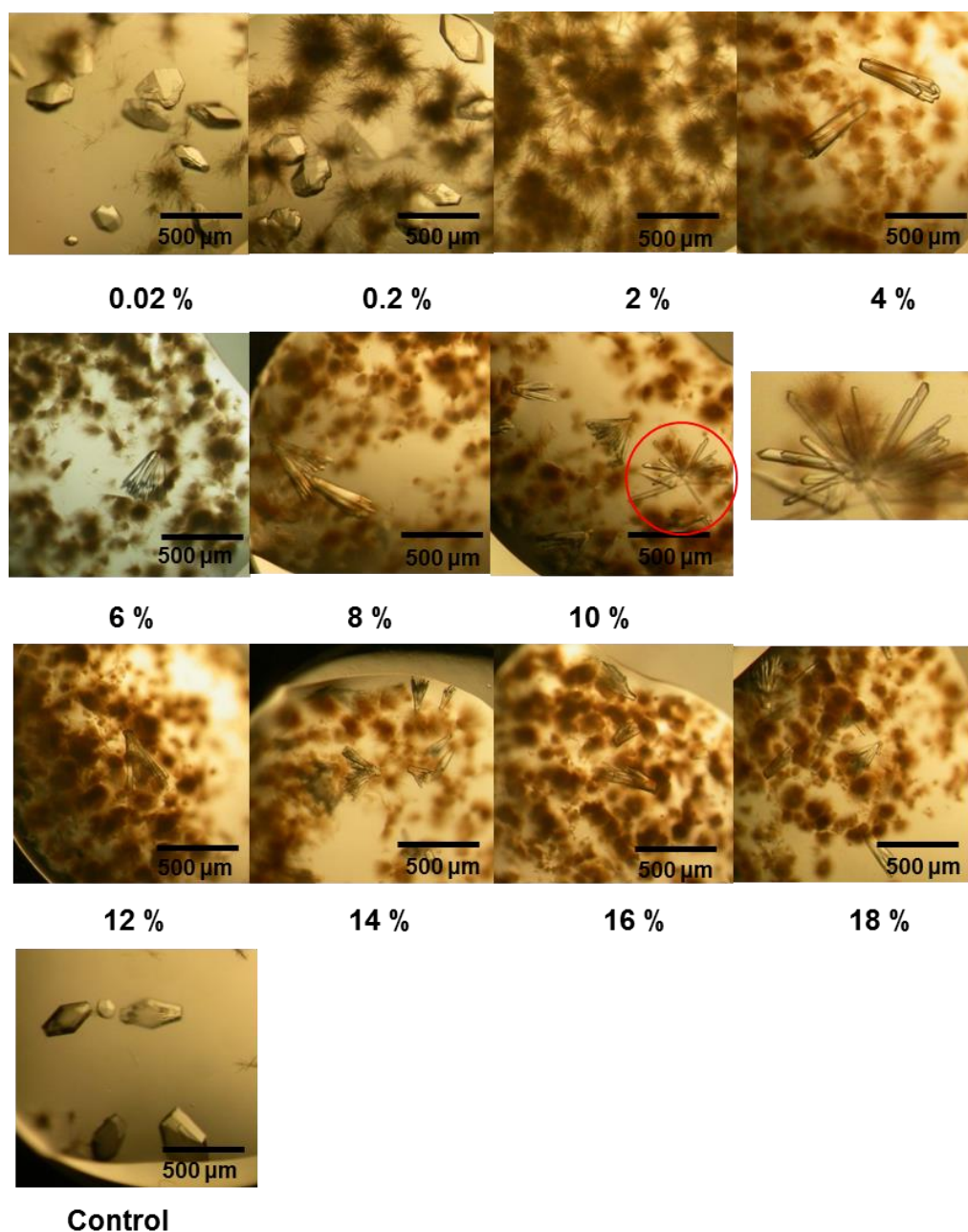


Figure 4-14b. Photomicrographs of HEWL crystals, grown under the tetragonal protocol, in the presence of p(DMAEMA) ($M_n \sim 17.1$ kDa) (quaternised ratio: 25 %) at various concentrations, with HEWL concentration: 50 mg/mL. Image labelled 'Control' represents crystals grown from sample wells without polymer. The scale bar was 500 μm .

Quaternised p(DMAEMA) (P2) ($M_n \sim 17.1$ kDa) (quaternised ratio: 25 %)

c) HEWL concentration: 75 mg/mL

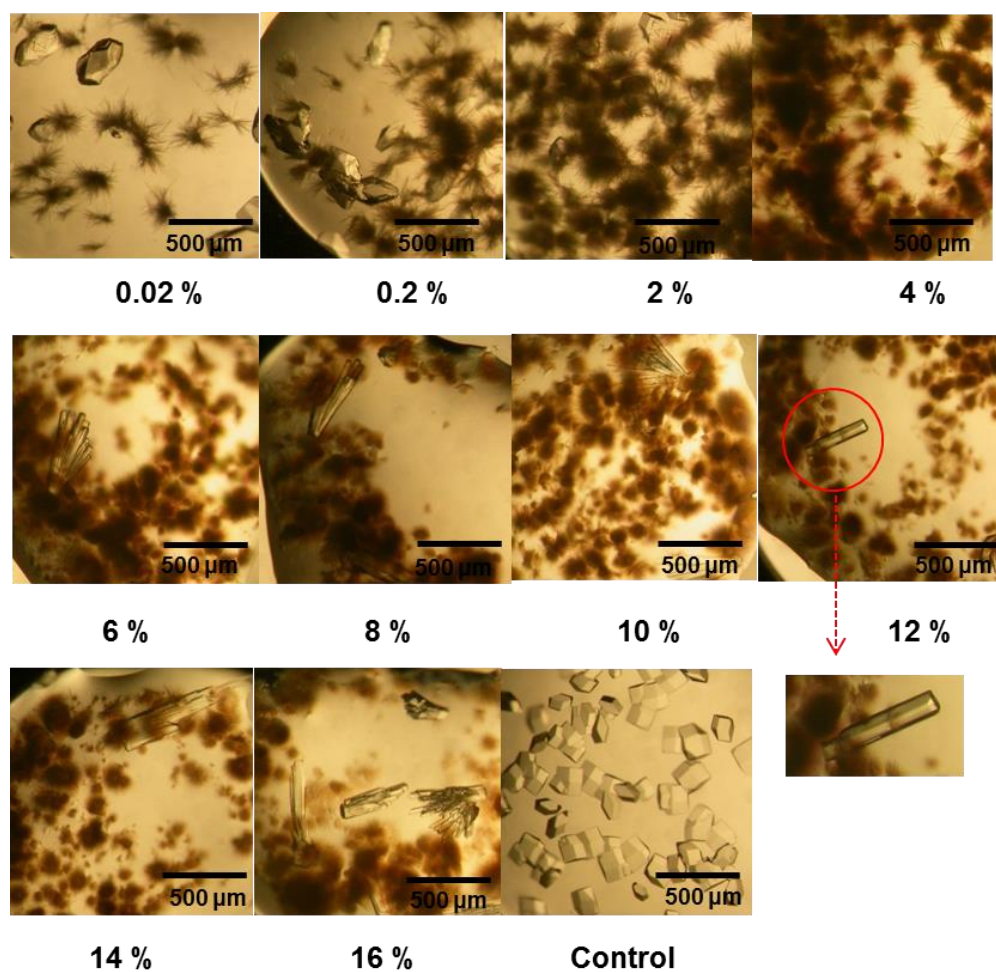


Figure 4-14c. Photomicrographs of HEWL crystals, grown under the tetragonal protocol, in the presence of (DMAEMA) ($M_n \sim 17.1$ kDa) (quaternised ratio: 25 %) at various concentrations, with HEWL concentration: 75 mg/mL. Image labelled 'Control' represents crystals grown from sample wells without polymer. The scale bar was 500 μm.

Quaternised p(DMAEMA) (P2) ($M_n \sim 17.1$ kDa) (quaternised ratio: 25 %)

d) HEWL concentration: 100 mg/mL

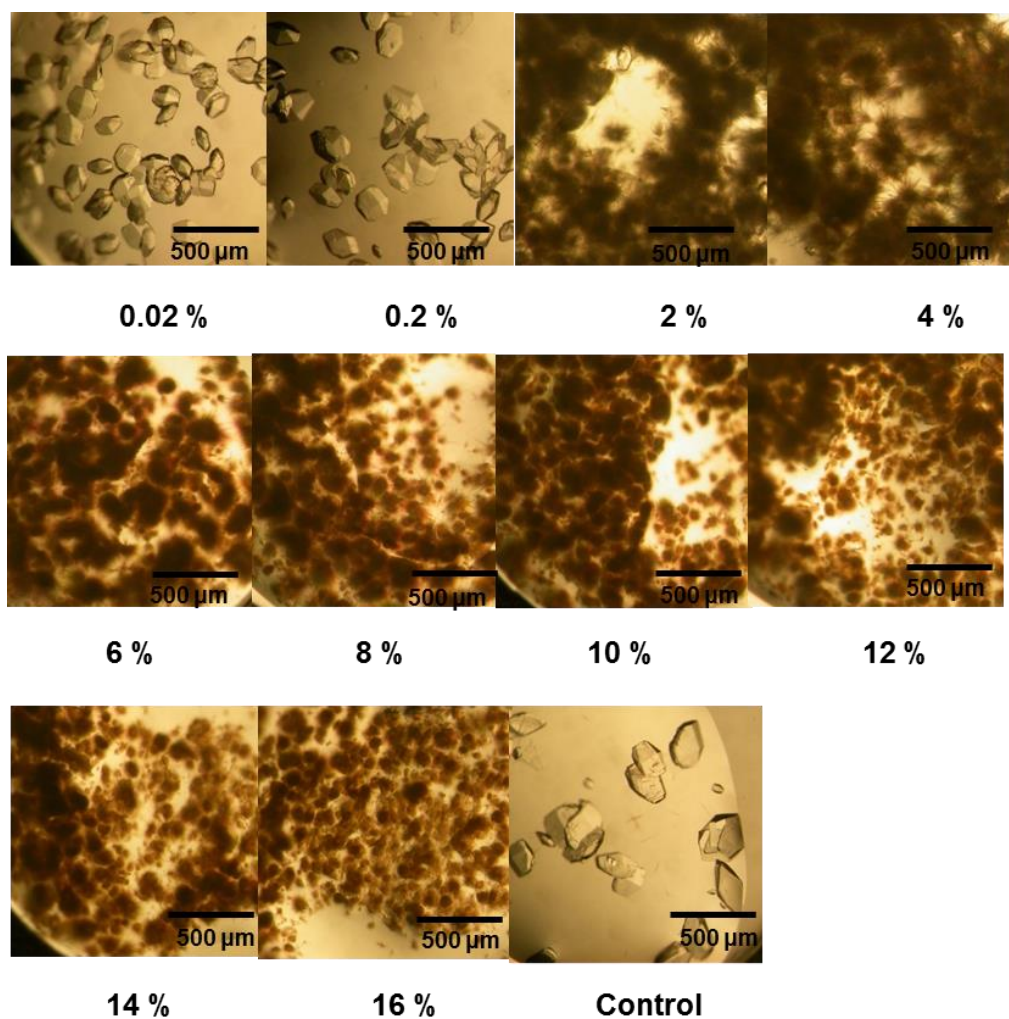


Figure 4-14d. Photomicrographs of HEWL crystals, grown under the tetragonal protocol, in the presence of (DMAEMA) ($M_n \sim 17.1$ kDa) (quaternised ratio: 25 %) at various concentrations, with HEWL concentration: 100 mg/mL. Image labelled 'Control' represents crystals grown from sample wells without polymer. The scale bar was 500 μm.

iii) Quaternised p(DMAEMA) (P2) ($M_n \sim 17.1$ kDa) (quaternised ratio: 50 %)

The following polymer solutions were prepared: quaternised p(DMAEMA) ($M_n \sim 17.1$ kDa) (quaternised ratio: 50 %) 0.02 %, 0.2 %, 2 %, 4 %, 6 %, 8 %, 10 % and 12 % (w/v) (Table 4-6).

Table 4-6. HEWL crystallisation plate set up: quaternised p(DMAEMA) (P2) ($M_n \sim 17.1$ kDa) (quaternised ratio: 50 %)

	1	2	3	4	5	6	7	8
0.25 M Na Acetate, 20 % NaCl	800 μ L (0.25 M Na Acetate, 20 % NaCl)	400 μ L (0.25 M Na Acetate, 20 % NaCl)	200 μ L (0.25 M Na Acetate, 20 % NaCl)	200 μ L (0.25 M Na Acetate, 20 % NaCl)	200 μ L (0.25 M Na Acetate, 20 % NaCl)	200 μ L (0.25 M Na Acetate, 20 % NaCl)	200 μ L (0.25 M Na Acetate, 20 % NaCl)	200 μ L (0.25 M Na Acetate, 20 % NaCl)
Quaternised p(DMAEMA) (50 %) 21.57 %	1.9 μ L (0.02 %)	9.3 μ L (0.2 %)	46 μ L (2 %)	93 μ L (4 %)	139 μ L (6 %)	185 μ L (8 %)	232 μ L (10 %)	278 μ L (12 %)
H ₂ O	1198.1 μ L	590.7 μ L	254 μ L	207 μ L	161 μ L	115 μ L	68 μ L	22 μ L
pH	4.8	4.8	4.8	4.8	4.8	4.8	4.8	4.8
0.25 M Na Acetate, 20 % NaCl								
Quaternised p(DMAEMA) (50 %) 21.57 %								
H ₂ O								
pH								
0.25 M Na Acetate, 20 % NaCl								
Quaternised p(DMAEMA) (50 %) 21.57 %								
H ₂ O								
pH								
0.25 M Na Acetate, 20 % NaCl	200 μ L (0.25 M Na Acetate, 20 % NaCl)							
Quaternised p(DMAEMA) (50 %) 21.57 %	0 μ L							
H ₂ O	300 μ L							
pH	4.8							

Figures 4-15a-d show the optical photomicrographs of HEWL crystals formed under quaternised p(DMAEMA) ($M_n \sim 17.1$ kDa) (quaternised ratio: 50 %) at various concentrations, with HEWL concentrations: 25, 50, 75 and 100mg/mL.

Quaternised p(DMAEMA) (P2) ($M_n \sim 17.1$ kDa) (quaternised ratio: 50 %)

a) HEWL concentration: 25 mg/mL

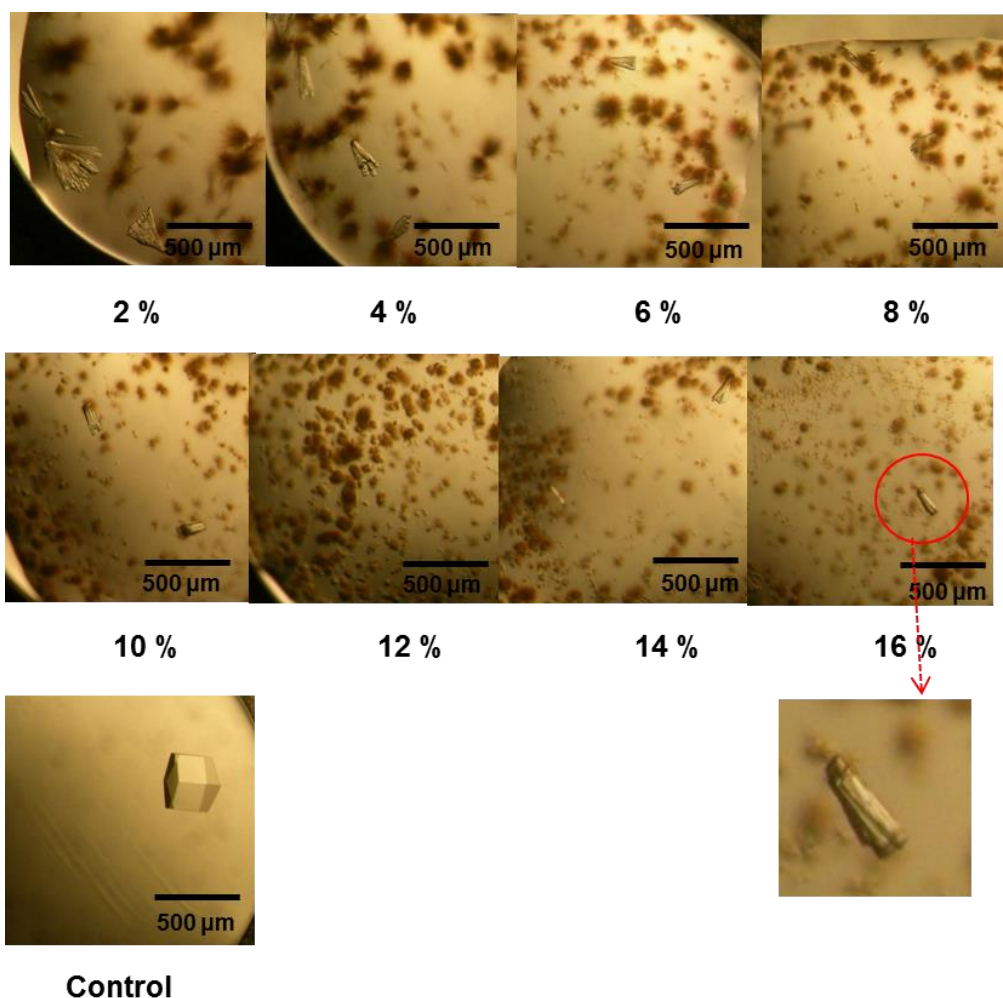


Figure 4-15a. Photomicrographs of HEWL crystals, grown under the tetragonal protocol, in the presence of p(DMAEMA) ($M_n \sim 17.1$ kDa) (quaternised ratio: 50 %) at various concentrations, with HEWL concentration: 25 mg/mL. Image labelled 'Control' represents crystals grown from sample wells without polymer. The scale bar was 500 μ m.

Quaternised p(DMAEMA) (P2) ($M_n \sim 17.1$ kDa) (quaternised ratio: 50 %)

b) HEWL concentration: 50 mg/mL

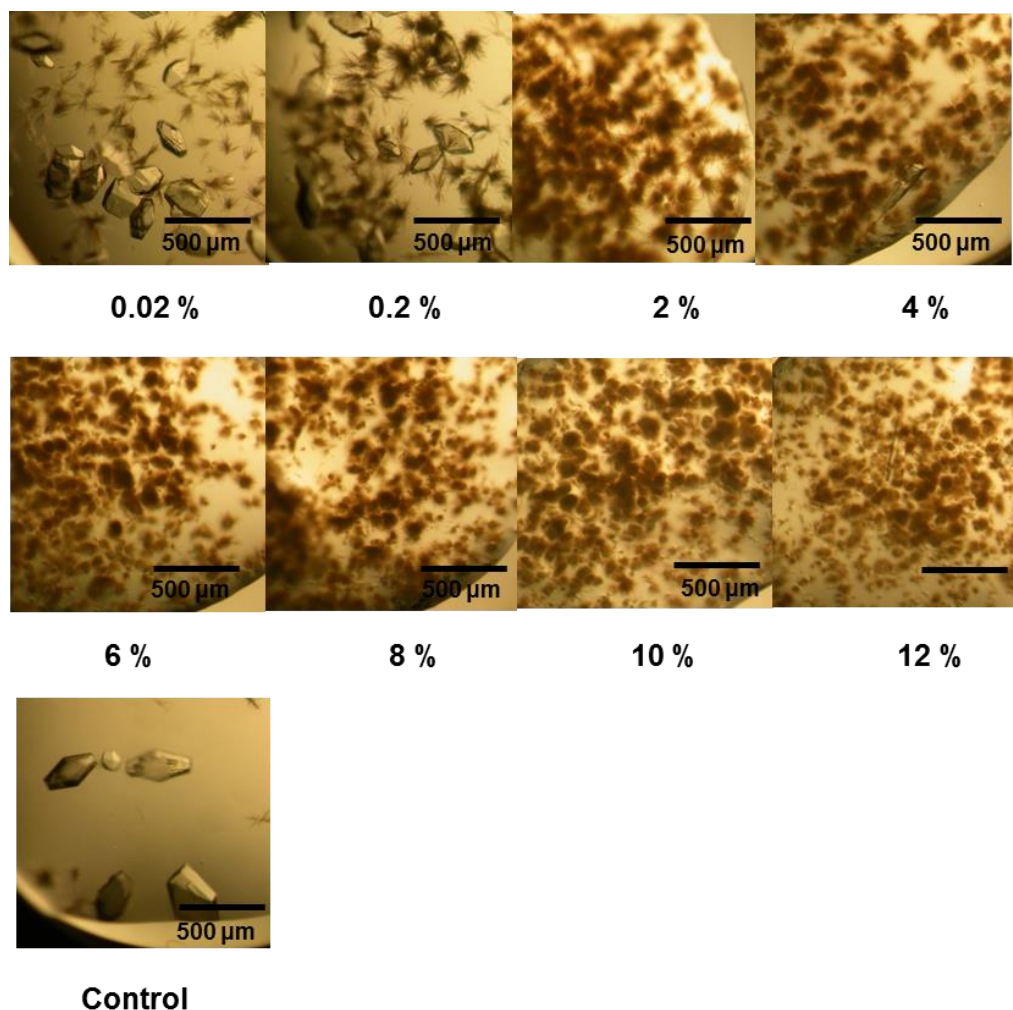


Figure 4-15b. Photomicrographs of HEWL crystals, grown under the tetragonal protocol, in the presence of p(DMAEMA) ($M_n \sim 17.1$ kDa) (quaternised ratio: 50 %) at various concentrations, with HEWL concentration: 50 mg/mL. Image labelled 'Control' represents crystals grown from sample wells without polymer. The scale bar was 500 μm.

Quaternised p(DMAEMA) (P2) ($M_n \sim 17.1$ kDa) (quaternised ratio: 50 %)

c) HEWL concentration: 75 mg/mL

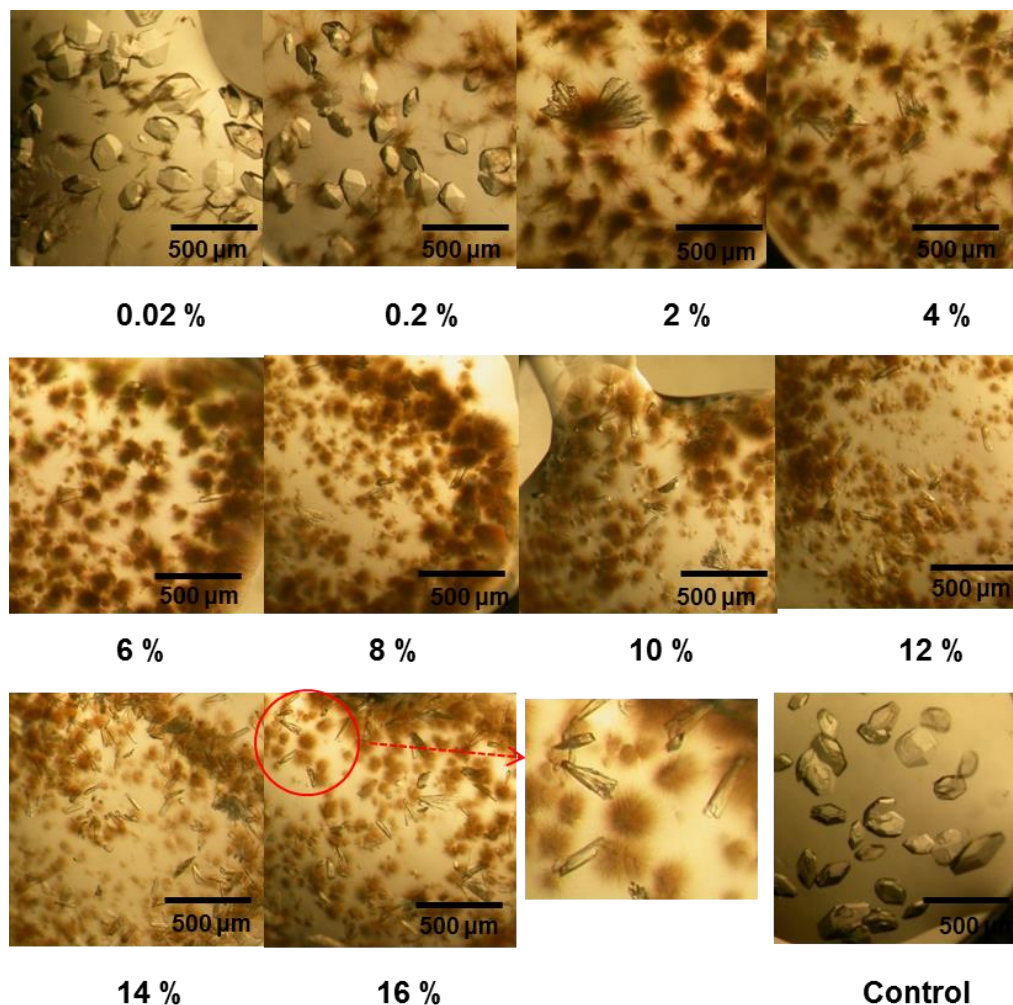


Figure 4-15c. Photomicrographs of HEWL crystals, grown under the tetragonal protocol, in the presence of p(DMAEMA) ($M_n \sim 17.1$ kDa) (quaternised ratio: 50 %) at various concentrations, with HEWL concentration: 75 mg/mL. Image labelled 'Control' represents crystals grown from sample wells without polymer. The scale bar was 500 μm .

Quaternised p(DMAEMA) (P2) ($M_n \sim 17.1$ kDa) (quaternised ratio: 50 %)

d) HEWL concentration: 100 mg/mL

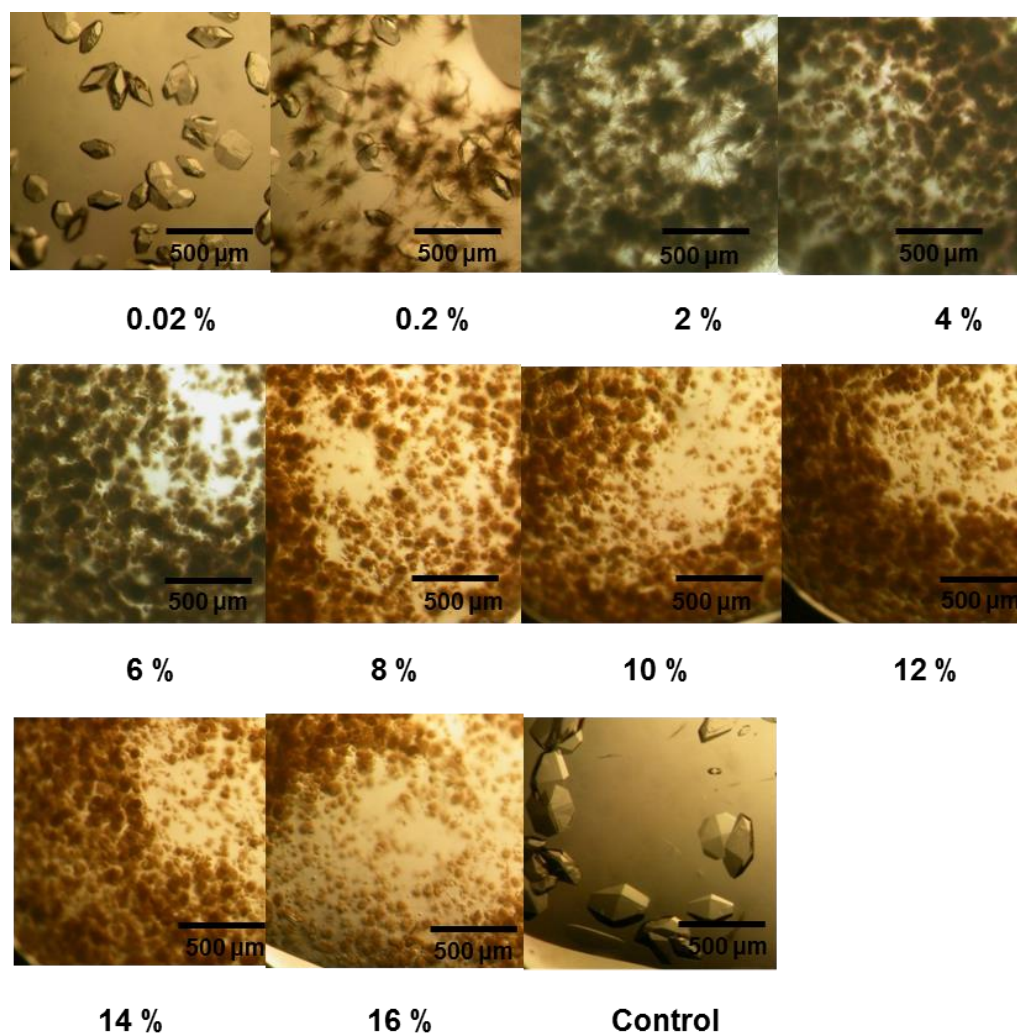


Figure 4-15d. Photomicrographs of HEWL crystals, grown under the tetragonal protocol, in the presence of p(DMAEMA) ($M_n \sim 17.1$ kDa) (quaternised ratio: 50 %) at various concentrations, with HEWL concentration: 100 mg/mL. Image labelled 'Control' represents crystals grown from sample wells without polymer. The scale bar was 500 μm .

iv) Quaternised p(DMAEMA) (P2) ($M_n \sim 17.1$ kDa) (quaternised ratio: 75 %)

The following polymer solutions were prepared: quaternised p(DMAEMA) (P2) ($M_n \sim 17.1$ kDa) (quaternised ratio: 75 %) 0.02 %, 0.2 %, 2 %, 4 %, 6 %, 8 %, 10 %, 12 %, 14 %, 16 %, 18 % and 20 % (w/v) (Table 4-7).

Table 4-7. HEWL crystallisation plate set up: quaternised p(DMAEMA) (P2) ($M_n \sim 17.1$ kDa) (quaternised ratio: 75 %)

	1	2	3	4	5	6	7	8	9	10	11	12
0.25 M Na Acetate, 20 % NaCl	800 μ L (0.25 M Na Acetate, 20 % NaCl)	400 μ L (0.25 M Na Acetate, 20 % NaCl)	200 μ L (0.25 M Na Acetate, 20 % NaCl)	200 μ L (0.25 M Na Acetate, 20 % NaCl)	200 μ L (0.25 M Na Acetate, 20 % NaCl)	200 μ L (0.25 M Na Acetate, 20 % NaCl)	200 μ L (0.25 M Na Acetate, 20 % NaCl)	200 μ L (0.25 M Na Acetate, 20 % NaCl)	200 μ L (0.25 M Na Acetate, 20 % NaCl)	200 μ L (0.25 M Na Acetate, 20 % NaCl)	200 μ L (0.25 M Na Acetate, 20 % NaCl)	200 μ L (0.25 M Na Acetate, 20 % NaCl)
Quaternised p(DMAEMA) (75 %) 34.64 %	1.2 μ L (0.02 %)	5.8 μ L (0.2 %)	29 μ L (2 %)	58 μ L (4 %)	87 μ L (6 %)	115 μ L (8 %)	144 μ L (10 %)	173 μ L (12 %)	202 μ L (14 %)	231 μ L (16 %)	260 μ L (18 %)	289 μ L (20 %)
H ₂ O	1198.8 μ L	594.2 μ L	271 μ L	242 μ L	213 μ L	185 μ L	156 μ L	127 μ L	98 μ L	69 μ L	40 μ L	11 μ L
pH	4.8	4.8	4.8	4.8	4.8	4.8	4.8	4.8	4.8	4.8	4.8	4.8
0.25 M Na Acetate, 20 % NaCl												
Quaternised p(DMAEMA) (75 %) 34.64 %												
H ₂ O												
pH												
0.25 M Na Acetate, 20 % NaCl												
Quaternised p(DMAEMA) (75 %) 34.64 %												
H ₂ O												
pH												
0.25 M Na Acetate, 20 % NaCl												
Quaternised p(DMAEMA) (75 %) 34.64 %												
H ₂ O												
pH												
0.25 M Na Acetate, 20 % NaCl												
Quaternised p(DMAEMA) (75 %) 34.64 %												
H ₂ O												
pH												
0.25 M Na Acetate, 20 % NaCl												
Quaternised p(DMAEMA) (75 %) 34.64 %												
H ₂ O												
pH												
0.25 M Na Acetate, 20 % NaCl												
Quaternised p(DMAEMA) (75 %) 34.64 %												
H ₂ O												
pH												

Figures 4-16a-d show images of HEWL crystals obtained under quaternised p(DMAEMA) (P2) ($M_n \sim 17.1$ kDa) (quaternised ratio: 75 %), with HEWL concentrations of 25, 50, 75 and 100mg/mL.

Quaternised p(DMAEMA) (P2) ($M_n \sim 17.1$ kDa) (quaternised ratio: 75 %)

a) HEWL concentration: 25 mg/mL

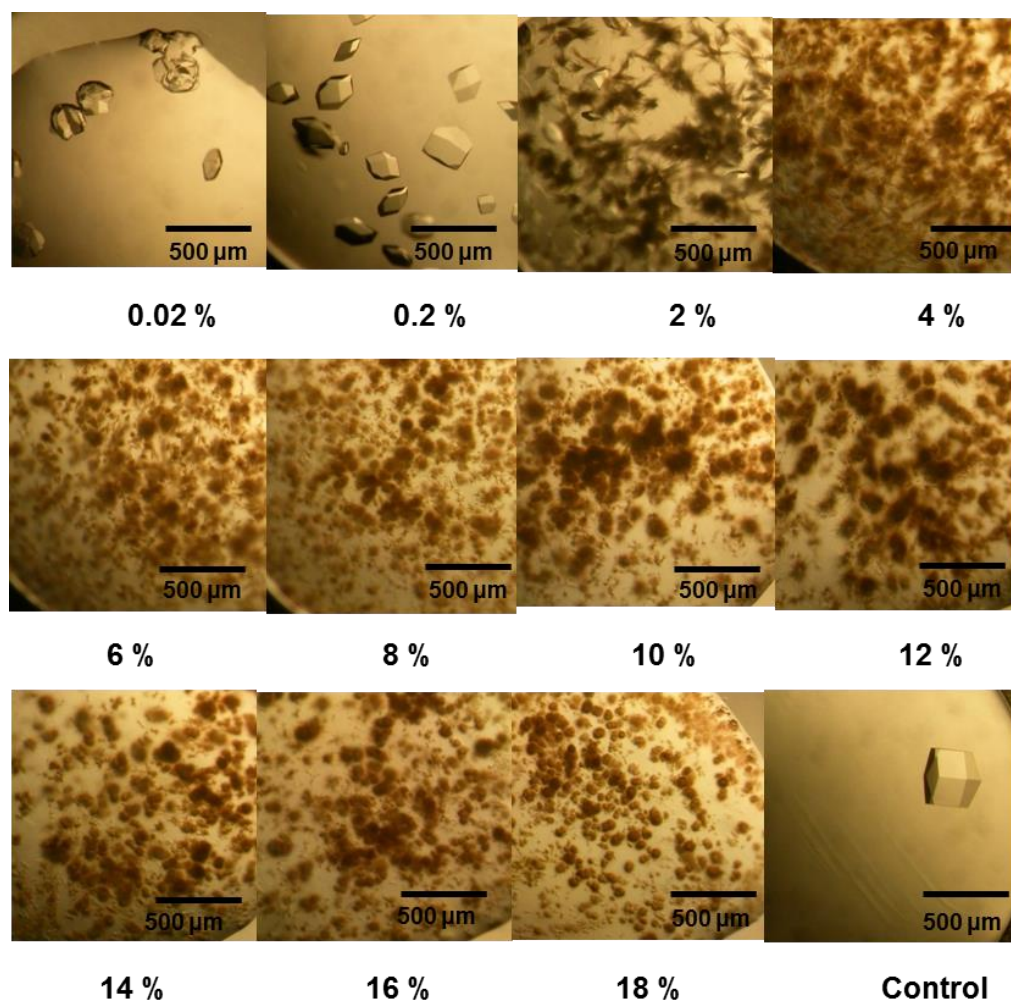


Figure 4-16a. Photomicrographs of HEWL crystals, grown under the tetragonal protocol, in the presence of p(DMAEMA) ($M_n \sim 17.1$ kDa) (quaternised ratio: 75 %) at various concentrations, with HEWL concentration: 25 mg/mL. Image labelled 'Control' represents crystals grown from sample wells without polymer. The scale bar was 500 μm.

Quaternised p(DMAEMA) (P2) ($M_n \sim 17.1$ kDa) (quaternised ratio: 75 %)

b) Lysozyme concentration: 50 mg/mL

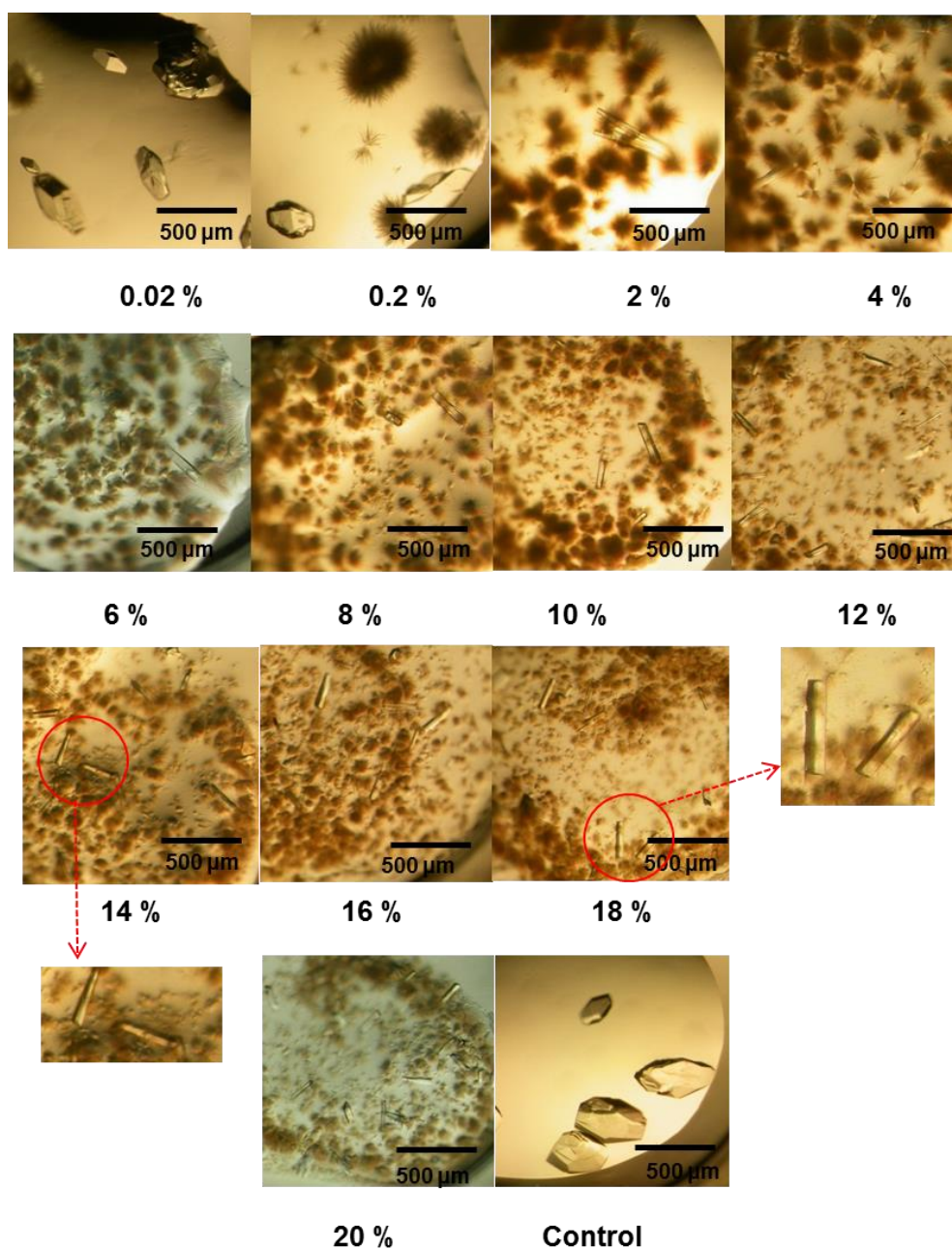
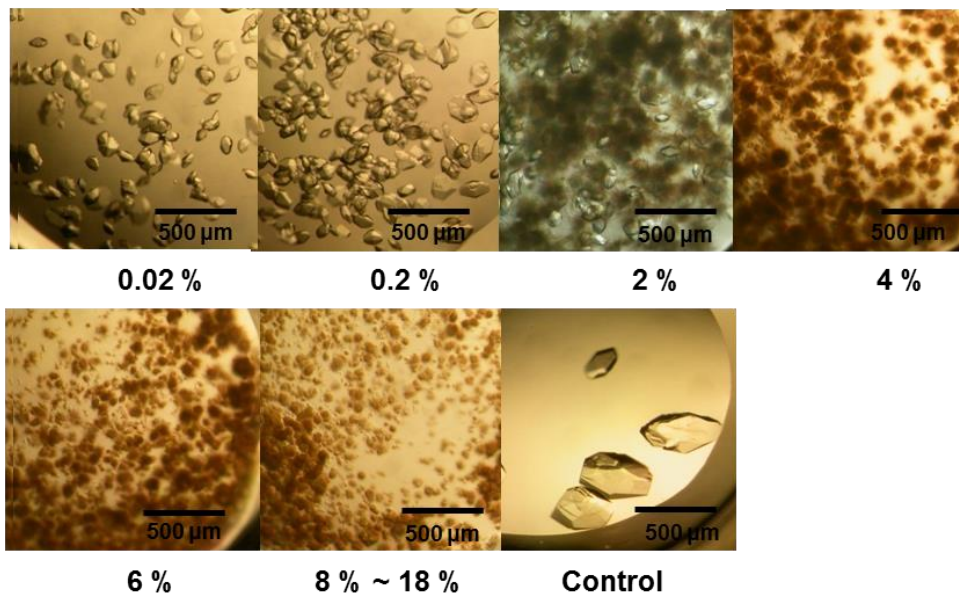


Figure 4-16b. Photomicrographs of HEWL crystals, grown under the tetragonal protocol, in the presence of p(DMAEMA) ($M_n \sim 17.1$ kDa) (quaternised ratio: 75 %) at various concentrations, with HEWL concentration: 50 mg/mL. Image labelled 'Control' represents crystals grown from sample wells without polymer. The scale bar was 500 μm .

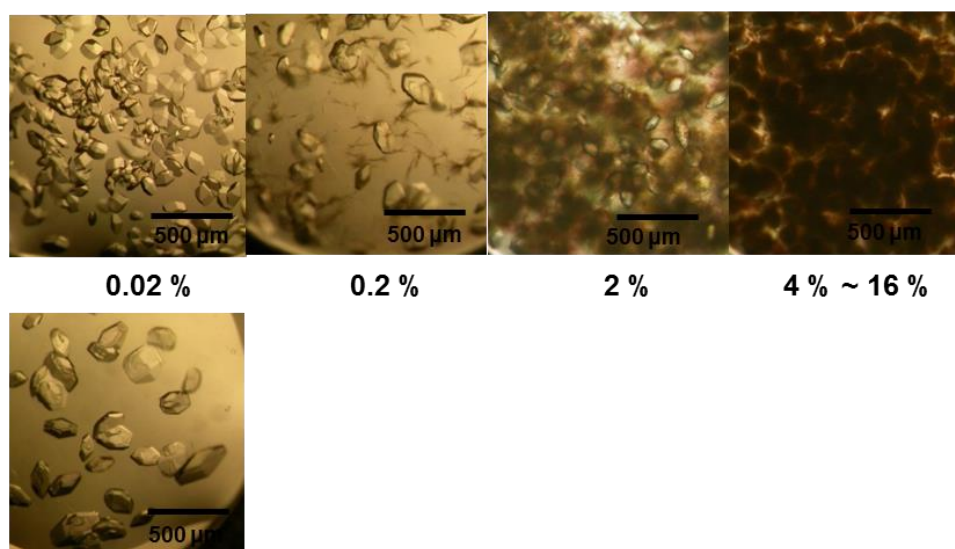
Quaternised p(DMAEMA) (P2) ($M_n \sim 17.1$ kDa) (quaternised ratio: 75 %)

c) HEWL concentration: 75 mg/mL; d) HEWL concentration: 100 mg/mL

c) HEWL concentration: 75 mg/ml



d) HEWL concentration: 100 mg/ml



Control

Figure 4-16c & d. Photomicrographs of HEWL crystals, grown under the tetragonal protocol, in the presence of p(DMAEMA) ($M_n \sim 17.1$ kDa) (quaternised ratio: 75 %) at various concentrations, with HEWL concentrations: 75 and 100 mg/mL. Images labelled 'Control' represent crystals grown from sample wells without polymer. The scale bar was 500 μm.

Figures 4-17a-d present optical micrographs of HEWL crystals obtained under quaternised p(DMAEMA) (P2) ($M_n \sim 17.1$ kDa) (quaternised ratio: 100 %), with HEWL concentrations: 25, 50, 75 and 100 mg/mL.

Quaternised p(DMAEMA) (P2) ($M_n \sim 17.1$ kDa) (quaternised ratio: 100 %)

a) HEWL concentration: 25 mg/mL

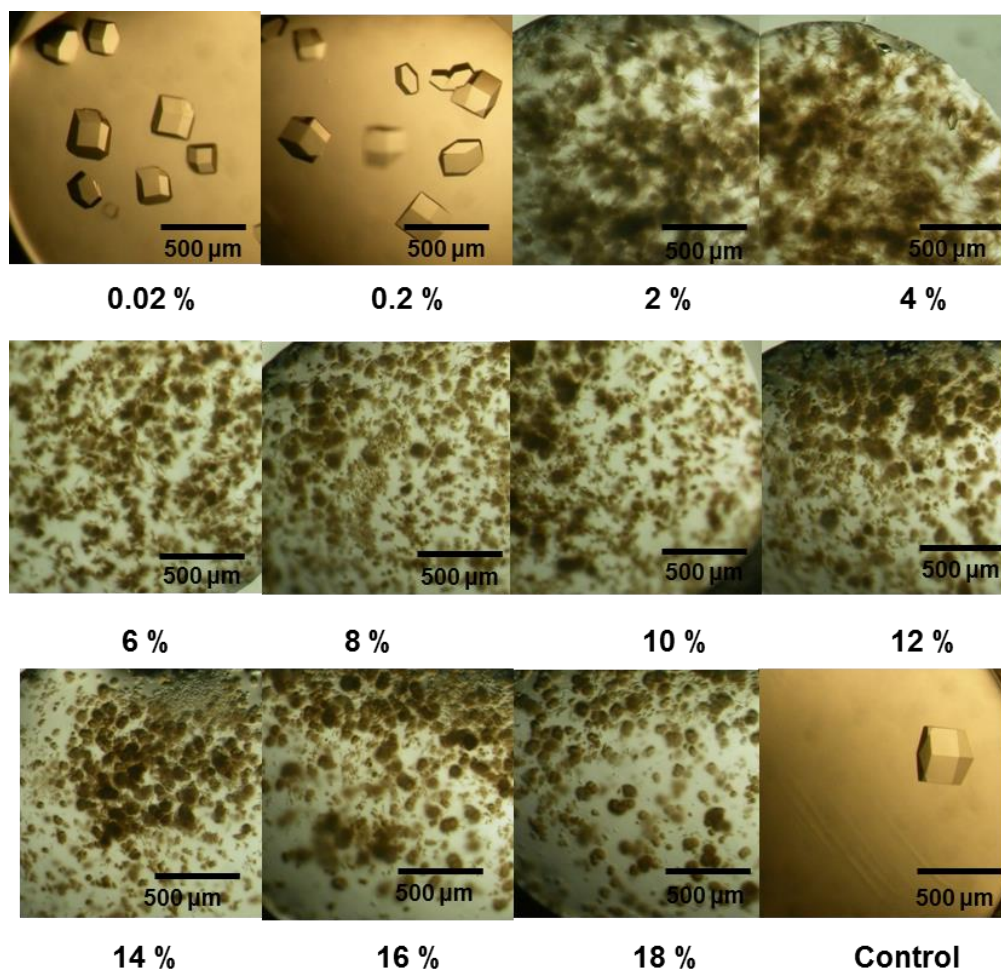


Figure 4-17a. Photomicrographs of HEWL crystals, grown under the tetragonal protocol, in the presence of p(DMAEMA) ($M_n \sim 17.1$ kDa) (quaternised ratio: 100 %) at various concentrations, with HEWL concentration: 25 mg/mL. Image labelled 'Control' represents crystals grown from sample wells without polymer. The scale bar was 500 μm.

Quaternised p(DMAEMA) (P2) ($M_n \sim 17.1$ kDa) (quaternised ratio: 100 %)

b) HEWL concentration: 50 mg/mL

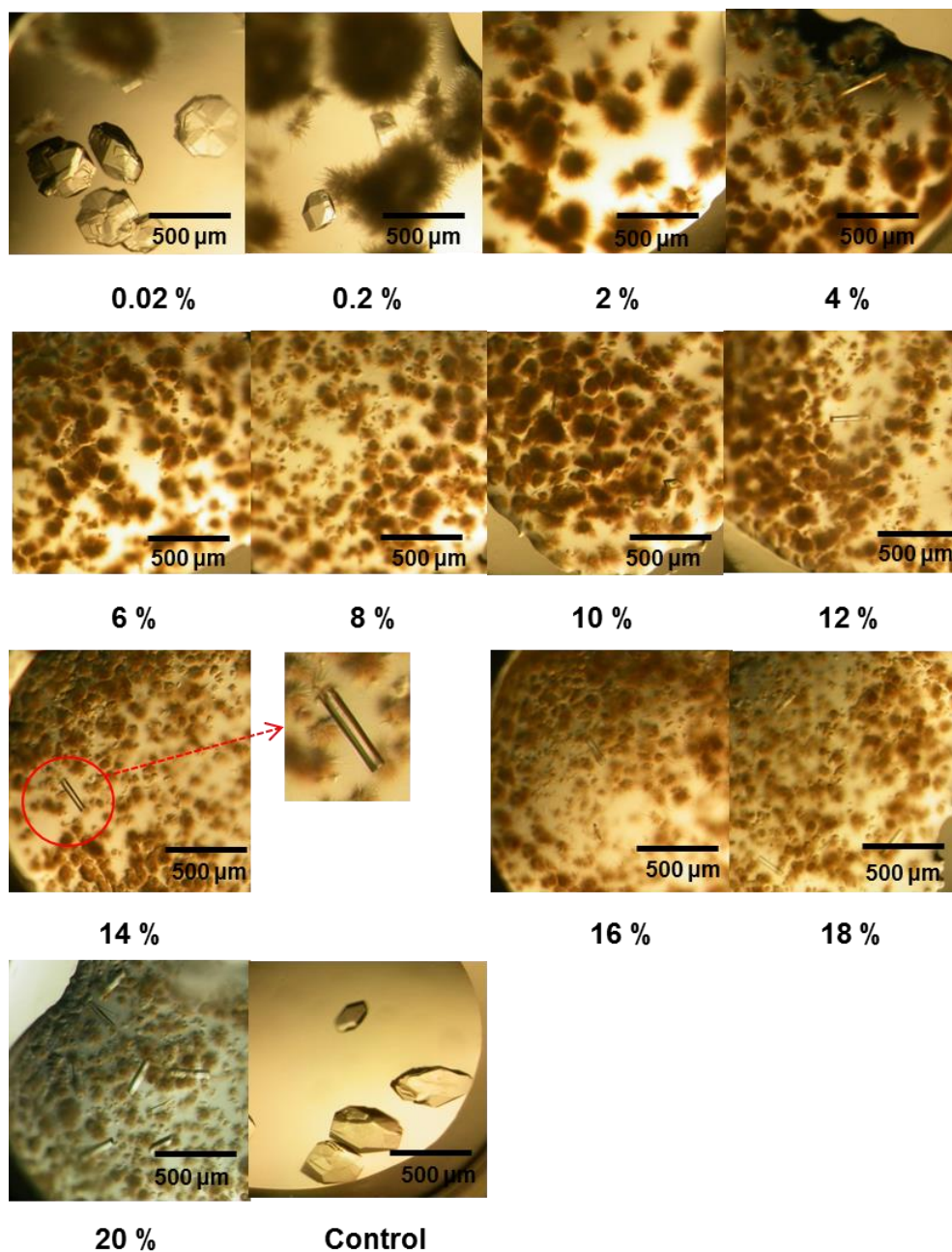
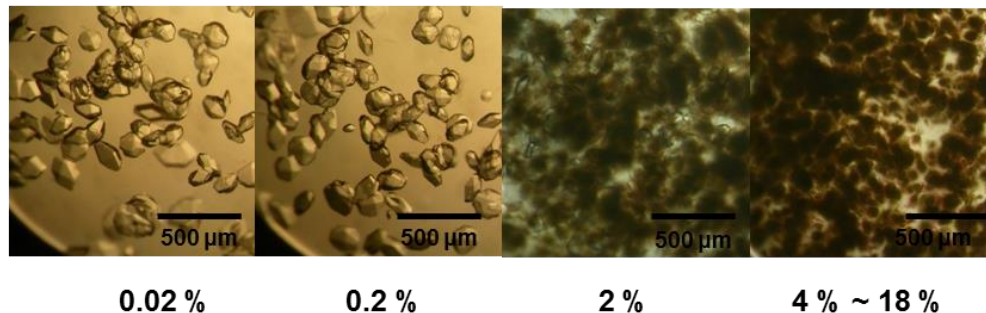


Figure 4-17b. Photomicrographs of HEWL crystals, grown under the tetragonal protocol, in the presence of p(DMAEMA) ($M_n \sim 17.1$ kDa) (quaternised ratio: 100 %) at various concentrations, with HEWL concentration: 50 mg/mL. Image labelled 'Control' represents crystals grown from sample wells without polymer. The scale bar was 500 μm .

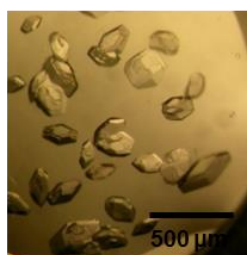
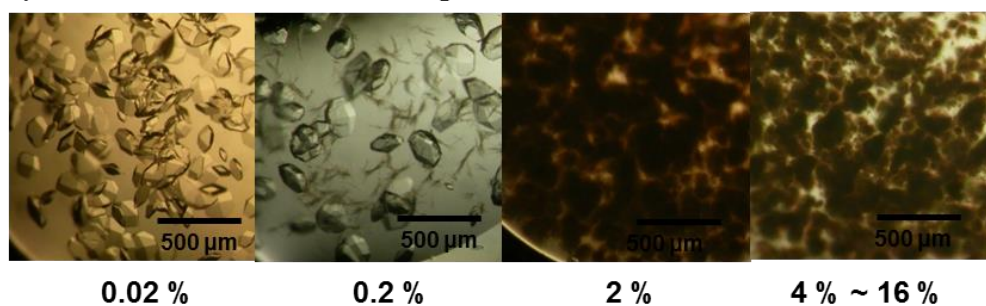
Quaternised p(DMAEMA) (P2) ($M_n \sim 17.1$ kDa) (quaternised ratio: 100 %)

c) HEWL concentration: 75 mg/mL; d) HEWL concentration: 100 mg/mL

c) HEWL concentration: 75 mg/ml



d) HEWL concentration: 100 mg/ml



Control

Figure 4-17c & d. Photomicrographs of HEWL crystals, grown under the tetragonal protocol, in the presence of p(DMAEMA) ($M_n \sim 17.1$ kDa) (quaternised ratio: 100 %) at various concentrations, with HEWL concentrations: 75 and 100 mg/mL. Images labelled 'Control' represent crystals grown from sample wells without polymer. The scale bar was 500 μm .

All above HEWL crystal images, including Figures 4-14a-d, 4-15a-d, 4-16a-d and 4-17a-d, show that HEWL crystallisation was clearly affected by the presence of quaternised p(DMAEMA) in solution. The rate of HEWL crystals formed in sample wells containing quaternised p(DMAEMA) was faster than that without added polymer. Various quaternised ratios of p(DMAEMA) had similar effects on HEWL crystallisation, even with different HEWL concentrations. Tetragonal crystals only were formed at lower concentrations (0.02 % ~ 0.2 % (w/v)). Upon increasing the concentration to above 2 %, quaternised p(DMAEMA) showed a visible and pronounced effect on the HEWL crystal formation; needles and monoclinic crystals were obtained (Figures 4-14b & c, 4-15a-c, 4-16b and 4-17b).

Therefore, quaternised p(DMAEMA) acted as solution additives significantly influenced the results of HEWL crystallisation. Moreover, quaternised p(DMAEMA) (P2) mediated-HEWL crystallisation followed a general morphology trend along with increasing polymer concentration: tetragonal → monoclinic & needle → needle, with tetragonal crystals forming at lower concentrations and monoclinic crystals & needle forming at higher polymer concentrations (Figure 4-18). In previous research, the absorption behavior of a high content of the cationic PDMAEMA on silicon wafers was controlled by a striving of the cationic segments for charge compensation by negative surface.²²⁶ Addition of quaternised p(DMAEMA), which exhibited a high cationic charge density, into HEWL solution, is therefore expected to alter the

electrostatic interactions between HEWL molecules and the solution.^{100, 118}

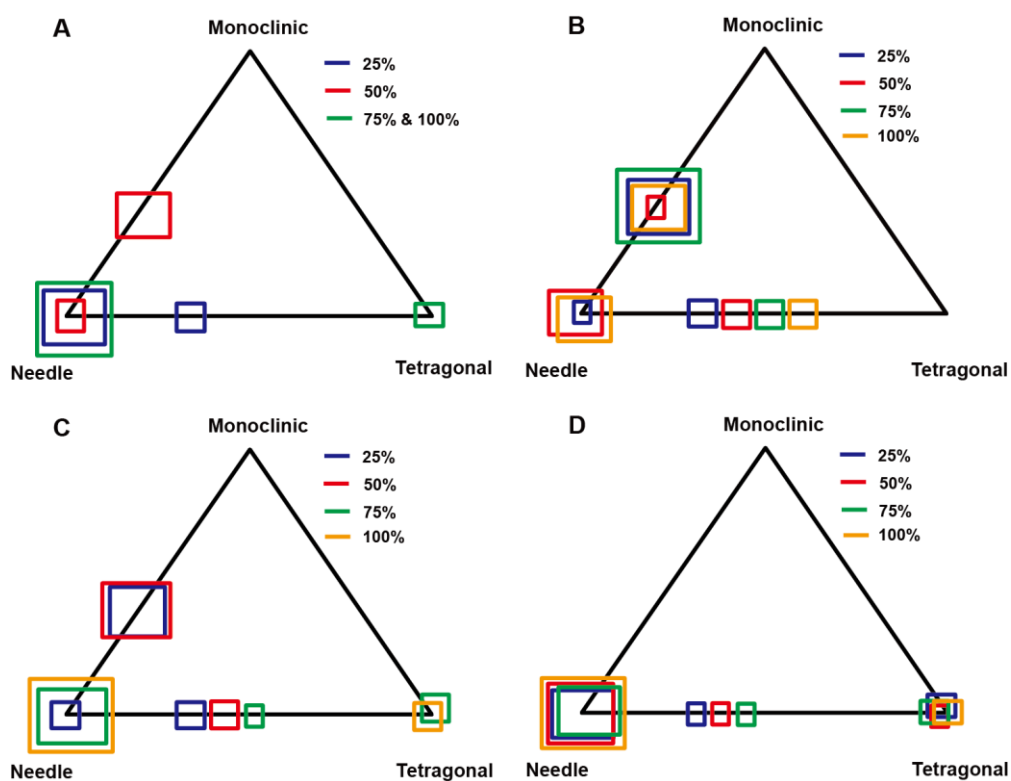


Figure 4-18. Schematic triangle graphs showing the changes in the morphology of HEWL crystals obtained in the presence of p(DMAEMA) with different degrees of quaternisation (25 %, 50 %, 75 % and 100 %). A) HEWL concentration: 25 mg/mL; B) HEWL concentration: 50 mg/mL; C) HEWL concentration: 75 mg/mL; D) HEWL concentration: 100 mg/mL. Three morphology phases: tetragonal, monoclinic and needle reside at the vertices of the triangle. The size of the colored squares quantitatively represents the possibility of crystal morphology shape.

Among all the above HEWL crystallisation experiments under quaternised p(DMAEMA) (P2), the experiment with quaternised ratio 75 % and HEWL concentration 50 mg/mL was the best condition for the formation of

monoclinic HEWL crystals. Therefore, photomicrograph data of this experiment (Figure 4-16b) was chosen for further image analysis. Figure 4-19 shows a full summary of HEWL crystals size and number distribution (tetragonal or monoclinic crystal). There was a significant effect on HEWL crystallisation depending on the concentration of cationic quaternised p(DMAEMA). For cationic HEWL, as the quaternised p(DMAEMA) (P2) concentration was increased, the size of monoclinic crystals decreased and the number of monoclinic crystals increased.

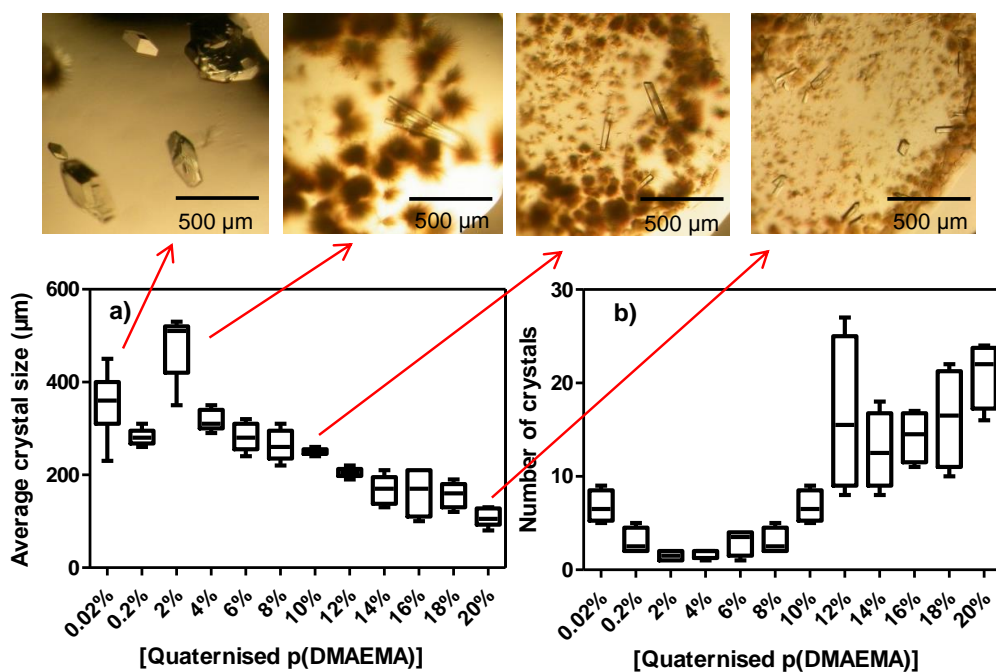


Figure 4-19. Summary of photomicrograph analysis showing changes in the size and number of HEWL crystals, grown in the presence of quaternised p(DMAEMA) (quaternised ratio: 75 %) at various concentrations, with HEWL concentration 50 mg/mL. a) Average length (μm) of the largest crystal (tetragonal or monoclinic) diameter; b) Experiment count for the number of crystals (tetragonal or monoclinic) per sample well. The scale bar was 500μm.

Figure 4-20 illustrates the diffraction patterns of HEWL crystal, grown in the presence of quaternised p(DMAEMA) (quaternised ratio: 75 %) by X-ray crystallography and Table 4-9 shows unit cell dimension of the HEWL crystal. Therefore, HEWL crystals obtained from quaternised p(DMAEMA) (P2)-mediated HEWL crystallisation, were confirmed as the monoclinic form by single crystal X-ray diffraction.

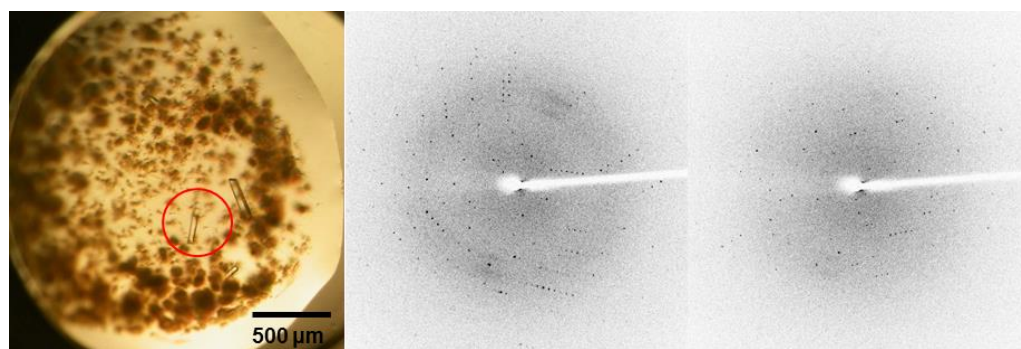


Figure 4-20. HEWL crystal photomicrograph and X-ray diffraction patterns yielded by the single HEWL crystal in the presence of cationic quaternised p(DMAEMA) (P2) (quaternised ratio: 75 %). Two scattering angles: 0 ± 1 degrees and 90 ± 1 degrees.

Table 4-9. Unit cell dimension of HEWL crystal formed in the presence of cationic quaternised p(DMAEMA) (P2) (quaternised ratio: 75 %)

Polymer	a, b, c (Å)	α, β, γ	Volume	Unit cell lattice
Quaternised p(DMAEMA)	26.82, 63.09, 58.73	$90^\circ, 93.2^\circ, 90^\circ$	99,213	Monoclinic

Representative Tukey plots of DLS data show protein aggregate growth in size as a function of time during crystallisation experiment (Figure 4-21). At the beginning of the experiment (T_0), the average size of the particles in the crystallisation solution was around 100 nm. After the addition of cationic quaternised p(DMAEMA) (P2), as the time increased, the rate of HEWL aggregates size increase was very slow. This may be because cationic quaternised p(DMAEMA) (P2) could lower the interfacial energy between cationic HEWL macromolecules and water by charge-charge repulsions, thus promoting nucleation and the formation of multiple crystal nuclei. Therefore, the size of each HEWL aggregate or crystal would increase very slowly. The size of pure quaternised p(DMAEMA) (P2) in solution was around 18 nm. DLS data details, including autocorrelation functions and radii distribution by intensity are shown in the Appendix Page 337.

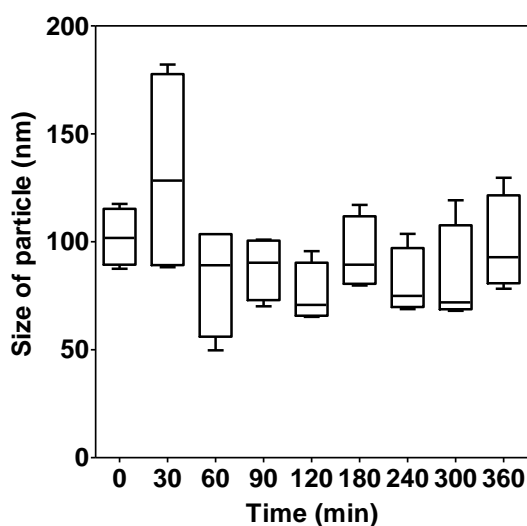


Figure 4-21. Variations of the size of HEWL aggregates or crystals in the solution as a function of time during crystallisation experiment induced by cationic quaternised p(DMAEMA) (P2) (quaternised ratio: 75 %).

Figure 4-22 presents SEM micrograph of HEWL crystal formed in the presence of quaternised p(DMAEMA) (P2). The SEM result shows that with the addition of cationic quaternised p(DMAEMA), the HEWL produced poor needles. Because of the poor stability of monoclinic crystals, and because they were normally surrounded by lots of HEWL needles, monoclinic crystals were not handled easily and it proved impossible to obtain SEM images in this research.

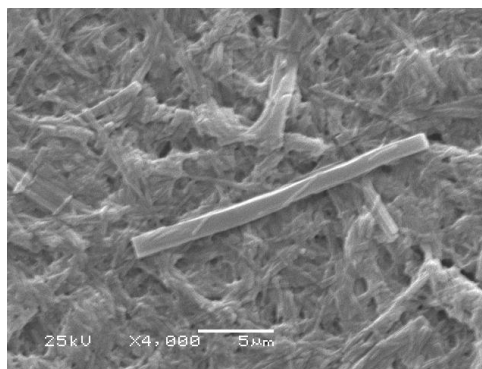


Figure 4-22. SEM micrograph of HEWL needles produced under tetragonal conditions in the presence of quaternised p(DMAEMA), -- x 4000 magnifications; the scale bar was 5 μ m.

4.3.2.2 HEWL crystallisation in the presence of p(DMAEMA-*stat*-PEGMA₄₇₅) (P3)

P(DMAEMA-*stat*-PEGMA₄₇₅) (P3) ($M_n \sim 52.9$ kDa) solutions with concentrations of 0.02 %, 0.2 %, 2 %, 4 %, 6 %, 8 %, 10 %, 12 %, 14 %, 16 %, 18 %, 20 % and 22 % (w/v) in 0.25 M sodium acetate, 20 % NaCl at pH 4.8 were prepared (Table 4-10). Each concentration was in triplicate for reproducibility.

Table 4-10. HEWL crystallisation plate: p(DMAEMA-*stat*-PEGMA₄₇₅) (P3)

	1	2	3	4	5	6	7	8	9	10	11	12
0.25 M Na Acetate, 20 % NaCl	800 µL (0.25 M Na Acetate, 20 % NaCl)	400 µL (0.25 M Na Acetate, 20 % NaCl)	200 µL (0.25 M Na Acetate, 20 % NaCl)									
Copolymer 38.96 % H ₂ O	1 µL (0.02 %) 1199 µL	5.1 µL (0.2 %) 594.9 µL	26 µL (2 %) 274 µL	51 µL (4 %) 249 µL	77 µL (6 %) 223 µL	103 µL (8 %) 197 µL	128 µL (10 %) 172 µL	154 µL (12 %) 146 µL	180 µL (14 %) 120 µL	205 µL (16 %) 95 µL	231 µL (18 %) 69 µL	257 µL (20 %) 43 µL
pH	4.8	4.8	4.8	4.8	4.8	4.8	4.8	4.8	4.8	4.8	4.8	4.8
0.25 M Na Acetate, 20 % NaCl	↓	↓	↓	↓	↓	↓	↓	↓	↓	↓	↓	↓
Copolymer 38.96 % H ₂ O	↓	↓	↓	↓	↓	↓	↓	↓	↓	↓	↓	↓
pH	↓	↓	↓	↓	↓	↓	↓	↓	↓	↓	↓	↓
0.25 M Na Acetate, 20 % NaCl	↓	↓	↓	↓	↓	↓	↓	↓	↓	↓	↓	↓
Copolymer 38.96 % H ₂ O	↓	↓	↓	↓	↓	↓	↓	↓	↓	↓	↓	↓
pH	↓	↓	↓	↓	↓	↓	↓	↓	↓	↓	↓	↓
0.25 M Na Acetate, 20 % NaCl	200 µL (0.25 M Na Acetate, 20 % NaCl)											
Copolymer 38.96 % H ₂ O	0 µL 300 µL											
pH	4.8	4.8	4.8	4.8	4.8	4.8	4.8	4.8	4.8	4.8	4.8	4.8
0.25 M Na Acetate, 20 % NaCl	↓	↓	↓	↓	↓	↓	↓	↓	↓	↓	↓	↓
Copolymer 38.96 % H ₂ O	↓	↓	↓	↓	↓	↓	↓	↓	↓	↓	↓	↓
pH	↓	↓	↓	↓	↓	↓	↓	↓	↓	↓	↓	↓
0.25 M Na Acetate, 20 % NaCl	200 µL (0.25 M Na Acetate, 20 % NaCl)											
Copolymer 38.96 % H ₂ O	18 µL 300 µL											
pH	4.8	4.8	4.8	4.8	4.8	4.8	4.8	4.8	4.8	4.8	4.8	4.8
0.25 M Na Acetate, 20 % NaCl	↓	↓	↓	↓	↓	↓	↓	↓	↓	↓	↓	↓
Copolymer 38.96 % H ₂ O	↓	↓	↓	↓	↓	↓	↓	↓	↓	↓	↓	↓
pH	↓	↓	↓	↓	↓	↓	↓	↓	↓	↓	↓	↓
0.25 M Na Acetate, 20 % NaCl	200 µL (0.25 M Na Acetate, 20 % NaCl)											
Copolymer 38.96 % H ₂ O	0 µL 300 µL											
pH	4.8	4.8	4.8	4.8	4.8	4.8	4.8	4.8	4.8	4.8	4.8	4.8
0.25 M Na Acetate, 20 % NaCl	↓	↓	↓	↓	↓	↓	↓	↓	↓	↓	↓	↓
Copolymer 38.96 % H ₂ O	↓	↓	↓	↓	↓	↓	↓	↓	↓	↓	↓	↓
pH	↓	↓	↓	↓	↓	↓	↓	↓	↓	↓	↓	↓

Figure 4-23 shows images of HEWL crystals obtained in the presence of p(DMAEMA-*stat*-PEGMA₄₇₅) (P3) at various concentrations, as solute in the

crystallisation solutions. Regular and small tetragonal HEWL crystals with the size of $\sim 100 \mu\text{m}$ formed within one day.

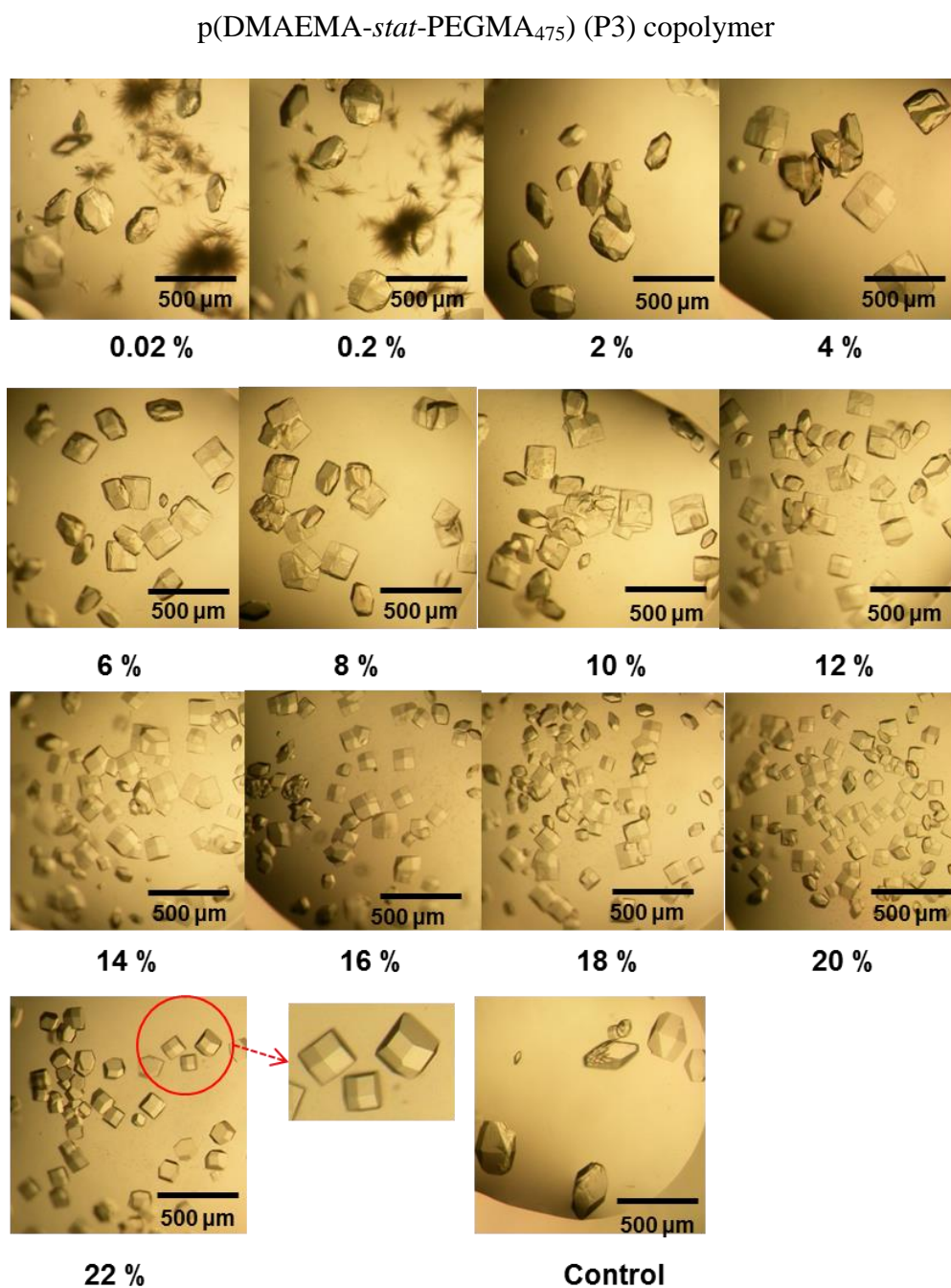


Figure 4-23. Photomicrographs of HEWL crystals, grown under the tetragonal protocol, in the presence of p(DMAEMA-*stat*-PEGMA₄₇₅) (P3) copolymer ($M_n \sim 52.9 \text{ kDa}$) at various concentrations. Image labelled 'Control' represents crystals grown from sample wells without polymer. The scale bar was $500 \mu\text{m}$.

A full summary of HEWL crystals size distribution by measuring the average length (μm) of the largest diameter of each crystal and number distribution depending on p(DMAEMA-*stat*-PEGMA₄₇₅) (P3) copolymer concentration was obtained by further image analysis (Figure 4-24). As the concentration of p(DMAEMA-*stat*-PEGMA₄₇₅) (P3) copolymer in solution was increased, the number of HEWL crystals appeared to increase and the size of the crystals decreased very clearly. Upon increasing the copolymer concentration to 20 %, the size of HEWL crystal decreased to $\sim 100 \mu\text{m}$.

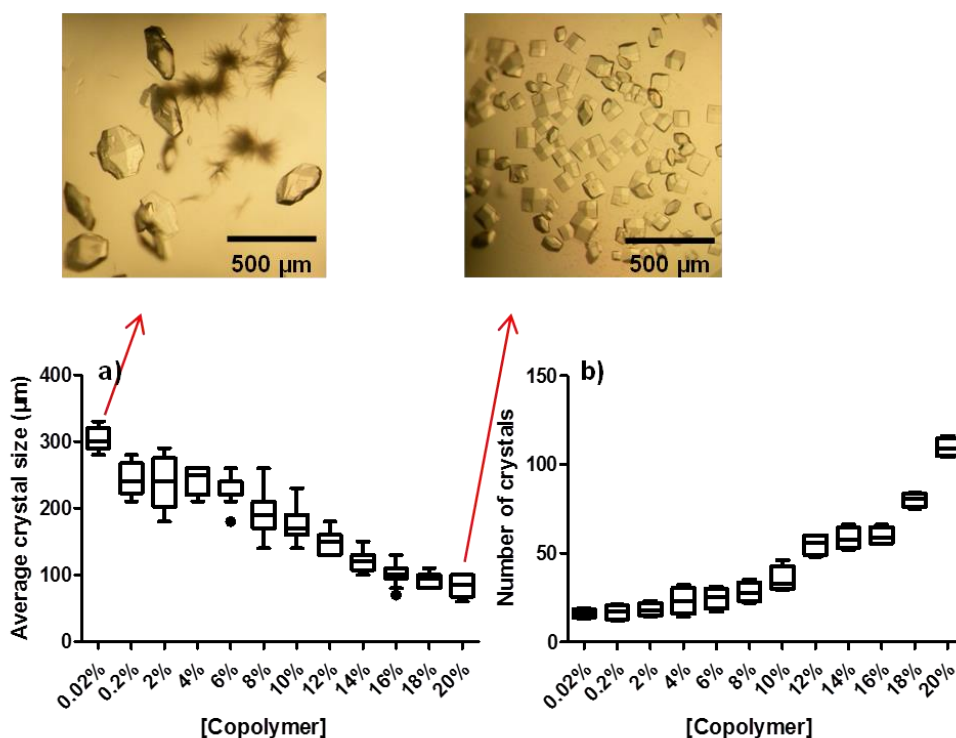


Figure 4-24. Summary of photomicrograph analysis showing changes in the size and number of HEWL crystals, grown in the presence of p(DMAEMA-*stat*-PEGMA₄₇₅) (P3) at various concentrations. a) Average length (μm) of the largest crystal diameter; b) Experiment count for the number of crystals per sample well. The scale bar was 500 μm .

Figure 4-25 illustrates the diffraction patterns of HEWL crystal, grown in the presence of p(DMAEMA-*stat*-PEGMA₄₇₅) (P3) by X-ray crystallography and Table 4-11 shows unit cell dimension of the HEWL crystal. Crystallisation of HEWL from the tetragonal-inducing protocol, when in the presence of cationic p(DMAEMA-*stat*-PEGMA₄₇₅) (P3), resulted in tetragonal crystals, which were confirmed by single crystal X-ray diffraction.

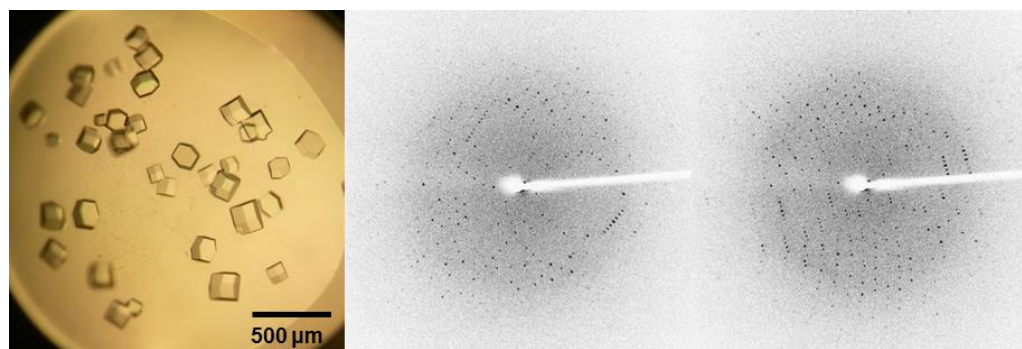


Figure 4-25. HEWL crystal photomicrograph and X-ray diffraction patterns yielded by the single HEWL crystal formed in the presence of cationic p(DMAEMA-*stat*-PEGMA₄₇₅) (P3). Two scattering angles: 0 ± 1 degrees and 90 ± 1 degrees.

Table 4-11. Unit cell dimension of HEWL crystal in the presence of cationic

p(DMAEMA-*stat*-PEGMA₄₇₅) (P3)

Polymer	a, b, c (Å)	α, β, γ	Volume	Unit cell lattice
P3	78.49, 78.49, 36.71	$90^\circ, 90^\circ, 90^\circ$	226,172	Tetragonal

P(DMAEMA-*stat*-PEGMA₄₇₅) (P3) copolymer might have different functions during HEWL crystallisation, due to the two components: neutral PEGMA₄₇₅

and cationic DMAEMA. As mentioned earlier, the neutral PEGMA₄₇₅ section might bind to water by H-bonding, compete with protein solutes for water and thus force protein solutes come out from the water solution. It could also lower the dielectric constant of the solution, leading to protein aggregation being promoted. At the crystallisation pH of 4.8, the cationic DMAEMA section had quaternary nitrogen with some positive charges, which could alter the electrostatic interactions between ionic HEWL macromolecules and the solution. There were likely to have been charge-charge repulsions between cationic DMAEMA and cationic HEWL macromolecules, which would lower the interface energy between HEWL macromolecules and water, consequently accelerated protein aggregation and the formation of multiple crystal nuclei for HEWL nucleation.

4.3.2.3 HEWL crystallisation in the presence of a mixture of two polymers: p(PEGMA₄₇₅) and p(DMAEMA) (P1 & P2) (molar ratio 9:1)

As mentioned above, p(DMAEMA-*stat*-PEGMA₄₇₅) (P3) affected the size of HEWL crystals very significantly. In order to compare the effects with p(DMAEMA-*stat*-PEGMA₄₇₅) copolymer, we set out to prepare a mixture of two polymers: p(PEGMA₄₇₅) and p(DMAEMA) (P1 & P2) for HEWL crystallisation. The following polymer solutions with a range of concentrations 0.02 %, 0.2 %, 2 %, 4 %, 6 %, 8 %, 10 %, 12 %, 14 %, 16 %, 18 % and 20 % (w/v) were prepared. Table 4-12 shows HEWL crystallisation plate in the

presents of a mixture of two polymers: p(PEGMA₄₇₅) and p(DMAEMA) (P1 & P2). Each concentration was in triplicate for reproducibility.

Table 4-12. HEWL crystallisation plate set up: a mixture of two polymers:

p(PEGMA₄₇₅) and p(DMAEMA) (P1 & P2)

	1	2	3	4	5	6	7	8	9	10	11	12
0.25 M Na Acetate, 20 % NaCl	800 µL (0.25 M Na Acetate, 20 % NaCl)	400 µL (0.25 M Na Acetate, 20 % NaCl)	200 µL (0.25 M Na Acetate, 20 % NaCl)	200 µL (0.25 M Na Acetate, 20 % NaCl)	200 µL (0.25 M Na Acetate, 20 % NaCl)	200 µL (0.25 M Na Acetate, 20 % NaCl)	200 µL (0.25 M Na Acetate, 20 % NaCl)	200 µL (0.25 M Na Acetate, 20 % NaCl)	200 µL (0.25 M Na Acetate, 20 % NaCl)	200 µL (0.25 M Na Acetate, 20 % NaCl)	200 µL (0.25 M Na Acetate, 20 % NaCl)	200 µL (0.25 M Na Acetate, 20 % NaCl)
Mixed polymers	1.2 µL (0.02 %)	6 µL (0.2 %)	30 µL (2 %)	60 µL (4 %)	89 µL (6 %)	119 µL (8 %)	149 µL (10 %)	179 µL (12 %)	209 µL (14 %)	239 µL (16 %)	268 µL (18 %)	298 µL (20 %)
33.52 % H ₂ O	1198.8 µL	594 µL	270 µL	240 µL	211 µL	181 µL	151 µL	121 µL	91 µL	61 µL	32 µL	2 µL
pH	4.8	4.8	4.8	4.8	4.8	4.8	4.8	4.8	4.8	4.8	4.8	4.8
0.25 M Na Acetate, 20 % NaCl												
Mixed polymers												
33.52 % H ₂ O												
pH												
0.25 M Na Acetate, 20 % NaCl												
Mixed polymers												
33.52 % H ₂ O												
pH												
0.25 M Na Acetate, 20 % NaCl	200 µL (0.25 M Na Acetate, 20 % NaCl)											
Mixed polymers	0 µL											
33.52 % H ₂ O	300 µL											
pH	4.8											
0.25 M Na Acetate, 20 % NaCl		200 µL (0.25 M Na Acetate, 20 % NaCl)										
Mixed polymers		0 µL										
33.52 % H ₂ O		300 µL										
pH		4.8										

Figure 4-26 shows the photomicrographs of HEWL crystals formed under a mixture of two polymers: p(PEGMA₄₇₅) and p(DMAEMA) (P1 & P2). A few large HEWL crystals formed within one day. From visual inspection, it is immediately clear that the results of crystallisation experiments are different from that obtained in the presents of p(DMAEMA-*stat*-PEGMA₄₇₅) (P3) copolymer, especially the crystal size and morphology shape. When the concentration of a mixture of two polymers: pPEGMA₄₇₅ and p(DMAEMA) (P1 & P2) in solution was increased to 20 % (w/v), the size of HEWL crystal was around 300 µm and the shape of some crystals was rhombohedral. But when in the presents of p(DMAEMA-*stat*-PEGMA₄₇₅) (P3) copolymer, the size was around 100 µm and the shape was exclusively tetragonal.

A mixture of two polymers: p(PEGMA₄₇₅) and p(DMAEMA) (P1 & P2) had two separate sections: neutral p(PEGMA₄₇₅) and cationic p(DMAEMA). However, unlike p(DMAEMA-*stat*-PEGMA₄₇₅) copolymer, those two sections affected HEWL crystallisation separately. It seems the influence of the neutral p(PEGMA₄₇₅) section was dominant in the crystallisation process

A mixture of two polymers: p(PEGMA₄₇₅) and p(DMAEMA) (P1 & P2)

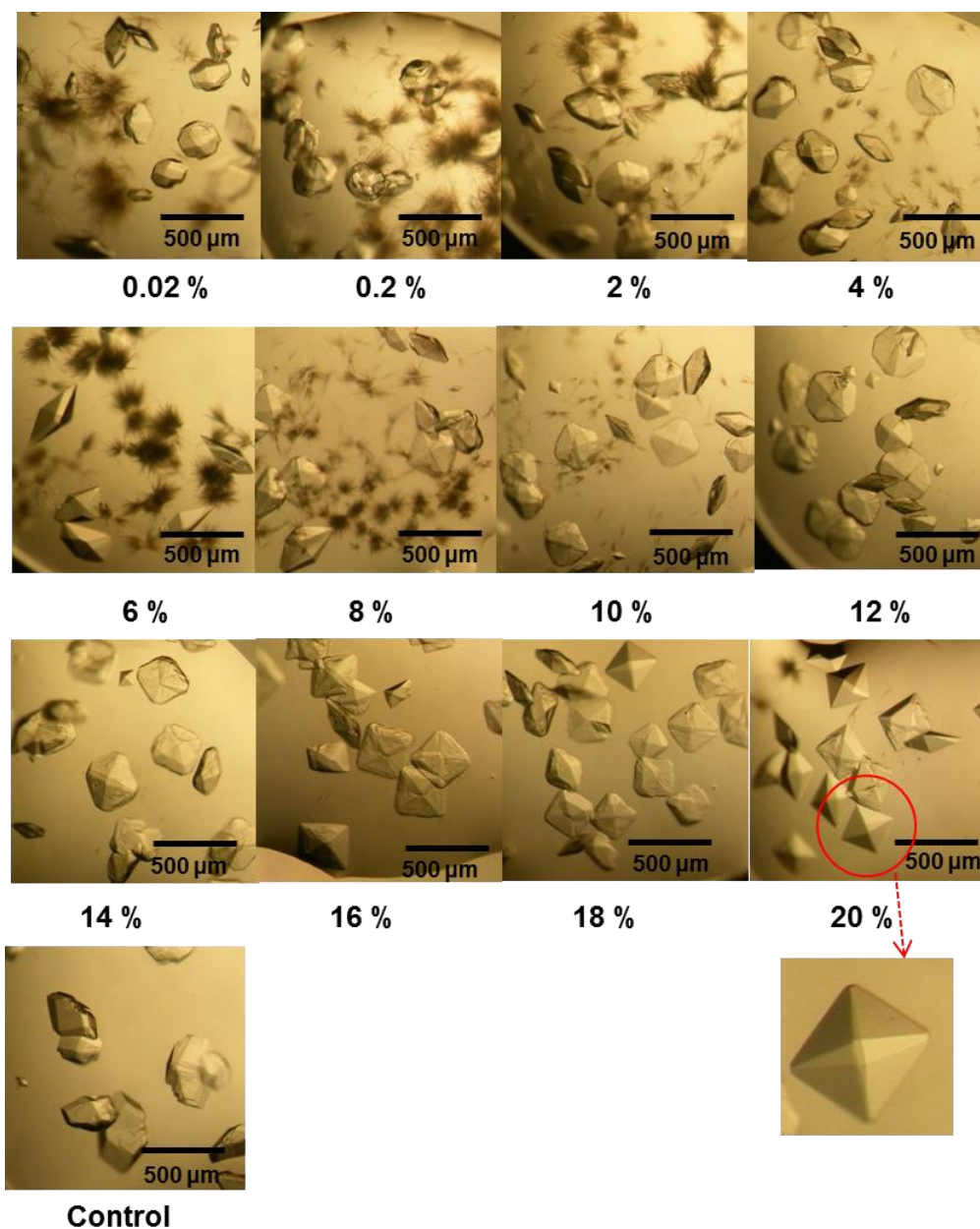


Figure 4-26. Photomicrographs of HEWL crystals, grown under the tetragonal protocol, in the presence of a mixture of two polymers: p(PEGMA₄₇₅) and p(DMAEMA) (P1 & P2) (molar ratio 9:1) at various concentrations. Image labelled 'Control' represents crystals grown from sample wells without polymer. The scale bar was 500 μm.

A full summary of HEWL crystals size distribution by measuring the average length (μm) of the largest diameter of each crystal and number distribution depending on a mixture of two polymers: p(PEGMA₄₇₅) and p(DMAEMA) (P1 & P2) concentration was obtained by further image analysis (Figure 4-27). As the concentration of a mixture of two polymers: p(PEGMA₄₇₅) and p(DMAEMA) (P1 & P2) in solution was increased, the number of HEWL crystals appeared to increase and the size of the crystals appeared to decrease.

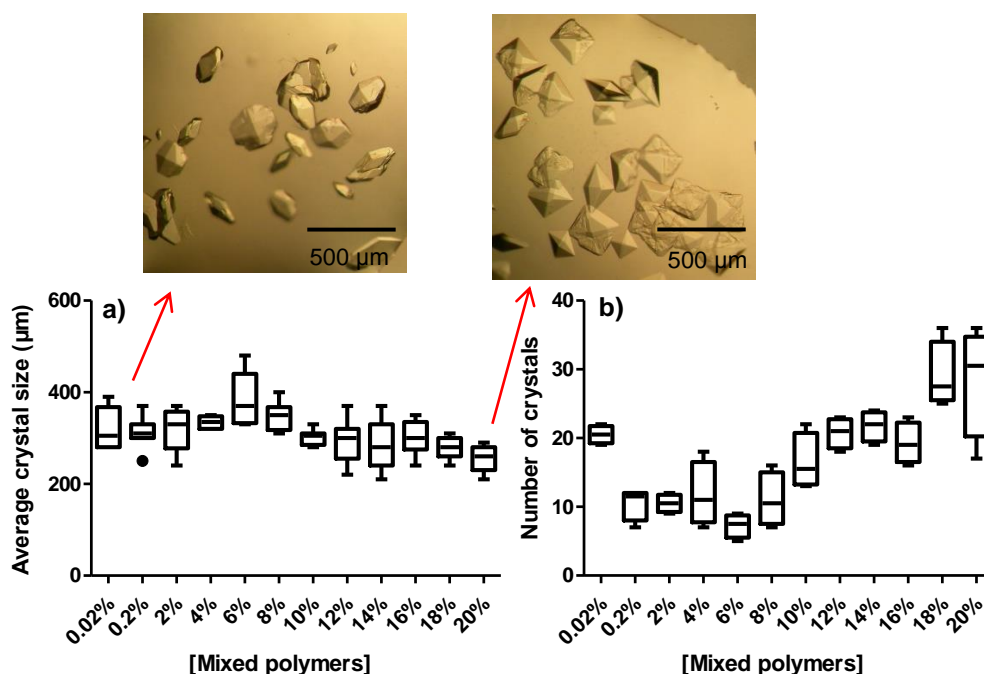


Figure 4-27. Summary of photomicrograph analysis showing changes in the size and number of HEWL crystals, grown in the presence of a mixture of two polymers: p(PEGMA₄₇₅) and p(DMAEMA) (P1 & P2) at various concentrations. a) Average length (μm) of the largest crystal diameter; b) Experiment count for the number of crystals per sample well. The scale bar was 500 μm .

Figure 4-28 illustrates the diffraction patterns of HEWL crystal, grown in the presence of a mixture of two polymers: p(PEGMA₄₇₅) and p(DMAEMA) (P1 & P2). Table 4-13 shows unit cell dimension of the HEWL crystal, identified as tetragonal by single crystal X-ray diffraction.

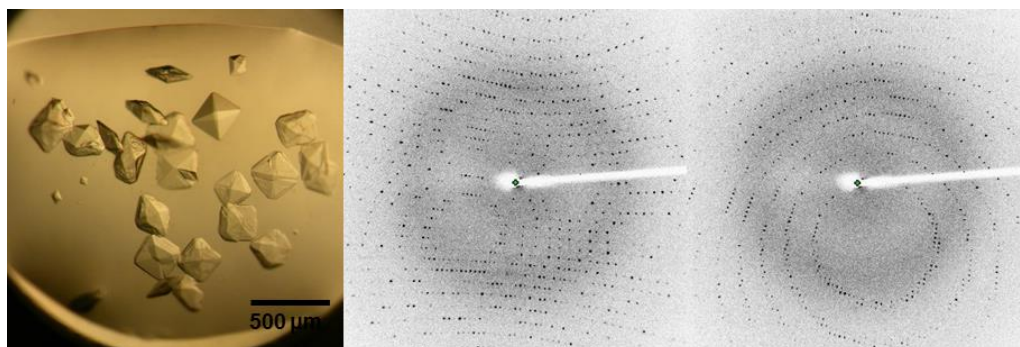


Figure 4-28. HEWL crystal photomicrograph and X-ray diffraction patterns yielded by the single HEWL crystal in the presence of a mixture of two polymers: p(PEGMA₄₇₅) and p(DMAEMA) (P1 & P2). Two scattering angles: 0 ± 1 degrees and 90 ± 1 degrees.

Table 4-13. Unit cell dimension of HEWL crystal in the presence of a mixture of two polymers: p(PEGMA₄₇₅) and p(DMAEMA) (P1 & P2)

Polymer	a, b, c (Å)	α, β, γ	Volume	Unit cell lattice
A mixture of two polymers: p(PEGMA ₄₇₅) and p(DMAEMA)	78.85, 78.85, 37.12	90 °, 90 °, 90 °	230,779	Tetragonal

Figure 4-29 shows Tukey plots of DLS data when in the presence of a mixture of two polymers: p(PEGMA₄₇₅) and p(DMAEMA) (P1 & P2). At the beginning of the experiment (T_0), the average size of the particles in the crystallisation

solution was around 180 nm. After the addition of a mixture of two polymers: p(PEGMA₄₇₅) and p(DMAEMA) (P1 & P2), as the time increased, a characteristic increase in HEWL aggregate size can be observed. After 395 minutes ($T_{395\text{min}}$), the average size of the particles in the crystallisation solution was around 900 nm. DLS data details, including autocorrelation functions and radii distribution by intensity are shown in the Appendix Page 337.

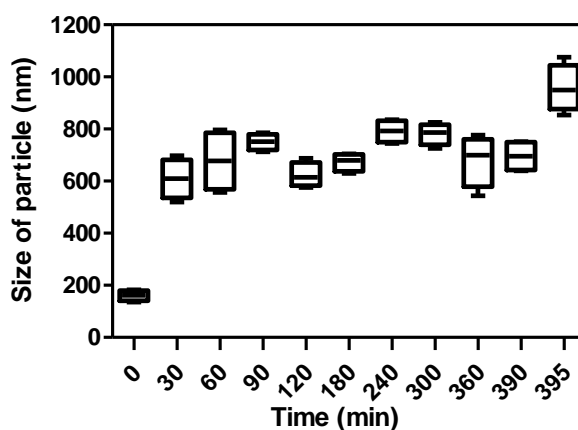


Figure 4-29. Variations of the size of HEWL aggregates or crystals in the solution as a function of time during crystallisation experiments induced by a mixture of two polymers: p(PEGMA₄₇₅) and p(DMAEMA) (P1 & P2).

4.3.2.4 HEWL crystallisation in the presence of p(DMAPMAM) (P4)

DMAPMAM, containing tertiary amines group was homopolymerised to form another cationic polymer. The following polymer solutions were prepared: p(DMAPMAM) (P4) (DPs 38, 83 and 150) 0.02 %, 0.2 %, 2 %, 4 %, 6 %, 8 %, 10 %, 12 % and 14 % (w/v) in 0.25 M sodium acetate and 20 % NaCl at pH 4.8 buffer solution. Tables 4-14a-c show HEWL crystallisation plating methods under p(DMAPMAM) (P4) (DPs 38, 83 and 150).

Table 4-14a. HEWL crystallisation plate set up: p(DMAPMAM) (P4) (DP 38)

	1	2	3	4	5	6	7	8	9
0.25 M Na Acetate, 20 % NaCl	400 µL (0.25 M Na Acetate, 20 % NaCl)	200 µL (0.25 M Na Acetate, 20 % NaCl)	100 µL (0.25 M Na Acetate, 20 % NaCl)	100 µL (0.25 M Na Acetate, 20 % NaCl)	100 µL (0.25 M Na Acetate, 20 % NaCl)	100 µL (0.25 M Na Acetate, 20 % NaCl)	100 µL (0.25 M Na Acetate, 20 % NaCl)	100 µL (0.25 M Na Acetate, 20 % NaCl)	100 µL (0.25 M Na Acetate, 20 % NaCl)
p(DMAPMAM) (DP 38)	0.5 µL (0.02 %)	3 µL (0.2 %)	13 µL (2 %)	26 µL (4 %)	39 µL (6 %)	53 µL (8 %)	66 µL (10 %)	79 µL (12 %)	92 µL (14 %)
H ₂ O	599.5 µL	297 µL	137 µL	124 µL	111 µL	97 µL	84 µL	71 µL	58 µL
pH	4.8	4.8	4.8	4.8	4.8	4.8	4.8	4.8	4.8
0.25 M Na Acetate, 20 % NaCl	↓	↓	↓	↓	↓	↓	↓	↓	↓
p(DMAPMAM) (DP 38)									
H ₂ O									
pH									
0.25 M Na Acetate, 20 % NaCl	↓	↓	↓	↓	↓	↓	↓	↓	↓
p(DMAPMAM) (DP 38)									
H ₂ O									
pH									
0.25 M Na Acetate, 20 % NaCl	200 µL (0.25 M Na Acetate, 20 % NaCl)	0 µL							
p(DMAPMAM) (DP 38)	0 µL								
H ₂ O	300 µL								
pH	4.8								
	↑	↑	↑	↑	↑	↑	↑	↑	↑

Table 4-14b. HEWL crystallisation plate set up: p(DMAPMAM) (P4) (DP 83)

	1	2	3	4	5	6	7	8	9
0.25 M Na Acetate, 20 % NaCl	400 μ L (0.25 M Na Acetate, 20 % NaCl)	200 μ L (0.25 M Na Acetate, 20 % NaCl)	100 μ L (0.25 M Na Acetate, 20 % NaCl)	100 μ L (0.25 M Na Acetate, 20 % NaCl)	100 μ L (0.25 M Na Acetate, 20 % NaCl)	100 μ L (0.25 M Na Acetate, 20 % NaCl)	100 μ L (0.25 M Na Acetate, 20 % NaCl)	100 μ L (0.25 M Na Acetate, 20 % NaCl)	100 μ L (0.25 M Na Acetate, 20 % NaCl)
p(DMAPMAM) (DP 83)	0.6 μ L (0.02 %)	3 μ L (0.2 %)	14 μ L (2 %)	28 μ L (4 %)	41 μ L (6 %)	55 μ L (8 %)	69 μ L (10 %)	83 μ L (12 %)	96 μ L (14 %)
H ₂ O	599.4 μ L	297 μ L	136 μ L	122 μ L	109 μ L	95 μ L	81 μ L	67 μ L	54 μ L
pH	4.8	4.8	4.8	4.8	4.8	4.8	4.8	4.8	4.8
0.25 M Na Acetate, 20 % NaCl									
p(DMAPMAM) (DP 83)									
H ₂ O									
pH									
0.25 M Na Acetate, 20 % NaCl									
p(DMAPMAM) (DP 83)									
H ₂ O									
pH									
0.25 M Na Acetate, 20 % NaCl	200 μ L (0.25 M Na Acetate, 20 % NaCl)								
p(DMAPMAM) (DP 83)	0 μ L								
H ₂ O	300 μ L								
pH	4.8								

Table 4-14c. HEWL crystallisation plate set up: p(DMAPMAM) (P4) (DP 150)

	1	2	3	4	5	6	7	8	9
0.25 M Na Acetate, 20 % NaCl	400 μ L (0.25 M Na Acetate, 20 % NaCl)	200 μ L (0.25 M Na Acetate, 20 % NaCl)	100 μ L (0.25 M Na Acetate, 20 % NaCl)	100 μ L (0.25 M Na Acetate, 20 % NaCl)	100 μ L (0.25 M Na Acetate, 20 % NaCl)	100 μ L (0.25 M Na Acetate, 20 % NaCl)	100 μ L (0.25 M Na Acetate, 20 % NaCl)	100 μ L (0.25 M Na Acetate, 20 % NaCl)	100 μ L (0.25 M Na Acetate, 20 % NaCl)
p(DMAPMAM) (DP 150)	0.5 μ L (0.02 %)	3 μ L (0.2 %)	13 μ L (2 %)	27 μ L (4 %)	40 μ L (6 %)	53 μ L (8 %)	67 μ L (10 %)	80 μ L (12 %)	93 μ L (14 %)
H ₂ O	599.5 μ L	297 μ L	137 μ L	123 μ L	110 μ L	97 μ L	83 μ L	70 μ L	57 μ L
pH	4.8	4.8	4.8	4.8	4.8	4.8	4.8	4.8	4.8
0.25 M Na Acetate, 20 % NaCl	↓	↓	↓	↓	↓	↓	↓	↓	↓
p(DMAPMAM) (DP 150)									
H ₂ O									
pH									
0.25 M Na Acetate, 20 % NaCl	↓	↓	↓	↓	↓	↓	↓	↓	↓
p(DMAPMAM) (DP 150)									
H ₂ O									
pH									
0.25 M Na Acetate, 20 % NaCl	200 μ L (0.25 M Na Acetate, 20 % NaCl)	↑	↑	↑	↑	↑	↑	↑	↑
p(DMAPMAM) (DP 150)	0 μ L								
H ₂ O	300 μ L								
pH	4.8								

Previous results showed that cationic quaternised p(DMAEMA) was able to control the morphology shape and alter the size of HEWL crystals. Similar as DMAEMA, monomer DMAPMAM has tertiary amine functionality, which can afford positive charges at crystallisation pH of 4.8. Figures 4-30a-c show the HEWL crystals obtained in the presence of p(DMAPMAM) (P4) (DPs 38, 83 and 150) with various concentrations (0.02 % ~ 20 % (w/v)), as solute in crystallisation solutions. From visual observation, cationic p(DMAPMAM) had an increased propensity for nucleating much more small crystals. It nucleated many uniform and small tetragonal HEWL crystals with the size of ~ 100 μm within one day. These HEWL crystals were identified as tetragonal by single crystal X-ray diffraction. Upon increasing the DP of p(DMAPMAM), the size of HEWL crystals slightly increased. The possible reason is that p(DMAPMAM) with higher DP had a larger molecular weight, which would increase the viscosity of the solution and slow the rate of protein crystal growth.²²⁷

a) p(DMAPMAm) (P4) (DP 38)

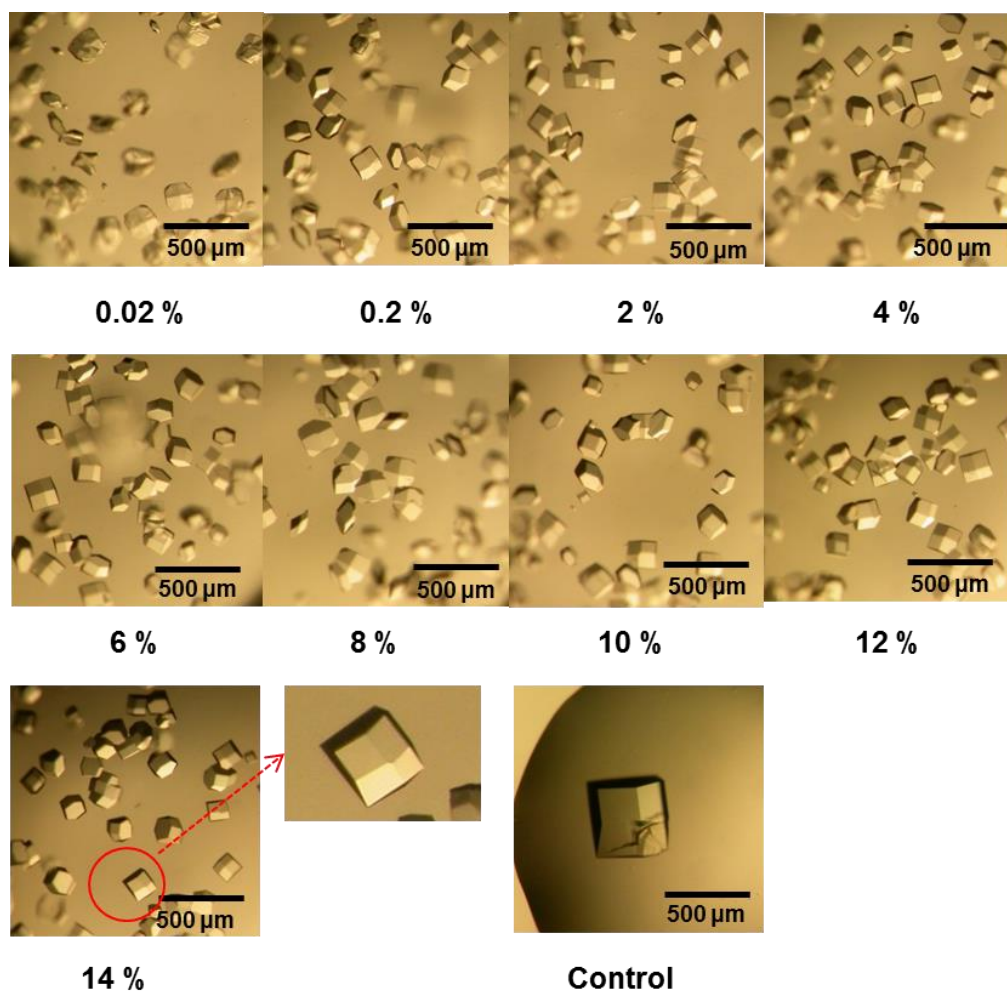


Figure 4-30a. Photomicrographs of HEWL crystals, grown under tetragonal crystal condition, in the presence of p(DMAPMAm) (P4) (DP 38) at various concentrations. Image labelled 'Control' represents crystals grown from sample wells without polymer. The scale bar was 500 μm .

b) p(DMAPMAm) (P4) (DP 83)

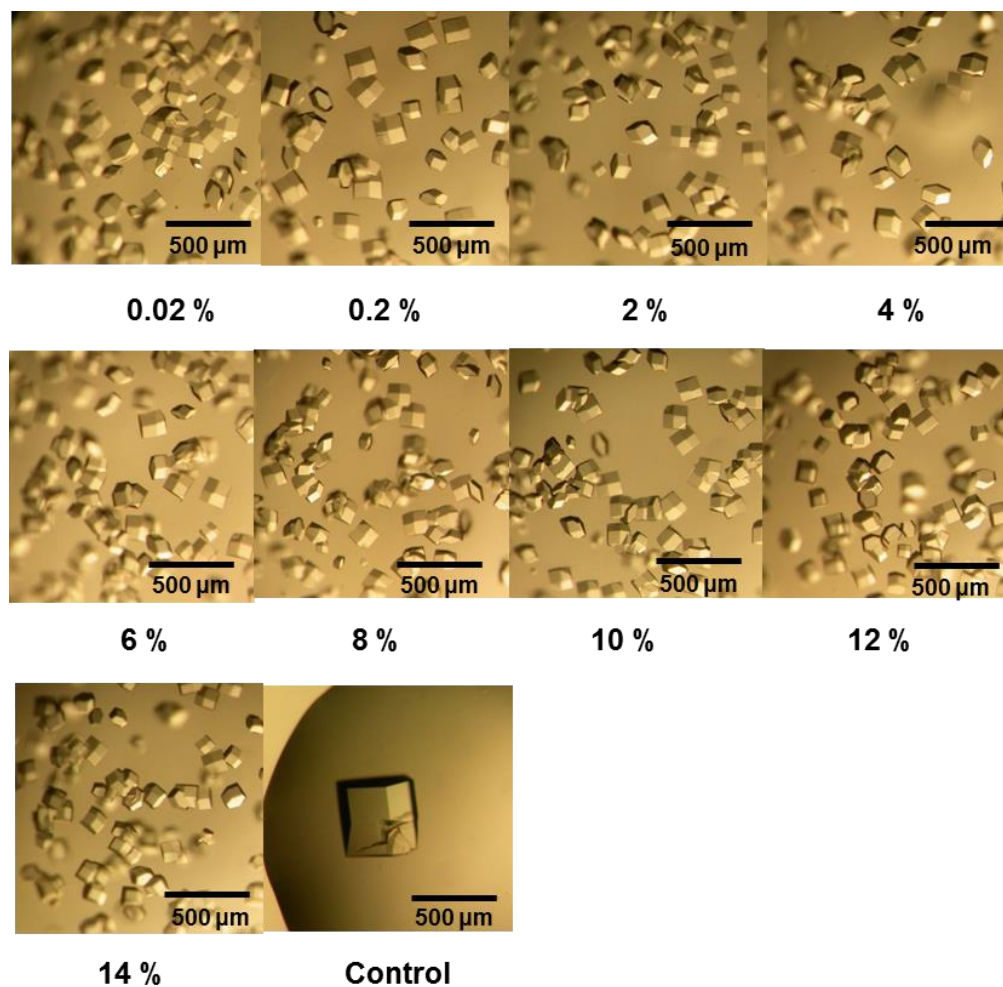


Figure 4-30b. Photomicrographs of HEWL crystals, grown under tetragonal crystal condition, in the presence of p(DMAPMAm) (P4) (DP 83) at various concentrations. Image labelled 'Control' represents crystals grown from sample wells without polymer. The scale bar was 500 μm.

c) p(DMAPMAm) (P4) DP 150

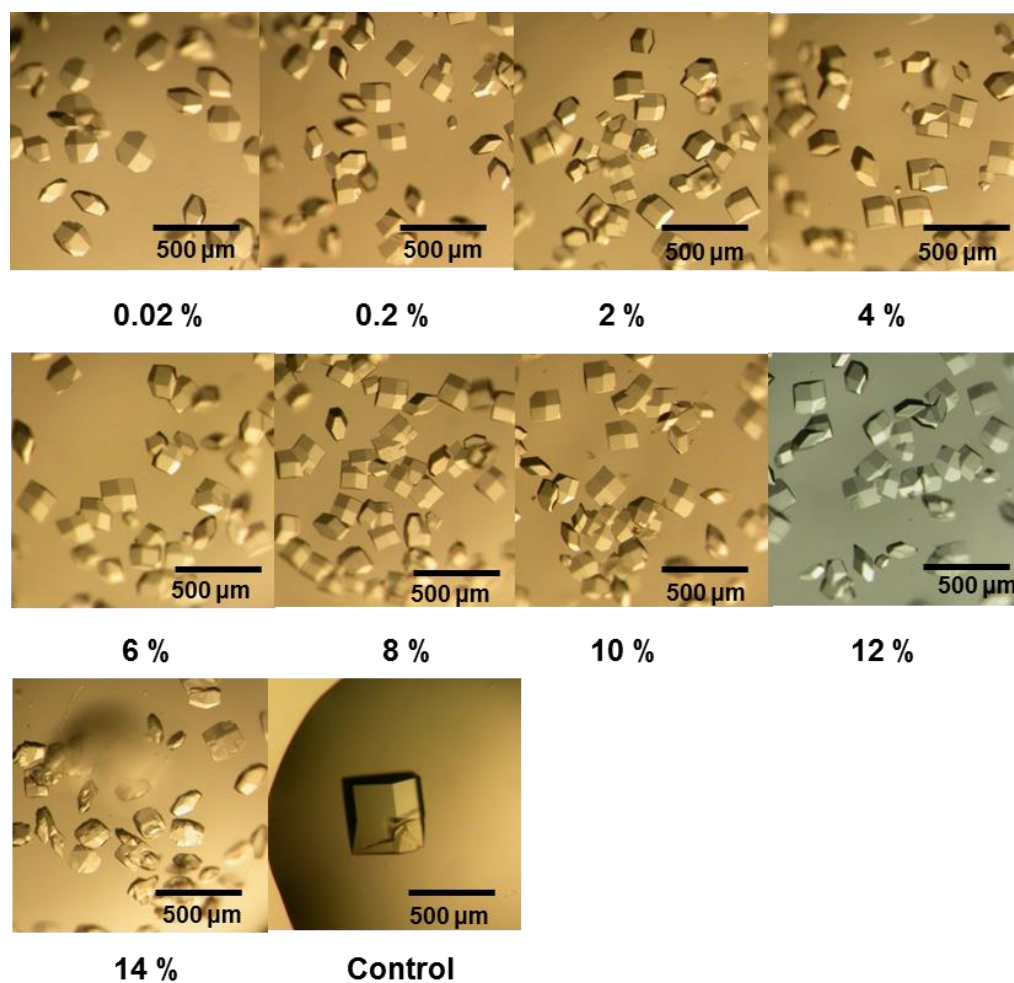


Figure 4-30c. Photomicrographs of HEWL crystals, grown under tetragonal crystal condition, in the presence of p(DMAPMAm) (P4) (DP 150) at various concentrations. Image labelled 'Control' represents crystals grown from sample wells without polymer. The scale bar was 500 μm.

A full coverage of crystal size distribution by measuring the average length (μm) of the largest crystal diameter and number distribution was obtained from p(DMAPMAm) (P4) (DP 83) (Figure 4-31). As the p(DMAPMAm) concentration was increased, the size of crystals decrease and the number of

crystals increased.

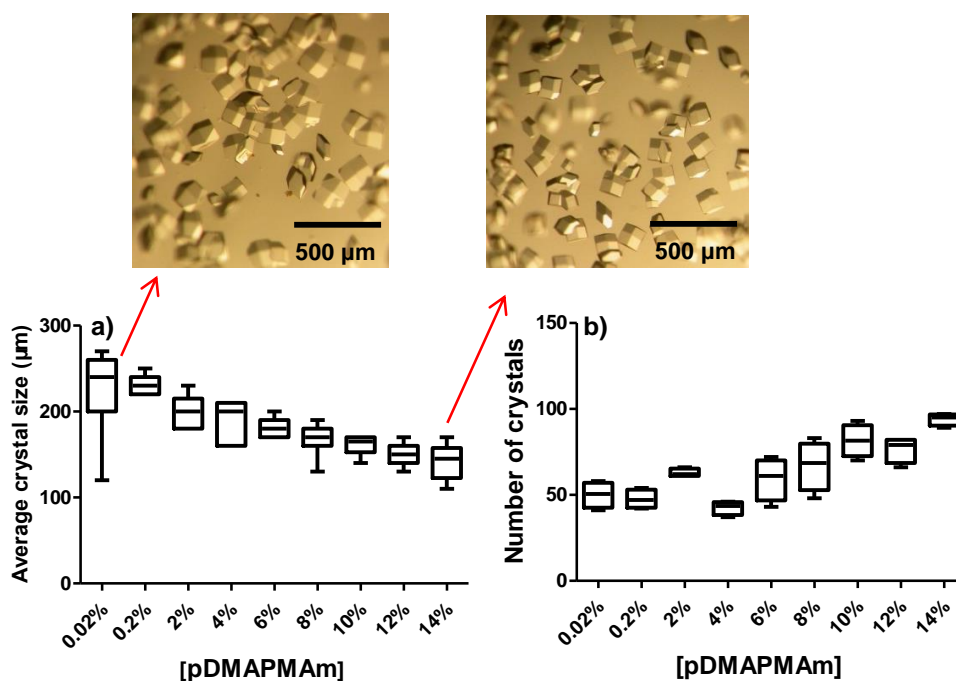


Figure 4-31. Summary of photomicrograph analysis of HEWL crystals, grown in the presence of p(DMAPMAm) (P4) (DP 83) at various concentrations. a) Average length (μm) of the largest crystal diameter; b) Experiment count for the number of crystals per sample well. The scale bar was $500\mu\text{m}$.

Figure 4-32 shows Tukey plots of DLS data of HEWL crystallisation in the presence of p(DMAPMAm) (P4). P(DMAPMAm) (P4) did not alter the size of HEWL aggregates or crystals clearly after 420 min. The size of pure p(DMAPMAm) (P4) in the solution without any protein was around 3 nm. Similar as quaternised p(DMAEMA) (P2), cationic p(DMAPMAm) (P4) could lower the interfacial energy between cationic HEWL macromolecules and water by charge-charge repulsions, thus promoted nucleation and the formation of multiple crystal nuclei. In turn, HEWL aggregates or crystals would grow

very slowly. DLS data details, including autocorrelation functions and radii distribution by intensity are shown in the Appendix Page 338.

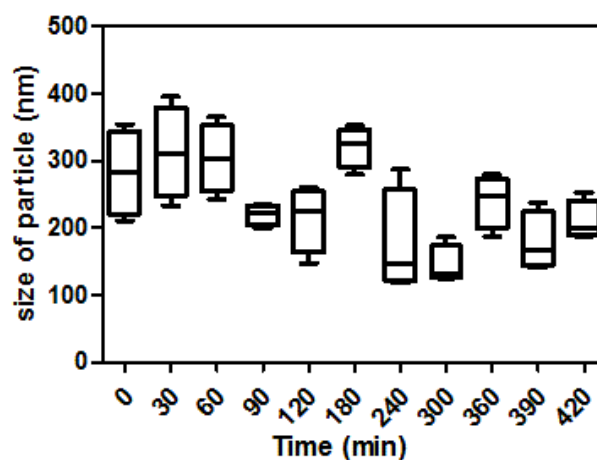


Figure 4-32. Variations of the size of HEWL aggregates or crystals in the solution as a function of time during crystallisation experiments induced by p(DMAPMAm) (P4).

In summary, cationic polymers had an increased propensity for nucleating small crystals. Figure 4-33 shows the hypothesis of mechanism of how cationic polymers mediated HEWL crystallisation.^{108, 226, 228, 229} There were likely to have been charge-charge repulsions between cationic polymer molecules and cationic HEWL macromolecules, lowering the interfacial energy between HEWL macromolecules and water, thus promoting protein-protein interactions at hydrophobic sites or anionic-cationic pair sites and subsequent crystallisation. In addition, cationic polymers might have bound to anionic residues on the HEWL chain leading to charge compensation by electrostatic interaction,¹⁰⁸ an increase of local concentration of HEWL macromolecules and the promotion of nucleation.

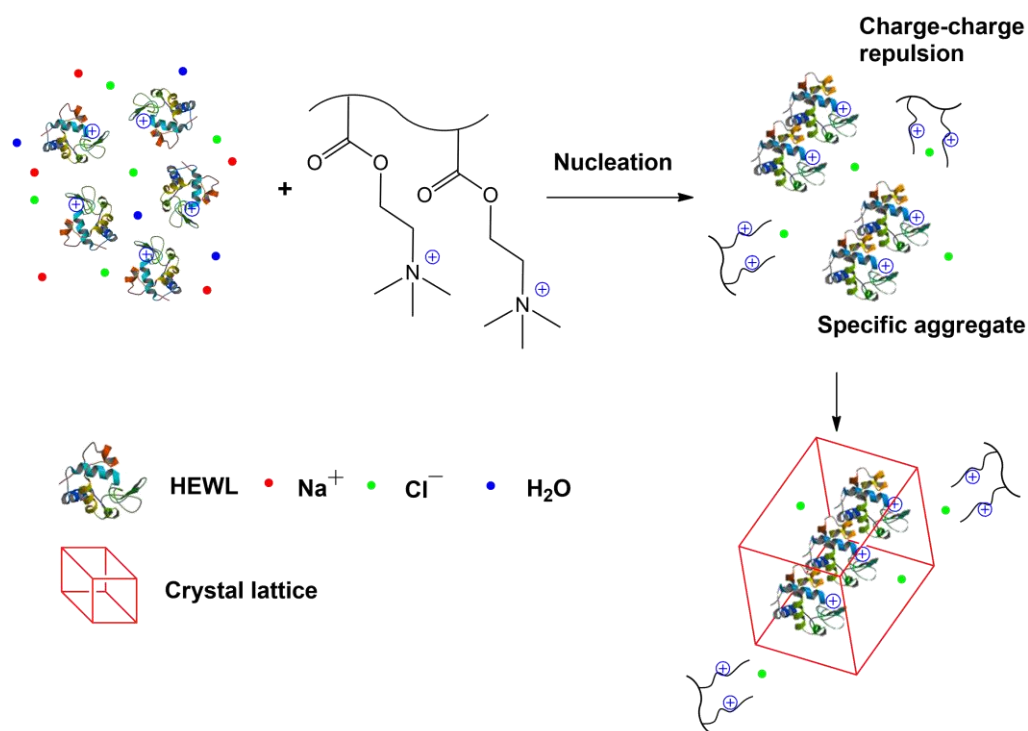


Figure 4-33. Hypothesis of mechanism of cationic polymer mediated HEWL crystallisation. Cationic polymer: charge-charge repulsions between cationic polymer and cationic HEWL. HEWL macromolecules are positively charged at tetragonal crystallisation pH of 4.8, i.e. cationic. Na^+ and Cl^- ions are from the crystallisation buffer solutions.

4.3.3 HEWL crystallisation in the presence of anionic polymers in solution

4.3.3.1 HEWL crystallisation in the presence of p(AMPS) (P5)

Monomer AMPS, containing ionisable sulfonic acid group can introduce some negative charges and homopolymerise to generate an anionic polymer P5. The following polymer solutions were prepared: p(AMPS) (P5) (DPs 53, 99 and 200): 0.02 %, 0.2 %, 2 %, 4 %, 6 %, 8 %, 10 %, 12 % and 14 % (w/v) in 0.25 M sodium acetate, 20 % NaCl, pH 4.8 buffer solution (Tables 4-15a-c).

Table 4-15a. HEWL crystallisation plate set up: p(AMPS) (P5) (DP 53)

	1	2	3	4	5	6	7	8	9
0.25 M Na Acetate, 20 % NaCl	400 μ L (0.25 M Na Acetate, 20 % NaCl)	200 μ L (0.25 M Na Acetate, 20 % NaCl)	100 μ L (0.25 M Na Acetate, 20 % NaCl)	100 μ L (0.25 M Na Acetate, 20 % NaCl)	100 μ L (0.25 M Na Acetate, 20 % NaCl)	100 μ L (0.25 M Na Acetate, 20 % NaCl)	100 μ L (0.25 M Na Acetate, 20 % NaCl)	100 μ L (0.25 M Na Acetate, 20 % NaCl)	100 μ L (0.25 M Na Acetate, 20 % NaCl)
p(AMPS) (DP 53)	0.6 μ L (0.02 %)	3 μ L (0.2 %)	14 μ L (2 %)	28 μ L (4 %)	42 μ L (6 %)	55 μ L (8 %)	69 μ L (10 %)	83 μ L (12 %)	97 μ L (14 %)
H ₂ O	599.4 μ L	297 μ L	136 μ L	122 μ L	108 μ L	95 μ L	81 μ L	67 μ L	53 μ L
pH	4.8	4.8	4.8	4.8	4.8	4.8	4.8	4.8	4.8
0.25 M Na Acetate, 20 % NaCl	↓	↓	↓	↓	↓	↓	↓	↓	↓
p(AMPS) (DP 53)									
H ₂ O									
pH									
0.25 M Na Acetate, 20 % NaCl	↓	↓	↓	↓	↓	↓	↓	↓	↓
p(AMPS) (DP 53)									
H ₂ O									
pH									
0.25 M Na Acetate, 20 % NaCl	↑	↑	↑	↑	↑	↑	↑	↑	↑
p(AMPS) (DP 53)									
H ₂ O									
pH									

Table 4-15b. HEWL crystallisation plate set up: p(AMPS) (P5) (DP 99)

	1	2	3	4	5	6	7	8
0.25 M Na Acetate, 20 % NaCl	400 μ L (0.25 M Na Acetate, 20 % NaCl)	200 μ L (0.25 M Na Acetate, 20 % NaCl)	100 μ L (0.25 M Na Acetate, 20 % NaCl)	100 μ L (0.25 M Na Acetate, 20 % NaCl)	100 μ L (0.25 M Na Acetate, 20 % NaCl)	100 μ L (0.25 M Na Acetate, 20 % NaCl)	100 μ L (0.25 M Na Acetate, 20 % NaCl)	100 μ L (0.25 M Na Acetate, 20 % NaCl)
p(AMPS) (DP 99) H ₂ O pH	0.7 μ L (0.02 %) 599.3 μ L 4.8	3 μ L (0.2 %) 297 μ L 4.8	17 μ L (2 %) 133 μ L 4.8	34 μ L (4 %) 116 μ L 4.8	50 μ L (6 %) 100 μ L 4.8	67 μ L (8 %) 83 μ L 4.8	84 μ L (10 %) 66 μ L 4.8	101 μ L (12 %) 49 μ L 4.8
0.25 M Na Acetate, 20 % NaCl	↓	↓	↓	↓	↓	↓	↓	↓
p(AMPS) (DP 99) H ₂ O pH								
0.25 M Na Acetate, 20 % NaCl	↓	↓	↓	↓	↓	↓	↓	↓
p(AMPS) (DP 99) H ₂ O pH								
0.25 M Na Acetate, 20 % NaCl	200 μ L (0.25 M Na Acetate, 20 % NaCl)	↑	↑	↑	↑	↑	↑	↑
p(AMPS) (DP 99) H ₂ O pH	0 μ L 300 μ L 4.8							

Table 4-15c. HEWL crystallisation plate set up: p(AMPS) (P5) (DP 200)

	1	2	3	4	5	6	7	8	9
0.25 M Na Acetate, 20 % NaCl	400 μ L (0.25 M Na Acetate, 20 % NaCl)	200 μ L (0.25 M Na Acetate, 20 % NaCl)	100 μ L (0.25 M Na Acetate, 20 % NaCl)	100 μ L (0.25 M Na Acetate, 20 % NaCl)	100 μ L (0.25 M Na Acetate, 20 % NaCl)	100 μ L (0.25 M Na Acetate, 20 % NaCl)	100 μ L (0.25 M Na Acetate, 20 % NaCl)	100 μ L (0.25 M Na Acetate, 20 % NaCl)	100 μ L (0.25 M Na Acetate, 20 % NaCl)
p(AMPS) (DP 200) H ₂ O	0.5 μ L (0.02 %) 599.5 μ L	3 μ L (0.2 %) 297 μ L	13 μ L (2 %) 137 μ L	26 μ L (4 %) 124 μ L	39 μ L (6 %) 111 μ L	52 μ L (8 %) 98 μ L	65 μ L (10 %) 85 μ L	79 μ L (12 %) 71 μ L	92 μ L (14 %) 58 μ L
pH	4.8	4.8	4.8	4.8	4.8	4.8	4.8	4.8	4.8
0.25 M Na Acetate, 20 % NaCl	↓	↓	↓	↓	↓	↓	↓	↓	↓
p(AMPS) (DP 200) H ₂ O									
pH									
0.25 M Na Acetate, 20 % NaCl	↓	↓	↓	↓	↓	↓	↓	↓	↓
p(AMPS) (DP 200) H ₂ O									
pH									
0.25 M Na Acetate, 20 % NaCl	↑	↑	↑	↑	↑	↑	↑	↑	↑
p(AMPS) (DP 200) H ₂ O	200 μ L (0.25 M Na Acetate, 20 % NaCl)								
pH	0 μ L 300 μ L 4.8								

Figures 4-34a-c show the images of HEWL crystals obtained in the presence of p(AMPS) (P5) (DPs 53, 99 and 200) with various concentrations (0.02 % ~ 20 % (w/v)). Anionic p(AMPS) nucleated a few large crystals, which were then identified as tetragonal by single crystal X-ray diffraction.

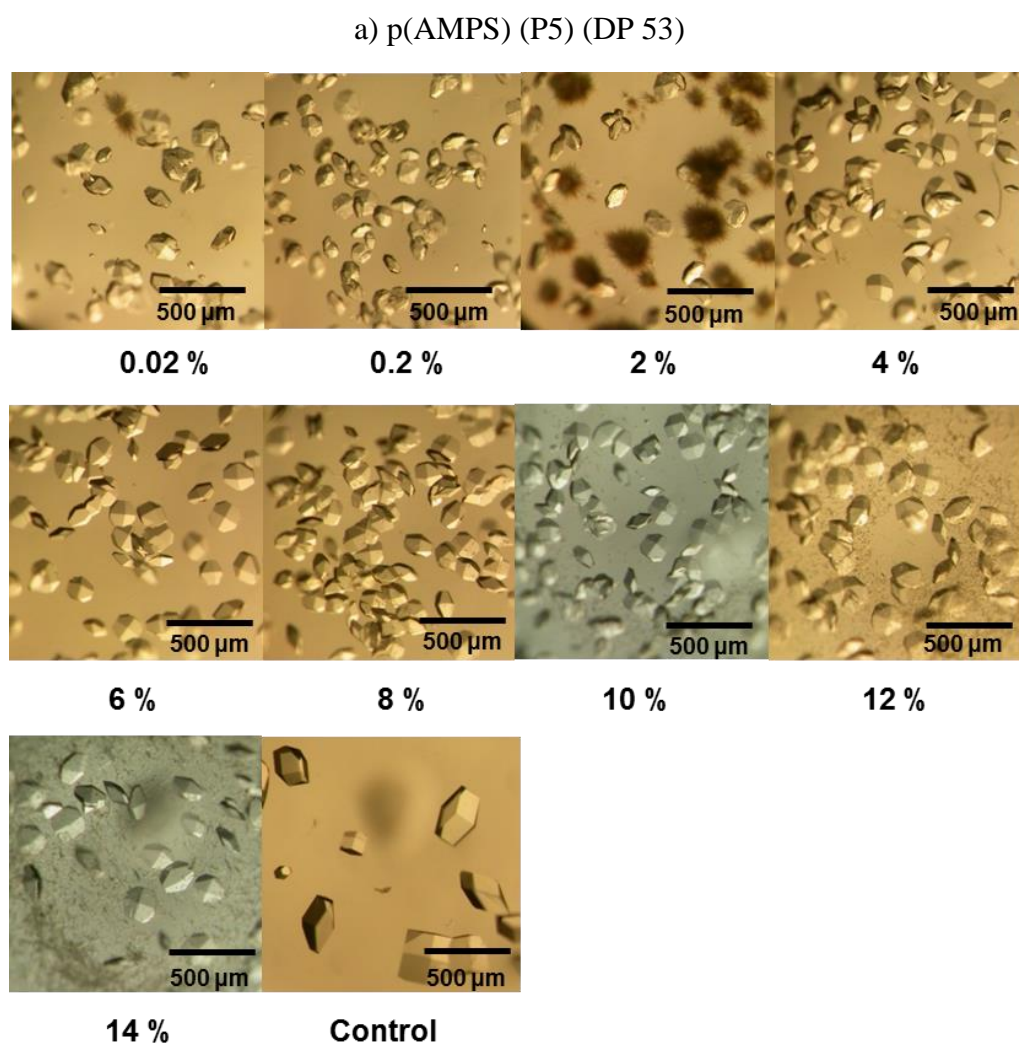


Figure 4-34a. Photomicrographs of HEWL crystals, grown under tetragonal crystal condition, in the presence of p(AMPS) (P5) (DP 53) at various concentrations. Image labelled 'Control' represents crystals grown from sample wells without polymer. The scale bar was 500 μm .

b) p(AMPS) (P5) (DP 99)

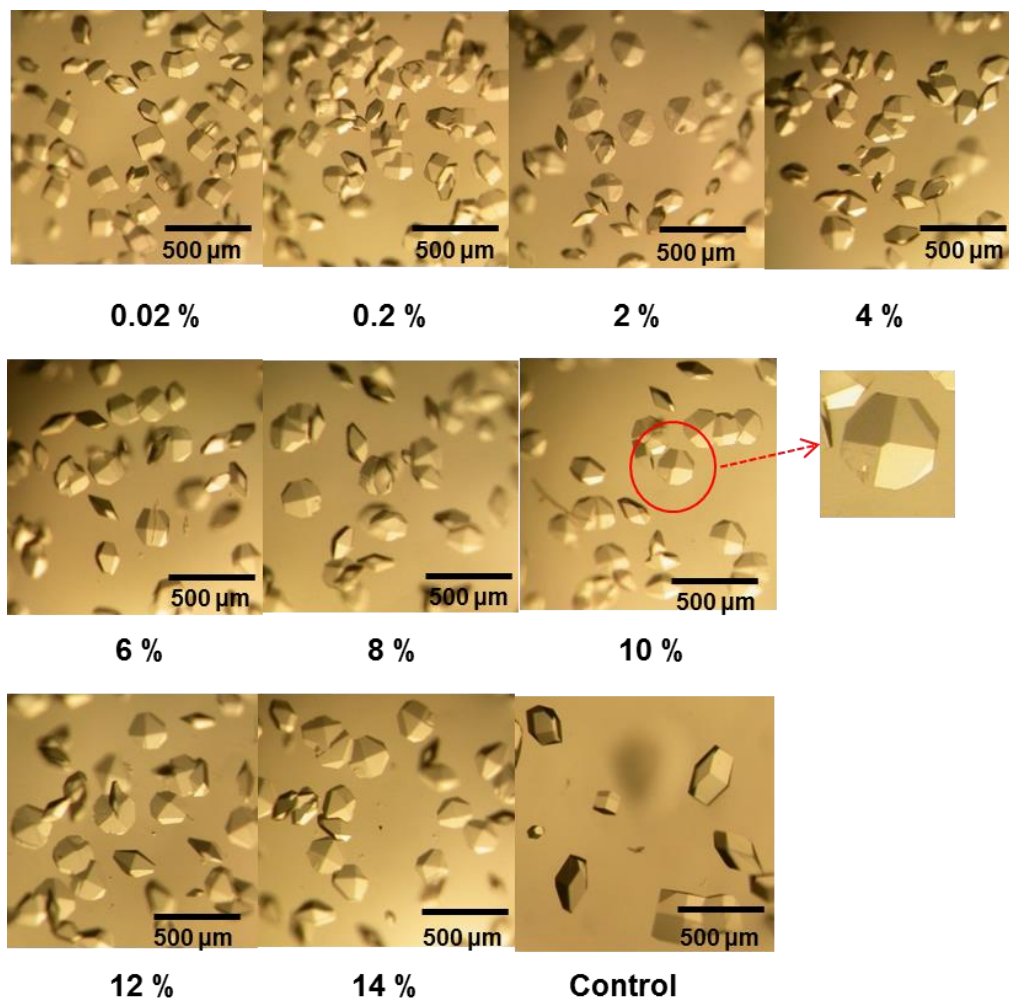


Figure 4-34b. Photomicrographs of HEWL crystals, grown under tetragonal crystal condition, in the presence of p(AMPS) (P5) (DP 99) at various concentrations. Image labelled 'Control' represents crystals grown from sample wells without polymer. The scale bar was 500 μm.

c) p(AMPS) (P5) (DP 200)

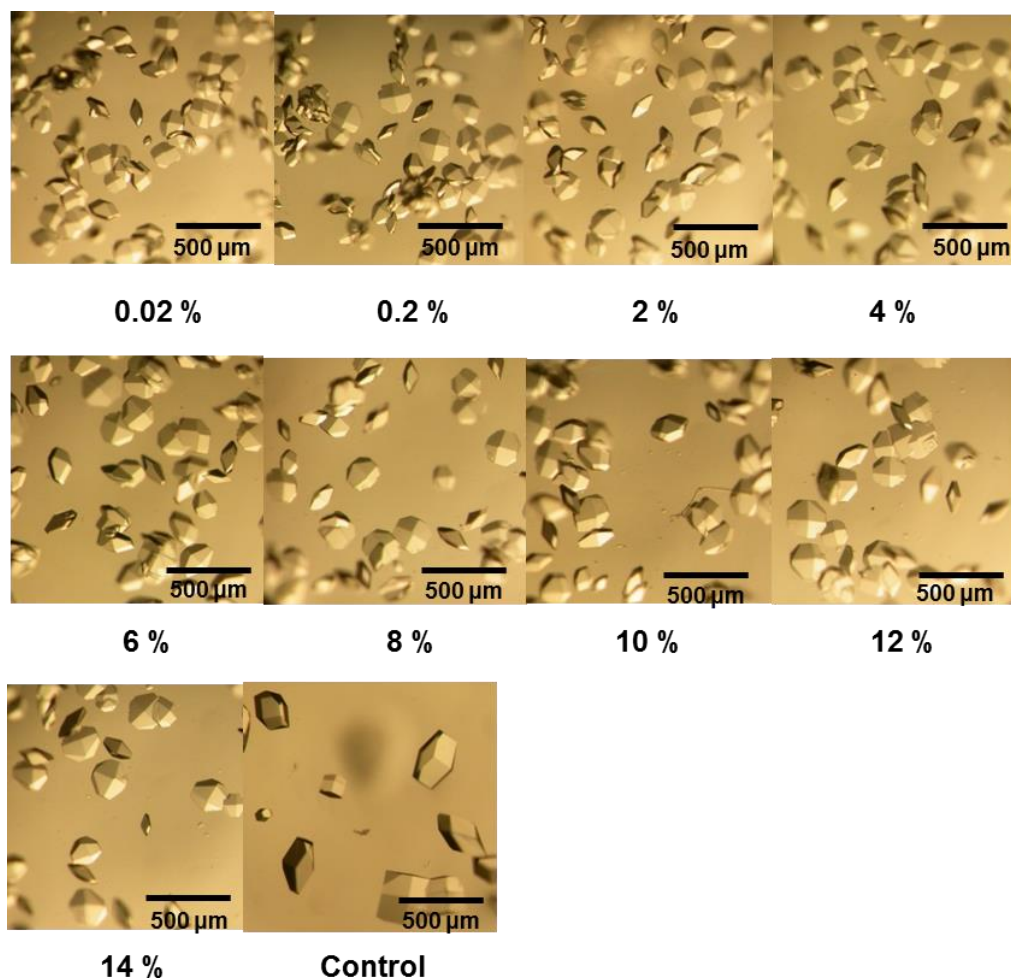


Figure 4-34c. Photomicrographs of HEWL crystals, grown under tetragonal crystal condition, in the presence of p(AMPS) (P5) (DP 200) at various concentrations. Image labelled ‘Control’ represents crystals grown from sample wells without polymer. The scale bar was 500 μm.

The HEWL images data obtained from the experiment in the presence of p(AMPS) (P5) (DP 99) was used for further image analysis. Figure 4-35 shows crystal size distribution by measuring the average length (μm) of the largest crystal diameter and number distribution was obtained from p(AMPS) (P5)

(DP 99). As the concentration of p(AMPS) (P5) in solution was increased, the number of HEWL crystals appeared to decrease and the size of the crystals appeared to increase.

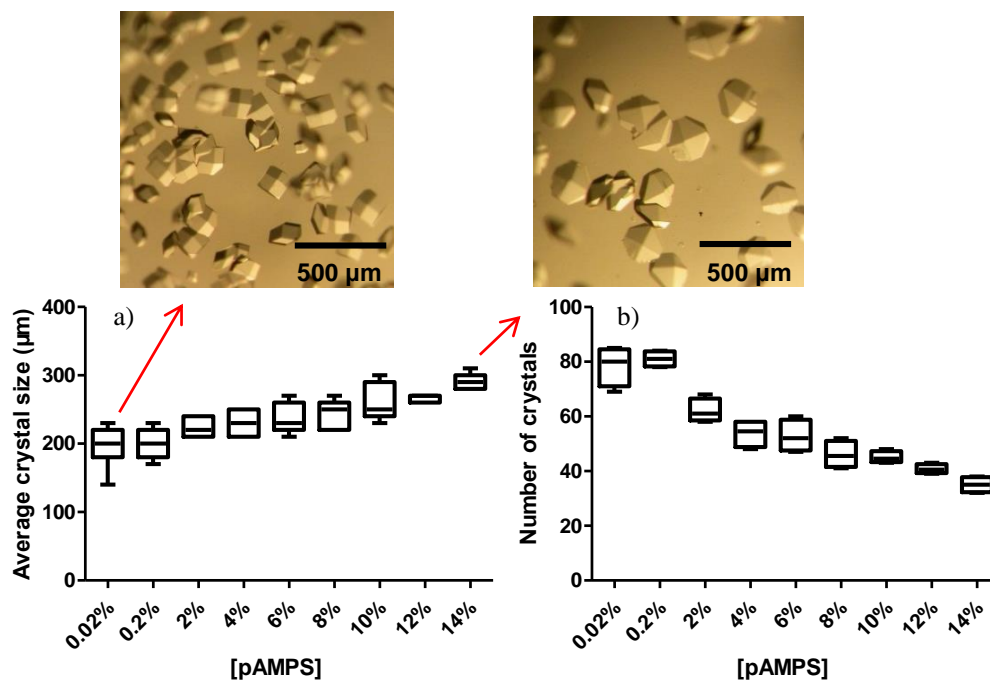


Figure 4-35. Summary of photomicrograph analysis showing changes in the size and number of HEWL crystals, grown in the presence of p(AMPS) (P5) (DP 99) at various concentrations. a) Average length (μm) of the largest crystal diameter; b) Experiment count for the number of crystals per sample well. The scale bar was $500\mu\text{m}$.

Figure 4-36 presents Tukey plots of DLS data when crystallised in the presence of p(AMPS) (P5). DLS data details, including autocorrelation functions and radii distribution by intensity are shown in the Appendix Page 338. At the beginning of the experiment (T_0), HEWL macromolecules were non-interacting in the solution. The average size of the particles in the

crystallisation solution was around 100 nm, measured by size distribution. With the addition of p(AMPS) (P5), HEWL crystallisation initiated and aggregates formed. As the time increased, HEWL aggregates grew in size. After 360 minutes, the average size of the particles in the crystallisation solution was around 400 nm. The size of pure p(AMPS) (P5) (DP 99) without any protein in the solution was around 4 nm.

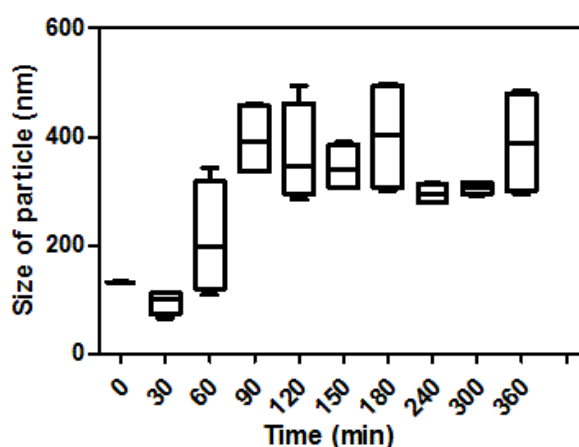


Figure 4-36. Variations of the size of HEWL aggregates or crystals in the solution as a function of time during crystallisation experiments induced by p(AMPS) (P5) (DP 99).

HEWL crystals were then taken out from the crystallisation plate, washed with crystallisation buffer solution. Then they were loaded onto aluminium stubs for SEM analysis. The SEM micrograph result (Figure 4-37) shows that with the addition of anionic p(AMPS) (P5), high quality HEWL crystal with sharp edges was formed. Moreover, HEWL crystals formed in the presence of anionic p(AMPS) (P5) were much more stable than that obtained without polymer.

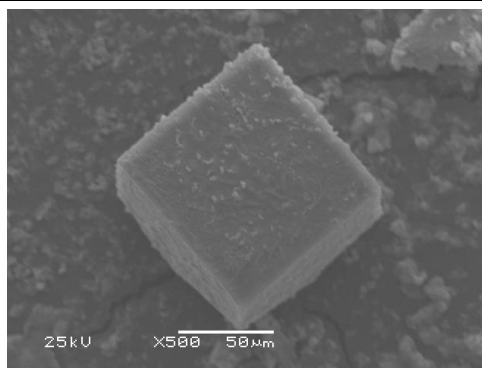


Figure 4-37. SEM micrograph of HEWL crystal produced under tetragonal conditions in the presence of p(AMPS) (P5), -- x 500 magnifications; the scale bar was 50 μm .

4.3.3.2 HEWL crystallisation in the presence of p(2-AmAA) (P6)

Another acrylamide monomer 2-AmAA, which has carboxyl group, was chosen to generate anionic homopolymers. The following polymer solutions were prepared: p(2-AmAA) (P6) (DP 18): 0.02 %, 0.2 %, 2 %, 3 %, 4 %, 5 %, 6 %, 7 % and 8 % (w/v); p(2-AmAA) (P6) (DP 46): 0.02 %, 0.2 %, 2 %, 3 %, 4 %, 5 %, 6 %, 7 % and 7.5 % (w/v); p(2-AmAA) (P6) (DP 72): 0.02 %, 0.2 %, 2 %, 4 %, 6 %, 8 %, 10 %, 12 % and 14 % (w/v); p(2-AmAA) (P6) (DP 150): 0.02 %, 0.2 %, 2 %, 4 %, 6 %, 8 %, 10 %, 12 % and 14 % (w/v) in 0.25 M sodium acetate and 20 % NaCl at pH 4.8 buffer solution. Tables 4-16a-d show HEWL crystallisation plates contained p(2-AmAA) (P6) (DPs 18, 46, 72 and 150) as solution additives.

Table 4-16a. HEWL crystallisation plate set up: p(2-AmAA) (P6) (DP 18)

	1	2	3	4	5	6	7	8	9
0.25 M Na Acetate, 20 % NaCl	400 µL (0.25 M Na Acetate, 20 % NaCl)	200 µL (0.25 M Na Acetate, 20 % NaCl)	100 µL (0.25 M Na Acetate, 20 % NaCl)						
p(2-AmAA) (DP 18) 14.02 %	1.4 µL (0.02 %)	7 µL (0.2 %)	36 µL (2 %)	53 µL (3 %)	71 µL (4 %)	89 µL (5 %)	107 µL (6 %)	125 µL (7 %)	143 µL (8 %)
H ₂ O	598.6 µL	293 µL	114 µL	97 µL	79 µL	61 µL	43 µL	25 µL	7 µL
pH	4.8	4.8	4.8	4.8	4.8	4.8	4.8	4.8	4.8
0.25 M Na Acetate, 20 % NaCl	↓	↓	↓	↓	↓	↓	↓	↓	↓
p(2-AmAA) (DP 18) 14.02 %									
H ₂ O									
pH									
0.25 M Na Acetate, 20 % NaCl	↓	↓	↓	↓	↓	↓	↓	↓	↓
p(2-AmAA) (DP 18) 14.02 %									
H ₂ O									
pH									
0.25 M Na Acetate, 20 % NaCl	200 µL (0.25 M Na Acetate, 20 % NaCl)	↑	↑	↑	↑	↑	↑	↑	↑
p(2-AmAA) (DP 18) 14.02 %	0 µL								
H ₂ O	300 µL								
pH	4.8								

Table 4-16b. HEWL crystallisation plate set up: p(2-AmAA) (P6) (DP 46)

	1	2	3	4	5	6	7	8	9
0.25 M Na Acetate, 20 % NaCl	400 μ L (0.25 M Na Acetate, 20 % NaCl)	200 μ L (0.25 M Na Acetate, 20 % NaCl)	100 μ L (0.25 M Na Acetate, 20 % NaCl)	100 μ L (0.25 M Na Acetate, 20 % NaCl)	100 μ L (0.25 M Na Acetate, 20 % NaCl)	100 μ L (0.25 M Na Acetate, 20 % NaCl)	100 μ L (0.25 M Na Acetate, 20 % NaCl)	100 μ L (0.25 M Na Acetate, 20 % NaCl)	100 μ L (0.25 M Na Acetate, 20 % NaCl)
p(2-AmAA) (DP 46) 12.49 %	1.6 μ L (0.02 %)	8 μ L (0.2 %)	40 μ L (2 %)	60 μ L (3 %)	80 μ L (4 %)	100 μ L (5 %)	120 μ L (6 %)	140 μ L (7 %)	150 μ L (7.5 %)
H ₂ O	598.4 μ L	292 μ L	110 μ L	90 μ L	70 μ L	50 μ L	30 μ L	10 μ L	0 μ L
pH	4.8	4.8	4.8	4.8	4.8	4.8	4.8	4.8	4.8
0.25 M Na Acetate, 20 % NaCl	↓	↓	↓	↓	↓	↓	↓	↓	↓
p(2-AmAA) (DP 46) 12.49 %									
H ₂ O									
pH									
0.25 M Na Acetate, 20 % NaCl	↓	↓	↓	↓	↓	↓	↓	↓	↓
p(2-AmAA) (DP 46) 12.49 %									
H ₂ O									
pH									
0.25 M Na Acetate, 20 % NaCl	↑	↑	↑	↑	↑	↑	↑	↑	↑
p(2-AmAA) (DP 46) 12.49 %									
H ₂ O	300 μ L								
pH	4.8								

Table 4-16c. HEWL crystallisation plate set up: p(2-AmAA) (P6) (DP 72)

	1	2	3	4	5	6	7	8	9
0.25 M Na Acetate, 20 % NaCl	400 μ L (0.25 M Na Acetate, 20 % NaCl)	200 μ L (0.25 M Na Acetate, 20 % NaCl)	100 μ L (0.25 M Na Acetate, 20 % NaCl)	100 μ L (0.25 M Na Acetate, 20 % NaCl)	100 μ L (0.25 M Na Acetate, 20 % NaCl)	100 μ L (0.25 M Na Acetate, 20 % NaCl)	100 μ L (0.25 M Na Acetate, 20 % NaCl)	100 μ L (0.25 M Na Acetate, 20 % NaCl)	100 μ L (0.25 M Na Acetate, 20 % NaCl)
p(2-AmAA) (DP 72) H ₂ O pH	0.5 μ L (0.02 %) 599.5 μ L 4.8	3 μ L (0.2 %) 297 μ L 4.8	13 μ L (2 %) 137 μ L 4.8	25 μ L (4 %) 125 μ L 4.8	38 μ L (6 %) 112 μ L 4.8	50 μ L (8 %) 100 μ L 4.8	63 μ L (10 %) 87 μ L 4.8	75 μ L (12 %) 75 μ L 4.8	88 μ L (14 %) 62 μ L 4.8
0.25 M Na Acetate, 20 % NaCl	↓	↓	↓	↓	↓	↓	↓	↓	↓
p(2-AmAA) (DP 72) H ₂ O pH									
0.25 M Na Acetate, 20 % NaCl	↓	↓	↓	↓	↓	↓	↓	↓	↓
p(2-AmAA) (DP 72) H ₂ O pH									
0.25 M Na Acetate, 20 % NaCl	200 μ L (0.25 M Na Acetate, 20 % NaCl)	↑	↑	↑	↑	↑	↑	↑	↑
p(2-AmAA) (DP 72) H ₂ O pH	0 μ L 300 μ L 4.8								

Table 4-16d. HEWL crystallisation plate set up: p(2-AmAA) (P6) (DP 150)

	1	2	3	4	5	6	7	8	9
0.25 M Na Acetate, 20 % NaCl	400 μ L (0.25 M Na Acetate, 20 % NaCl)	200 μ L (0.25 M Na Acetate, 20 % NaCl)	100 μ L (0.25 M Na Acetate, 20 % NaCl)	100 μ L (0.25 M Na Acetate, 20 % NaCl)	100 μ L (0.25 M Na Acetate, 20 % NaCl)	100 μ L (0.25 M Na Acetate, 20 % NaCl)	100 μ L (0.25 M Na Acetate, 20 % NaCl)	100 μ L (0.25 M Na Acetate, 20 % NaCl)	100 μ L (0.25 M Na Acetate, 20 % NaCl)
p(2-AmAA) (DP 150) H ₂ O pH	0.8 μ L (0.02 %) 599.2 μ L 4.8	4 μ L (0.2 %) 296 μ L 4.8	21 μ L (2 %) 129 μ L 4.8	42 μ L (4 %) 108 μ L 4.8	63 μ L (6 %) 87 μ L 4.8	83 μ L (8 %) 67 μ L 4.8	104 μ L (10 %) 46 μ L 4.8	126 μ L (12 %) 25 μ L 4.8	146 μ L (12 %) 4 μ L 4.8
0.25 M Na Acetate, 20 % NaCl	↓	↓	↓	↓	↓	↓	↓	↓	↓
p(2-AmAA) (DP 150) H ₂ O pH									
0.25 M Na Acetate, 20 % NaCl	↓	↓	↓	↓	↓	↓	↓	↓	↓
p(2-AmAA) (DP 150) H ₂ O pH									
0.25 M Na Acetate, 20 % NaCl	200 μ L (0.25 M Na Acetate, 20 % NaCl)	↑	↑	↑	↑	↑	↑	↑	↑
p(2-AmAA) (DP 150) H ₂ O pH	0 μ L 300 μ L 4.8								

Figures 4-38a-d show the images of HEWL crystals formed in the presence of p(2-AmAA) (P6) (DPs 18, 46, 72 and 150) at various concentrations. From visual observation, HEWL needles formed under p(2-AmAA) (P6) with lower DPs of 18 and 46 at lower concentrations (Figures 4-38a, < 4 %; Figures 4-38b, < 7 % (w/v)). However, as the concentration of p(2-AmAA) (P6) with DPs of 18 and 46 was increased, there were no HEWL needles formed. It is reported that HEWL needles can be grown in the presence of acid-functionalised polymers.¹⁰⁴ When HEWL crystallisation in the presence of p(2-AmAA) (P6) with higher DPs of 79 and 108, smaller uniform HEWL crystals were obtained (Figure 4-38c and d). The pKa of p(2-AmAA) (P6) was 5.92, measured by titration. At pH 4.8, p(2-AmAA) (P6) was a weakly anionic polymer. Because the crystallisation pH of HEWL being close (pH 4.8) to the pKa value of p(2-AmAA) (P6), and thus a smaller number of anionic carboxyls remaining on the p(2-AmAA) (P6) at pH of 4.8 compared to anionic p(AMPS) (P5). All these small HEWL crystals formed in the presence of anionic p(2-AmAA) (P6) were identified as tetragonal by single crystal X-ray diffraction later.

a) p(2-AmAA) (P6) (DP 18)

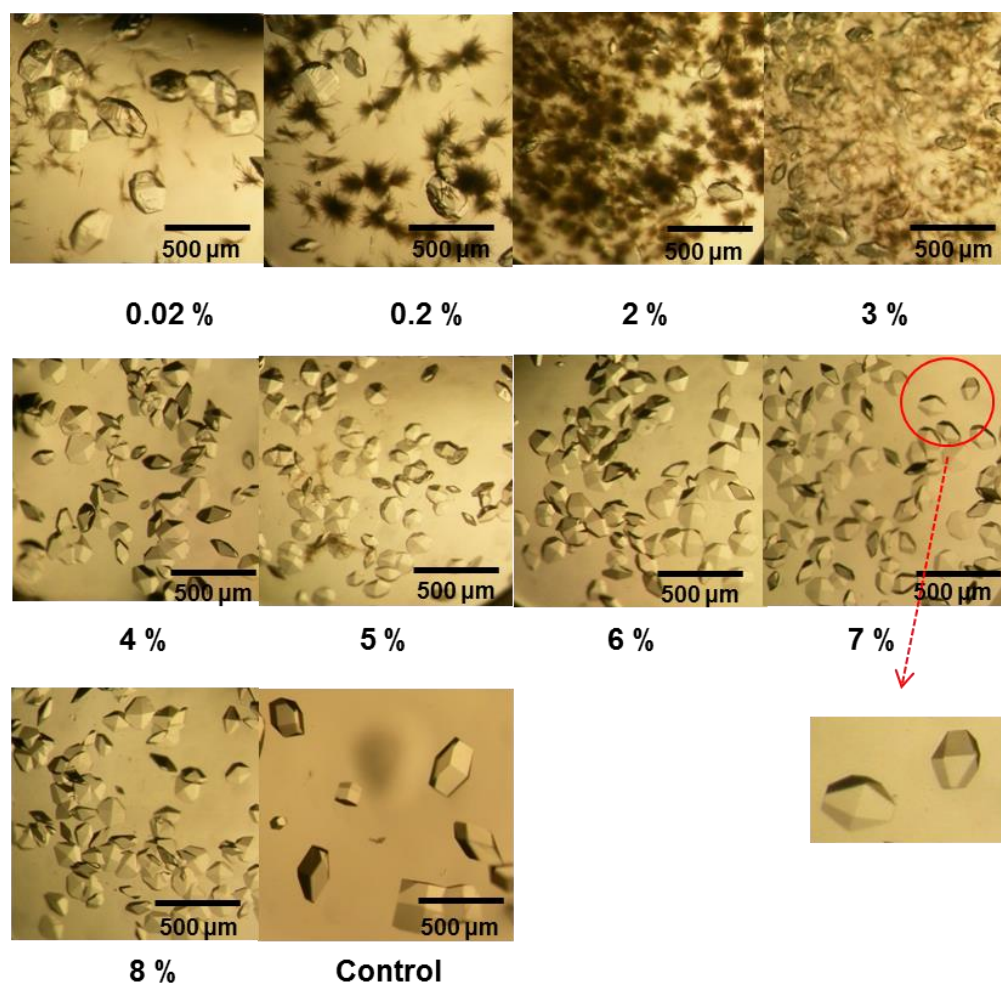


Figure 4-38a. Photomicrographs of HEWL crystals, grown under tetragonal crystal condition, in the presence of p(2-AmAA) (P6) (DP 18) at various concentrations. Image labelled 'Control' represents crystals grown from sample wells without polymer. The scale bar was 500 μm.

b) p(2-AmAA) (P6) (DP 46)

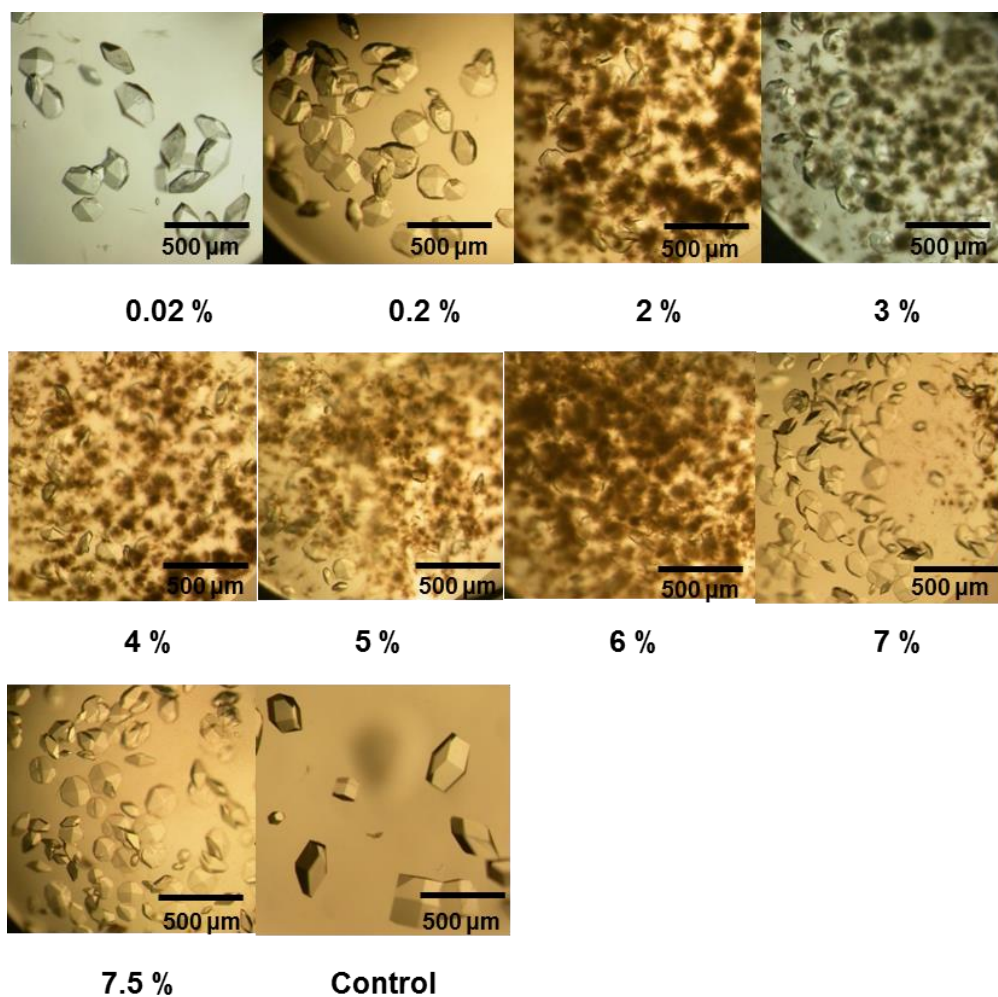


Figure 4-38b. Photomicrographs of HEWL crystals, grown under tetragonal crystal condition, in the presence of p(2-AmAA) (P6) (DP 46) at various concentrations. Image labelled 'Control' represents crystals grown from sample wells without polymer. The scale bar was 500 μm.

c) p(2-AmAA) (P6) (DP 72)

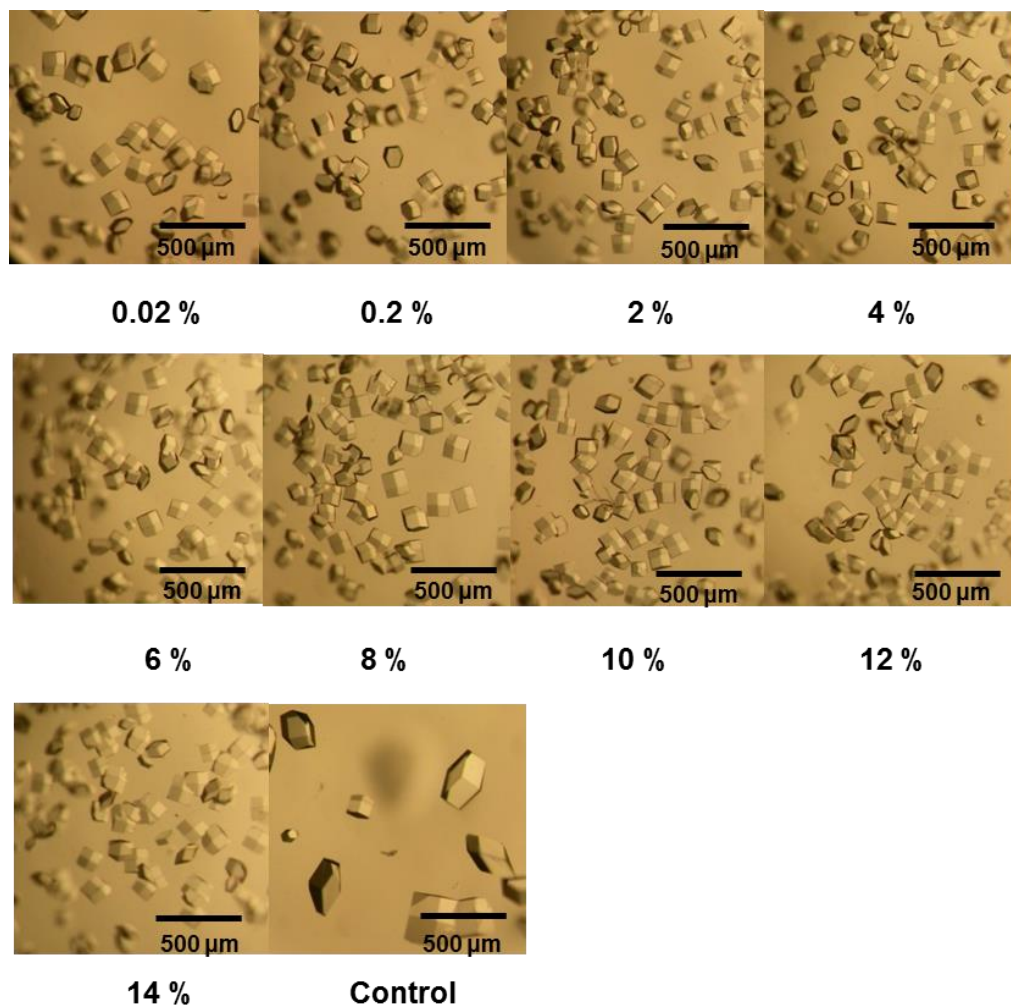


Figure 4-38c. Photomicrographs of HEWL crystals, grown under tetragonal crystal condition, in the presence of p(2-AmAA) (P6) (DP 72) at various concentrations. Image labelled 'Control' represents crystals grown from sample wells without polymer. The scale bar was 500 μm.

d) p(2-AmAA) (P6) (DP 150)

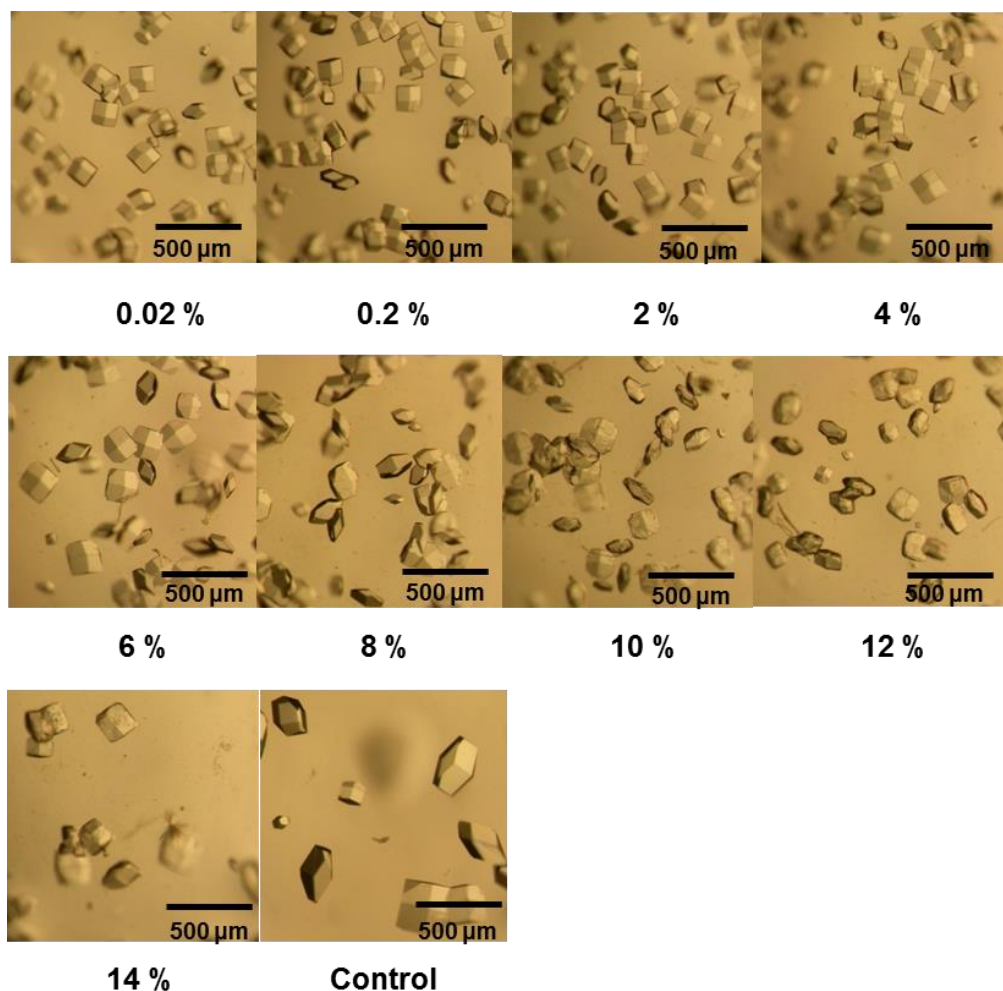


Figure 4-38d. Photomicrographs of HEWL crystals, grown under tetragonal crystal condition, in the presence of p(2-AmAA) (P6) (DP 150) at various concentrations. Image labelled 'Control' represents crystals grown from sample wells without polymer. The scale bar was 500 μm.

The HEWL images data obtained from p(2-AmAA) (P6) (DP 72) was used for further image analysis. Figure 4-39 shows crystal size distribution by measuring the average length (μm) of the largest crystal diameter and number distribution was obtained from p(2-AmAA) (P6) (DP 72). As the concentration

of p(2-AmAA) (P6) in solution was increased, the number of HEWL crystals decreased and the size of the crystals appeared to increase slightly.

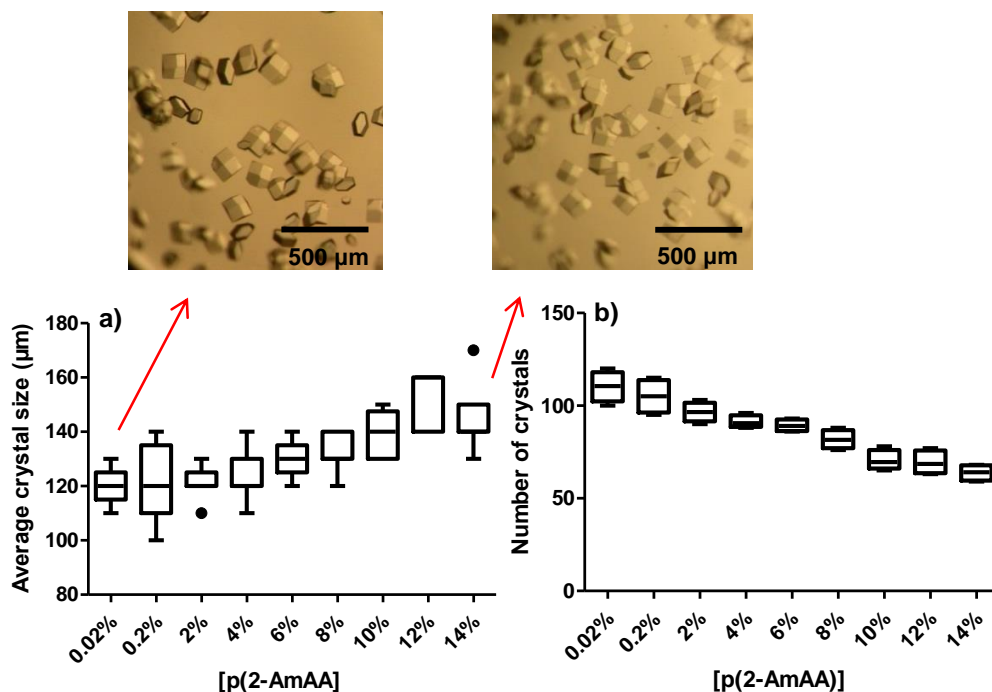


Figure 4-39. Summary of photomicrograph analysis showing changes in the size and number of HEWL crystals, grown in the presence of p(2-AmAA) (P6) (DP 72) at various concentrations. a) Average length (μm) of the largest crystal diameter; b) Experiment count for the number of crystals per sample well. The scale bar was 500μm.

Figure 4-40 illustrates the diffraction patterns of HEWL crystal grown in the presence of p(2-AmAA) (P6) (DPs 18 and 46) using X-ray crystallography. Table 4-17 shows unit cell dimensions of those HEWL crystals. All the HEWL crystals formed in the presence of anionic p(2-AmAA) (P6) were identified as tetragonal by single crystal X-ray diffraction.

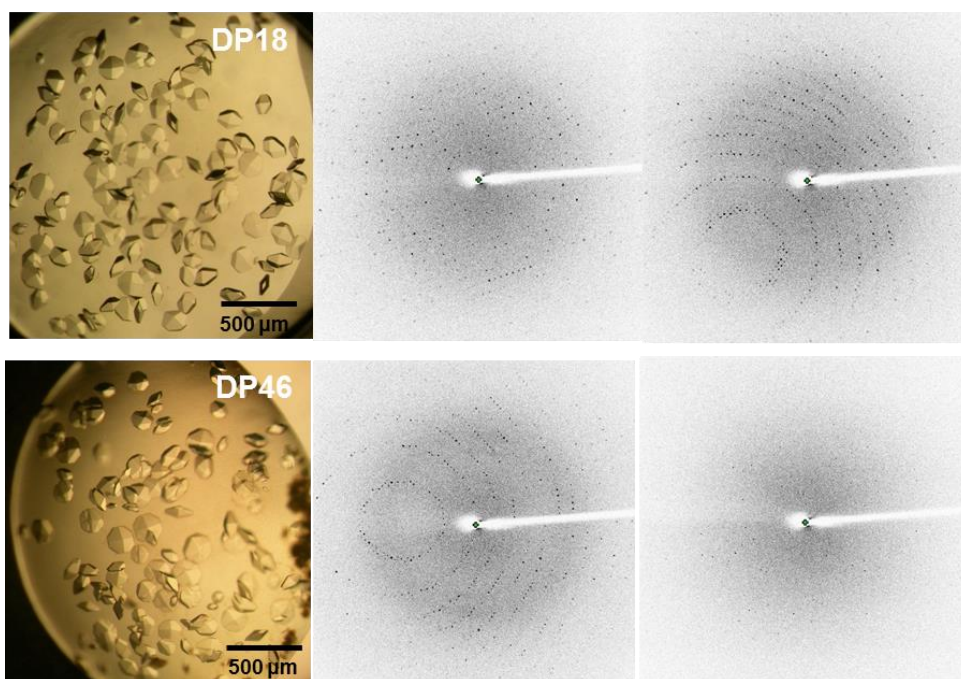


Figure 4-40. HEWL crystal photomicrographs and X-ray diffraction patterns yielded by the single HEWL crystal in the presence of p(2-AmAA) (P6) with DP of 18 and 46. Two scattering angles: 0 ± 1 degrees and 90 ± 1 degrees.

Table 4-17. Unit cell dimensions of HEWL crystal in the presence of anionic p(2-AmAA) (P6) with DP of 18 and 46

Polymer	a, b, c (Å)	α, β, γ	Volume	Unit cell lattice
p(2-AmAA) DP 18	78.87, 78.87, 37.10	$90^\circ; 90^\circ; 90^\circ$	230,794	Tetragonal
p(2-AmAA) DP 46	79.13, 79.13, 37.16	$90^\circ; 90^\circ; 90^\circ$	232,678	Tetragonal

Figure 4-41 shows Tukey plots of DLS data when crystallised under p(2-AmAA) (P6). DLS data details, including autocorrelation functions and radii distribution by intensity are shown in the Appendix Page 339. At the beginning of the experiment (T_0), the average size of the particles in

crystallisation solution was around 30 nm, measured by size distribution. With the addition of p(2-AmAA) (P6), HEWL aggregates grew in size. After 360 minutes, the average size of the particles in crystallisation solution was around 180 nm. The size of pure p(2-AmAA) (P6) without any protein was around 3 nm.

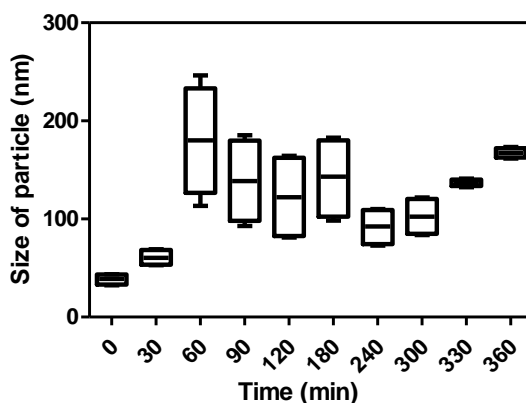


Figure 4-41. Variations of the size of HEWL aggregates or crystals in the solution as a function of time during crystallisation experiments induced by p(2-AmAA) (P6).

4.3.3.3 HEWL crystallisation in the presence of p(4-AmBA) (P7)

4-AmBA, which has the carboxyl group and a higher molar mass than 2-AmAA, was also chosen to generate anionic homopolymers. The following polymer solutions were prepared: p(4-AmBA) (P7) (DP 21): 0.02 %, 0.2 %, 2 %, 3 %, 4 %, 5 %, 6 %, 7 % and 8 % (w/v); p(4-AmBA) (P7) (DPs 50, 100 and 200): 0.02 %, 0.2 %, 2 %, 4 %, 6 %, 8 %, 10 %, 12 % and 14 % (w/v) in 0.25 M sodium acetate, 20 % NaCl, pH 4.8 buffer solution. Tables 4-18a-d show HEWL crystallisation plates contained p(4-AmBA) (P7) (DPs 21, 50,

100 and 200) as solution additives.

Table 4-18a. HEWL crystallisation plate set up: p(4-AmBA) (P7) (DP 21)

	1	2	3	4	5	6
0.25 M Na Acetate, 20 % NaCl	400 μ L (0.25 M Na Acetate, 20 % NaCl) 1.2 μ L (0.02 %)	200 μ L (0.25 M Na Acetate, 20 % NaCl) 6 μ L (0.2 %)	100 μ L (0.25 M Na Acetate, 20 % NaCl) 30 μ L (2 %)	100 μ L (0.25 M Na Acetate, 20 % NaCl) 61 μ L (4 %)	100 μ L (0.25 M Na Acetate, 20 % NaCl) 91 μ L (6 %)	100 μ L (0.25 M Na Acetate, 20 % NaCl) 122 μ L (8 %)
p(4-AmBA) (DP 21) 16.41 % H ₂ O pH	598.8 μ L 4.8	294 μ L 4.8	120 μ L 4.8	89 μ L 4.8	59 μ L 4.8	28 μ L 4.8
0.25 M Na Acetate, 20 % NaCl	↓	↓	↓	↓	↓	↓
p(4-AmBA) (DP 21) 16.41 % H ₂ O pH	↓	↓	↓	↓	↓	↓
0.25 M Na Acetate, 20 % NaCl	↓	↓	↓	↓	↓	↓
p(4-AmBA) (DP 21) 16.41 % H ₂ O pH	↓	↓	↓	↓	↓	↓
0.25 M Na Acetate, 20 % NaCl	200 μ L (0.25 M Na Acetate, 20 % NaCl) 0 μ L	↑	↑	↑	↑	↑
p(4-AmBA) (DP 21) 16.41 % H ₂ O pH	300 μ L 4.8					

Table 4-18b. HEWL crystallisation plate set up: p(4-AmBA) (P7) (DP 50)

	1	2	3	4	5	6	7	8	9
0.25 M Na Acetate, 20 % NaCl	400 μ L (0.25 M Na Acetate, 20 % NaCl)	200 μ L (0.25 M Na Acetate, 20 % NaCl)	100 μ L (0.25 M Na Acetate, 20 % NaCl)	100 μ L (0.25 M Na Acetate, 20 % NaCl)	100 μ L (0.25 M Na Acetate, 20 % NaCl)	100 μ L (0.25 M Na Acetate, 20 % NaCl)	100 μ L (0.25 M Na Acetate, 20 % NaCl)	100 μ L (0.25 M Na Acetate, 20 % NaCl)	100 μ L (0.25 M Na Acetate, 20 % NaCl)
p(4-AmBA) (DP 50)	0.5 μ L (0.02 %)	3 μ L (0.2 %)	13 μ L (2 %)	25 μ L (4 %)	38 μ L (6 %)	51 μ L (8 %)	63 μ L (10 %)	76 μ L (12 %)	88 μ L (14 %)
H ₂ O	599.5 μ L	297 μ L	137 μ L	125 μ L	112 μ L	99 μ L	87 μ L	74 μ L	62 μ L
pH	4.8	4.8	4.8	4.8	4.8	4.8	4.8	4.8	4.8
0.25 M Na Acetate, 20 % NaCl	↓	↓	↓	↓	↓	↓	↓	↓	↓
p(4-AmBA) (DP 50)									
H ₂ O									
pH									
0.25 M Na Acetate, 20 % NaCl	↓	↓	↓	↓	↓	↓	↓	↓	↓
p(4-AmBA) (DP 50)									
H ₂ O									
pH									
0.25 M Na Acetate, 20 % NaCl	200 μ L (0.25 M Na Acetate, 20 % NaCl)	↑	↑	↑	↑	↑	↑	↑	↑
p(4-AmBA) (DP 50)	0 μ L								
H ₂ O	300 μ L								
pH	4.8								

Table 4-18c. HEWL crystallisation plate set up: p(4-AmBA) (P7) (DP 100)

	1	2	3	4	5	6	7	8	9
0.25 M Na Acetate, 20 % NaCl	400 μ L (0.25 M Na Acetate, 20 % NaCl)	200 μ L (0.25 M Na Acetate, 20 % NaCl)	100 μ L (0.25 M Na Acetate, 20 % NaCl)	100 μ L (0.25 M Na Acetate, 20 % NaCl)	100 μ L (0.25 M Na Acetate, 20 % NaCl)	100 μ L (0.25 M Na Acetate, 20 % NaCl)	100 μ L (0.25 M Na Acetate, 20 % NaCl)	100 μ L (0.25 M Na Acetate, 20 % NaCl)	100 μ L (0.25 M Na Acetate, 20 % NaCl)
p(4-AmBA) (DP 100)	0.5 μ L (0.02 %)	3 μ L (0.2 %)	13 μ L (2 %)	25 μ L (4 %)	38 μ L (6 %)	50 μ L (8 %)	64 μ L (10 %)	76 μ L (12 %)	88 μ L (14 %)
H ₂ O	599.5 μ L	297 μ L	137 μ L	125 μ L	112 μ L	100 μ L	86 μ L	74 μ L	62 μ L
pH	4.8	4.8	4.8	4.8	4.8	4.8	4.8	4.8	4.8
0.25 M Na Acetate, 20 % NaCl	↓	↓	↓	↓	↓	↓	↓	↓	↓
p(4-AmBA) (DP 100)									
H ₂ O									
pH									
0.25 M Na Acetate, 20 % NaCl	↓	↓	↓	↓	↓	↓	↓	↓	↓
p(4-AmBA) (DP 100)									
H ₂ O									
pH									
0.25 M Na Acetate, 20 % NaCl	200 μ L (0.25 M Na Acetate, 20 % NaCl)	↑	↑	↑	↑	↑	↑	↑	↑
p(4-AmBA) (DP 100)	0 μ L								
H ₂ O	300 μ L								
pH	4.8								

Table 4-18d. HEWL crystallisation plate set up: p(4-AmBA) (P7) (DP 200)

	1	2	3	4	5	6	7	8	9
0.25 M Na Acetate, 20 % NaCl	400 μ L (0.25 M Na Acetate, 20 % NaCl)	200 μ L (0.25 M Na Acetate, 20 % NaCl)	100 μ L (0.25 M Na Acetate, 20 % NaCl)	100 μ L (0.25 M Na Acetate, 20 % NaCl)	100 μ L (0.25 M Na Acetate, 20 % NaCl)	100 μ L (0.25 M Na Acetate, 20 % NaCl)	100 μ L (0.25 M Na Acetate, 20 % NaCl)	100 μ L (0.25 M Na Acetate, 20 % NaCl)	100 μ L (0.25 M Na Acetate, 20 % NaCl)
p(4-AmBA) (DP 200) H ₂ O	0.5 μ L (0.02 %) 599.5 μ L	3 μ L (0.2 %) 297 μ L	13 μ L (2 %) 137 μ L	26 μ L (4 %) 124 μ L	38 μ L (6 %) 112 μ L	51 μ L (8 %) 99 μ L	64 μ L (10 %) 86 μ L	77 μ L (12 %) 73 μ L	90 μ L (14 %) 60 μ L
pH	4.8	4.8	4.8	4.8	4.8	4.8	4.8	4.8	4.8
0.25 M Na Acetate, 20 % NaCl	↓	↓	↓	↓	↓	↓	↓	↓	↓
p(4-AmBA) (DP 200) H ₂ O									
pH									
0.25 M Na Acetate, 20 % NaCl	↓	↓	↓	↓	↓	↓	↓	↓	↓
p(4-AmBA) (DP 200) H ₂ O									
pH									
0.25 M Na Acetate, 20 % NaCl	200 μ L (0.25 M Na Acetate, 20 % NaCl)	↑	↑	↑	↑	↑	↑	↑	↑
p(4-AmBA) (DP 200) H ₂ O	0 μ L								
pH	300 μ L 4.8								

Figures 4-42a-d present images of HEWL crystals obtained in the presence of p(4-AmBA) (P7) (DPs 21, 50, 100 and 200) at various concentrations. From visual observation, large HEWL crystals were formed under p(4-AmBA) with lower DP of 21 (Figure 4-42a). However, smaller uniform HEWL crystals were obtained when in the presence of p(4-AmBA) (P7) with higher DP of 50, 100 and 200 (Figure 4-42b-d). The pKa of p(4-AmBA) (P7) was 6.26, measured by titration. At pH 4.8, p(4-AmBA) (P7) was a weakly anionic polymer. Similar to p(2-AmAA) (P6), due to the crystallisation pH of HEWL being close (pH 4.8) to the pKa value of p(4-AmBA) (P7), a small number of anionic carboxyls remaining on the p(4-AmBA) (P7) at pH of 4.8. p(4-AmBA) with lower DP of 21 might have very few anionic carboxyls, and therefore might compete with protein solutes for water and result in dehydration of protein macromolecules rather than by electrostatic interaction. All these HEWL crystals formed in the presence of anionic p(4-AmBA) (P7) were identified as tetragonal by single crystal X-ray diffraction.

a) p(4-AmBA) (P7) (DP 21)

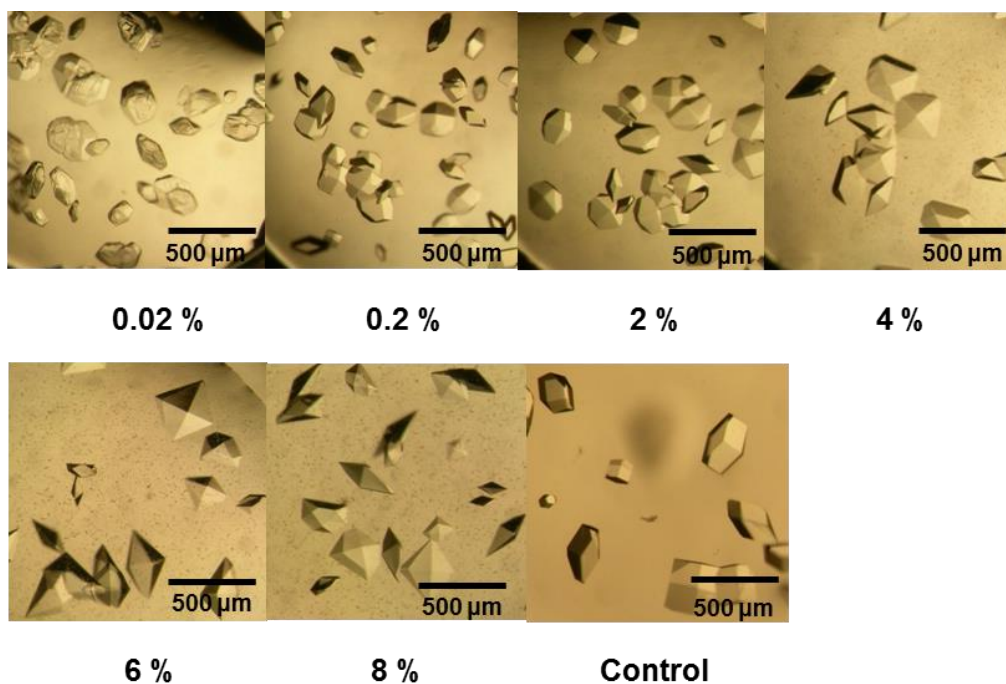


Figure 4-42a. Photomicrographs of HEWL crystals, grown under tetragonal crystal condition, in the presence of p(4-AmBA) (P7) (DP 21) at various concentrations. Image labelled 'Control' represents crystals grown from sample wells without polymer. The scale bar was 500 μm.

b) p(4-AmBA) (P7) (DP 50)

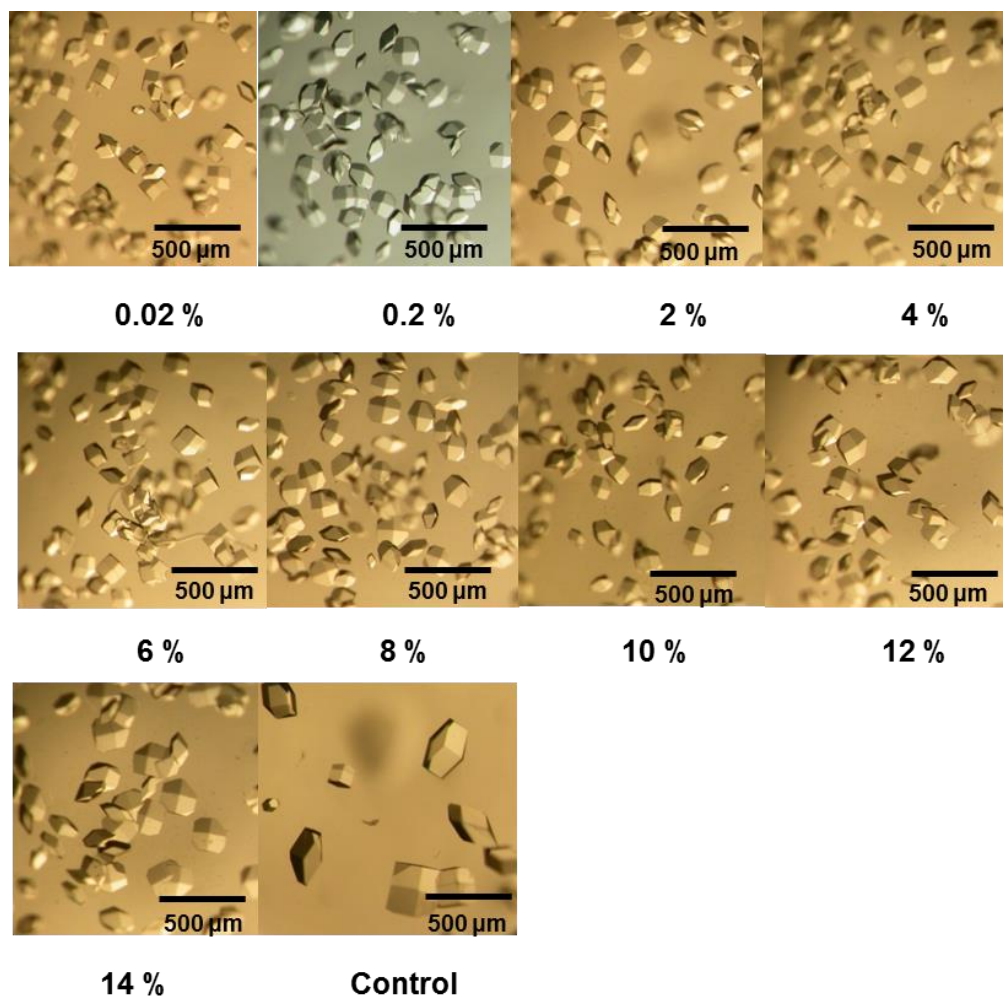


Figure 4-42b. Photomicrographs of HEWL crystals, grown under tetragonal crystal condition, in the presence of p(4-AmBA) (P7) (DP 50) at various concentrations. Image labelled 'Control' represents crystals grown from sample wells without polymer. The scale bar was 500 μm.

c) p(4-AmBA) (P7) (DP 100)

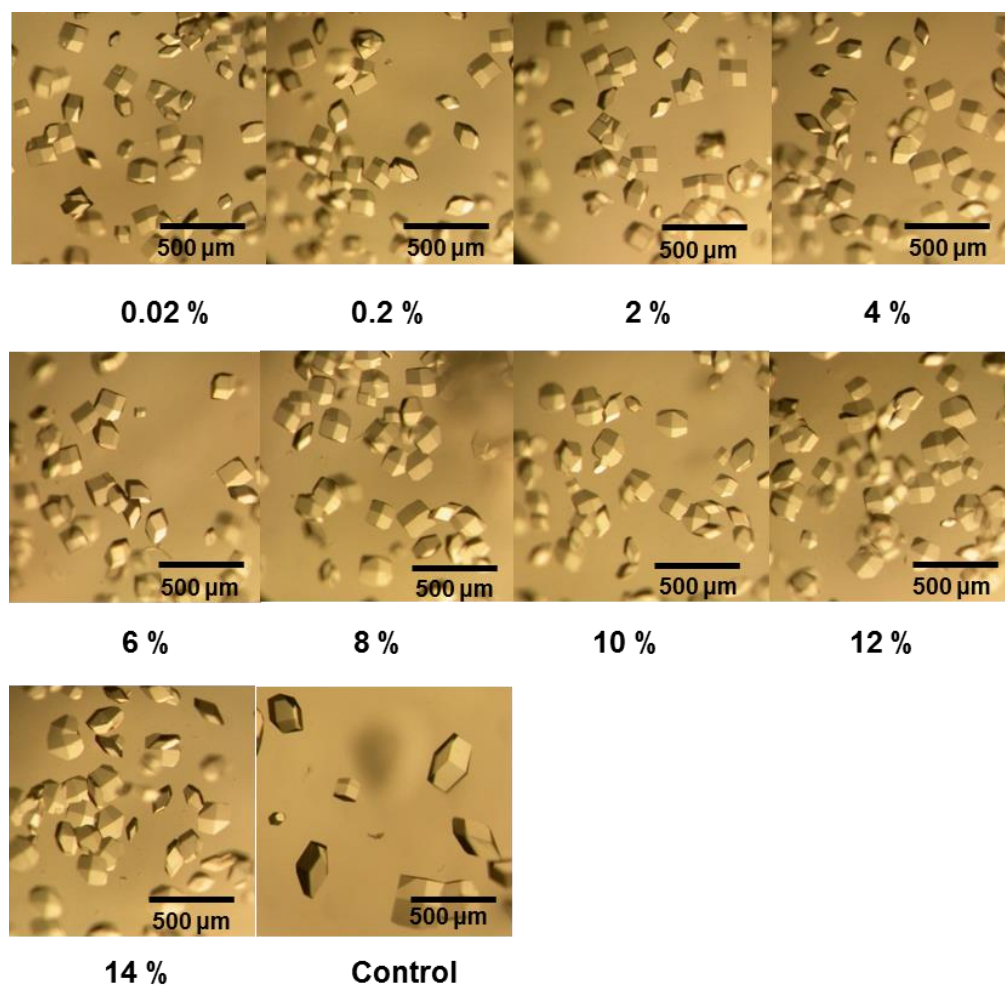


Figure 4-42c. Photomicrographs of HEWL crystals, grown under tetragonal crystal condition, in the presence of p(4-AmBA) (P7) (DP 100) at various concentrations. Image labelled 'Control' represents crystals grown from sample wells without polymer. The scale bar was 500 μm.

d) p(4-AmBA) (P7) (DP 200)

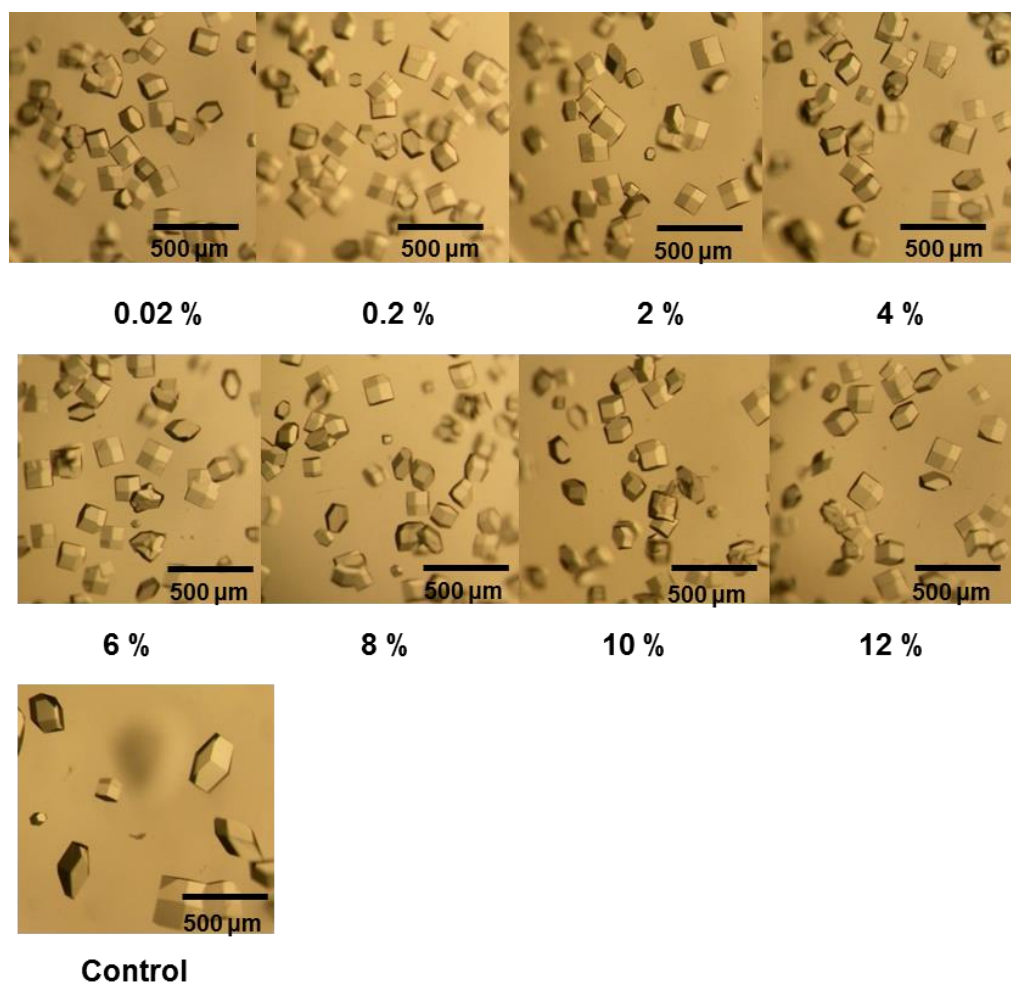


Figure 4-42d. Photomicrographs of HEWL crystals, grown under tetragonal crystal condition, in the presence of p(4-AmBA) (P7) (DP 200) at various concentrations. Image labelled 'Control' represents crystals grown from sample wells without polymer. The scale bar was 500 μm.

The HEWL images data obtained from p(4-AmBA) (P7) (DP 100) was used for further image analysis. Crystal size and number distribution data (Figure 4-43) shows that as the concentration of p(4-AmBA) (P7) (DP 100) in solution was increased, the number of HEWL crystals decreased and the size of the crystals appeared to increase slightly.

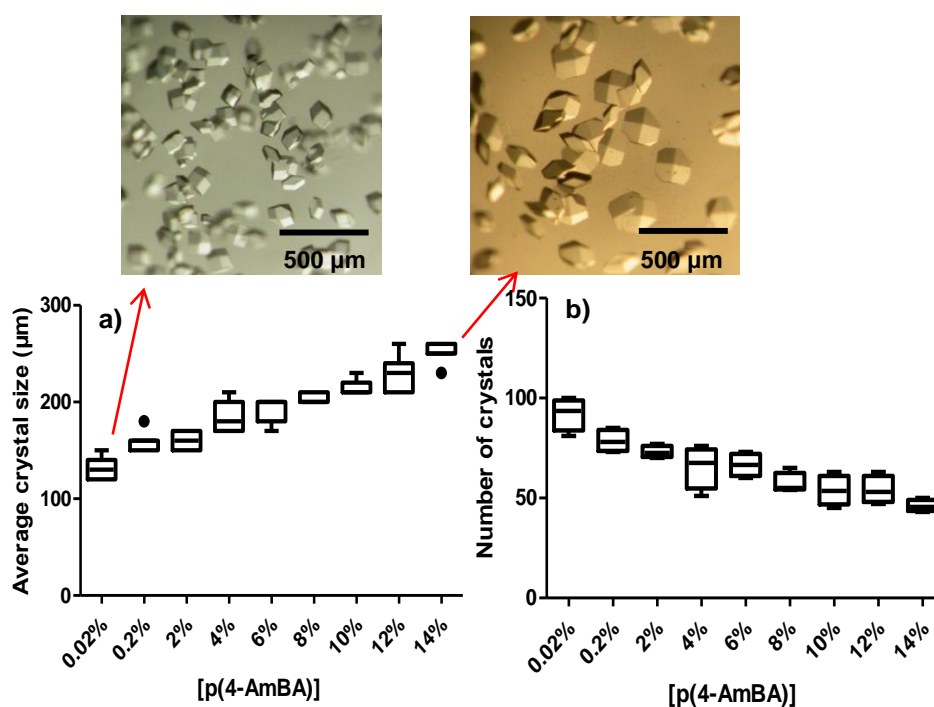


Figure 4-43. Summary of photomicrograph analysis showing changes in the size and number of HEWL crystals, grown in the presence of p(4-AmBA) (P7) (DP 100) at various concentrations. a) Average length (μm) of the largest crystal diameter; b) Experiment count for the number of crystals per sample well. The scale bar was 500μm.

Figure 4-44 illustrates the diffraction patterns of HEWL crystal, grown in the presence of p(4-AmBA) (P7) using X-ray crystallography. Table 4-19 shows

unit cell dimension of the HEWL tetragonal crystal.

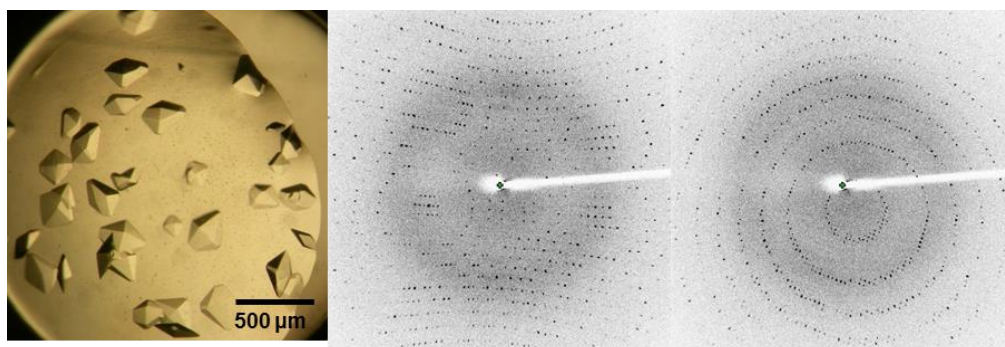


Figure 4-44. HEWL crystal photomicrograph and X-ray diffraction patterns yielded by the single HEWL crystal in the presence of p(4-AmBA) (P7). Two scattering angles: 0 ± 1 degrees and 90 ± 1 degrees.

Table 4-19. Unit cell dimension of HEWL crystal in the presence of anionic

p(4-AmBA) (P7)

Polymer	a, b, c (Å)	α, β, γ	Volume	Unit cell lattice
p(4-AmBA)	78.75, 78.75, 37.08	$90^\circ, 90^\circ, 90^\circ$	229,956	Tetragonal

Figure 4-45 shows Tukey plots of DLS data when HEWL crystallised in the presence of p(4-AmBA) (P7). DLS data details, including autocorrelation functions and radii distribution by intensity are shown in the Appendix Page 339. At the beginning of the experiment (T_0), the average size of the particles in crystallisation solution was around 20 nm, measured by size distribution. With the addition of p(4-AmBA) (P7), HEWL aggregates grew in size. After 360 minutes, the average size of the particles in crystallisation solution was around 70 nm. The size of pure p(4-AmBA) (P7) without any protein was around 3 nm.

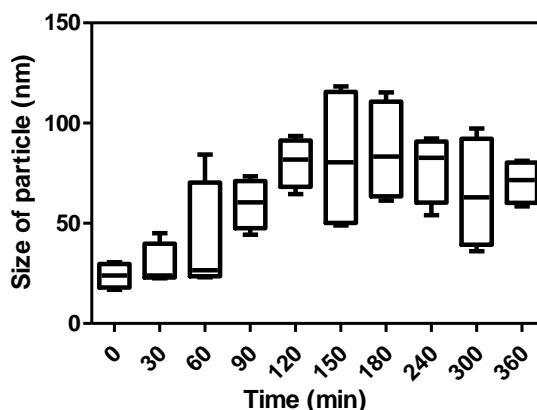


Figure 4-45. Variations of the size of HEWL aggregates or crystals in the solution as a function of time during crystallisation experiments induced by p(4-AmBA) (P7).

In summary, the influence of anionic polymers on HEWL crystallisation was less than that of the cationic polymers regarding crystal shape, but the anionic polymers did alter the size of HEWL crystals. Figure 4-46 shows the hypothesis of how anionic polymers mediated HEWL crystallisation. As mentioned earlier, some researchers reported polymers containing cationic segments had an absorption behavior on negative surface, which controlled by charge compensation.^{226, 108} We proposed that anionic polymers might favor binding cationic HEWL macromolecules for charge compensation via electrostatic interaction,¹⁰⁸ thus, they would either lower the protein and water interfacial energy and act as nucleation centers by the absorption of HEWL macromolecules, or slow down the rate of HEWL crystal further growth. Therefore, they acted as not only nucleators in solution but also as inhibitors.¹⁰⁰

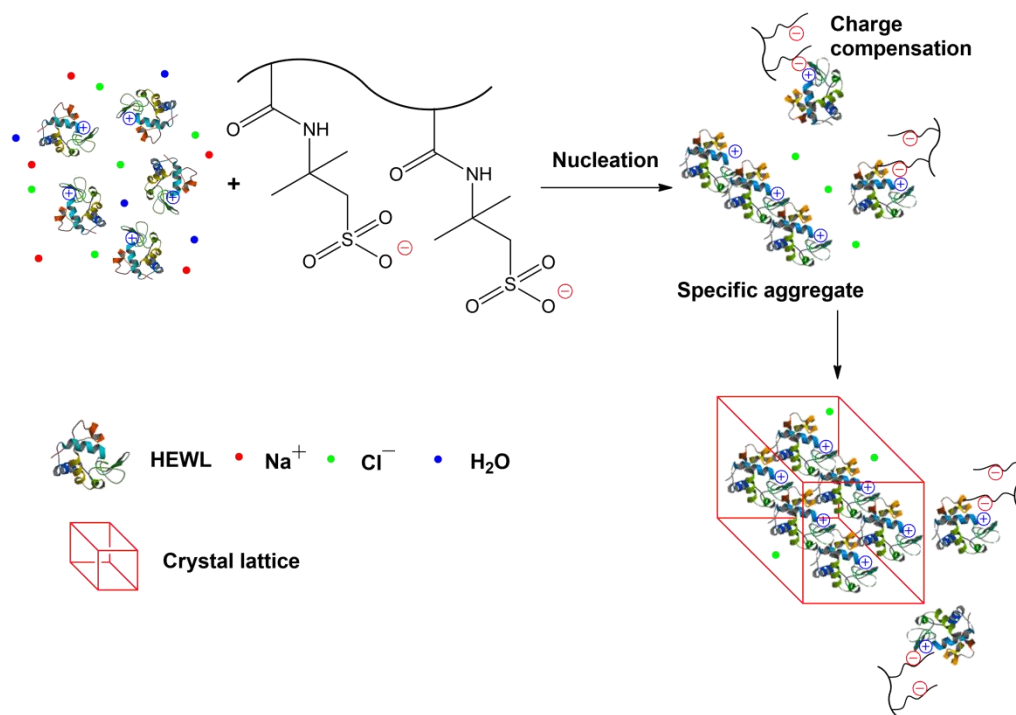


Figure 4-46. Hypothesis of mechanism of anionic polymer mediated HEWL crystallisation. Anionic polymer: binding cationic HEWL for charge compensation. HEWL macromolecules are positively charged at tetragonal crystallisation pH of 4.8, i.e. cationic. Na⁺ and Cl⁻ ions come from the crystallisation buffer solutions.

4.3.4 HEWL crystallisation in the presence of cationic/zwitterionic polymer in solution: p(METMAC-*co*-MEDSAH) (P8)

A cationic/zwitterionic copolymer with both positive charges and zwitterionic components was applied to HEWL crystallisation. The following polymer solutions were prepared: p(METMAC-*co*-MEDSAH) (P8): 0.02 %, 0.2 %, 2 %, 4 %, 6 %, 8 %, 10 %, 12 % and 14 % (w/v) in 0.25 M sodium acetate, 20 % NaCl, pH 4.8 buffer solution (Table 4-20).

Table 4-20. HEWL crystallisation plate: p(METMAC-co-MEDSAH) (P8)

	1	2	3	4	5	6	7	8	9
0.25 M Na Acetate, 20 % NaCl	800 µL (0.25 M Na Acetate, 20 % NaCl)	200 µL (0.25 M Na Acetate, 20 % NaCl)	100 µL (0.25 M Na Acetate, 20 % NaCl)	100 µL (0.25 M Na Acetate, 20 % NaCl)	100 µL (0.25 M Na Acetate, 20 % NaCl)	100 µL (0.25 M Na Acetate, 20 % NaCl)	100 µL (0.25 M Na Acetate, 20 % NaCl)	100 µL (0.25 M Na Acetate, 20 % NaCl)	100 µL (0.25 M Na Acetate, 20 % NaCl)
p(TMAEMA-co-MEDSA) 37.64 %	1.1 µL (0.02 %)	2.7 µL (0.2 %)	13.3 µL (2 %)	27 µL (4 %)	40 µL (6 %)	53 µL (8 %)	66 µL (10 %)	80 µL (12 %)	93 µL (14 %)
H ₂ O	1198.9 µL	297.3 µL	136.7 µL	123 µL	110 µL	97 µL	84 µL	70 µL	57 µL
pH	4.8	4.8	4.8	4.8	4.8	4.8	4.8	4.8	4.8
0.25 M Na Acetate, 20 % NaCl	↓	↓	↓	↓	↓	↓	↓	↓	↓
p(TMAEMA-co-MEDSA) 37.64 %									
H ₂ O									
pH									
0.25 M Na Acetate, 20 % NaCl	↓	↓	↓	↓	↓	↓	↓	↓	↓
p(TMAEMA-co-MEDSA) 37.64 %									
H ₂ O									
pH									
0.25 M Na Acetate, 20 % NaCl	200 µL (0.25 M Na Acetate, 20 % NaCl)	↑	↑	↑	↑	↑	↑	↑	↑
p(TMAEMA-co-MEDSA) 37.64 %	0 µL								
H ₂ O	300 µL								
pH	4.8								

Figure 4-47 shows the HEWL crystals obtained in the presence of p(METMAC-*co*-MEDSAH) (P8) at various concentrations. With the effects of both cation and zwitterionic sulfobetaine, p(METMAC-*co*-MEDSAH) (P8) nucleated a few crystals with complex shape. There were significant etch defects on the surface of crystals.

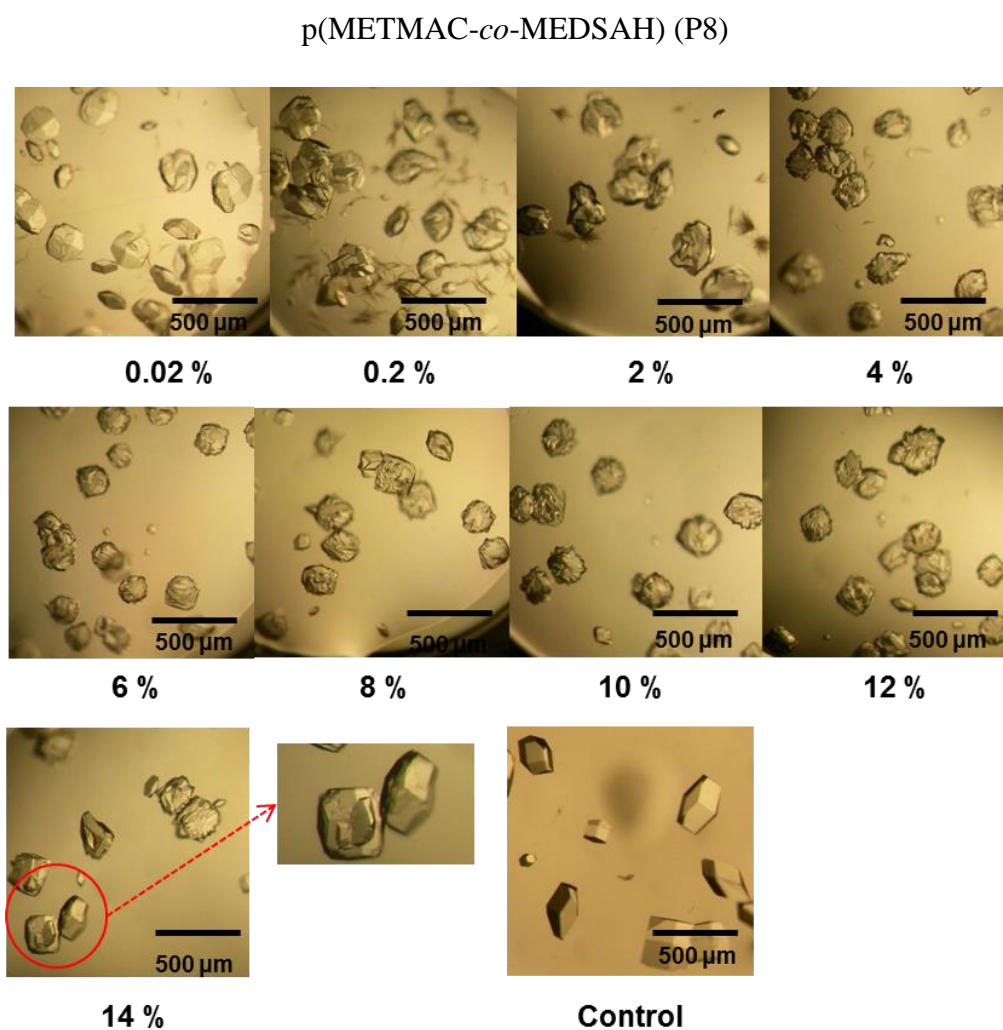


Figure 4-47. Photomicrographs of HEWL crystals, grown under tetragonal crystal condition, in the presence of p(METMAC-*co*-MEDSAH) (P8) at various concentrations. Image labelled 'Control' represents crystals grown from sample wells without polymer. The scale bar was 500 μm.

Figure 4-48 presents image analysis of HEWL crystals grown in the presence of p(METMAC-*co*-MEDSAH) (P8). As the concentration of p(METMAC-*co*-MEDSAH) (P8) in solution was increased, the size of the crystals did not vary clearly, but, the shape of crystals appeared to be more complex.

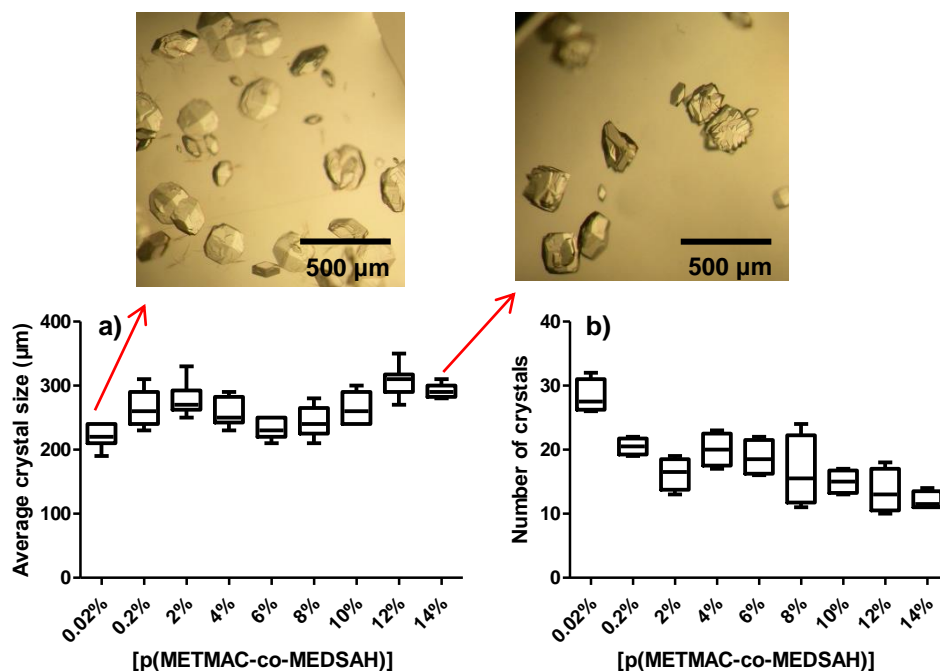


Figure 4-48. Summary of photomicrograph analysis showing changes in the size and number of HEWL crystals, grown in the presence of p(METMAC-*co*-MEDSAH) (P8). a) Average length (μm) of the largest crystal diameter; b) Experiment count for the number of crystals per sample well.

Cationic/zwitterionic copolymer might have different functions during HEWL crystallisation (Figure 4-49). It might complex with HEWL macromolecules for charge compensation and promoted nucleation; or may have charge-charge repulsions between cationic/zwitterionic polymer and cationic HEWL

macromolecules; after nucleation, it also might absorb on certain faces of crystals and influence the direction of crystal further growth.¹⁰⁰ In these ways, the HEWL crystals might have complex shape; however, the crystal form was still tetragonal.

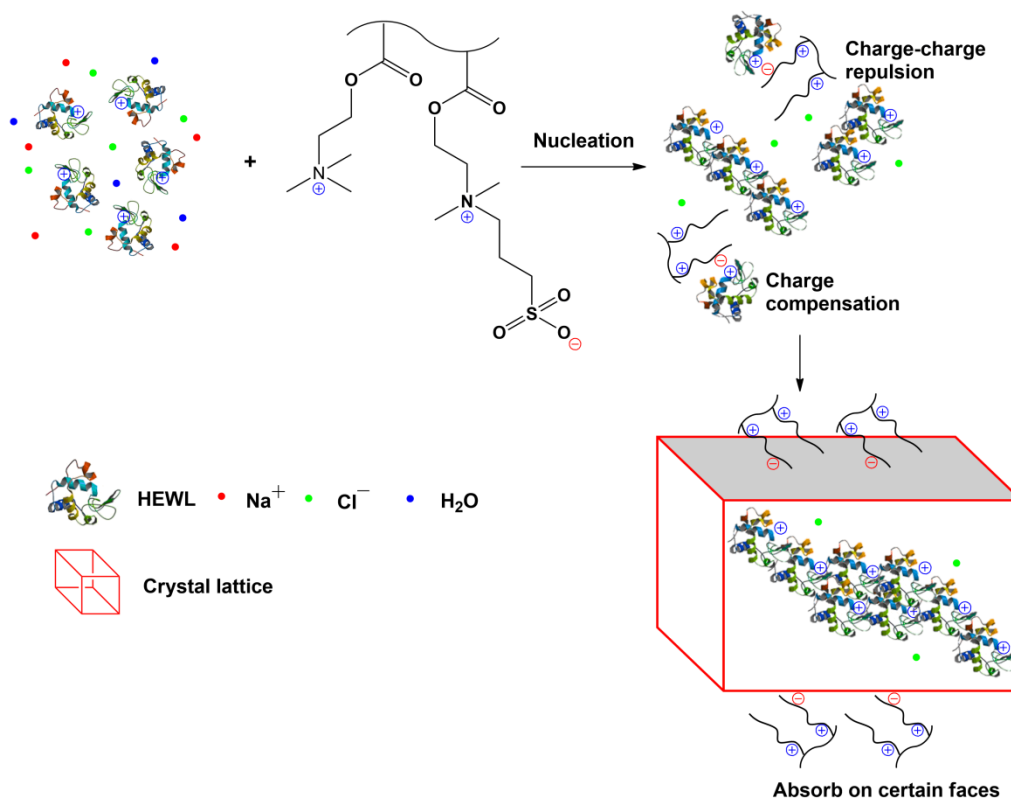


Figure 4-49. Hypothesis of mechanisms of cationic/zwitterionic polymer mediated HEWL crystallisation. It can act via multiple mechanisms, i.e. charge-charge repulsions between cationic/zwitterionic polymer and cationic HEWL macromolecules; or it can complex with HEWL macromolecules for charge compensation; or it can absorb on certain faces of crystals and influence the direction of crystal further growth. HEWL macromolecules are positively charged at tetragonal crystallisation pH of 4.8, i.e. cationic. Na⁺ and Cl⁻ ions are from the crystallisation buffer solutions.

4.4 Conclusions

In this chapter, four classes of materials with varying degrees of charge, molecular weight and backbone structure were investigated for their roles as additives in HEWL solution, including one neutral polymer: p(PEGMA₄₇₅) (P1); three cationic polymers: quaternised p(DMAEMA) (P2) with a series of quaternised ratios: 25 %, 50 %, 75 % and 100 %, a random copolymer p(DMAEMA-*stat*-PEGMA₄₇₅) (P3) and p(DMAPMAm) (P4) (DPs: 38, 83 and 150); three anionic polymers: p(AMPS) (P5) (DPs: 53, 99 and 200), p(2-AmAA) (P6) (DPs: 18, 46, 72 and 150) and p(4-AmBA) (P7) (DPs: 21, 50, 100 and 200); and one cationic/zwitterionic copolymer: p(METMAC-*co*-MEDSAH) (P8) (Table 4-21). Crystallisation experiments were performed on 96-well plates, by using the sitting drop vapour diffusion technique. The results show that these polymers have different effects on protein crystallisation, depending on the functionality and charge of polymers.

Table 4-21. Summary of polymers applied to HEWL crystallisation

Poly-neutral	p(PEGMA ₄₇₅)
Poly-cationic	Quaternised p(DMAEMA) (quaternised ratios: 25 %, 50 %, 75 % and 100 %)
	p(DMAEMA- <i>stat</i> -PEGMA ₄₇₅)
	p(DMAPMAm) (DPs: 38, 83 and 150)
Poly-anionic	p(AMPS) (DPs: 53, 99 and 200)
	p(2-AmAA) (DPs: 18, 46, 72 and 150)
	p(4-AmBA) (DPs: 21, 50, 100 and 200)
Poly-cationic/zwitterionic	p(METMAC- <i>co</i> -MEDSAH)

The first protein we selected was HEWL. The pI of HEWL is 11.35, therefore when at its crystallisation pH 4.8, HEWL macromolecules are positively charged, i.e. cationic. HEWL crystallisation under conditions favouring the tetragonal form resulted in exclusively tetragonal crystals within 1-2 days without any polymer. Neutral p(PEGMA₄₇₅) (P1) as a precipitant, competed with protein solutes for water and thus promoted HEWL crystallisation via a dehydration mechanism,¹²⁵ resulting in a few large tetragonal crystals. Cationic polymers had an increased propensity for nucleating many small crystals by altering the electrostatic interactions between HEWL molecules and the solution. Moreover, instead of tetragonal crystals, two other forms of HEWL crystals were obtained when crystallised in the presence of quaternised p(DMAEMA) (P2): needles and monoclinic crystals. Anionic polymers could influence the size of HEWL crystals by attracting cationic HEWL macromolecules for charge compensation.¹⁰⁸ Anionic p(AMPS) (P5) nucleated a few large crystals. However, smaller HEWL crystals were obtained when applied weakly anionic p(2-AmAA) (P6) and p(4-AmBA) (P7), due to the pKa values of p(2-AmAA) (P6) and p(4-AmBA) (P7) being close to the crystallisation pH 4.8. With the effects of both cation and zwitterionic sulfobetaine, p(METMAC-*co*-MEDSAH) (P8) nucleated a few crystals with complex shape.

In conclusion, all these results illustrate that polymers acting as solution additives can mediate protein crystallisation through favourable interactions

between polymer and protein or the surrounding solvent system. They are found to influence strongly the resultant crystal size and shape, even crystal packing motifs; and have the ability to obtain multiple polymorphs from one crystallisation condition, which could save time for new constructs.

CHAPTER 5

5. Application of Polymers to Concanavalin A (Con A) Crystallisation

5.1 Introduction

Concanavalin A (Con A) was first crystallised by Sumner and Howell,^{168, 169} and Greer *et al.* preliminarily reported its crystallographic studies.¹⁷⁰ Currently, there are several common structurally characterised crystal forms of concanavalin A (Con A), which bound to manganese and calcium ions, including orthorhombic $I222$ (form I),¹⁸¹ triclinic $P1$ (form II),¹⁷¹ orthorhombic $C222_1$ (form III)¹⁷², orthorhombic $C222_1$ (form IV)⁹⁹ and orthorhombic $P2_12_12_1$ (form V).⁹⁹

As mentioned in Chapter 4, various polymers we prepared have clear effects on HEWL crystal size, shape, crystal packing motifs, and polymorphic forms under crystallisation conditions favouring HEWL tetragonal polymorph. In addition to HEWL, which is cationic under conditions in which it is normally crystallised, we also aimed to evaluate whether those polymers were suitable for other proteins, especially anionic proteins. Therefore, concanavalin A (Con A) was chosen as first model anionic protein for further crystallisation studies. The isoelectric point (pI) of Con A is 4.5,²²⁷ but crystallisation of this protein is normally carried out at pH 8.5, at which point Con A molecules are negatively charged overall (Table 5-1).

Table 5-1. Summary of concanavalin A (Con A)

Protein	pI ^a	Mw (kDa)	Crystallisation pH
Con A 	4.5	25.5	8.5

^a Isoelectric point (pI) is the pH at which a particular molecule or surface carries no net electrical charge.

Three classes of polymers were selected for further Con A crystallisation experiments, including neutral, cationic and anionic polymers. Based on the results of HEWL crystallisation, polymers with different degrees of charge and backbone structure have dramatically influenced the crystallisation results, especially the cationic quaternised p(DMAEMA) (P2). Among the anionic polymers we prepared, the expected pKa value of p(AMPS) (P5) (~ 0.86) was the smallest; thus, it would have more negative charges at the crystallisation pH of 8.5 than other two anionic polymers: p(2-AmAA) (P6) and p(4-AmBA) (P7). Therefore, in this chapter, we chose three key polymers from each class for their role as additives in Con A crystallisation: neutral p(PEGMA₄₇₅) (P1), cationic quaternised p(DMAEMA) (P2) (quaternised ratio: 75 %) and anionic p(AMPS) (P5) (DP 99). Figure 5-1 shows a summary of hypothesis of the interaction of various polymers with anionic concanavalin A (Con A) in the protein crystallisation process.

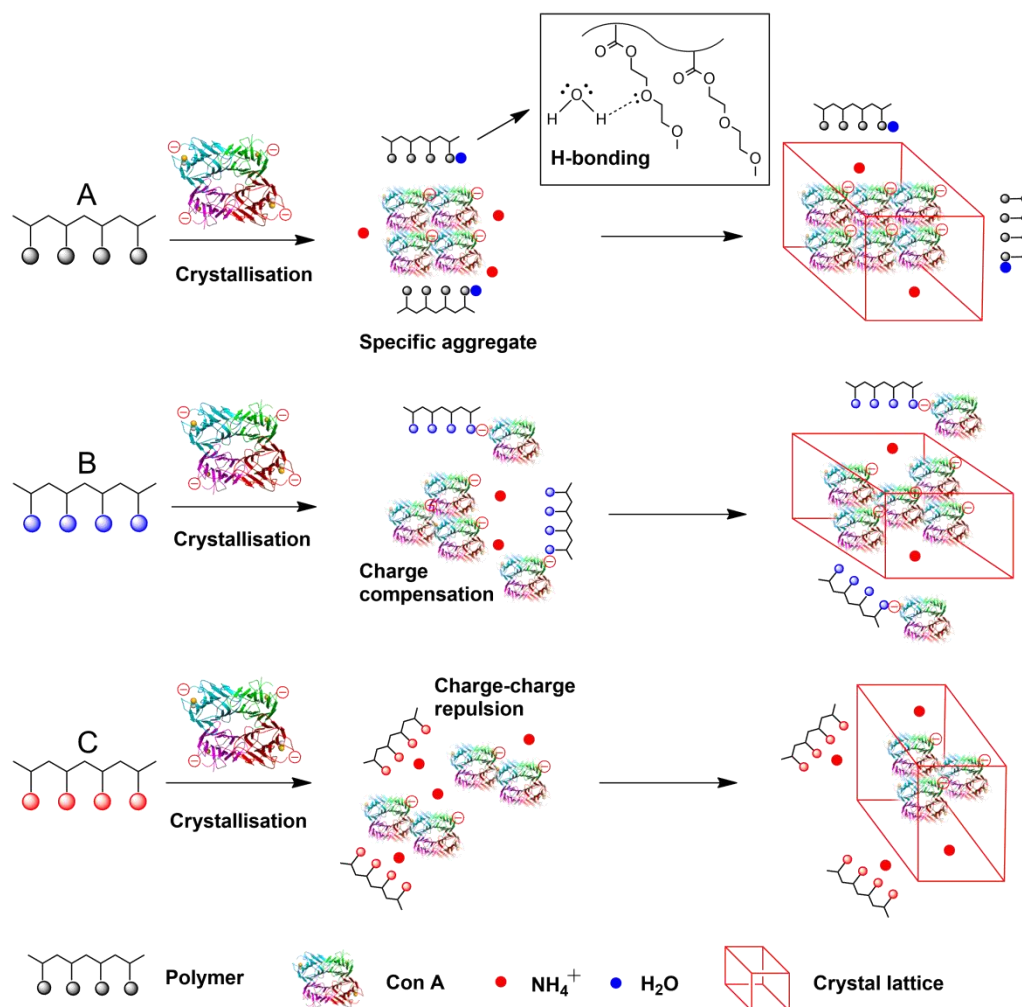


Figure 5-1. Schematic representation of the interaction of various polymers with anionic concanavalin A (Con A) in the protein crystallisation process. (A) Neutral polymer: H-bonding with water and thus promoting protein crystallisation via a dehydration mechanism. (B) Cationic polymer: attracting anionic Con A for charge compensation. (C) Anionic polymer: charge-charge repulsions between anionic polymer and anionic Con A. Con A macromolecules are anionic when at crystallisation pH 8.5. NH₄⁺ ions are derived from the crystallisation buffer solutions.

5.2 Methods

5.2.1 Crystallisation technique and plate

Con A was crystallised using the sitting drop vapour diffusion technique as described in Chapter 4 for HEWL. MRC 2 Well Crystallisation Plates (Swissci) (UVP plate, 96 reservoir wells) were purchased from Hampton Research. Specifically, a solution (50 μL) of tested polymer buffer was pipetted in triplicate in the reservoir wells. Protein solution (1 μL) and buffered polymer solution (as described above, 1 μL) were pipetted into sample wells of the crystallisation plate.

5.2.2 Preparation of polymer solutions and stock buffer solutions

The stock polymer solutions in H_2O at a concentration of $\sim 40\%$ (w/v) were prepared. In order to use polymers as part of the solution in Con A crystallisation, it was necessary, to alter the pH to around 8.5 by using HCl (1 M) or NaOH (2 M). The stock buffer solutions of 1 M ammonium sulfate and 10 mM Tris buffer at pH 8.5 and 20 mM Tris buffer at pH 8.0 were also prepared and filtered using a 0.2 μm cellulose acetate membrane filter.

The following polymer solutions were prepared at a final volume of 2 mL, 1 mL, 500 μL or 250 μL : 0.02 % (w/v), 0.2 % (w/v), 2 % (w/v), 4 % (w/v), 6 % (w/v), 8 % (w/v), 10 % (w/v), 12 % (w/v), 14 % (w/v), 16 % (w/v), 18 % (w/v), 20 % (w/v), 22 % (w/v) and 24 % (w/v) in 1 M ammonium sulfate and 10 mM Tris buffer at pH 8.5. Polymers had dissolved completely in all solutions.

5.2.3 Crystallisation protocol for Con A crystals^{181, 209}

Con A from *Canavalia ensiformis* (Jack bean) was purchased from Sigma (Product Number: C7275, CAS Number: 11028-71-0, pI: 4.5, 4.7, 5.1, 5.5). 20 mM Tris buffer at pH 8.0 was prepared and filtered through a 0.2 µm cellulose acetate membrane filter. This was used to prepare the 70 mg/mL Con A solution, which was then centrifuged at 13,000 rpm for 5 min at 4 °C.

Con A was crystallised using the sitting drop vapour diffusion technique as described in Chapter 4 for HEWL. A drop of 1:1 protein:polymer solution was usually used here. Con A solution (1 µL, 70 mg/mL Con A in 20 mM Tris buffer at pH 8.0) and buffered polymer solution (1 µL, 1 M ammonium sulfate and 10 mM Tris buffer at pH 8.5) were pipetted into each sample well, and buffered polymer solution (50 µL) was pipetted into each reservoir well of the crystallisation plate. Con A in each sample well was 35 mg/mL. For control, some wells contained no polymer in their reservoir and sample solutions. The entire crystallisation plate system was sealed using transparent sealing tape and monitored using optical microscopy. Crystallisation occurred over a couple of days at 19 °C.

5.2.4 Crystal imaging

Optical images of Con A crystals were directly collected by a Leica Stereomicroscope (63 x magnifications), with a Leica fan-cooled light source, connected to a Nikon Coolpix 4500 digital camera (4.0 megapixels).

5.2.5 X-ray crystallography

Con A crystals were determined by single crystal X-ray diffraction recorded at room temperature on an X-ray generator with high-flux Osmic confocal multi-layer optics. Con A crystals were cryoprotected with mother liquor containing 30 % glycerol, then flash-frozen in a nitrogen-gas stream.^{99, 210}

5.2.6 DLS studies

For the DLS experiments on Con A crystal growth, Con A was crystallised using the batch crystallisation method. A protein solution of 30 mg/mL Con A in 20 mM Tris buffer at pH 8.0 was mixed with a polymer solution of 1 M ammonium sulfate and 10 mM Tris buffer at pH 8.5. Three classes of polymers, containing neutral polymer: p(PEGMA₄₇₅) (P1), cationic polymer: quaternised p(DMAEMA) (P2) (quaternised ratio: 75 %) and anionic polymer: p(AMPS) (P5) (DP 99) were used here. Crystal growth time: 2 hours. Control experiments contained no polymer in the crystallisation solution.

5.2.7 SEM analysis

Con A crystals grown in the presence of selected polymers neutral p(PEGMA₄₇₅) (P1), cationic quaternised p(DMAEMA) (P2) (quaternised ratio: 75 %) and anionic p(AMPS) (P5) by using sitting drop vapour diffusion method were subjected to SEM analysis in this project.

5.3 Results and discussion

5.3.1 Con A crystallisation in the presence of neutral polymer in solution:

p(PEGMA₄₇₅) (P1)

By using the above mentioned pH-altered stock buffer solution, the following

p(PEGMA₄₇₅) (P1) solutions with various concentrations were prepared:

0.02 %, 0.2 %, 2 %, 4 %, 6 %, 8 %, 10 % and 12 % (w/v) (Table 5-2).

Table 5-2. Con A crystallisation plate set up: p(PEGMA₄₇₅)

1 M ammonium sulfate and 10 mM Tris buffer	100 μ L (1 M ammonium sulfate and 10 mM Tris buffer)	0.3 μ L (0.02 %)	149.7 μ L	8.5	↓				
p(PEGMA ₄₇₅) H ₂ O pH	100 μ L (1 M ammonium sulfate and 10 mM Tris buffer)	2.6 μ L (0.2 %)	147.4 μ L	8.5	↓				
1 M ammonium sulfate and 10 mM Tris buffer	100 μ L (1 M ammonium sulfate and 10 mM Tris buffer)	26 μ L (2 %)	124 μ L	8.5	↓				
p(PEGMA ₄₇₅) H ₂ O pH	100 μ L (1 M ammonium sulfate and 10 mM Tris buffer)	52 μ L (4 %)	98 μ L	8.5	↓				
1 M ammonium sulfate and 10 mM Tris buffer	100 μ L (1 M ammonium sulfate and 10 mM Tris buffer)	77 μ L (6 %)	73 μ L	8.5	↓				
p(PEGMA ₄₇₅) H ₂ O pH	100 μ L (1 M ammonium sulfate and 10 mM Tris buffer)	103 μ L (8 %)	47 μ L	8.5	↓				
1 M ammonium sulfate and 10 mM Tris buffer	100 μ L (1 M ammonium sulfate and 10 mM Tris buffer)	129 μ L (10 %)	21 μ L	8.5	↓				
p(PEGMA ₄₇₅) H ₂ O pH	100 μ L (1 M ammonium sulfate and 10 mM Tris buffer)	155 μ L (12 %)	0 μ L	8.5	↓				
1 M ammonium sulfate and 10 mM Tris buffer	100 μ L (1 M ammonium sulfate and 10 mM Tris buffer)	0 μ L	150 μ L	8.5	↑				
p(PEGMA ₄₇₅) H ₂ O pH	100 μ L (1 M ammonium sulfate and 10 mM Tris buffer)	0 μ L	150 μ L	8.5	↑				

Figure 5-2 shows images of Con A crystals formed in the presence of p(PEGMA₄₇₅) (P1). Con A solutions produced small crystals with sizes of around 60 μm within 1 week in the absence of polymer (Figure 5-2, Control). When p(PEGMA₄₇₅) (P1) was added to the solution, the size and number of Con A crystals were found to vary very clearly. Neutral polymer p(PEGMA₄₇₅) (P1) resulted in a few large rectangular crystals.

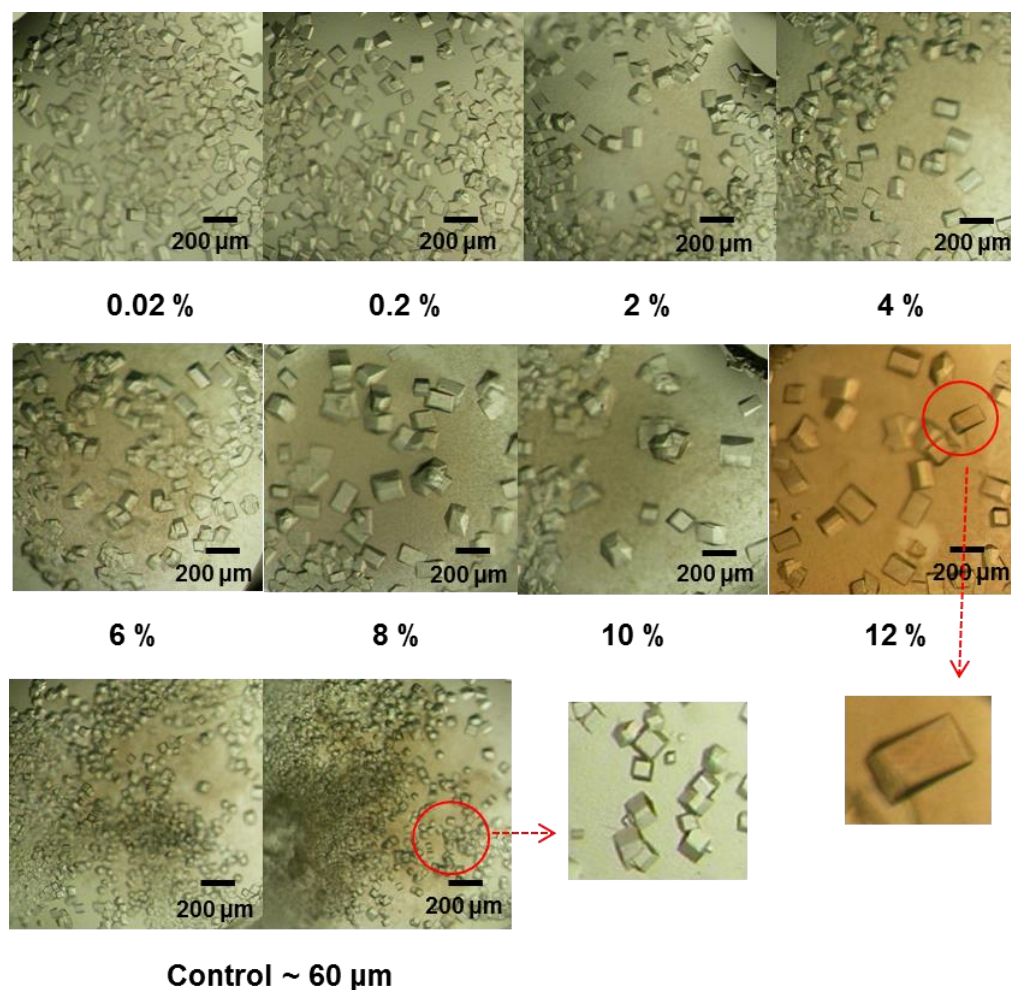


Figure 5-2. Selected photomicrographs of Con A crystals, grown in the presence of p(PEGMA₄₇₅) (P1) at various concentrations. Image labelled 'Control' represents Con A crystals grown from sample wells without polymer. The scale bar was 200 μm .

Con A crystal size and number distribution depending on neutral p(PEGMA₄₇₅) (P1) concentration was obtained by further image analysis (Figure 5-3). For anionic Con A, as the concentration of p(PEGMA₄₇₅) (P1) in solution was increased, the number of Con A crystals appeared to decrease, and the size of the crystals appeared to increase.

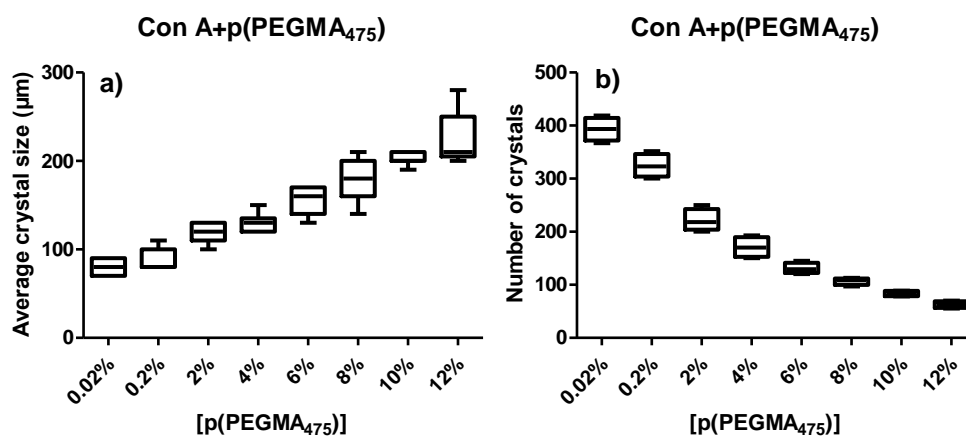


Figure 5-3. Summary of photomicrograph analysis of Con A crystals, grown in the presence of p(PEGMA₄₇₅) (P1) at various concentrations. a) Average length (μm) of the largest crystal diameter; b) Experiment count for the number of crystals per sample well.

Diffraction data were collected for Con A crystals by single crystal X-ray diffraction recorded at room temperature. Figure 5-4 illustrates the diffraction patterns of Con A crystals formed in the absence of polymer (Control) and in the presence of p(PEGMA₄₇₅) (P1) by X-ray crystallography; and Table 5-3 shows diffraction data of Con A crystals, which confirmed as orthorhombic (space group: $C222_1$, form IV).

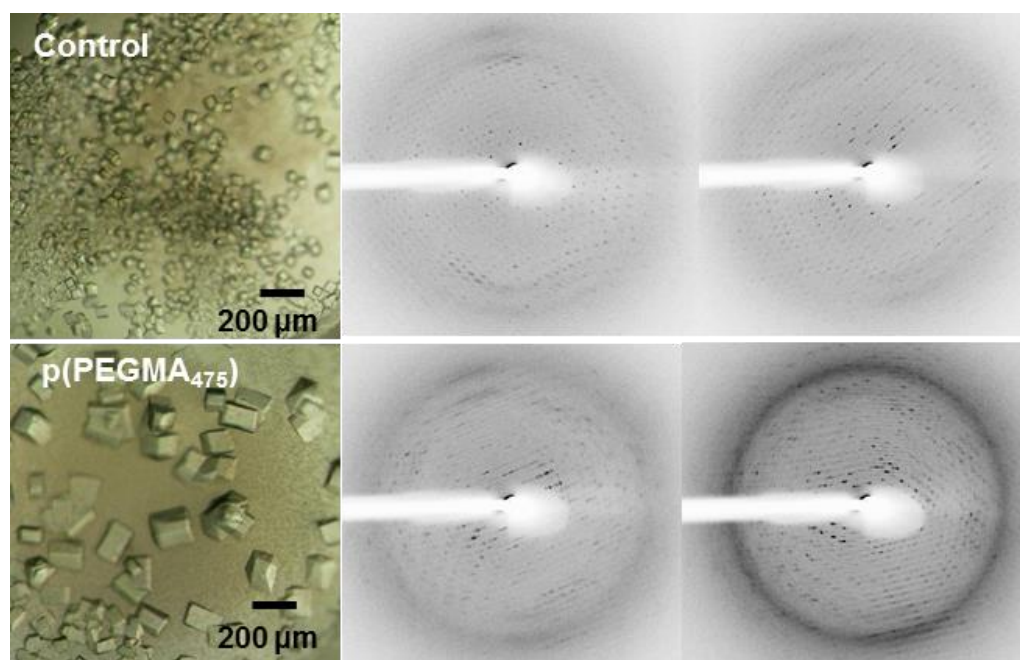


Figure 5-4. Con A crystals photomicrographs and X-ray diffraction patterns yielded by the single Con A crystal in the presence of neutral p(PEGMA₄₇₅) (P1). Image labelled ‘Control’ represents Con A crystals grown from sample wells without p(PEGMA₄₇₅) (P1). Two scattering angles: 0 ± 1 degrees and 90 ± 1 degrees.

Table 5-3. Diffraction data collection for Con A crystals formed in the absence (Control) and presence of neutral p(PEGMA₄₇₅) (P1)

	Control	p(PEGMA ₄₇₅) (P1)
Space group	$C222_1$	$C222_1$
Unit cell lattice	Orthorhombic	Orthorhombic
Cell dimensions: a, b, c (Å)	101.4, 119.2, 250.2	102.0, 119.4, 251.0
α, β, γ	$90^\circ, 90^\circ, 90^\circ$	$90^\circ, 90^\circ, 90^\circ$
Resolution (Å)	50-2.8	50-2.8
Crystal-to-detector distance	170 mm	170 mm
Con A form	Form IV	Form IV

100 μL of 2 mg/mL p(PEGMA₄₇₅) (P1) in 1 M ammonium sulfate and 10 mM Tris buffer at pH 8.5 was mixed with 100 μL of 30 mg/mL Con A in 20 mM Tris buffer at pH 8.0; then dispensed to a VISCOTEK DLS Quartz cell. Figure 5-5 shows a summary of DLS data of Con A crystallisation under neutral p(PEGMA₄₇₅) (P1) at time points T_0 and $T_{120\text{min}}$. Figure 5-5a shows autocorrelation functions, which were analysed by DLS to obtain the distribution of particle radii, as shown in Figure 5-5b.

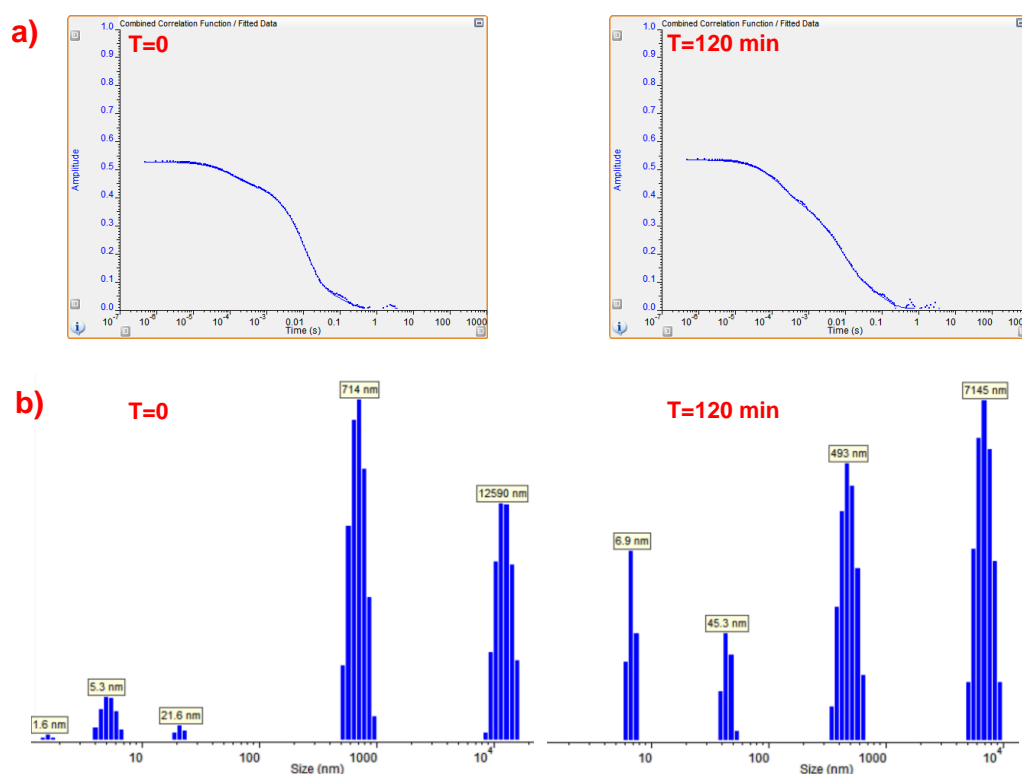


Figure 5-5. Summary of DLS data of Con A crystallisation under neutral p(PEGMA₄₇₅) (P1) at time points T_0 and $T_{120\text{min}}$: a) representative autocorrelation functions; b) radii distribution by intensity.

Representative Tukey plots of DLS data further illustrate protein aggregates growing in size as a function of time during Con A crystallisation experiments

under neutral p(PEGMA₄₇₅) (P1) (Figure 5-6). At the beginning of the experiment (T_0), the average size of the particles in the crystallisation solution was around 4 μm , measured by size distribution. With the addition of p(PEGMA₄₇₅) (P1), Con A crystallisation initiated and aggregates formed. As the time increased, Con A aggregates grew in size. After 120 minutes, the average size of the particles in the crystallisation solution was around 9 μm . The size of pure neutral p(PEGMA₄₇₅) (P1) without any protein in solution was around 7 nm.

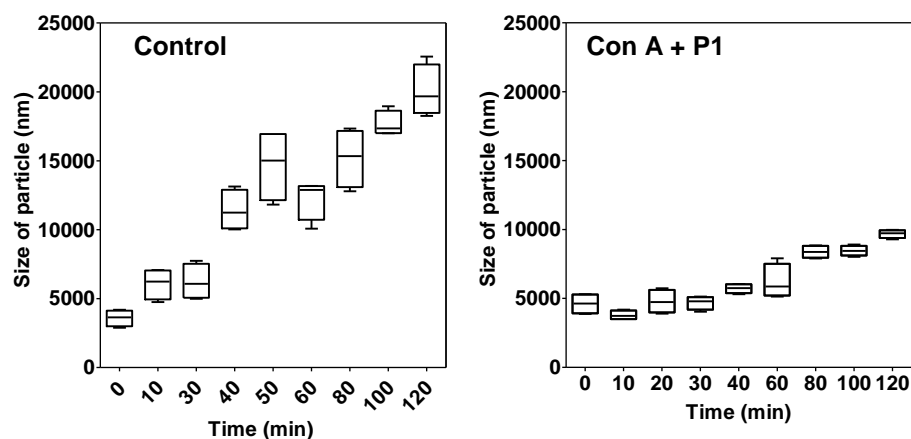


Figure 5-6. Variations of the size of Con A aggregates or crystals in the solution as a function of time during crystallisation experiments induced by neutral p(PEGMA₄₇₅) (P1). Tukey plots labelled ‘Control’ represent Con A aggregates or crystals grown from in the absence of polymer.

Con A crystals were taken out from the crystallisation plates then washed with crystallisation buffer solutions for SEM analysis. Figure 5-7 contains micrographs of Con A crystals grown in the absence (a) and presence of neutral p(PEGMA₄₇₅) (P1) (b). Con A crystals were poorly defined and had significant

etch defects without applied polymer (Figure 5-7a). With the addition of neutral p(PEGMA₄₇₅) (P1), Con A crystals had round edges with significant etch defects, however, p(PEGMA₄₇₅) (P1) still improved the size and shape of Con A crystal (Figure 5-7b). Compared with optical microscopy images, SEM images of Con A crystals did not look so well. This may be because of poor mechanical properties and stability of protein crystals.

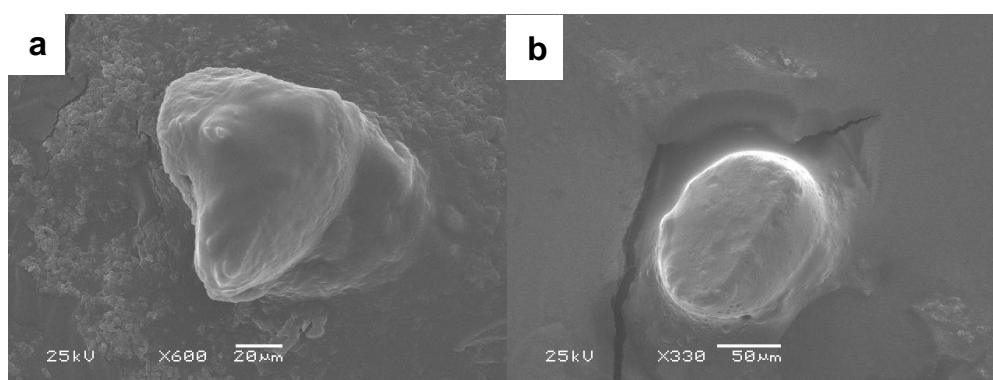


Figure 5-7. SEM micrographs of Con A crystals formed by sitting drop method: a) control, without any polymer, -- x 600 magnifications; the scale bar was 20 μm ; b) in the presence of p(PEGMA₄₇₅) (P1), -- x 330 magnifications; the scale bar was 50 μm .

All above results suggest neutral p(PEGMA₄₇₅) (P1) had a similar effect on crystal formation to that which occurred in HEWL crystallisation. Figure 5-8 presents a proposed mechanism of neutral polymer mediated Con A crystallisation. Neutral p(PEGMA₄₇₅) (P1) competed with protein solutes for water and dehydrated protein macromolecules.¹²⁵ Moreover, p(PEGMA₄₇₅) might have ‘volume-excluded effects’ by hydrophobic exclusion of protein

solutes.²²⁴ It could also lower the dielectric constant of the solution, consequently protein aggregation and phase separation was promoted. Therefore, Con A macromolecules were compelled to associate with each other.

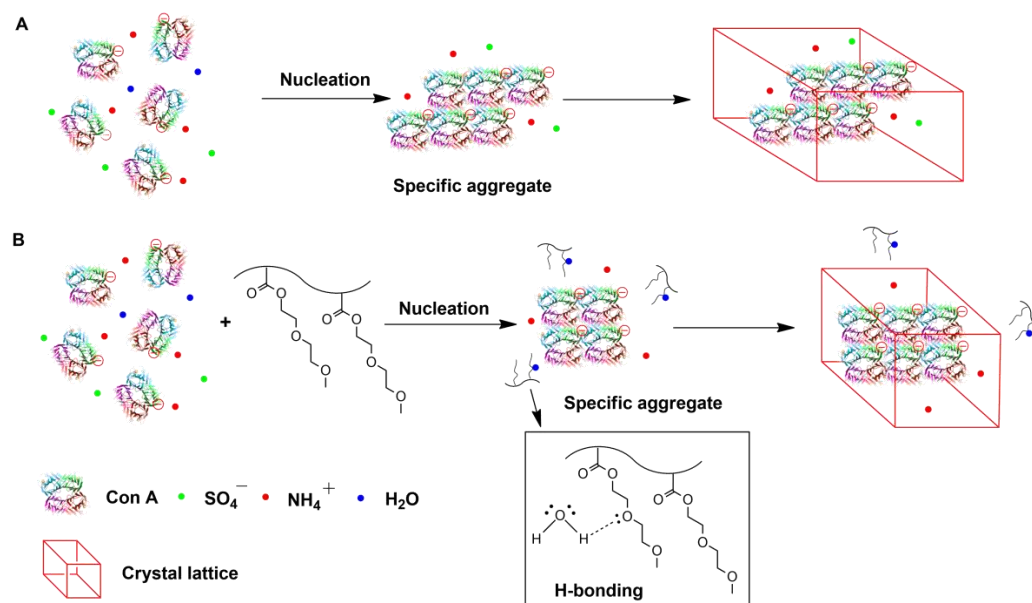


Figure 5-8. Schematic representation of hypothesis of anionic Con A crystallisation process in the absence of polymer (A); and the interaction of neutral p(PEGMA₄₇₅) (P1) with anionic Con A in the protein crystallisation process (B). Con A macromolecules are negatively charged at crystallisation pH of 8.5, i.e. anionic. NH_4^+ and SO_4^- ions come from the crystallisation buffer solutions.

5.3.2 Con A crystallisation in the presence of cationic polymer in solution: quaternised p(DMAEMA) (P2)

The following quaternised p(DMAEMA) (P2) (quaternised ratio: 75 %) solutions with various concentrations were prepared: 0.02 %, 0.2 %, 2 %, 4 %, 6 %, 8 %, 10 %, 12 % and 14 % (w/v) (Table 5-4).

Table 5-4. Con A crystallisation plate set up: quaternised p(DMAEMA) (P2)

	1	2	3	4	5	6	7	8	9
1 M ammonium sulfate and 10 mM Tris buffer	100 μ L (1 M ammonium sulfate and 10 mM Tris buffer)	100 μ L (1 M ammonium sulfate and 10 mM Tris buffer)	100 μ L (1 M ammonium sulfate and 10 mM Tris buffer)	100 μ L (1 M ammonium sulfate and 10 mM Tris buffer)	100 μ L (1 M ammonium sulfate and 10 mM Tris buffer)	100 μ L (1 M ammonium sulfate and 10 mM Tris buffer)	100 μ L (1 M ammonium sulfate and 10 mM Tris buffer)	100 μ L (1 M ammonium sulfate and 10 mM Tris buffer)	100 μ L (1 M ammonium sulfate and 10 mM Tris buffer)
Quaternised p(DMAEMA) (75%)	0.1 μ L (0.02%)	1.3 μ L (0.2%)	13 μ L (2%)	25 μ L (4%)	38 μ L (6%)	50 μ L (8%)	63 μ L (10%)	75 μ L (12%)	88 μ L (14%)
H ₂ O	149.9 μ L	148.7 μ L	137 μ L	125 μ L	112 μ L	100 μ L	87 μ L	75 μ L	62 μ L
pH	8.5	8.5	8.5	8.5	8.5	8.5	8.5	8.5	8.5
1 M ammonium sulfate and 10 mM Tris buffer	↓	↓	↓	↓	↓	↓	↓	↓	↓
Quaternised p(DMAEMA) (75%)									
H ₂ O									
pH									
1 M ammonium sulfate and 10 mM Tris buffer	↓	↓	↓	↓	↓	↓	↓	↓	↓
Quaternised p(DMAEMA) (75%)									
H ₂ O									
pH									
1 M ammonium sulfate and 10 mM Tris buffer	↑	↑	↑	↑	↑	↑	↑	↑	↑
Quaternised p(DMAEMA) (75%)									
H ₂ O									
pH									

Figure 5-9 shows Con A crystals formed in the presence of quaternised p(DMAEMA) (P2). Cationic polymer was likely to nucleate a few large block shape crystals.

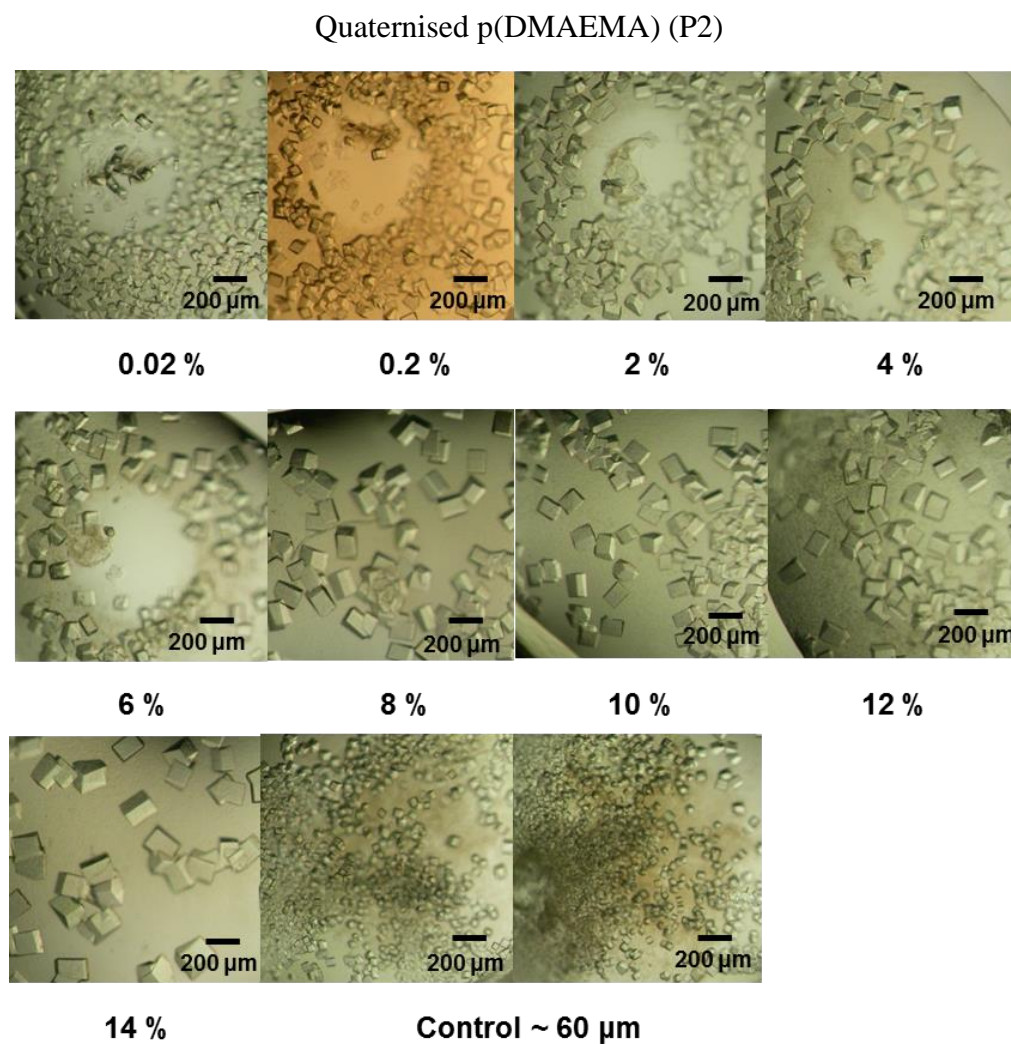


Figure 5-9. Photomicrographs showing changes in the size and shape of Con A crystals, grown in the presence of quaternised p(DMAEMA) (P2) (quaternised ratio: 75 %) at various concentrations. Image labelled ‘Control’ represents crystals grown from sample wells without polymer. The scale bar was 200 µm.

Figure 5-10 shows image analysis of Con A crystal size distribution by measuring the average length (μm) of the largest diameter of each crystal and number distribution depending on quaternised p(DMAEMA) (P2) concentration. For anionic Con A, as the concentration of quaternised p(DMAEMA) (P2) in solution was increased, the number of Con A crystals appeared to decrease, and the size of the crystals appeared to increase.

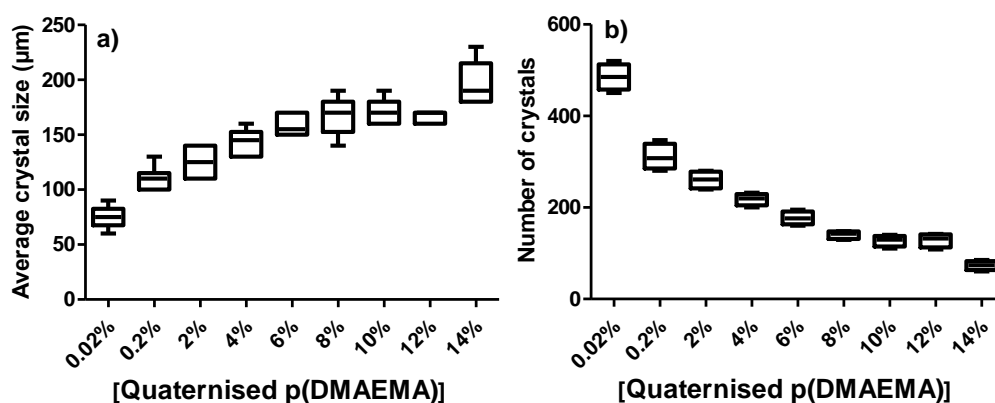


Figure 5-10. Summary of photomicrograph analysis of Con A crystals, grown in the presence of quaternised p(DMAEMA) (P2) at various concentrations. a) Average length (μm) of the largest crystal diameter. b) Experiment count for the number of crystals per sample well.

100 μL of 2 mg/mL quaternised p(DMAEMA) (P2) in 1 M ammonium sulfate and 10 mM Tris buffer at pH 8.5 was mixed with 100 μL of 30 mg/mL Con A in 20 mM Tris buffer at pH 8.0 for DLS study. Figure 5-11 shows a summary of DLS data of Con A crystallisation under cationic quaternised p(DMAEMA) (P2) at time points T_0 and $T_{120\text{min}}$. Figure 5-11a shows autocorrelation functions, which were analysed by DLS to obtain the distribution of particle radii, as

shown in Figure 5-11b.

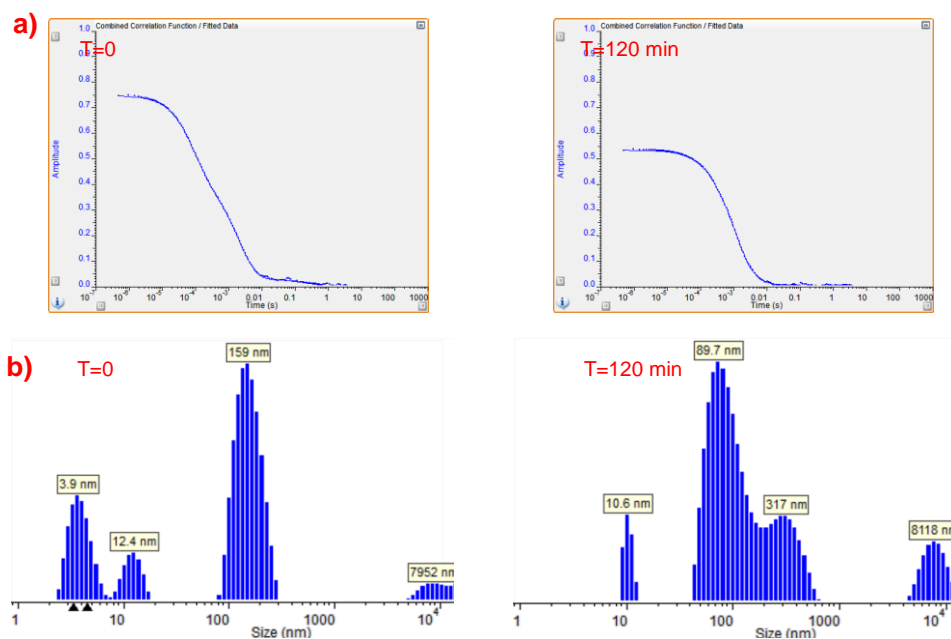


Figure 5-11. Summary of DLS data of Con A crystallisation under quaternised p(DMAEMA) (P2) at time points T_0 and $T_{120\text{min}}$: a) representative autocorrelation functions; b) radii distribution by intensity.

Representative Tukey plots of DLS data show Con A aggregates growing in size in the presence of quaternised p(DMAEMA) (P2) as a function of time during crystallisation experiments as shown in Figure 5-12. At the beginning of the experiment (T_0), the average size of the particles in the crystallisation solution was around 300 nm, measured by size distribution. With the addition of quaternised p(DMAEMA) (P2), an increase in size of the Con A aggregates was observed. After 120 minutes ($T_{120\text{min}}$), the average size of the aggregates in the crystallisation solution was around 1000 nm. The size of pure quaternised p(DMAEMA) (P2) in solution was around 18 nm.

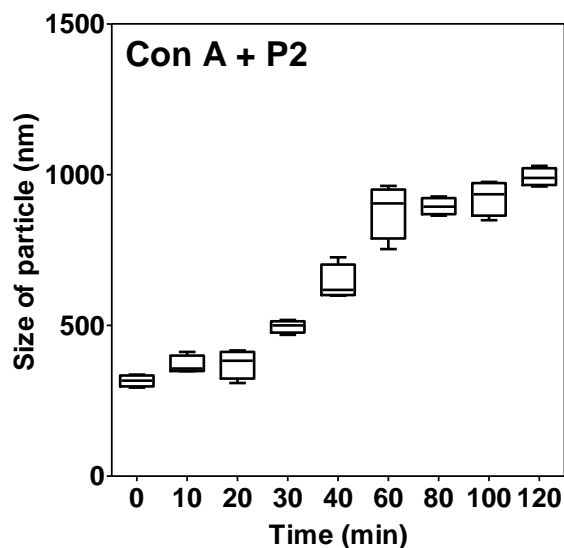


Figure 5-12. Variations of the size of Con A aggregates or crystals in the solution as a function of time during crystallisation experiments induced by cationic quaternised p(DMAEMA) (P2).

The SEM micrograph result of Con A crystals is shown in Figure 5-13. Con A crystals formed under quaternised p(DMAEMA) (P2) also had round edges with significant etch defects, due to poor mechanical properties and stability of protein crystals.

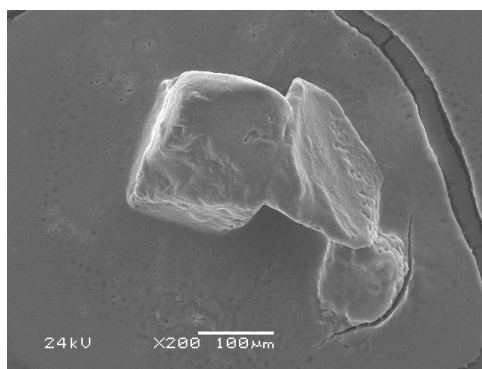


Figure 5-13. SEM micrographs of Con A crystals formed in the presence of quaternised p(DMAEMA) (P2), -- x 200 magnifications; the scale bar was 100 μm .

In summary of all above results obtained in the presence of cationic quaternised p(DMAEMA) (P2), for anionic proteins, such as Con A, the cationic polymer was likely to have attracted anionic Con A macromolecules by electrostatic interaction for charge compensation in the crystallisation process (Figure 5-14). Therefore, the cationic polymer would either lower the protein and water interfacial energy and act as nucleation centers by the absorption of Con A macromolecules, or slow down the rate of further growth of Con A crystal.

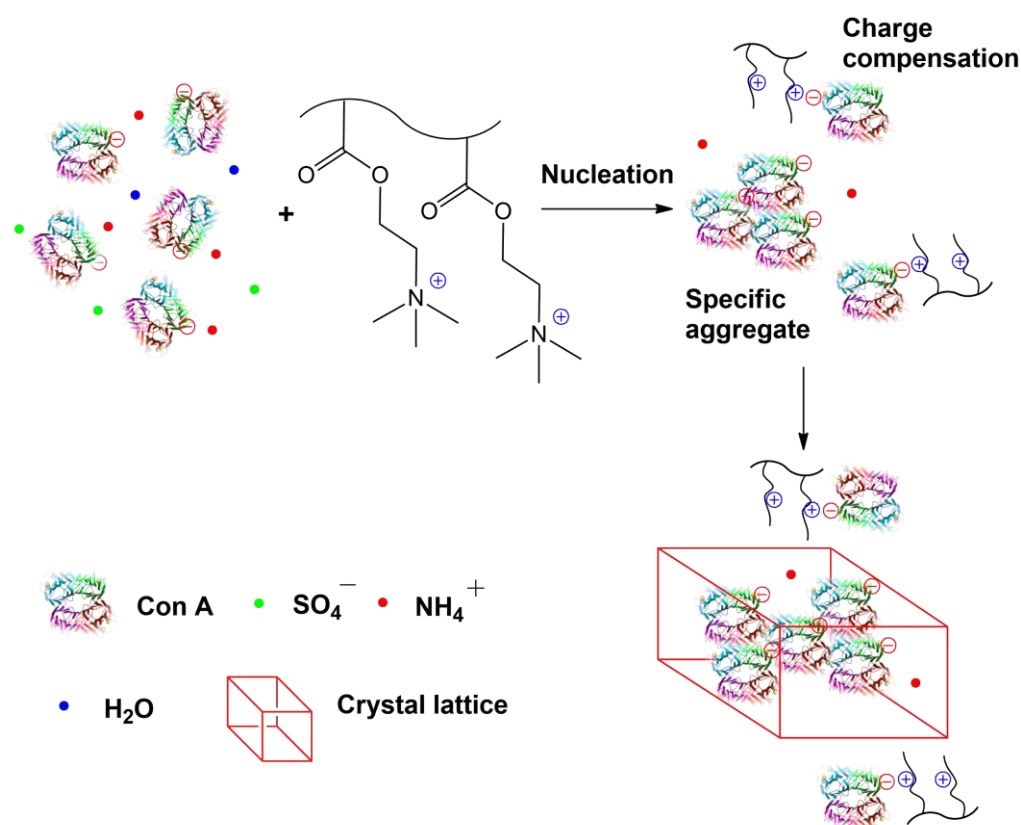


Figure 5-14. Hypothesis of mechanism of cationic polymer mediated Con A crystallisation. Cationic polymer attracted anionic Con A for charge compensation. Con A macromolecules were anionic when at crystallisation pH 8.5. NH_4^+ and SO_4^- ions were from the crystallisation buffer solutions.

Figure 5-15 shows images of Con A crystals formed in the presence of p(AMPS) (P5) (DP 99). Anionic p(AMPS) (P5) accelerated Con A aggregation and the formation of multiple nuclei, produced many small crystals with sizes of $\sim 20 \mu\text{m}$.

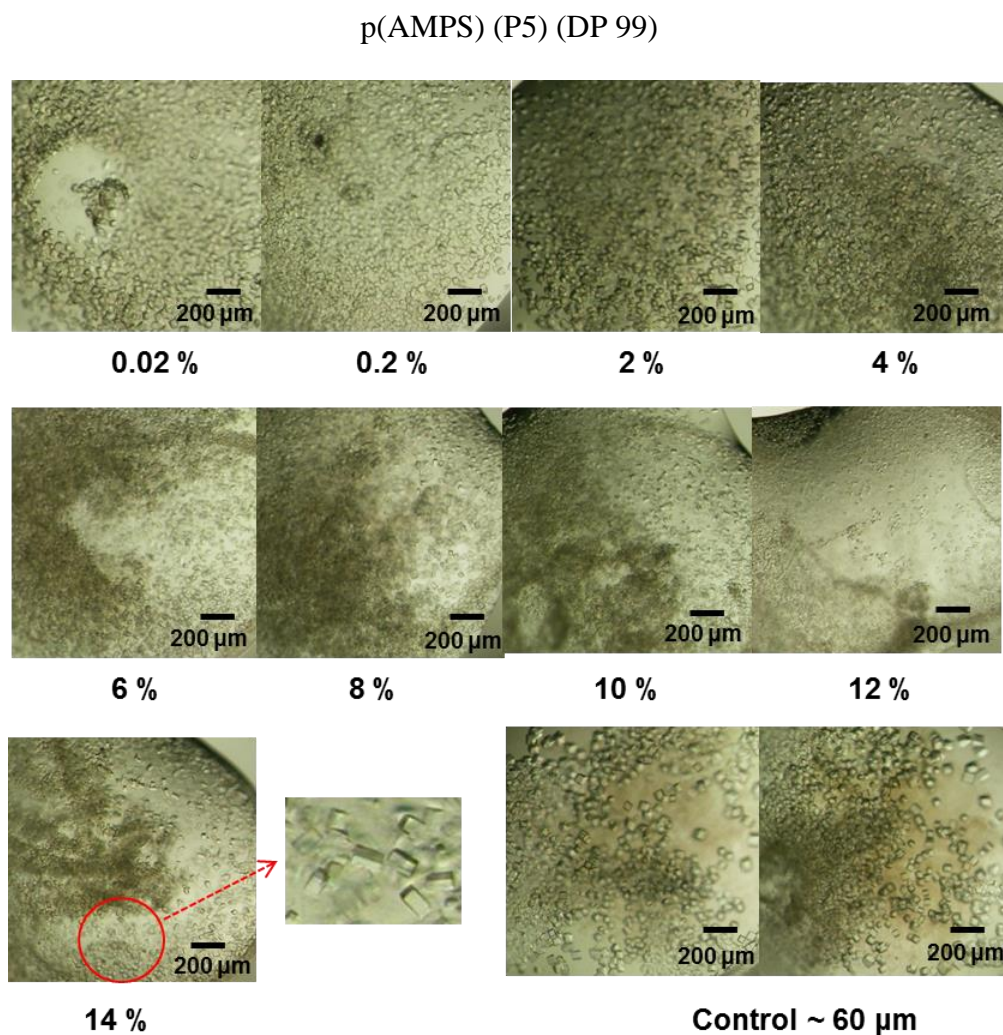


Figure 5-15. Photomicrographs of Con A crystals, grown in the presence of p(AMPS) (P5) (DP 99) at various concentrations. Images labelled ‘Control’ represent crystals grown from sample wells without polymer. The scale bar was $200 \mu\text{m}$.

Image analysis of photomicrograph data by measuring the average length (μm) of the largest diameter of each crystal depending on p(AMPS) (P5) concentration was obtained (Figure 5-16). However, it was not easy to obtain the number distribution, due to the amount of small crystals in the whole sample well was too large. For anionic Con A, as the concentration of p(AMPS) (P5) in solution was increased, the size of crystals appeared to decrease. At the concentration of 14 % (w/v), the size of Con crystal was around 20 μm .

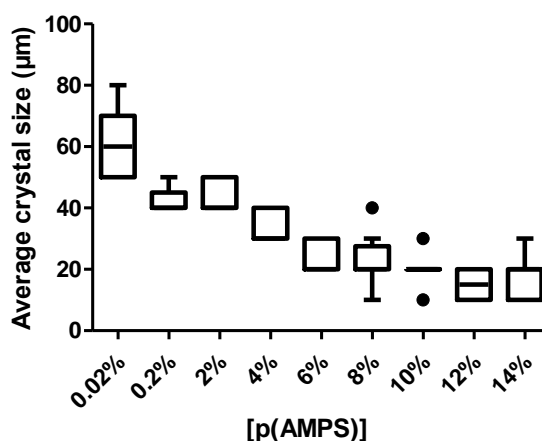


Figure 5-16. Summary of photomicrograph analysis of Con A crystals, grown in the presence of p(AMPS) (P5) at various concentrations.

100 μL of 2 mg/mL p(AMPS) (P5) in 1 M ammonium sulfate and 10 mM Tris buffer at pH 8.5 was mixed with 100 μL of 30 mg/mL Con A in 20 mM Tris buffer at pH 8.0; then dispensed to a VISCOTEK DLS Quartz cell for DLS study. Figure 5-17 shows a summary of DLS data of Con A crystallisation under anionic p(AMPS) (P5) at time points T_0 and $T_{100\text{min}}$. Figure 5-17a shows autocorrelation functions, which were analysed by DLS to obtain the distribution of particle radii, as shown in Figure 5-17b and c.

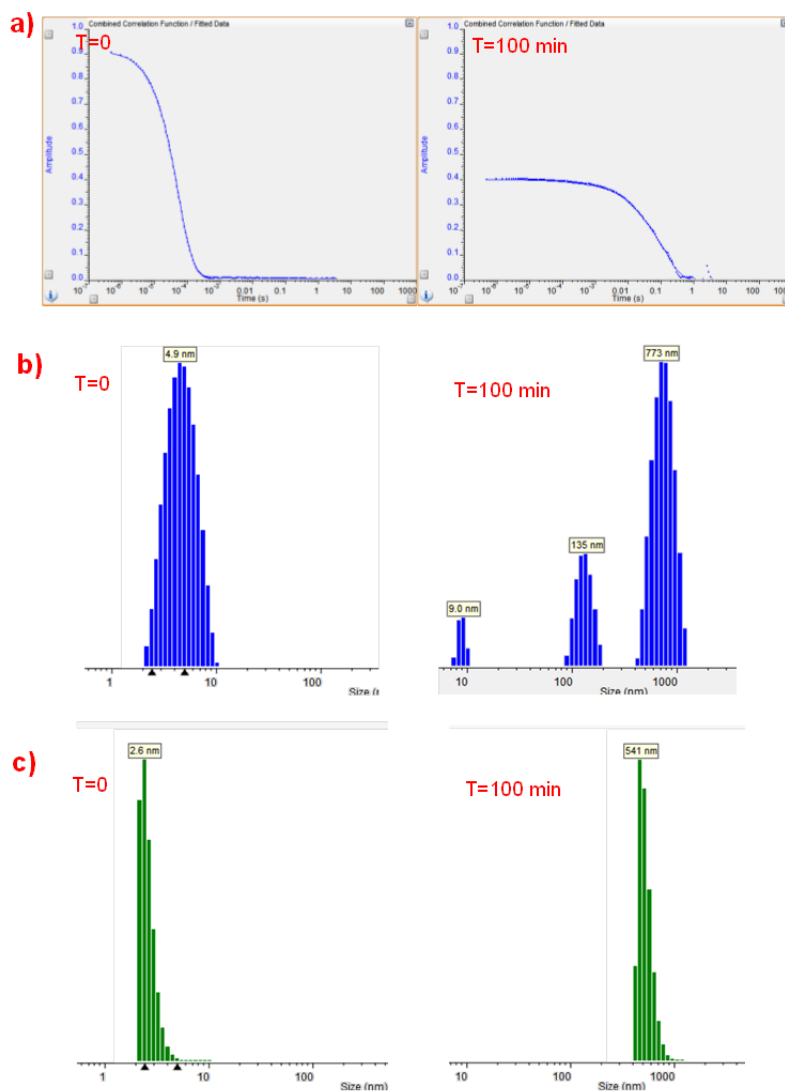


Figure 5-17. Summary of DLS data of Con A crystallisation under anionic p(AMPS) (P5) DP (99) at time points T_0 and $T_{100\text{min}}$: a) representative autocorrelation functions; b) radii distribution by intensity; c) radii distribution by number.

Representative Tukey plots of above DLS data show an increase in the size of protein aggregates when in the presence of p(AMPS) (P5) as a function of time during crystallisation experiments (Figure 5-18). Con A aggregates growing in size can be observed during the crystallisation experiment. At the beginning of

the experiment (T_0), Con A macromolecules were non-interacting in the solution. The decay time was very short. The average size of the particles in crystallisation solution was around 5 nm, measured by size distribution. With the addition of anionic p(AMPS) (P5), Con A crystallisation initiated and aggregates formed. As the time increased, Con A aggregates grew in size. Large particles diffused slower than small particles, and the correlation function decayed at a slower rate. After 120 minutes ($T_{120\text{min}}$), the average size of the particles in crystallisation solution was around 700 nm. The size of pure p(AMPS) (P5) (DP 99) without any protein was around 4 nm.

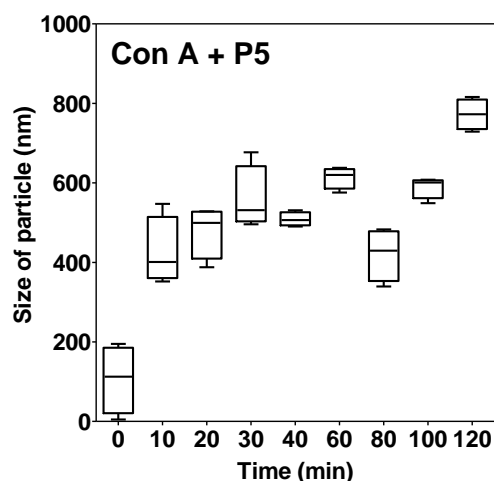


Figure 5-18. Variations of the size of Con A aggregates or crystals in the solution as a function of time during crystallisation experiments induced by anionic p(AMPS) (P5).

Con A crystals were then taken out from the crystallisation plates, washed with 1 M ammonium sulfate and 10 mM Tris buffer solution at pH 8.5 for SEM study. The SEM micrograph result (Figure 5-19) shows that although Con A

crystals had slight rounded edges under p(AMPS) (P5), however, they were better than that obtained under neutral p(PEGMA₄₇₅) (P1) and cationic quaternised p(DMAEMA) (P2). This may suggest that p(AMPS) (P5) could enhance the stability of Con A crystals.

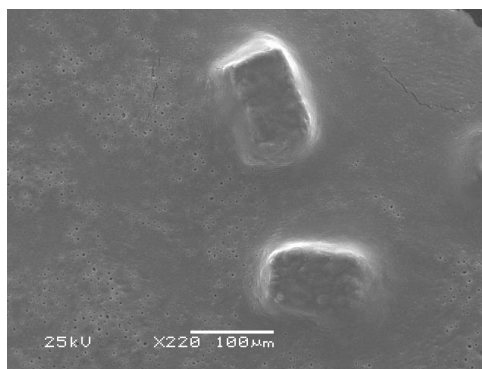


Figure 5-19. SEM micrograph of Con A crystals formed in the presence of p(AMPS) (P5), -- x 220 magnifications; the scale bar was 100 μm .

In summary of the above results obtained in the presence of p(AMPS) (P5), we proposed that at Con A crystallisation pH of 8.5, anionic polymer molecules had some negative charges, resulting in ‘charge-charge’ repulsions between anionic polymer molecules and anionic Con A macromolecules, lowering the interfacial energy between Con A macromolecules and water, thus, leading to the promotion of the nucleation rate and formation of multiple nuclei (Figure 5-20).^{226, 108}

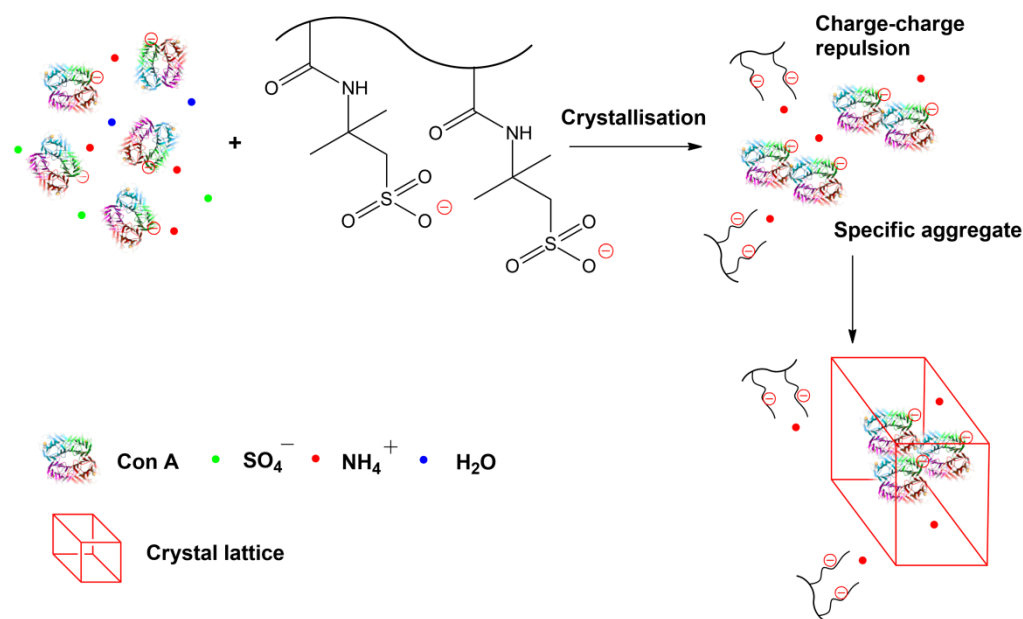


Figure 5-20. Hypothesis of mechanism of anionic polymer mediated Con A crystallisation. Anionic polymer: charge-charge repulsions between anionic polymer and anionic Con A. Con A macromolecules were anionic when at crystallisation pH 8.5. NH_4^+ and SO_4^- ions were from the crystallisation buffer solutions.

5.4 Conclusions

In this chapter, three polymers with varying degrees of charge, molecular weight and backbone structure were selected from each class and investigated as solution additives for Con A crystallisation, including neutral p(PEGMA₄₇₅) (P1), cationic quaternised p(DMAEMA) (P2) with quaternised ratio: 75 % and anionic p(AMPS) (P5). Crystallisation experiments were performed on 96-well plates using the sitting drop vapour diffusion technique as well.

Con A crystallisation experiments produced small orthorhombic crystals (space group: $C222_1$, form IV) with sizes of $\sim 60 \mu\text{m}$ within 1 week in the absence of

polymer. When polymers were utilised, the sizes and numbers of crystals were found to vary with the types of polymers added to solution, however, the form of crystals was still orthorhombic. Neutral polymers resulted in a few large block-shaped crystals with sizes of $\sim 200 \mu\text{m}$, suggesting a similar effect on crystal formation to that which occurred in HEWL crystallisation. Cationic polymers were likely to have attracted anionic Con A macromolecules by electrostatic interaction for charge compensation, and nucleated a few large crystals as well with sizes of $\sim 150 \mu\text{m}$. Anionic polymers accelerated Con A aggregation and produced many smaller crystals with sizes of $\sim 20 \mu\text{m}$ within four days. In conclusion, all these results illustrate that polymers with varying net charges, acted as solution additives to mediate protein crystallisation and have the ability to alter the size of protein crystals.

CHAPTER 6

6. Application of Polymers to Bovine Liver Catalase (BLC) Crystallisation

6.1 Introduction

Bovine liver catalase (BLC) was crystallised by Sumner and Dounce in 1937.¹⁸⁵ BLC has three structurally characterised crystal forms: trigonal $P3_221$ (form I),¹⁸⁶ orthorhombic $P2_12_12_1$ (form II)¹⁸⁷ and another orthorhombic (form III).¹⁸⁸ Forms I and II of BLC have been fully characterised using single X-ray diffraction previously. Form III only has previously been analysed by electron microscopy and powder X-ray diffraction.^{230, 231, 232, 233} It is very difficult to obtain high quality single BLC crystals, by using traditional growth methods. Moreover, BLC crystals are extremely thin ($<1 \mu\text{m}$),²³¹ it is therefore hard to get X-ray diffraction pattern. Recently, Matzger *et al.* utilised polymer-induced heteronucleation (PIHn) approach; i.e. cross-linked polymer films as heteronucleants, for BLC crystallisation, and got crystals suitable for single crystal X-ray diffraction (form III).^{188, 99} However, whether polymers were used as ‘additives’ in solution can mediate BLC crystallisation successfully or not, rarely has been studied.

Therefore, in addition to HEWL and Con A, a third model protein: bovine liver catalase (BLC), was chosen as model anionic protein for further crystallisation studies. The isoelectric point (pI) of BLC is 5.4,²²² and when at crystallisation

pH of 6.8, BLC macromolecules will carry some negative charges, hence being a weakly anionic protein at this pH (Table 6-1).

Table 6-1. Summary of bovine liver catalase (BLC)

Protein	pI ^a	Mw (kDa)	Crystallisation pH
BLC 	5.4	60	6.8

^a Isoelectric point (pI) is the pH at which a particular molecule or surface carries no net electrical charge.

As described in Chapter 5, in order to evaluate the effect of those polymers with different degrees of charge and backbone structure on other proteins, especially anionic proteins, three key polymers from each class, neutral p(PEGMA₄₇₅) (P1), cationic quaternised p(DMAEMA) (P2) (quaternised ratio: 75 %) and anionic p(AMPS) (P5) (DP 99) were also applied for BLC crystallisation by using sitting drop vapour diffusion crystallisation protocols. The crystallisation condition used here was first reported by McPherson and co-workers.²¹⁰ Figure 6-1 shows a summary of hypothesis of the interaction of various polymers with weakly anionic bovine liver catalase (BLC) in the protein crystallisation process.

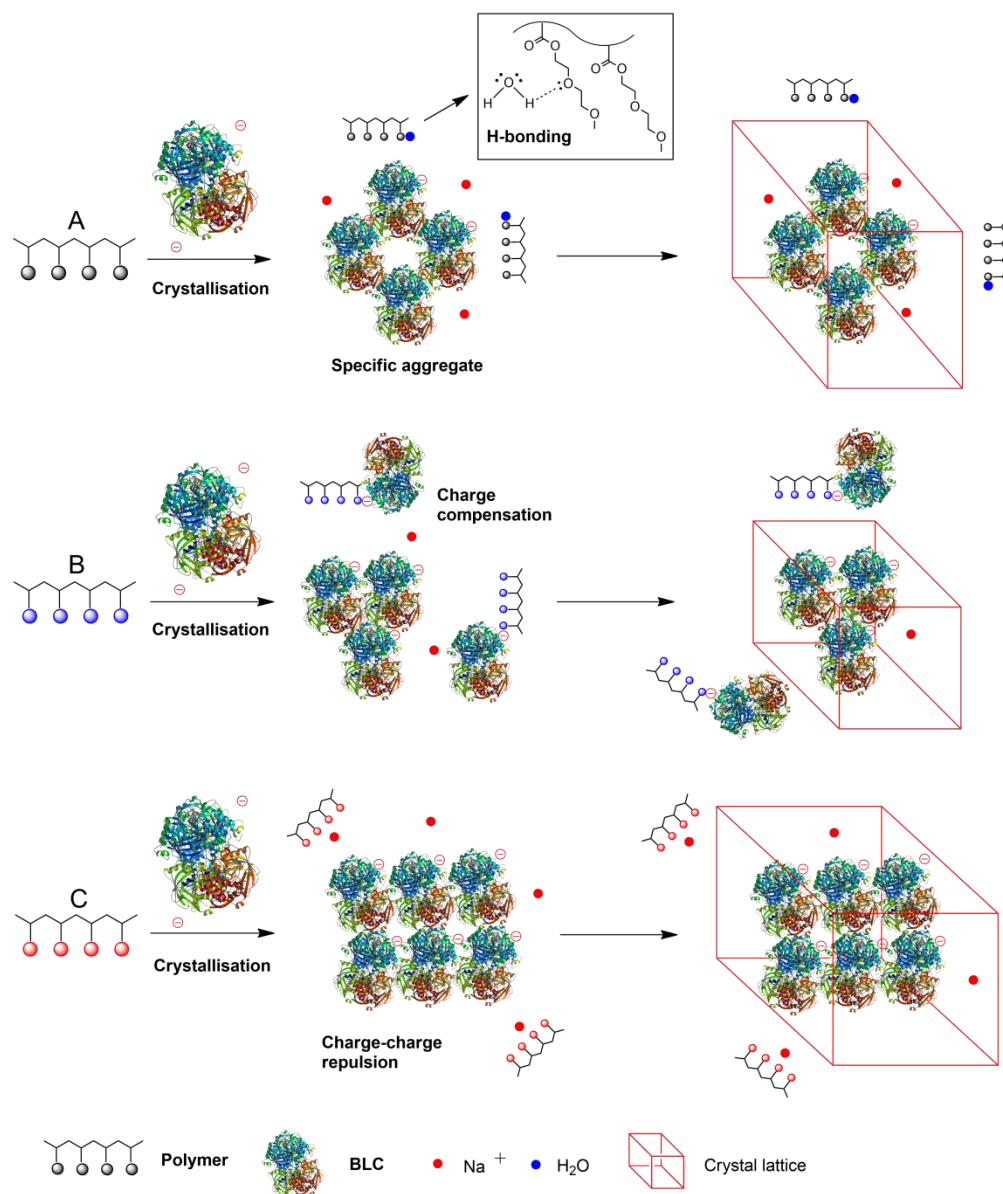


Figure 6-1. Schematic representation of the interaction of various polymers with anionic bovine liver catalase (BLC) in the protein crystallisation process. (A) Neutral polymer: H-bonding with water and thus promoting protein crystallisation via a dehydration mechanism. (B) Cationic polymer: attracting anionic BLC for charge compensation. (C) Anionic polymer: charge-charge repulsions between anionic polymer and anionic BLC. BLC macromolecules are weakly anionic when at crystallisation pH 6.8. Na^+ ions are derived from the crystallisation buffer solutions.

6.2 Methods

6.2.1 Crystallisation technique and plate

BLC was also crystallised using the sitting drop vapour diffusion technique as described in Chapter 4 for HEWL. MRC 2 Well Crystallisation Plates (Swissci) (UVP plate, 96 reservoir wells) were purchased from Hampton Research. Specifically, a solution (50 μL) of tested polymer buffer was pipetted in triplicate in the reservoir wells. Protein solution (1 μL) and buffered polymer solution (as described above, 1 μL) were pipetted into sample wells of the crystallisation plate.

6.2.2 Preparation of polymer solutions and stock buffer solutions

Similar as procedures described in Chapter 4, the stock polymer solution was prepared and adjusted to the BLC crystallisation pH of 6.8. The stock buffer solutions of 12 % PEG 4000 and 0.05 M sodium phosphate buffer at pH 6.8 and 0.05 M sodium phosphate buffer at pH 6.8 were prepared and filtered using a 0.2 μm cellulose acetate membrane filter. By using the above mentioned pH-altered polymer solutions and the stock buffer solutions, the following polymer solutions were prepared: 0.02 %, 0.2 %, 2 %, 4 %, 6 %, 8 %, 10 %, 12 %, 14 %, 16 %, 18 %, 20 %, 22 % and 24 % (w/v) in 12 % PEG 4000 and 0.05 M sodium phosphate buffer at pH 6.8. All polymers dissolved completely in the buffer solutions.

6.2.3 Crystallisation protocol for BLC crystals^{209, 211}

Catalase from bovine liver (BLC) was purchased from Sigma (Product Number: C40, EC Number: 1.11.1.6, CAS Number: 9001-05-2, pI: 5.4). 0.05 M sodium phosphate buffer at pH 6.8 was prepared and filtered through a 0.2 μm cellulose acetate membrane filter. A protein solution of 40 mg/mL BLC was prepared and then centrifuged at 13,000 rpm for 5 min at 4 $^{\circ}\text{C}$.

BLC was crystallised following the sitting drop vapour diffusion procedures, in a similar manner to HEWL crystallisation in Chapter 4, with a BLC solution of 40 mg/mL BLC in 0.05 M sodium phosphate buffer at pH 6.8 and a polymer solution of 12 % PEG 4000 and 0.05 M sodium phosphate buffer at pH 6.8 in the sample well, and 50 μL of tested polymer buffer in the reservoir well.²¹⁰ For control experiments, some reservoir and sample wells contained no polymer. The entire crystallisation plate system was sealed using transparent sealing tape and incubated at 19 $^{\circ}\text{C}$.

6.2.4 Crystal imaging

Optical photomicrographs of BLC crystals were directly collected by a Leica Stereomicroscope (63 x magnifications), with a Leica fan-cooled light source, connected to a Nikon Coolpix 4500 digital camera.

6.2.5 X-ray crystallography

BLC crystallographic parameters were determined by single crystal X-ray

diffraction recorded at room temperature on an X-ray generator with high-flux Osmic confocal multi-layer optics. BLC crystals were cryoprotected with mother liquor containing 30 % ethylene glycol, then flash-frozen in a nitrogen-gas stream.^{99, 210}

6.2.6 DLS studies

Similar to HEWL, the batch crystallisation method was applied for a DLS time study of BLC crystallisation. Because the optimum intensity range for DLS measurement is 300-8000, a protein solution of 20 mg/mL BLC in 0.05 M sodium phosphate buffer at pH 6.8 was mixed with a polymer solution in 12 % PEG 4000 and 0.05 M sodium phosphate buffer at pH 6.8 to induce BLC crystallisation. Three classes of polymers, comprising neutral polymer: p(PEGMA₄₇₅) (P1), cationic polymer: quaternised p(DMAEMA) (P2) (quaternised ratio: 75 %) and anionic polymer: p(AMPS) (P5) (DP 99) were utilised here. Temperature: 19 °C. Crystal growth time: 2 hours.

6.3 Results and discussion

6.3.1 BLC crystallisation in the presence of neutral polymer in solution:

p(PEGMA₄₇₅) (P1)

By using the above mentioned pH-altered stock buffer solution, the following p(PEGMA₄₇₅) (P1) solutions with various concentrations were prepared: 0.02 %, 0.2 %, 2 %, 4 %, 6 %, 8 %, 10 %, 12 % and 14 % (w/v) in 12 % PEG

4000 and 0.05 M sodium phosphate buffer at pH 6.8. Table 6-2 shows BLC crystallisation plate set up and Figure 6-2 shows images of BLC crystals grown from solutions containing neutral p(PEGMA₄₇₅) (P1).

Table 6-2. BLC crystallisation plate set up: p(PEGMA₄₇₅)

	1	2	3	4	5	6	7	8	9
12 % PEG 4000 and 0.05 M sodium phosphate buffer	100 µL (12 % PEG 4000 and 0.05 M sodium phosphate buffer)	100 µL (12 % PEG 4000 and 0.05 M sodium phosphate buffer)	100 µL (12 % PEG 4000 and 0.05 M sodium phosphate buffer)	100 µL (12 % PEG 4000 and 0.05 M sodium phosphate buffer)	100 µL (12 % PEG 4000 and 0.05 M sodium phosphate buffer)	100 µL (12 % PEG 4000 and 0.05 M sodium phosphate buffer)	100 µL (12 % PEG 4000 and 0.05 M sodium phosphate buffer)	100 µL (12 % PEG 4000 and 0.05 M sodium phosphate buffer)	100 µL (12 % PEG 4000 and 0.05 M sodium phosphate buffer)
p(PEGMA ₄₇₅) 37 %	0.1 µL (0.02 %)	1.4 µL (0.2 %)	14 µL (2 %)	27 µL (4 %)	41 µL (6 %)	54 µL (8 %)	68 µL (10 %)	81 µL (12 %)	95 µL (14 %)
H ₂ O	149.9 µL	148.6 µL	136 µL	123 µL	109 µL	96 µL	82 µL	69 µL	55 µL
pH	6.8	6.8	6.8	6.8	6.8	6.8	6.8	6.8	6.8
12 % PEG 4000 and 0.05 M sodium phosphate buffer									
p(PEGMA ₄₇₅) 37 %									
H ₂ O									
pH									
12 % PEG 4000 and 0.05 M sodium phosphate buffer									
p(PEGMA ₄₇₅) 37 %									
H ₂ O									
pH									
12 % PEG 4000 and 0.05 M sodium phosphate buffer	100 µL (12 % PEG 4000 and 0.05 M sodium phosphate buffer)								
p(PEGMA ₄₇₅) 37 %	0 µL								
H ₂ O	150 µL								
pH	6.8								

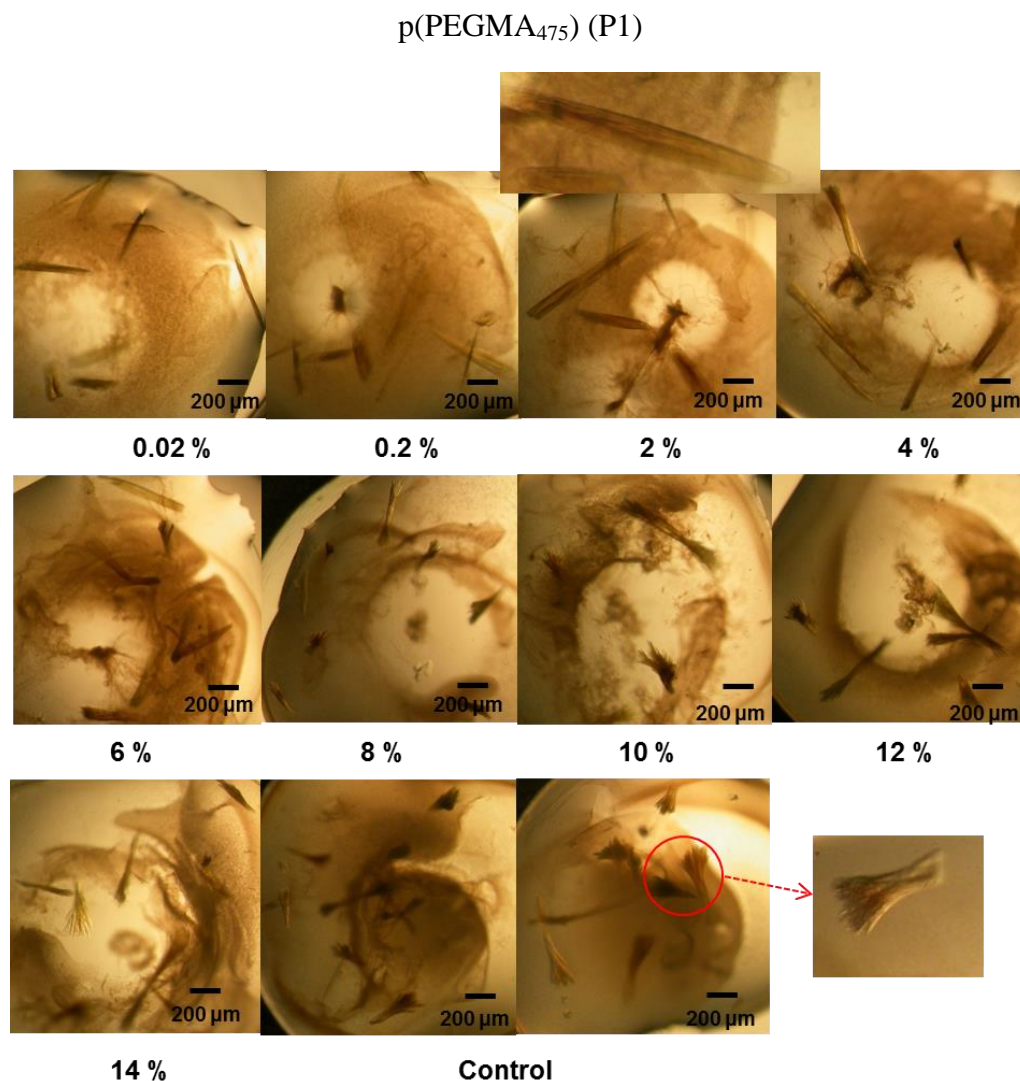


Figure 6-2. Selected photomicrographs of BLC crystals, grown in the presence of p(PEGMA₄₇₅) (P1) at various concentrations. Image labelled ‘Control’ represents BLC crystals grown from sample wells without polymer. The scale bar was 200 μm.

BLC crystal formation in the absence of added polymer occurred after two weeks and resulted in needle crystals outgrowth from a single point in a ‘wheatsheaf’ morphology (Figure 6-2, Control). However, it proved difficult to obtain good quality single crystals without any added polymer. The literature

reports that orthorhombic BLC crystals typically exhibit an extremely high defect density and incorporate great numbers of misoriented microcrystals.²¹⁰

Neutral polymer p(PEGMA₄₇₅) (P1) nucleated a few long crystals at lower concentrations (< 4 %, w/v). However, the quality of these crystals was poor and it was not possible to determine their structure by single crystal X-ray diffraction.

The solutions in the sample wells were not clear enough for fully automated image analysis; therefore, we did both manual and automated analysis. A full summary of BLC crystals size distribution by measuring the average length (μm) of the largest diameter of each crystal and number distribution depending on neutral p(PEGMA₄₇₅) (P1) concentration was obtained by further image analysis (Figure 6-3). For anionic BLC, as the concentration of p(PEGMA₄₇₅) (P1) in solution was increased, the size of crystals increased first. However, as shown in Figure 6-2 above, when the concentration of neutral p(PEGMA₄₇₅) (P1) was above 4 %, ‘wheatsheaf’ shape BLC crystals formed rather than large and thin crystals. As the concentration of p(PEGMA₄₇₅) (P1) was increased, the size of ‘wheatsheaf’ shape BLC crystals decreased slightly.

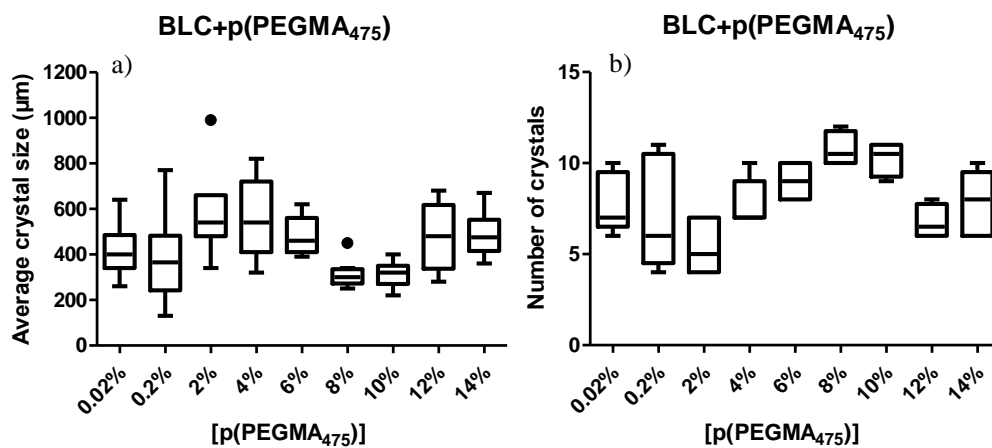


Figure 6-3. Summary of photomicrograph analysis of BLC crystals, grown in the presence of p(PEGMA₄₇₅) (P1) at various concentrations. a) Average length (µm) of the largest crystal diameter. b) Experiment count for the number of crystals per sample well.

For the DLS study, a protein solution of 20 mg/mL BLC in 0.05 M sodium phosphate buffer at pH 6.8 mixed with a polymer solution in 12 % PEG 4000 and 0.05 M sodium phosphate buffer at pH 6.8 was employed, which was then dispensed to a VISCOTEK DLS Quartz cell. The control experiment contained no polymer in the crystallisation solution. Figure 6-4 shows a summary of DLS data of BLC crystallisation under neutral p(PEGMA₄₇₅) (P1) at time points T_0 and $T_{120\text{min}}$. Figure 6-4a shows autocorrelation functions, which were analysed by DLS to obtain the distribution of particle radii, as shown in Figure 6-4b.

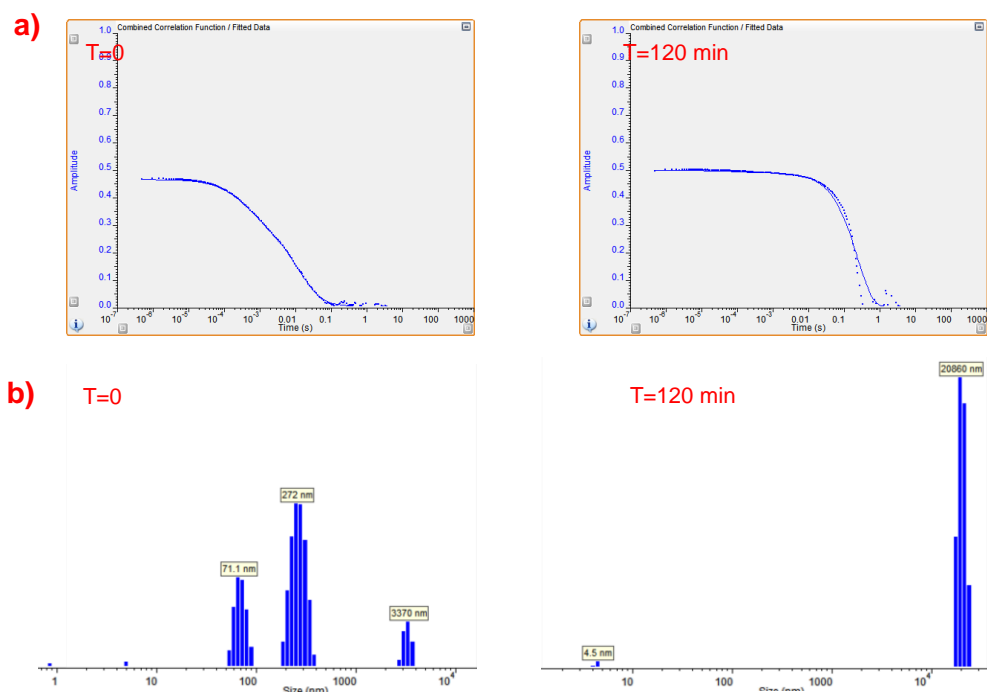


Figure 6-4. Summary of DLS data of BLC crystallisation under neutral p(PEGMA₄₇₅) (P1) at time points T_0 and $T_{120\text{min}}$: a) representative autocorrelation functions; b) radii distribution by intensity.

Figure 6-5 illustrate representative Tukey plots of the above DLS data. The characteristic increase in the size of BLC aggregates can be observed in all cases. At the beginning of the experiment (T_0) under p(PEGMA₄₇₅) (P1), the average size of the particles in the crystallisation solution was around 0.9 μm , measured by size distribution. With the addition of p(PEGMA₄₇₅) (P1), BLC crystallisation initiated and aggregates formed. As the time increased, BLC aggregates grew in size. After 120 minutes ($T_{120\text{min}}$), the average size of the particles in the crystallisation solution was around 2 μm . As a control, the experiment was also carried out without polymer.

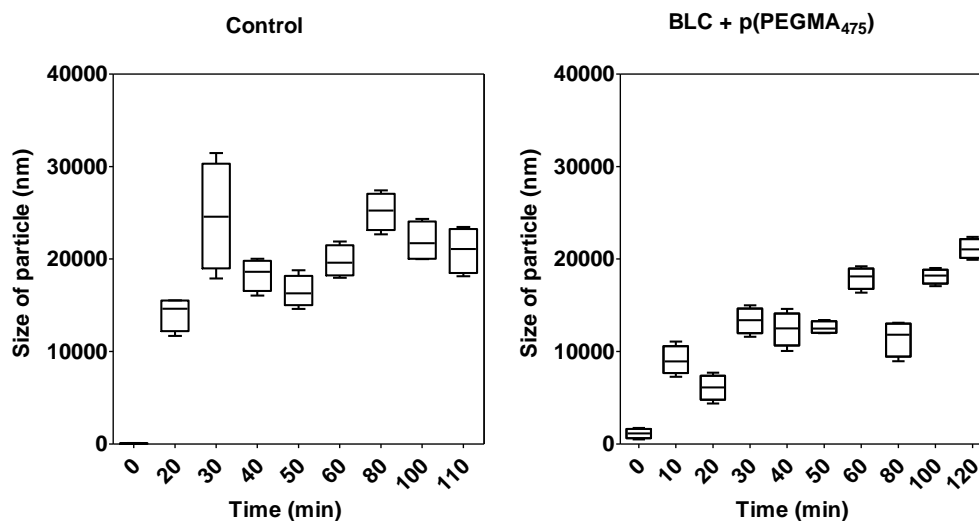


Figure 6-5. Variations of the size of BLC aggregates or crystals in the solution as a function of time during crystallisation experiments induced by neutral p(PEGMA₄₇₅) (P1). Tukey plots labelled ‘Control’ represent crystals grown from solutions without polymer.

The above results suggest that neutral p(PEGMA₄₇₅) (P1) competed with protein solutes for water, and thereby acted as a precipitant to mediate BLC crystallisation, leading to protein aggregation similar to HEWL and Con A (Figure 6-6B).¹²⁵ Therefore, BLC macromolecules were compelled to associate with each other. However, as the concentration of p(PEGMA₄₇₅) (P1) in solution increased, the increased number of nucleation sites caused by the high concentration of precipitant in combination with the increased viscosity of these solutions, promoted the formation of needle crystal outgrowth from a single point in the ‘wheatsheaf’ morphology.²¹⁰

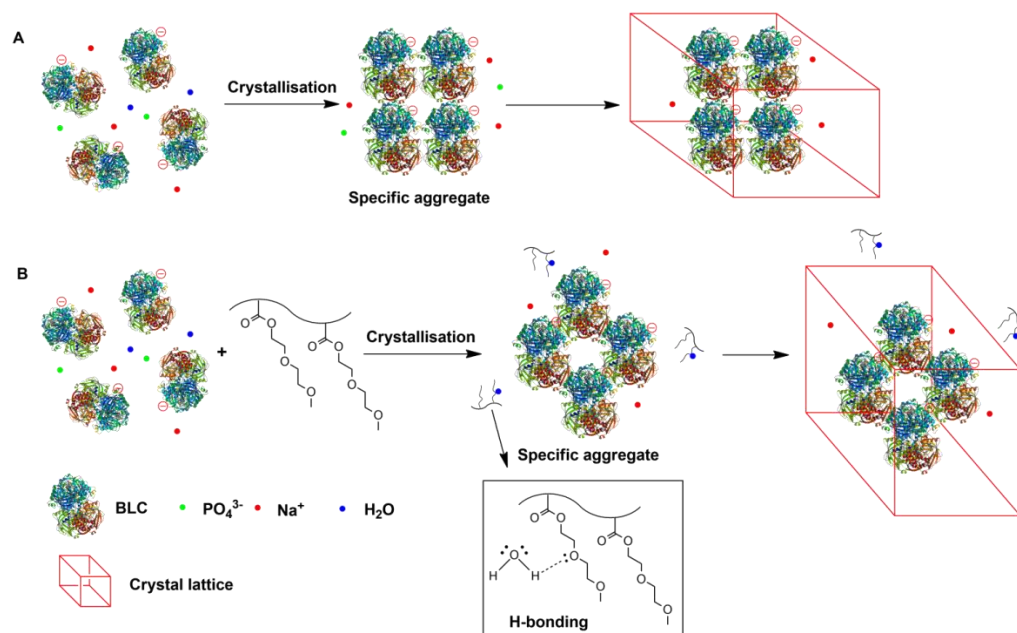


Figure 6-6. Schematic representation of hypothesis of anionic BLC crystallisation process in the absence of polymer (A); and the interaction of neutral p(PEGMA₄₇₅) (P1) with anionic BLC in the protein crystallisation process (B). BLC macromolecules are negatively charged at crystallisation pH of 6.8, i.e. weakly anionic. Na⁺ and PO₄³⁻ ions are from the crystallisation buffer solutions.

6.3.2 BLC crystallisation in the presence of cationic polymer in solution: quaternised p(DMAEMA) (P2)

The following quaternised p(DMAEMA) (P2) (quaternised ratio: 75 %) solutions with various concentration were prepared: 0.02 %, 0.2 %, 2 %, 4 %, 6 %, 8 %, 10 % and 12 % (w/v). Table 6-3 shows BLC crystallisation plate set up and Figure 6-7 shows images of BLC crystals formed in the presence of quaternised p(DMAEMA) (P2).

Table 6-3. BLC crystallisation plate set up: quaternised p(DMAEMA) (P2)

	1	2	3	4	5	6	7	8
12 % PEG 4000 and 0.05 M sodium phosphate buffer	100 µL (12 % PEG 4000 and 0.05 M sodium phosphate buffer)	100 µL (12 % PEG 4000 and 0.05 M sodium phosphate buffer)	100 µL (12 % PEG 4000 and 0.05 M sodium phosphate buffer)	100 µL (12 % PEG 4000 and 0.05 M sodium phosphate buffer)	100 µL (12 % PEG 4000 and 0.05 M sodium phosphate buffer)	100 µL (12 % PEG 4000 and 0.05 M sodium phosphate buffer)	100 µL (12 % PEG 4000 and 0.05 M sodium phosphate buffer)	100 µL (12 % PEG 4000 and 0.05 M sodium phosphate buffer)
Quaternised p(DMAEMA) (75 %)	0.3 µL (0.02 %)	2.5 µL (0.2 %)	25 µL (2 %)	50 µL (4 %)	75 µL (6 %)	100 µL (8 %)	125 µL (10 %)	150 µL (12 %)
H ₂ O	149.7 µL	147.5 µL	125 µL	100 µL	75 µL	50 µL	25 µL	0 µL
pH	6.8	6.8	6.8	6.8	6.8	6.8	6.8	6.8
12 % PEG 4000 and 0.05 M sodium phosphate buffer	↓	↓	↓	↓	↓	↓	↓	↓
Quaternised p(DMAEMA) (75 %)								
H ₂ O								
pH								
12 % PEG 4000 and 0.05 M sodium phosphate buffer	↓	↓	↓	↓	↓	↓	↓	↓
Quaternised p(DMAEMA) (75 %)								
H ₂ O								
pH								
12 % PEG 4000 and 0.05 M sodium phosphate buffer	↑	↑	↑	↑	↑	↑	↑	↑
Quaternised p(DMAEMA) (75 %)								
H ₂ O	100 µL (12 % PEG 4000 and 0.05 M sodium phosphate buffer)	0 µL						
pH	150 µL	6.8						

Quaternised p(DMAEMA) (P2)

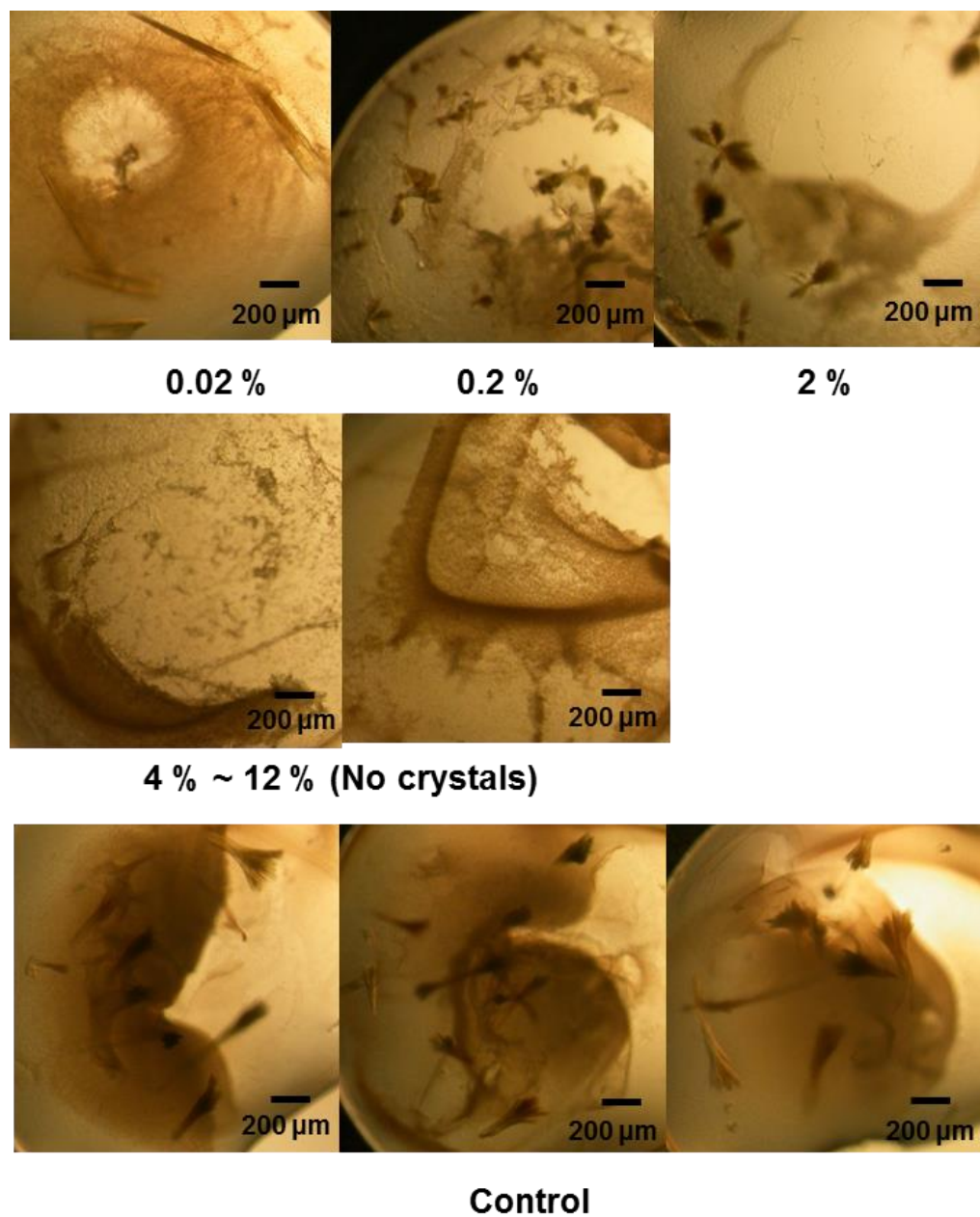


Figure 6-7. Photomicrographs of BLC crystals, grown in the presence of quaternised p(DMAEMA) (P2) at various concentrations. Images labelled 'Control' represent crystals grown from sample wells without polymer. The scale bar was 200 μm.

From visual inspection of Figure 6-7, when cationic quaternised p(DMAEMA) (P2) was utilised, long and thin crystals were formed at concentration of 0.02 % (w/v). A few needles with a ‘sea-urchin’ morphology formed at lower concentrations (0.2 % ~ 2 %, w/v). However, as the concentration of cationic quaternised p(DMAEMA) (P2) in solution increased, it was hard to get BLC crystals, almost no BLC crystals were formed by using cationic quaternised p(DMAEMA) (P2) at higher concentrations. There may be several reasons. First, BLC was not easy to crystallise by using orthorhombic $P2_12_12_1$ crystallisation condition because orthorhombic BLC growth mechanism was complicated.²¹⁰ Moreover, at pH 8.5, cationic quaternised p(DMAEMA) (P2) might favor attracting anionic BLC macromolecules by electrostatic interaction, resulting in the suppression of BLC crystallisation. Thus, insufficient BLC macromolecules could aggregate together and form nuclei.

Figure 6-8 shows a summary of DLS data of BLC crystallisation from solution containing cationic quaternised p(DMAEMA) (P2) at time points T_0 and $T_{120\text{min}}$. Moreover, representative Tukey plots of DLS data are shown in Figure 6-9. An increase in size of BLC aggregates was observed during the crystallisation experiments. At the beginning of the experiment (T_0), the average size of the particles in the crystallisation solution was around 400 nm, measured by size distribution. With the addition of quaternised p(DMAEMA) (P2), BLC aggregates grew in size. After 120 minutes ($T_{120\text{min}}$), the average size of the particles in crystallisation solution was around 8000 nm.

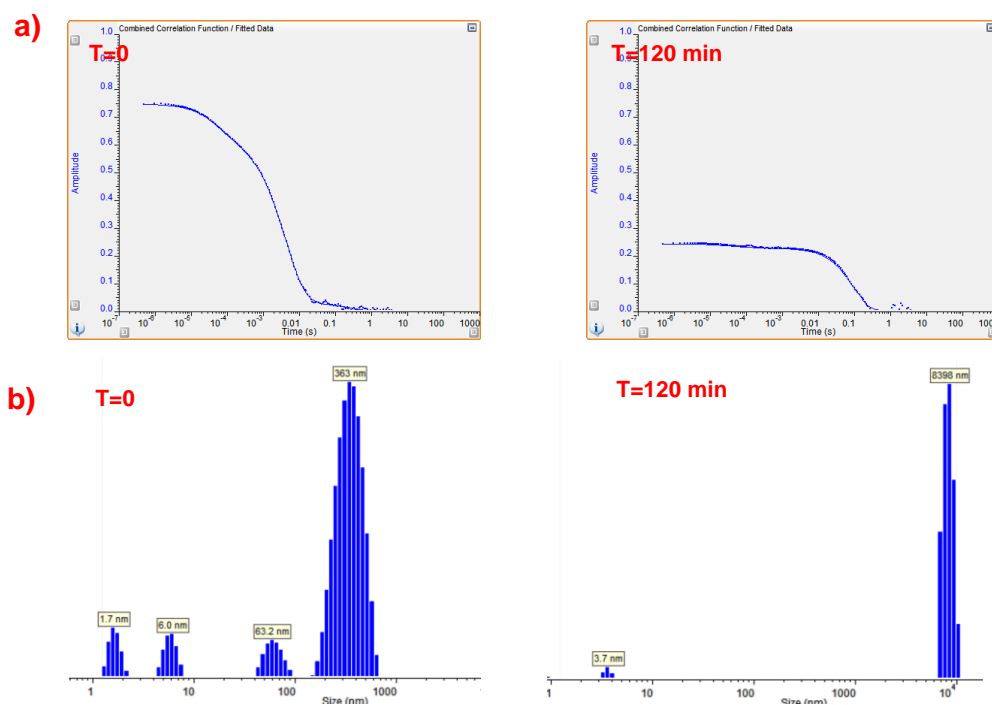


Figure 6-8. Summary of DLS data of BLC crystallisation under cationic quaternised p(DMAEMA) (P2) at time points T_0 and $T_{120\text{min}}$: a) representative autocorrelation functions; b) radii distribution by intensity.

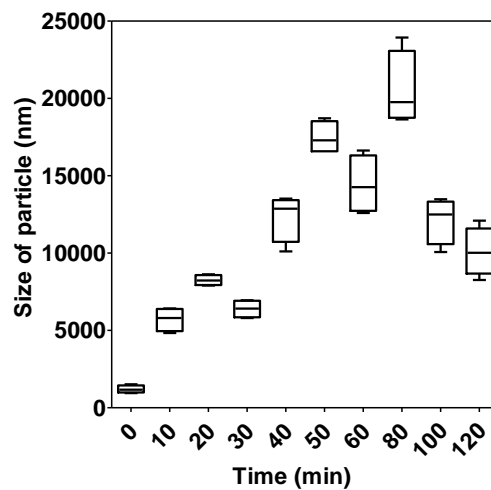


Figure 6-9. Variations of the size of BLC aggregates or crystals in the solution as a function of time during crystallisation experiments induced by cationic quaternised p(DMAEMA) (P2).

**6.3.3 BLC crystallisation in the presence of anionic polymer in solution:
p(AMPS) (P5)**

The following p(AMPS) (P5) solutions with various concentrations were prepared: 0.02 %, 0.2 %, 2 %, 4 %, 6 %, 8 %, 10 %, 12 %, 14 % and 16 % (w/v) in 12 % PEG 4000 and 0.05 M sodium phosphate buffer at pH 6.8 (Table 6-4).

Table 6-4. BLC crystallisation plate set up: p(AMPS) (P5) (DP 99)

	1	2	3	4	5	6	7	8	9	10
12 % PEG 4000 and 0.05 M sodium phosphate buffer	100 µL (12 % PEG 4000 and 0.05 M sodium phosphate buffer)	100 µL (12 % PEG 4000 and 0.05 M sodium phosphate buffer)	100 µL (12 % PEG 4000 and 0.05 M sodium phosphate buffer)	100 µL (12 % PEG 4000 and 0.05 M sodium phosphate buffer)	100 µL (12 % PEG 4000 and 0.05 M sodium phosphate buffer)	100 µL (12 % PEG 4000 and 0.05 M sodium phosphate buffer)	100 µL (12 % PEG 4000 and 0.05 M sodium phosphate buffer)	100 µL (12 % PEG 4000 and 0.05 M sodium phosphate buffer)	100 µL (12 % PEG 4000 and 0.05 M sodium phosphate buffer)	100 µL (12 % PEG 4000 and 0.05 M sodium phosphate buffer)
p(AMPS)(DP 99)	0.1 µL (0.02 %)	1.3 µL (0.2 %)	13 µL (2 %)	26 µL (4 %)	39 µL (6 %)	52 µL (8 %)	65 µL (10 %)	78 µL (12 %)	91 µL (14 %)	104 µL (16 %)
H ₂ O	149.9 µL	148.7 µL	137 µL	124 µL	111 µL	98 µL	85 µL	72 µL	59 µL	46 µL
pH	6.8	6.8	6.8	6.8	6.8	6.8	6.8	6.8	6.8	6.8
12 % PEG 4000 and 0.05 M sodium phosphate buffer										
p(AMPS)(DP 99)										
H ₂ O										
pH										
12 % PEG 4000 and 0.05 M sodium phosphate buffer										
p(AMPS)(DP 99)										
H ₂ O										
pH										
12 % PEG 4000 and 0.05 M sodium phosphate buffer										
p(AMPS)(DP 99)										
H ₂ O										
pH										

Figure 6-10 shows photomicrographs of BLC crystals formed in the presence of p(AMPS) (P5). When p(AMPS) (P5) was used for BLC crystallisation, the size and shape of BLC crystals were found to vary very clearly. Anionic p(AMPS) (P5) promoted BLC aggregation, with single crystals being obtained in 10 days.

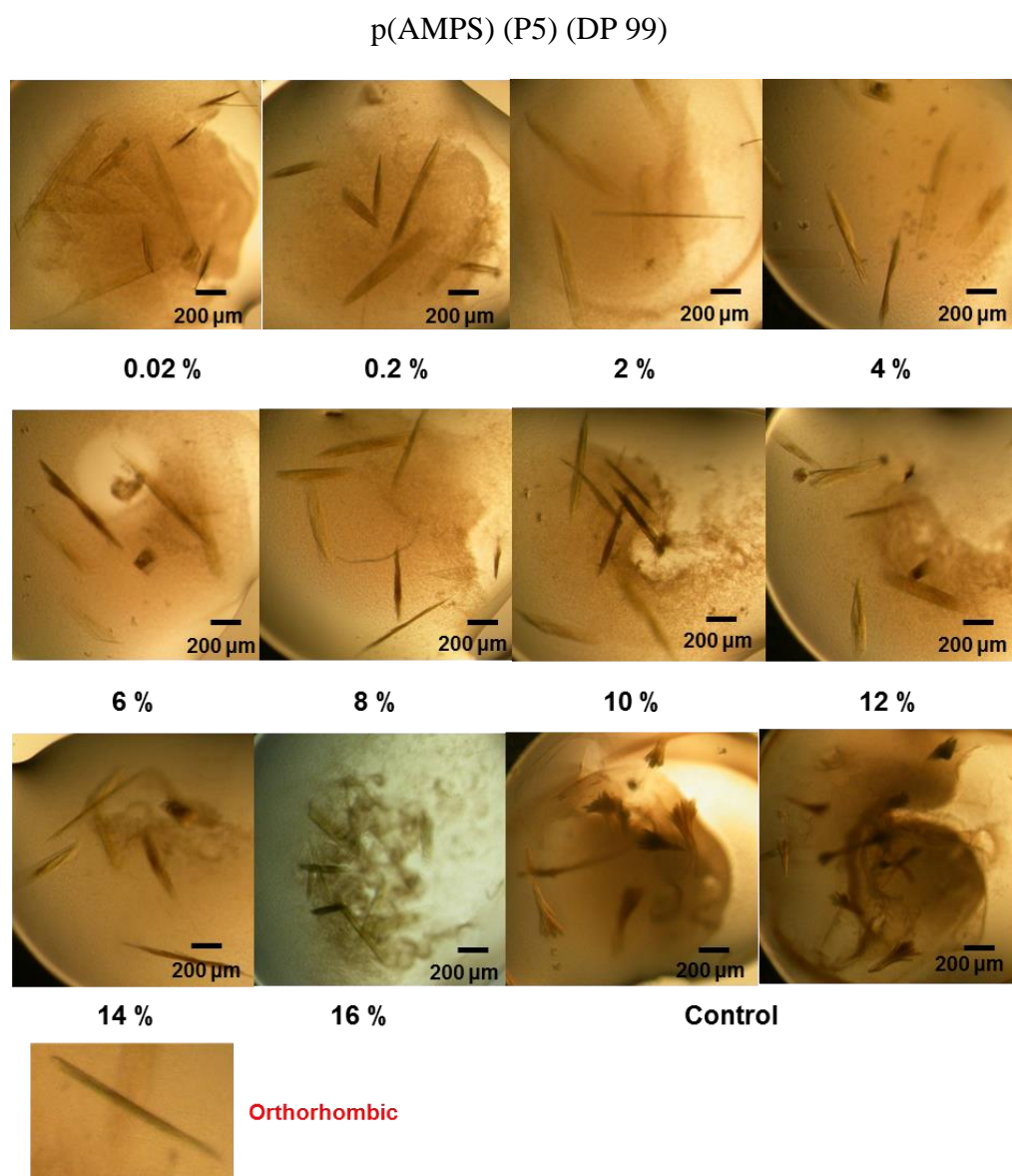


Figure 6-10. Photomicrographs of BLC crystals formed in the presence of p(AMPS) (P5) at various concentrations. Images labelled ‘Control’ represent crystals grown from sample wells without polymer. The scale bar was 200 μm.

Figure 6-11 shows image analysis of BLC crystals size distribution by measuring the average length (μm) of the largest diameter of each crystal and number distribution depending on anionic p(AMPS) (P5) concentration. For weakly anionic BLC, as the concentration of p(AMPS) (P5) in solution was increased, the number of BLC crystals appeared to increase and the size of the crystals appeared to decrease slightly.

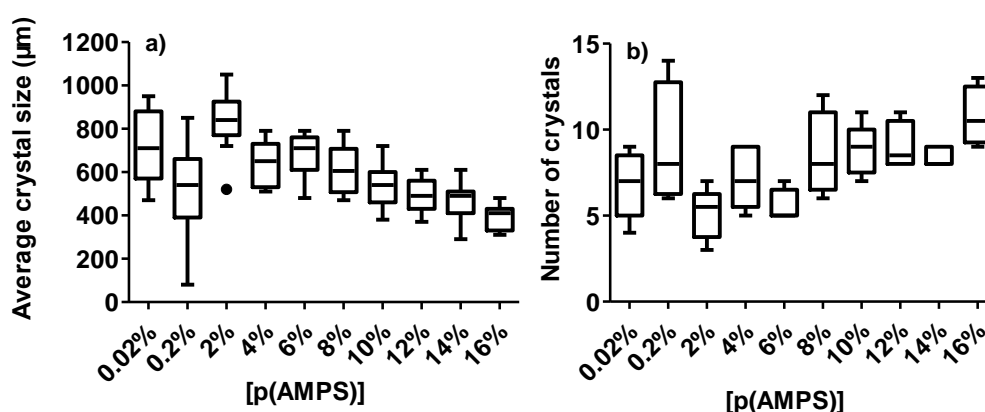


Figure 6-11. Summary of photomicrograph analysis of BLC crystals, grown in the presence of p(AMPS) (P5) at various concentrations. a) Average length (μm) of the largest crystal diameter; b) Experiment count for the number of crystals per sample well.

Figure 6-12 illustrates the diffraction patterns of BLC crystal formed in the presence of anionic p(AMPS) (P5) by X-ray crystallography. X-ray diffraction identified the crystal form was orthorhombic (space group: $P2_12_12_1$, form III) (Table 6-5). BLC crystals of form III reported previously were extremely thin ($< 1 \mu\text{m}$) and hard to characterise fully using single crystal X-ray diffraction.²³¹

Furthermore, BLC form III has rarely been studied; thus the use of polymers as

solution additives might be useful in further BLC crystal characterisation.

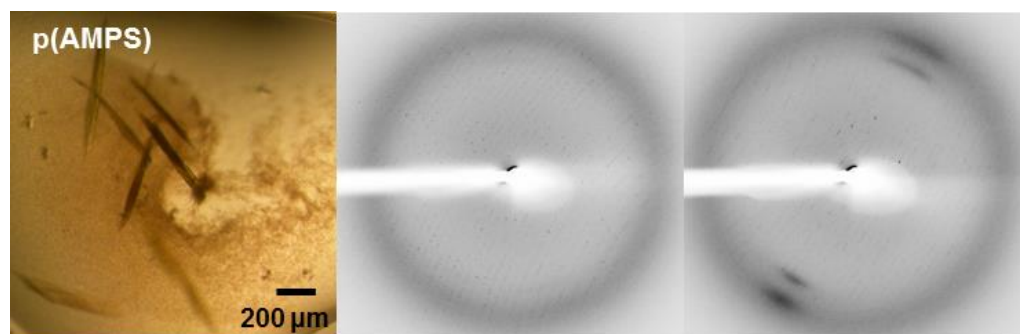


Figure 6-12. BLC crystal photomicrograph and X-ray diffraction patterns yielded by the single BLC crystal in the presence of anionic p(AMPS) (P5).

Two scattering angles: 0 ± 1 degrees and 90 ± 1 degrees.

Table 6-5. Diffraction data collection for BLC crystal

	BLC form III
Space group	$P2_12_12_1$
Unit cell lattice	Orthorhombic
Cell dimensions: a, b, c (Å)	69.3, 174.1, 191.5
α , β , γ	90° , 90° , 90°
Resolution (Å)	50-2.8
Crystal-to-detector distance	170 mm

Figure 6-13 shows a summary of DLS data of BLC crystallisation under anionic p(AMPS) (P5) at time points T_0 and $T_{120\text{min}}$. Figure 6-13a shows autocorrelation functions, which were analysed by DLS to obtain the distribution of particle radii, as shown in Figure 6-13b.

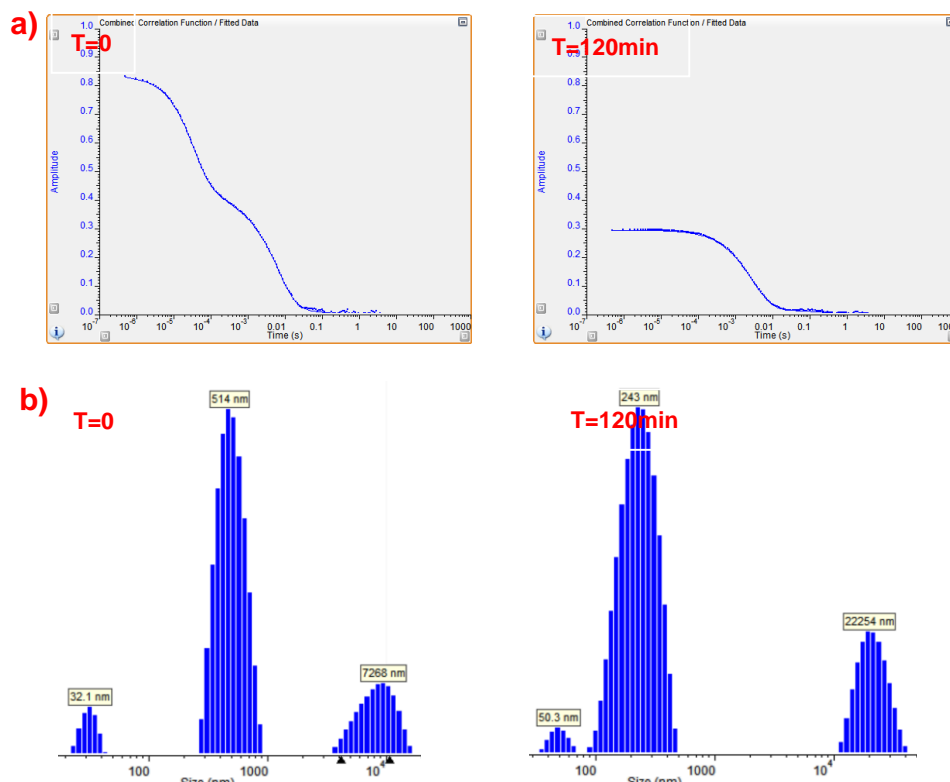


Figure 6-13. Summary of DLS data of BLC crystallisation under anionic p(AMPS) (P5) at time points T_0 and $T_{120\text{min}}$: a) representative autocorrelation functions; b) radii distribution by intensity.

Furthermore, representative Tukey plots of above DLS data are shown in Figure 6-14. At the beginning of the experiment (T_0), the average size of the particles in the crystallisation solution was around $1.5 \mu\text{m}$, measured by size distribution. With the addition of anionic p(AMPS) (P5), BLC aggregates grew in size. After 120 minutes ($T_{120\text{min}}$), the average size of the particles in the crystallisation solution was around $5 \mu\text{m}$.

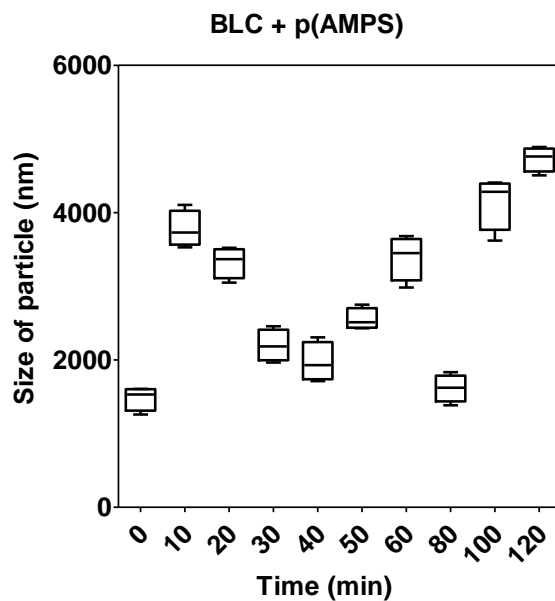


Figure 6-14. Variations of the size of BLC aggregates or crystals in the solution as a function of time during crystallisation experiments induced by anionic p(AMPS) (P5).

Figure 6-15 illustrates the proposed mechanism of anionic polymer mediated BLC crystallisation. Similar to Con A, at BLC crystallisation pH of 6.8, anionic p(AMPS) (P5) molecules had some negative charges. There were expected to be ‘charge-charge’ repulsions between anionic polymer molecules and anionic BLC macromolecules, thus, anionic polymer lowered the interfacial energy between BLC macromolecules and water, leading to the promotion of BLC nucleation rate.^{226, 108}

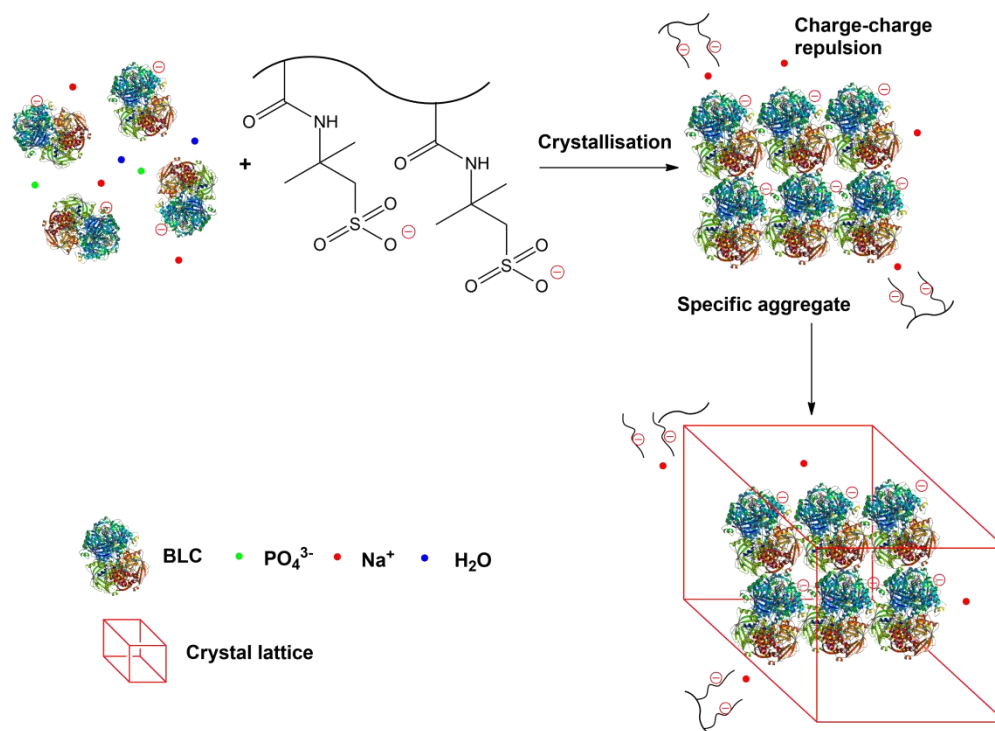


Figure 6-15. Hypothesis of mechanism of anionic polymer mediated BLC crystallisation. Anionic polymer: charge-charge repulsions between anionic polymer and anionic BLC. BLC macromolecules are weakly anionic when at crystallisation pH 6.8. Na^+ and PO_4^{3-} ions come from the crystallisation buffer solutions.

6.4 Conclusions

In this chapter, similar to Con A, three key polymers with varying degrees of charge were selected from each class and utilised as solution additives for BLC crystallisation: neutral p(PEGMA₄₇₅) (P1), cationic quaternised p(DMAEMA) (P2) with quaternised ratio: 75 % and anionic p(AMPS) (P5). BLC crystallisation experiments were also performed on 96-well plates using the sitting drop vapour diffusion technique.

The isoelectric point (pI) of BLC is 5.4 therefore at its crystallisation pH of 6.8 BLC is a weakly anionic protein. BLC crystal formation in the absence of added polymers occurred after two weeks and resulted in needle crystals outgrowth in a 'wheatsheaf' morphology. Neutral p(PEGMA₄₇₅) (P1) nucleated a few long crystals at lower concentrations (< 4 %, w/v). However, it was not possible to determine their structure by single crystal X-ray diffraction. When cationic quaternised p(DMAEMA) (P2) was utilised, a few needles with a 'sea-urchin' morphology formed at lower concentrations (< 2 %, w/v). However, as the concentration of quaternised p(DMAEMA) (P2) in solution increased, suppression of BLC crystallisation occurred. By contrast, anionic polymers promoted BLC aggregation, with single crystals being obtained in 10 days. X-ray diffraction identified these crystals as orthorhombic (space group: $P2_12_12_1$, form III). These results illustrate that polymers can nucleate protein crystals produce diffraction-quality single crystals, which makes structural elucidation possible.

CHAPTER 7

7. Discussion, Conclusions and Future Work

7.1 Discussion and conclusions

Protein assemblies, either in the form of crystals or supramolecular nanoparticles, are important in areas ranging from basic biochemical research through to pharmaceutical application. In addition to characterisation purposes,^{3,5} there are other applications where defined assemblies of proteins, either crystals or self-assembled protein nanoparticles are desirable, including industrial biocatalysis⁹ and therapeutic protein formulations.^{25,28} The ability to prepare a given crystal or self-assembled structure from protein molecules, however, remains extremely challenging. A variety of approaches have been used to aid the production of protein crystals; the most common involves the addition of nucleants, or surface-active materials into the crystallisation solution.⁷⁰ Synthetic polymers are important additives for protein crystallisation control as there are many possible chemistries which can be introduced into the backbone and side-chains, giving a very wide range of functional behaviour.^{5, 100, 101} Proteins have become particular targets for polymer-mediated crystallisation in recent years owing to their growing importance in pharmaceutical applications. Soluble polymeric additives can influence the biomolecule crystallisation process leading to changes in size, habit and even polymorph of the final crystals.⁷¹ Literature reviews in Chapter

I introduced previous studies of synthetic polymers used as solution additives for the control of crystallisation. Although tremendous efforts have been made, only a very few functional polymers have been studied as additives in protein crystallisation. There are many factors which can affect crystallisation, the majority of which are still poorly understood. Moreover, the mechanisms governing the interactions between polymer additives and emerging protein assemblies are elusive and need to be further confirmed.

The work presented in this thesis has concentrated on the application of polymers as ‘additives’ into the protein solution, i.e. dissolved polymers in the solution to mediate proteins crystallisation. In order to probe some of the factors involved in polymer-mediated protein crystallisation, we set out to prepare different classes of polymers with varying degrees of charge, molecular weight and backbone structure, and then to study their roles as additives in model protein solutions. The guiding hypothesis was that specific functional polymers in solution could alter the rate of protein crystallisation from solutions, and thereby influence the shape, size, and/or polymorph of the resultant crystals.

Four classes of materials were investigated for their effects on protein crystallisation studies: neutral, cationic, anionic and cationic/zwitterionic polymers. We chose poly(ethylene glycol) methyl ether methacrylate₄₇₅ (PEGMA₄₇₅), as a neutral methacrylate derivative of PEG to obtain a polymer, p(PEGMA₄₇₅), analogous to PEG but with hydrophilic side-chain functionality

and a hydrophobic main-chain. Two monomers containing tertiary amines groups were selected to afford positive charges, including one methacrylate monomer 2-(dimethylamino)ethyl methacrylate (DMAEMA) which was either homopolymerised or copolymerised with PEGMA₄₇₅, and one methacrylamide monomer N-(3-(dimethylamido)propyl)methacrylamide (DMAPMAM), which was also homopolymerised to form cationic polymers. Three acrylamide-based main chain monomers, including 2-acrylamido-2-methyl-1-propanesulfonic acid (AMPS), 2-acrylamidoacetic acid (2-AmAA) and 4-acrylamidobutanoic acid (4-AmBA), which have ionisable sulfonic acid or carboxyl groups, were selected to generate anionic water soluble homopolymers. Moreover, a cationic/zwitterionic copolymer of [2-(methacryloyloxy)ethyl]trimethylammonium chloride (METMAC) and N-[2-(methacryloyloxy)ethyl]-dimethyl-(2-sulfoethan)aminium hydroxide (MEDSAH) with both positive charges and zwitterionic components was prepared in order to span an even wider range of charge-charge interactions.

P(PEGMA₄₇₅) (P1), p(DMAEMA) (P2), and p(DMAEMA-*stat*-PEGMA₄₇₅) (P3) were prepared via ATRP routes.¹⁴³ N-Methylation of p(DMAEMA) with different degrees of quaternisation was carried out to vary the total permanent cation content.^{199, 200} P(DMAPMAM) (P4), p(AMPS) (P5), p(2-AmAA) (P6) and p(4-AmBA) (P7) were synthesised using RAFT methods.²⁰² A cationic/zwitterionic copolymer of p(METMAC-*co*-MEDSAH) (P8) was prepared at a METMAC:MEDSAH molar ratio of 1:1. Polymers with different

charge, molecular weight and backbone structure were prepared in good yields. Three model proteins crystallisation systems were studied here: hen egg white lysozyme (HEWL); concanavalin A (Con A); and bovine liver catalase (BLC). A simple model linking polymer charge to protein pI and crystallisation rate was proposed. Crystallisation experiments were performed on 96-well plates, by using the sitting drop vapour diffusion technique.

The first study was carried out on HEWL crystallisation. Figure 7-1 presents selected optical photomicrographs of HEWL crystals grown utilising different polymers as additives in the crystallisation process. The pI of HEWL is 11.35, therefore when at its crystallisation pH 4.8, HEWL macromolecules are positively charged, i.e. cationic. HEWL crystallisation under conditions favouring the tetragonal form resulted in exclusively tetragonal crystals within 1-2 days without any polymer (Figure 7-1, Control). When in the presence of polymers, most of the HEWL crystals were readily identified by their distinctive morphology as tetragonal. However, different polymers have clearly influenced the results of the crystallisation experiments, especially the crystal morphology.

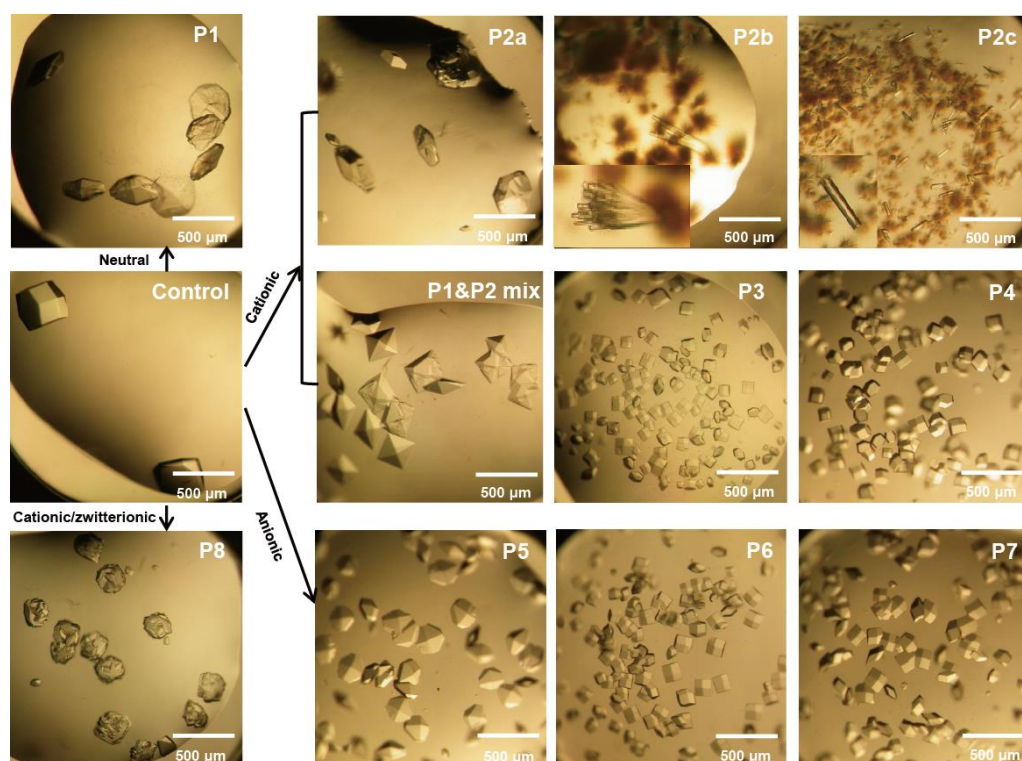


Figure 7-1. Selected optical photomicrographs of HEWL crystals formed under conditions of tetragonal crystal-inducing protocol, in the presence of neutral, cationic, anionic and cationic/zwitterionic polymers as solutes in the crystallisation solutions. Image labelled ‘Control’ represents crystals grown from sample wells without polymer. Neutral polymer: P1. Cationic polymers: P2-4. P2a: 0.02 % w/v p(DMAEMA), P2b: 2 % w/v p(DMAEMA), P2c: 12 % w/v p(DMAEMA). Anionic polymers: P5-7, P6 and P7 were weakly anionic at pH 4.8. Cationic/zwitterionic polymer: P8.

Neutral p(PEGMA₄₇₅) (P1) nucleated a few large HEWL tetragonal crystals (Figure 7-1, P1). It was expected that p(PEGMA₄₇₅), as a neutral methacrylate derivative of PEG and an H-bond acceptor, might compete with protein solutes for water and thus promote protein crystallisation via a dehydration

mechanism (Figure 7-2, A).¹²⁵ Moreover, p(PEGMA₄₇₅) may have ‘volume-excluded effects’ by hydrophobic exclusion of protein solutes.²²⁴

Neutral polymers of this type could also reduce the dielectric constant of the crystallisation solution, leading to an increase of the effective distance over which protein electrostatic effects would take place,²²⁵ consequently protein aggregation and phase separation was promoted.¹⁰⁸ In turn, HEWL macromolecules may have been more able to associate with each other.

Cationic polymers had an increased propensity for nucleating many small crystals (Figure 7-1, P2c, P3 and P4). In Figure 7-1, P2a-c show the images of HEWL crystals obtained using quaternised p(DMAEMA) at three different concentrations. The HEWL crystal form was tetragonal when crystallised from 0.02 % (w/v) quaternised p(DMAEMA) (Figure 7-1, P2a). Upon increasing the concentration to above 2 % (w/v), the HEWL crystal form was clearly different from a typical tetragonal character (Figure 7-1, P2b). Instead of tetragonal, two other forms of HEWL crystals, including needles and monoclinic crystals were obtained, when crystallised from otherwise identical solutions in the presence of 12 % (w/v) quaternised p(DMAEMA) (Figure 7-1, P2c). Moreover, quaternised p(DMAEMA) mediated-HEWL crystallisation followed a general trend, with tetragonal crystals forming at lower concentrations of polymer and monoclinic crystals & needle forming at higher polymer concentrations. Addition of quaternised p(DMAEMA) into HEWL solution, which exhibited a high cationic charge density, was expected to alter the electrostatic interactions

between HEWL molecules and the solution.^{118, 100} Cationic p((DMAEMA)-*stat*-PEGMA₄₇₅) (P3) and p(DMAPMAm) (P4) nucleated many uniform and small tetragonal HEWL crystals with the sizes around 100 μm within one day (Figure 7-1, P3 and P4). There were likely to have been charge-charge repulsions between cationic polymers molecules and cationic HEWL macromolecules, lowering the interfacial energy between HEWL macromolecules and water, thus promoting protein-protein interactions at hydrophobic sites or anionic-cationic pair sites and subsequent crystallisation (Figure 7-2, B). In addition, cationic polymers might have bound to anionic residues on the HEWL chain leading to charge compensation by electrostatic interaction,¹⁰⁸ an increase of local concentration of HEWL macromolecules and the promotion of nucleation. Mixed polymers solutions of p(DMAEMA) and p(PEGMA₄₇₅) (molar ratio 1:9) were also applied for HEWL crystallisation to compare the effects with P3 and formed a few large tetragonal crystals with sizes of $\sim 300 \mu\text{m}$, implying the influence of the neutral p(PEGMA₄₇₅) section was dominant in the crystallisation process (Figure 7-1, P1 & P2 mix).

The influence of anionic polymers on HEWL crystallisation was less than that of the cationic polymers regarding crystal shape, but the anionic polymers did alter the size of HEWL crystals (Figure 7-1, P5-7). Anionic p(AMPS) nucleated a few large crystals with mean size around 300 μm (Figure 7-1, P5). However, smaller HEWL crystals were obtained when p(2-AmAA) and p(4-AmBA) were added (Figure 7-1, P6 and P7). This was likely a

consequence of the crystallisation pH of HEWL being close (pH 4.8) to the expected pKa values of p(2-AmAA) and p(4-AmBA), and thus a smaller number of anionic carboxyl groups remaining on these polymers compared to the cationic polymers at the same pH. The HEWL crystals formed in the presence of anionic polymers were identified as tetragonal by single crystal X-ray diffraction. Anionic polymers might favor attracting cationic HEWL macromolecules for charge compensation by electrostatic interaction (Figure 7-2, C),¹⁰⁸ thus, they would either lower the protein and water interfacial energy and act as nucleation centers by the absorption of HEWL macromolecules, or slow down the rate of further growth. Therefore, they acted as not only nucleators in solution but also as inhibitors.¹⁰⁰

Cationic and zwitterionic sulfobetaine p(METMAC-*co*-MEDSAH) nucleated a few crystals with complex shape (Figure 7-1, P8). The combined cationic/zwitterionic copolymer was expected to have a variety of functions during HEWL crystallisation (Figure 7-2, D). One expected action was complexation with HEWL macromolecules, leading to charge compensation and promotion of nucleation. After nucleation, this polymer also might absorb on certain faces of crystals and influence the direction of crystal further growth.¹⁰⁰ From a first principles hypothesis, the HEWL crystals would thus be expected to be of different shape when crystallised with zwitterionic polymers compared to the purely cationic; however, the crystal form was still tetragonal.

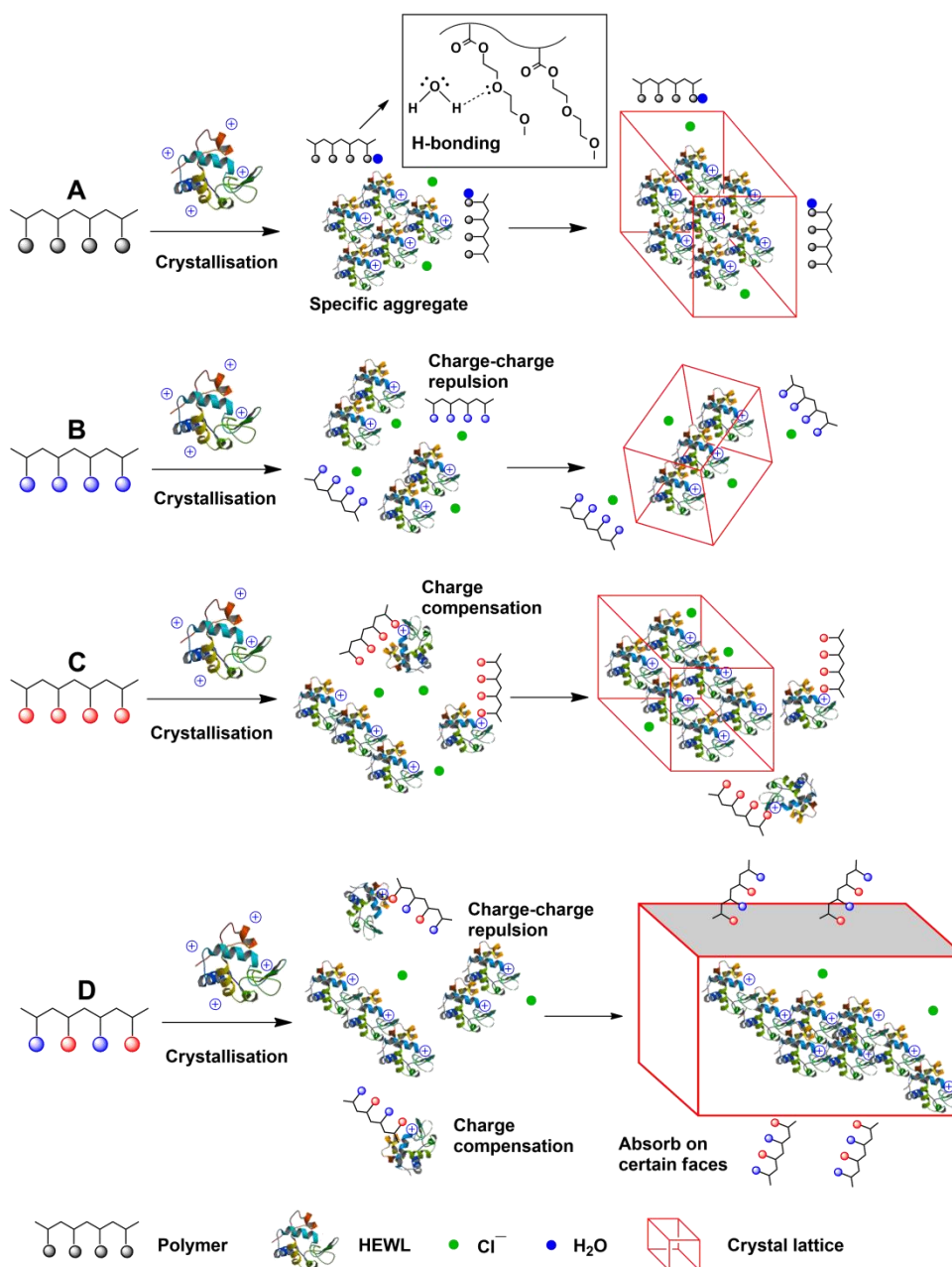


Figure 7-2. Schematic representation of the interaction of various polymers with cationic HEWL in the protein crystallisation process. (A) Neutral polymer: H-bonding with water and thus promoting protein crystallisation via a dehydration mechanism. (B) Cationic polymer: charge-charge repulsions between cationic polymer and cationic HEWL. (C) Anionic polymer: binding cationic HEWL for charge compensation. (D) Cationic/zwitterionic polymer: have a variety of functions during HEWL crystallisation. HEWL macromolecules are positively charged at tetragonal crystallisation pH of 4.8.

To investigate further the influence of these polymers on protein crystallisation, we selected representative polymers from each class and carried out crystallisation assays with a range of polymer concentrations. Figure 7-3 outlines a summary evaluation of HEWL crystal size distribution, which was obtained by measuring the average length (μm) of the largest diameter of each crystal at each polymer concentration using ImageJ software. There was a clear effect on HEWL crystallisation depending on the concentration of polymer. For HEWL (cationic at crystallisation pH), as the concentration of neutral polymer in solution was increased, the size of crystals increased (Figure 7-3, P1). However, the size of HEWL crystals decreased when the concentration of cationic polymer was increased (Figure 7-3, P2-4). A slight increase in average size of HEWL crystals formed was observed when anionic polymer concentration increased (Figure 7-3, P5-7). Perhaps surprisingly, the hybrid cationic/zwitterionic copolymer P8 caused a slight increase in crystal size, suggesting perhaps a greater role for the pendant sulfonate anions at the side-chain termini than the trimethylammonium headgroups on the co-monomer (Figure 7-3, P8). At lower concentrations, polymers may have served as nucleation centres via bridging interactions to promote nucleation, whereas when the concentration was increased, it is possible that charged polymers could stabilise or coat emergent small protein aggregates and inhibit further growth of crystals,^{100, 234} and that multiple mechanisms can be involved. Indeed, the influence of polymers in protein crystallisation has been suggested

to include the stages before nucleation, as well as initial nucleation and subsequent crystal growth.¹⁰⁰ Therefore, in addition to the chemical functionality of polymers, it is likely that the concentration of polymers can play significant roles in modifying the protein crystallisation process.

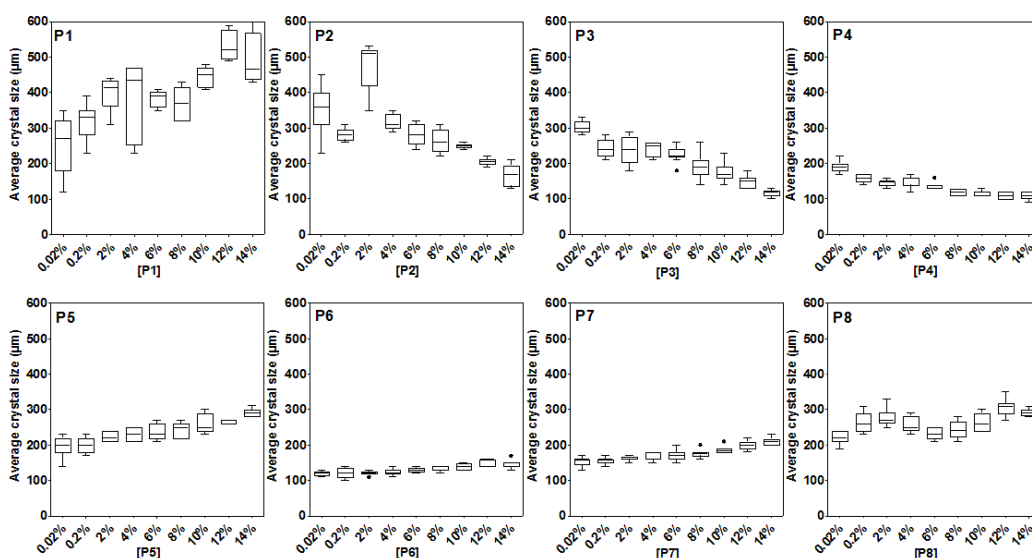


Figure 7-3. Summary of photomicrograph analysis showing changes in the size of HEWL crystals, grown in the presence of different classes of polymers at various concentrations. Neutral polymer: P1; cationic polymers: P2-4; anionic polymers: P5-7, P6 and P7 were weakly anionic at pH 4.8. Cationic/zwitterionic polymer: P8

The second model protein investigated was Con A. The pI of Con A is 4.5, but crystallisation of this protein is normally carried out at pH 8.5, at which point Con A molecules are negatively charged overall. Three polymers were then selected from each class for further experiments: neutral p(PEGMA₄₇₅) (P1), cationic quaternised p(DMAEMA) (P2) and anionic p(AMPS) (P5). Con A

solutions produced small crystals with sizes of $\sim 60 \mu\text{m}$ within 1 week without any polymer, which were orthorhombic (Figure 7-4, Control). When polymers were utilised, the sizes and numbers of crystals were found to vary with the types of polymers added to solution, however, the form of the crystals was still orthorhombic. Neutral polymer P1 resulted in a few large block-shaped crystals (Figure 7-4, P1), suggesting a similar dehydration mechanism to that which occurred in HEWL crystallisation. Cationic polymer P2 was expected to bind anionic Con A and nucleated a few large crystals (Figure 7-4, P2). By contrast the anionic polymer P5 was postulated to decrease the interfacial energy between Con A macromolecules and water by charge-charge repulsions between anionic polymer and anionic Con A, resulting in the promotion of protein aggregation and formation of many smaller crystals within four days (Figure 7-4, P5).

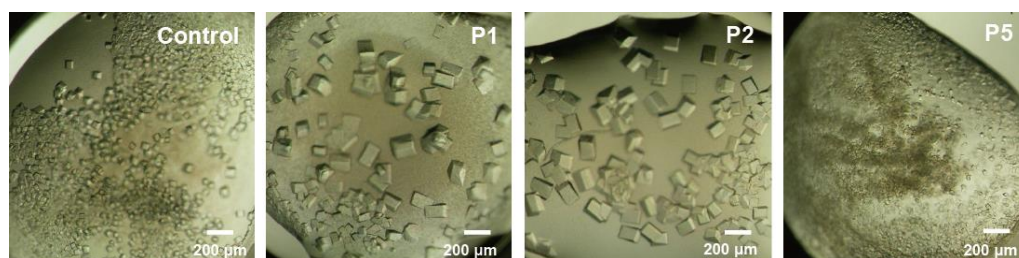


Figure 7-4. Optical images showing changes of Con A crystals, in the presence of different polymers: neutral p(PEGMA₄₇₅) (P1), cationic quaternised p(DMAEMA) (P2) and anionic p(AMPS) (P5). Image labelled ‘Control’ represents crystals grown from sample wells without polymer.

Moreover, for anionic Con A, as the concentration of neutral polymer in

solution was increased, the size of Con A crystals increased (Figure 7-5, P1). The effects of cationic and anionic polymers on Con A crystallisation were predicted from this simple model to be opposite from the effects on HEWL. The size of Con A crystals increased when the concentration of cationic polymer was increased (Figure 7-5 P2). However, the size of Con A crystals decreased when the concentration of anionic polymer was increased (Figure 7-5, P5). All these results together illustrate that polymers with varying net charges have the ability to control the size of protein crystals.

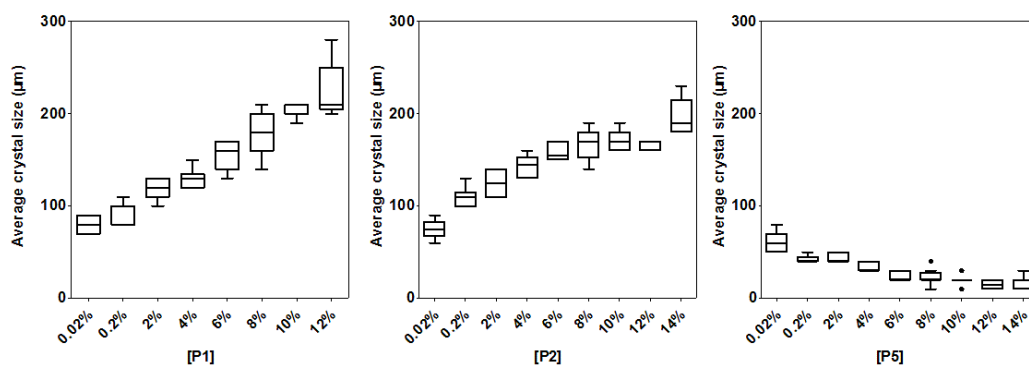


Figure 7-5. Summary of photomicrograph analysis showing changes in the size of Con A crystals, grown in the presence of different classes of polymers at various concentrations. Neutral polymer: P1; cationic polymer: P2; anionic polymer: P5.

The third model protein was BLC. The pI of BLC is 5.4 but at its crystallisation pH of 6.8 BLC is a weakly anionic protein. Similar to Con A, three polymers were also selected from each class for further BLC crystallisation experiments: neutral p(PEGMA₄₇₅) (P1), cationic quaternised p(DMAEMA) (P2) and anionic p(AMPS) (P5). BLC crystal formation in the

absence of added polymers occurred after two weeks and resulted in needle crystal outgrowth with a ‘wheatsheaf’ morphology (Figure 7-6, Control). It was hard to get single crystals without any polymer. When in the presence of neutral p(PEGMA₄₇₅) (P1), poor quality crystals were obtained and it was not possible to determine their structure by single crystal X-ray diffraction. Cationic quaternised p(DMAEMA) (P2) produced a few needles with a ‘sea-urchin’ morphology formed at lower concentrations, but suppression of BLC crystallisation occurred at higher concentration. By contrast, anionic polymers promoted BLC aggregation and produced single crystals in 10 days, which were identified as orthorhombic (space group: $P2_12_12_1$, form III) by X-ray diffraction. BLC crystals of form III reported previously were extremely thin ($< 1 \mu\text{m}$) and hard to characterise fully using single crystal X-ray diffraction.²³¹ It should be noted that BLC form III has rarely been studied; thus the use of polymers as solution additives might be useful in further BLC crystal characterisation.

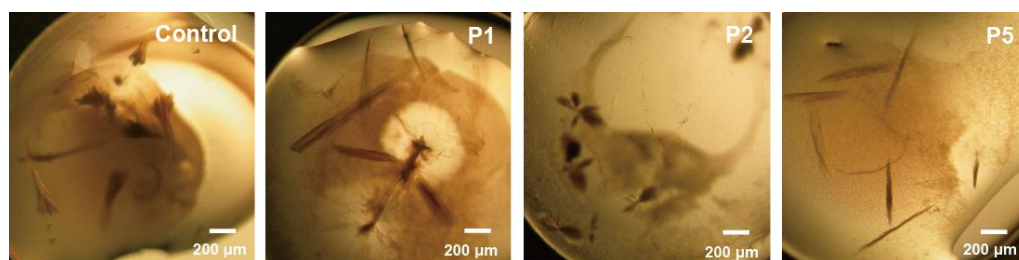


Figure 7-6. Optical images showing changes of BLC crystals, in the presence of different polymers: neutral p(PEGMA₄₇₅) (P1), cationic quaternised p(DMAEMA) (P2) and anionic p(AMPS) (P5). Image labelled ‘Control’ represents crystals grown from sample wells without polymer.

Light scattering experiments were carried out to evaluate the HEWL and Con A aggregation process directly in the presence of crystallisation solutions and polymers with varying net charges. Protein crystallisation was initiated by mixing protein with polymer solutions, leading to immediate supersaturation and formation of protein aggregates. Based on the effects of each polymer on crystal size and morphology in prior experiments, we predicted (Figure 7-7, A) and subsequently evaluated (Figure 7-7, B-D) the effects of each polymer on the growth of cationic HEWL and anionic Con A crystals.

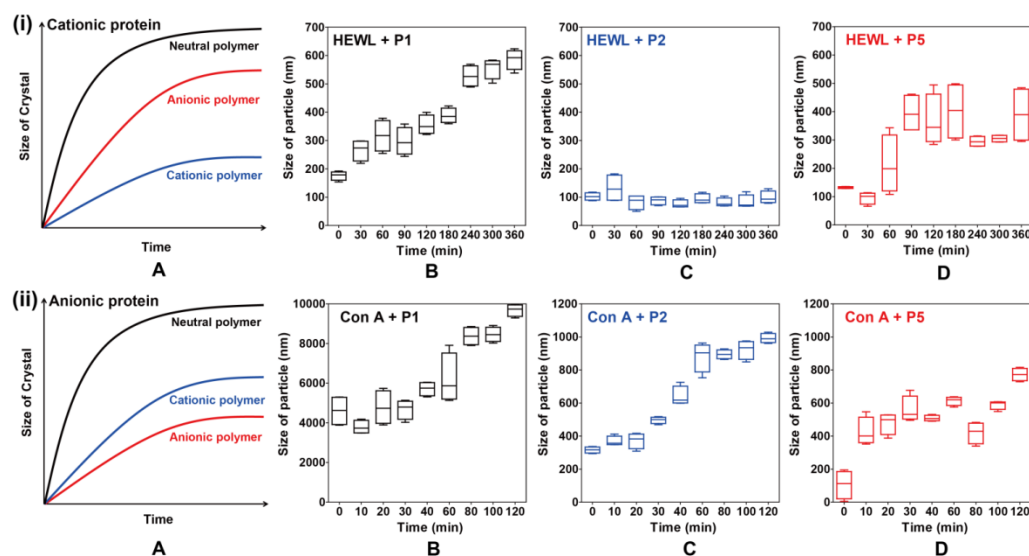


Figure 7-7. Predicted growth of HEWL ((i)A) and Con A ((ii)A) particles during crystallisation; and actual variations in the size of HEWL ((i)B-D) and Con A ((ii)B-D) aggregates or crystals in the solution as a function of time during crystallisation experiments induced by different polymers by DLS. Black represents the application of neutral polymers; blue represents the application of cationic polymers; red represents the application of anionic polymers.

At the beginning of the experiment, protein macromolecules were free and non-interacting in the solution. After the addition of various polymers, a characteristic increase in protein aggregate size can be observed in all cases. As time increased, the rate of protein aggregation growth followed two distinct sequences. With the addition of neutral p(PEGMA₄₇₅) (P1), cationic quaternised p(DMAEMA) (P2) and anionic p(AMPS) (P5) in crystallisation solutions, the size of HEWL aggregates increased up to around 600 nm, 120 nm and 400 nm respectively, while Con A aggregates increased up to around 10000 nm, 1000 nm and 800 nm. Therefore, for HEWL, particle size increased most rapidly for neutral polymer > anionic polymer > cationic polymer (Figure 7-7(i), B-D), whereas for the rate of the growth of Con A aggregation the sequence was: neutral polymer > cationic polymer > anionic polymer (Figure 7-7(ii), B-D). These DLS data indicated that as time increased, protein aggregates increased in size, presumably until the critical nuclei were reached and crystals began to grow. As mentioned above, neutral polymers competed with proteins for water and thus promoted protein crystallisation. Cationic polymers were expected to lower the interfacial energy between cationic HEWL macromolecules and water by charge-charge repulsions, thus promoting nucleation; while the same polymers were likely to attract anionic Con A macromolecules for charge compensation, thus slowing down the rate of crystal growth. The effects of anionic polymer on HEWL and Con A crystallisation were predicted from this simple model to be opposite from

cationic polymers, and to a first approximation this pattern was observed. We thus propose that DLS measurements can be used as a simple qualitative screen to predict the outcome for protein crystallisation experiments.

In conclusion, a series of polymers with varying degrees of charge, molecular weight and backbone structure have been successfully prepared and applied to the crystallisation of HEWL, Con A and BLC via sitting drop vapour diffusion techniques. These polymers acted as solution additives to mediate protein crystallisation through favourable interactions between polymer and protein or the surrounding solvent system; and were found to influence strongly the resultant crystal sizes, shapes and polymorphs. Experiments in which polymers and proteins exhibited different charges suggested possible mechanisms of how these polymers might affect protein crystallisation. Moreover, ‘first principles’ structure-function relationships linking the types of polymers used in these experiments and the protein crystal habits produced were generated. These relationships might be used as models to guide a wide range of protein crystallisation experiments in the future. Therefore, polymers as solution additives may perhaps be tuned to control the size, quality, shape and even polymorph of protein crystals for use in pharmaceutical, biotechnological or chemical applications.

7.2 Future work

In this study, we used the whole range of polymers with varying degrees of

charge, molecular weight and backbone structure as solution ‘additives’ for HEWL crystallisation experiments, however, due to the time limit, we selected three key polymers from each class for Con A and BLC crystallisation experiments. Therefore, the whole range of polymers should be applied in the future Con A and BLC crystallisation experiments.

Based on the effects of each polymer on crystal size and morphology in the experiments, we suggested some mechanisms of how the polymers affect protein crystallisation, and proposed possible models of ‘first principles’ structure-function relationships linking the types of polymers used in these experiments and the protein crystal habits produced. However, the study of these models is still on its early stage. Because there are so many factors which can affect crystallisation, many of which are still poorly understood, these mechanisms are still somewhat tenuous and need to be further investigated. Obviously, this is the key issue to solve in the future.

A series of polymers were prepared and successfully applied as ‘additives’ to influence protein crystal size, outer crystal shape, even crystal packing motifs. However, future work should involve the investigation of more polymer additives with various possible functionalities, including soluble polymer additives and insoluble polymer surfaces, such as molecularly imprinted polymers (MIPs). The results will aid in better understanding of the mechanisms we proposed.

Moreover, the structure-function relationships linking the types of polymers

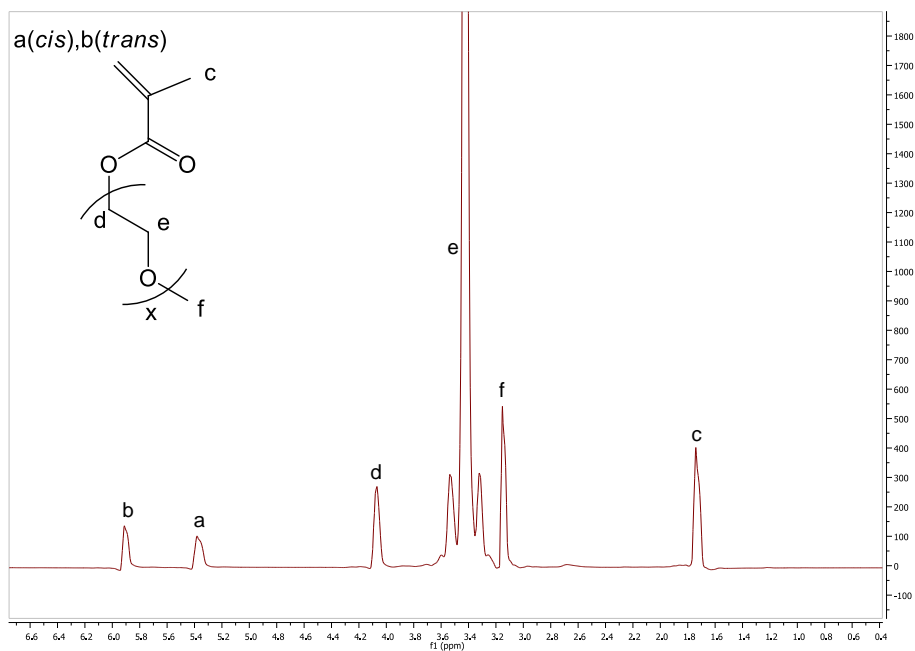
and the protein crystal habits produced might be used as models to guide a wide range of protein crystallisation experiments in the future. Therefore, polymers as solution additives may perhaps be tuned to control the size, quality, shape and even polymorph of protein crystals for use in pharmaceutical, biotechnological or chemical applications.

APPENDIX

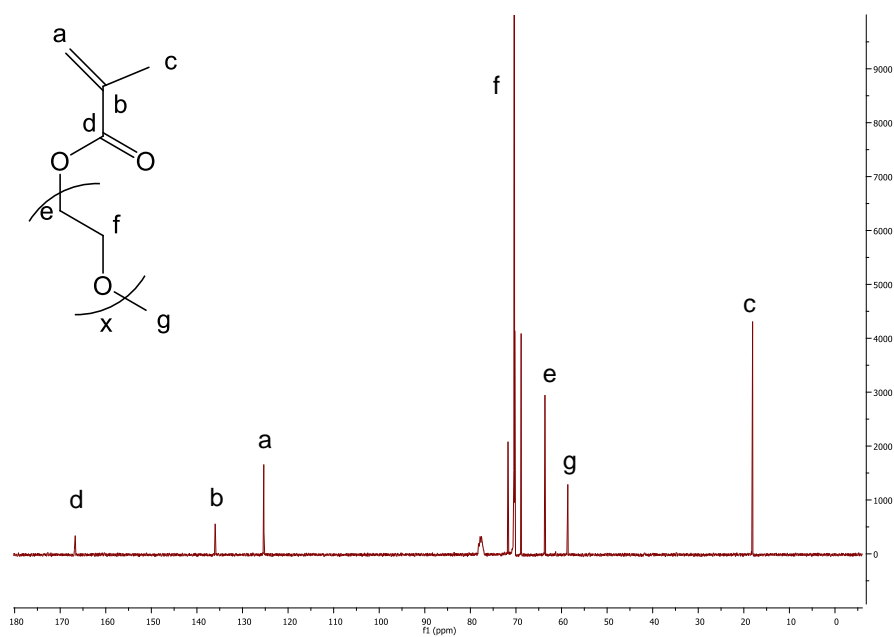
Supporting spectroscopy graphs

Monomer PEGMA₄₇₅

Proton NMR

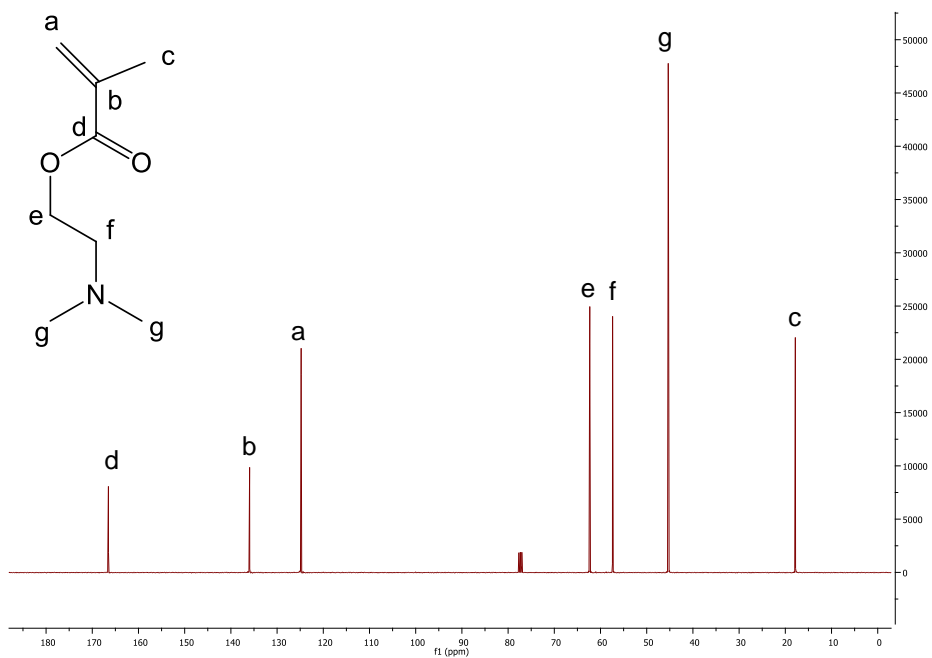


Carbon NMR



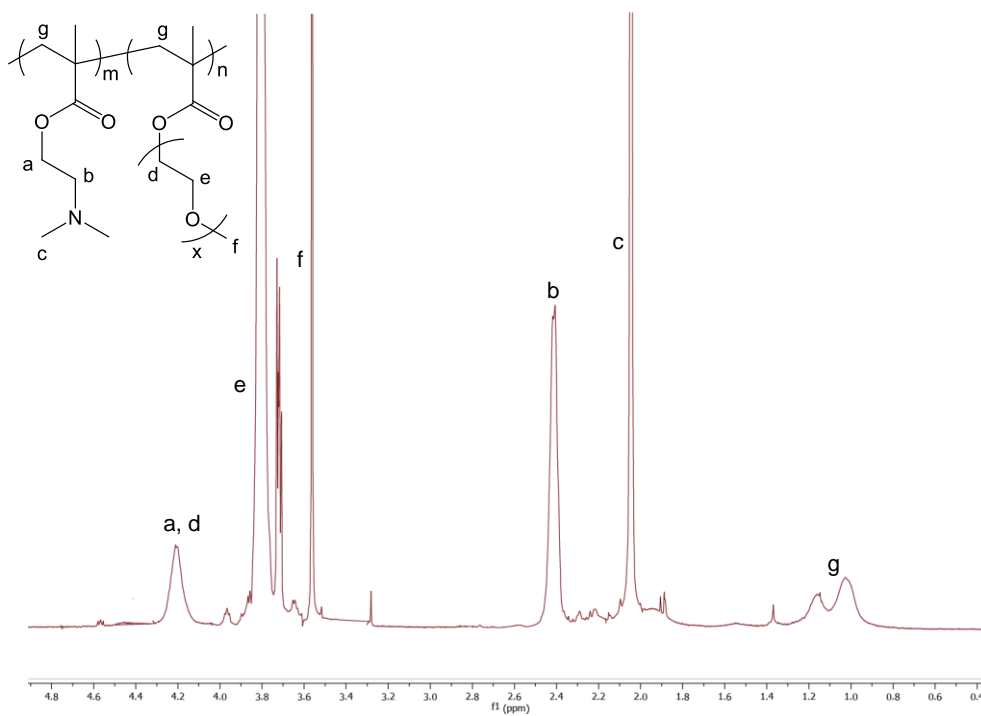
Monomer DMAEMA

Carbon NMR



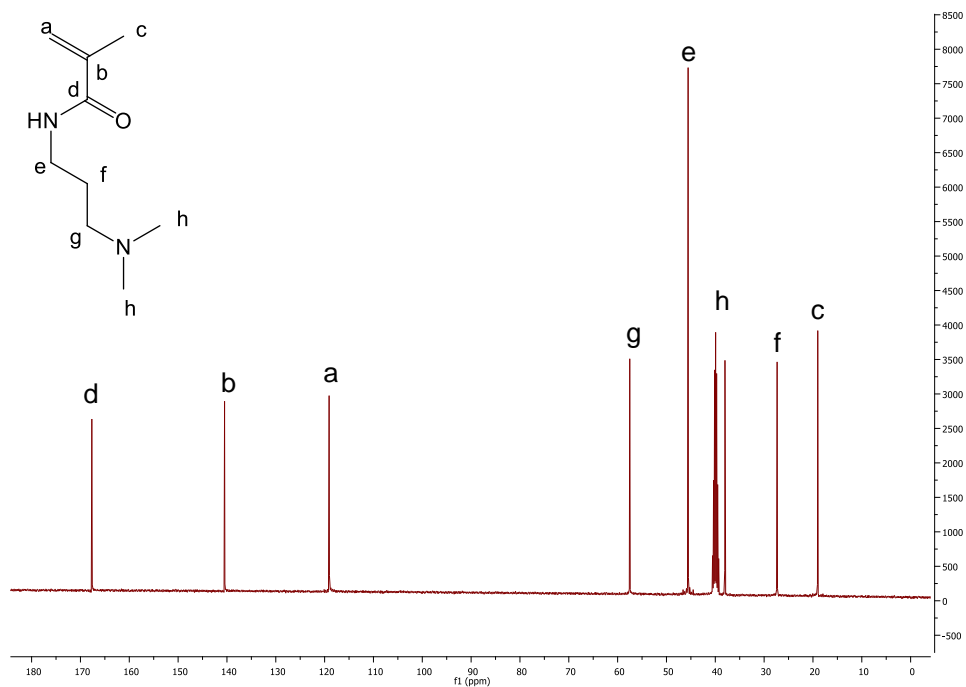
Polymer p(DMAEMA-*stat*-PEGMA₄₇₅)

Proton NMR



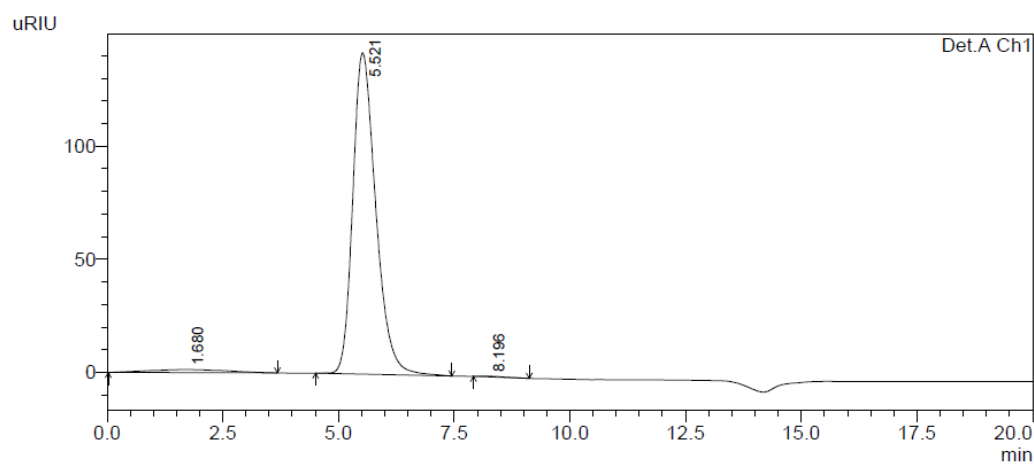
Monomer DMAPMAm

Carbon NMR



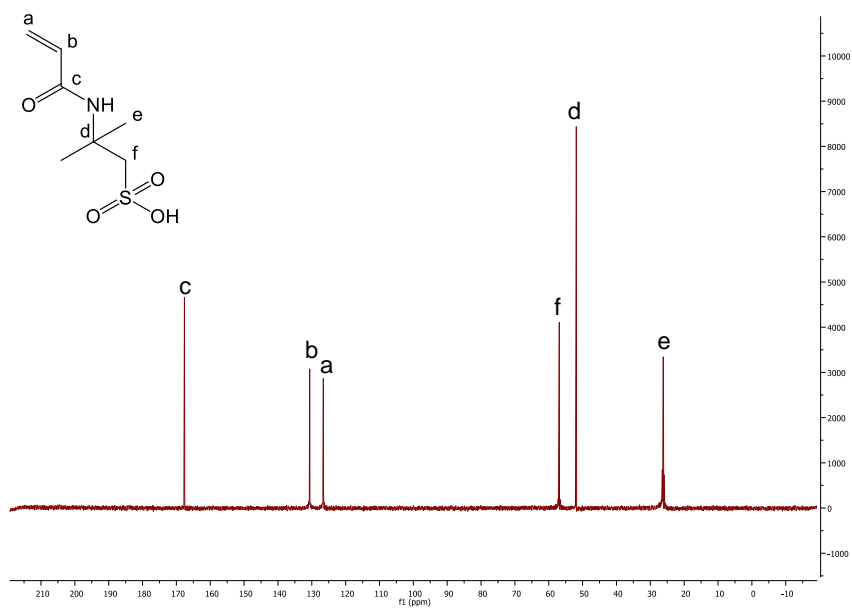
Polymer p(DMAPMAm)

GPC



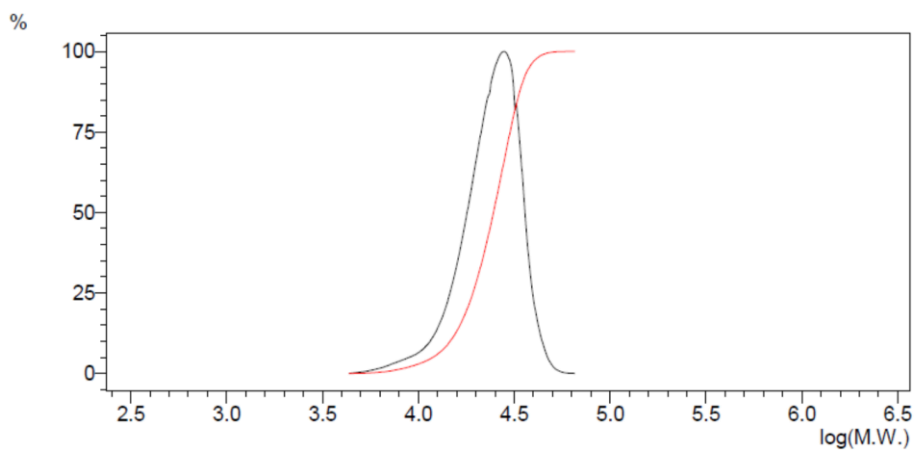
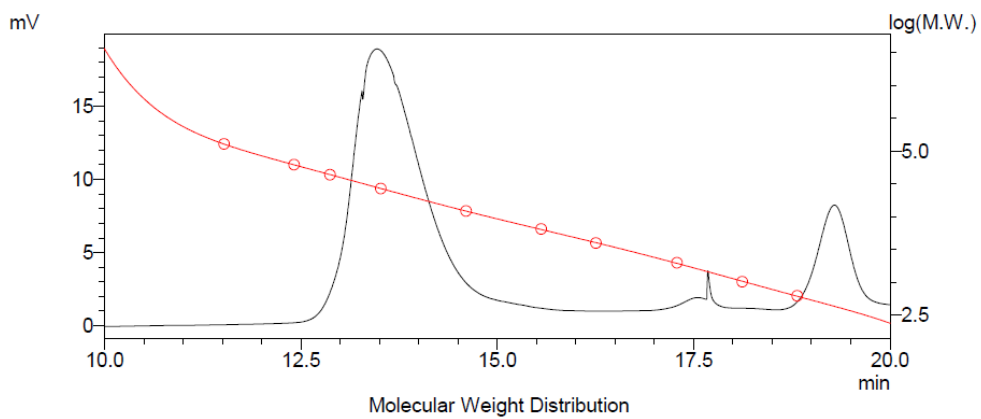
Monomer AMPS

Carbon NMR



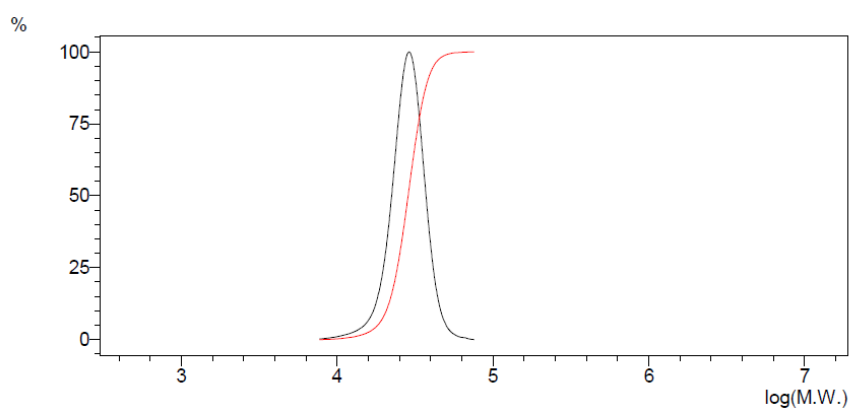
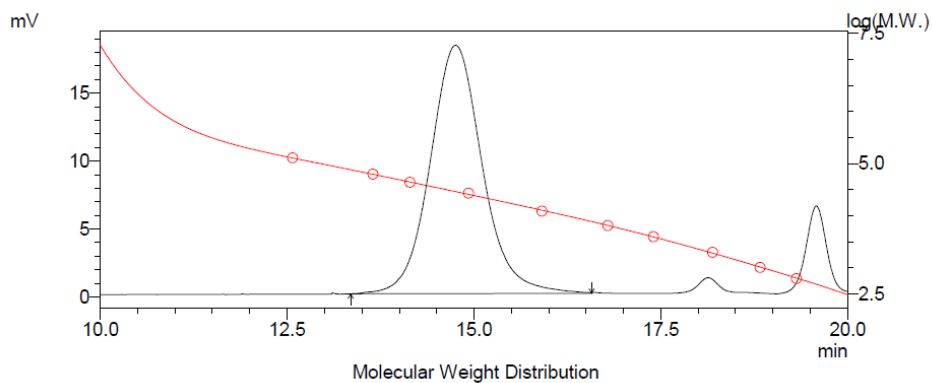
Polymer p(AMPS)

GPC



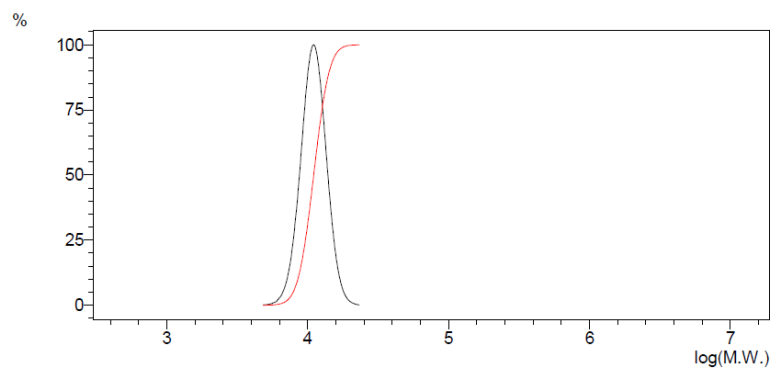
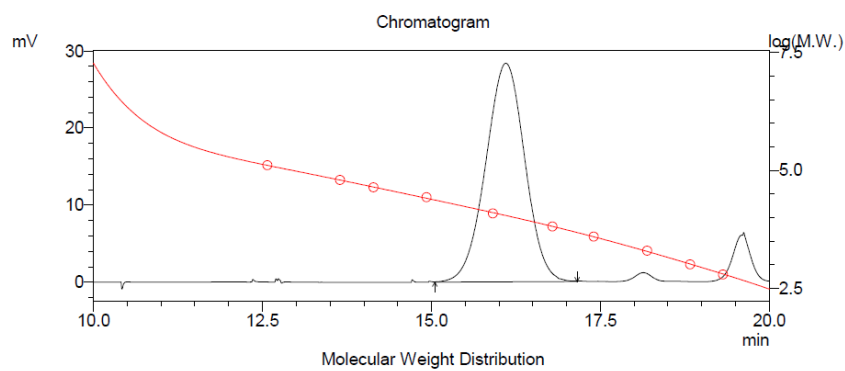
Polymer p(2-AmAA)

GPC



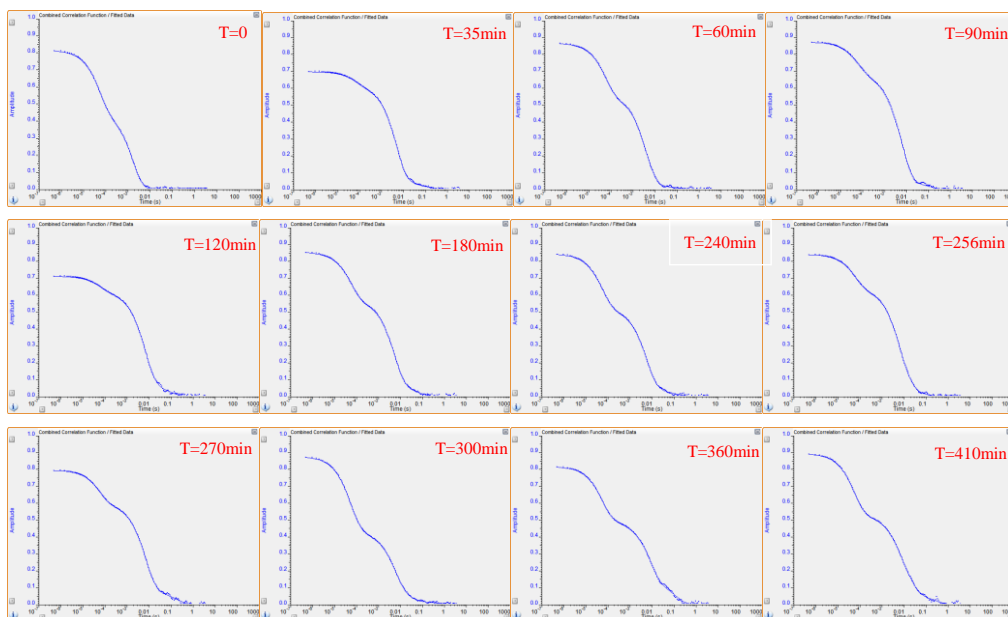
Polymer p(4-AmBA)

GPC

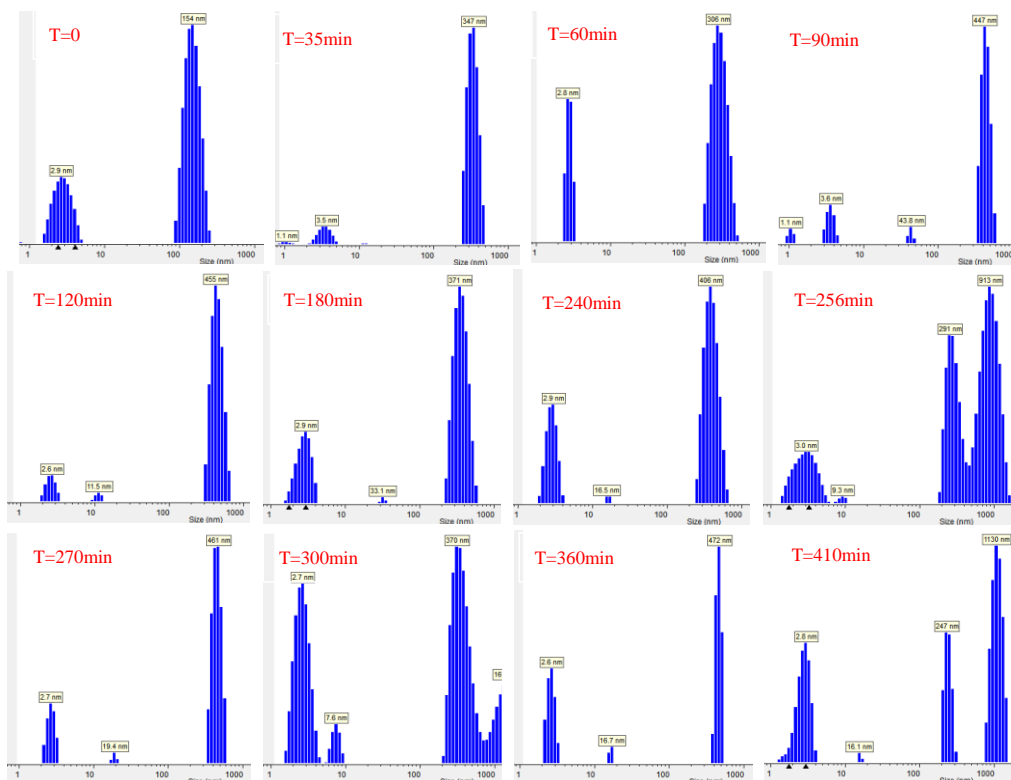


DLS analysis - HEWL crystal growth: control without polymer

Combined correlation function

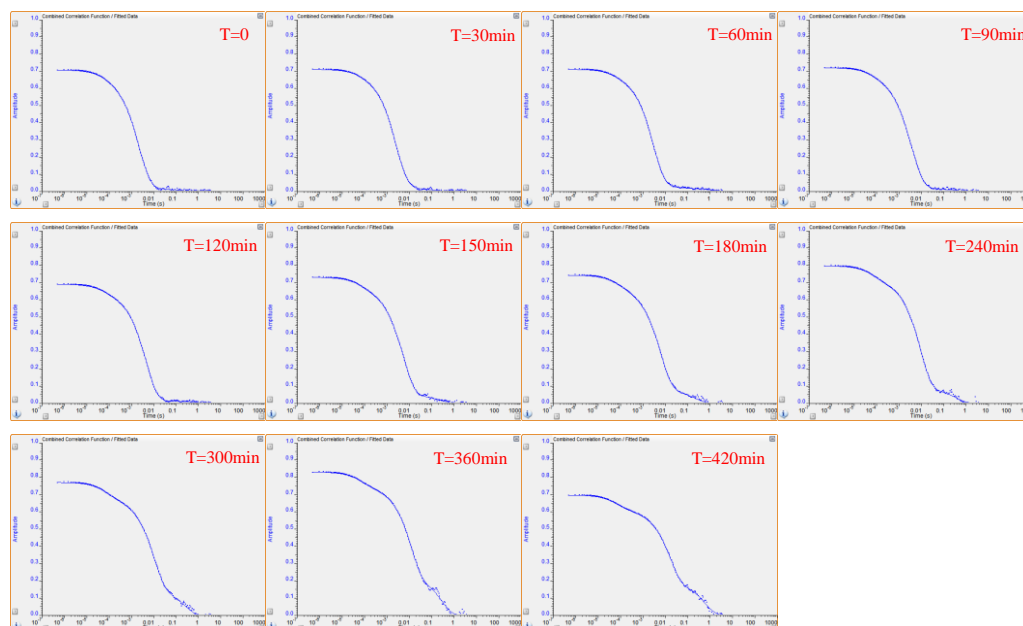


Intensity distribution

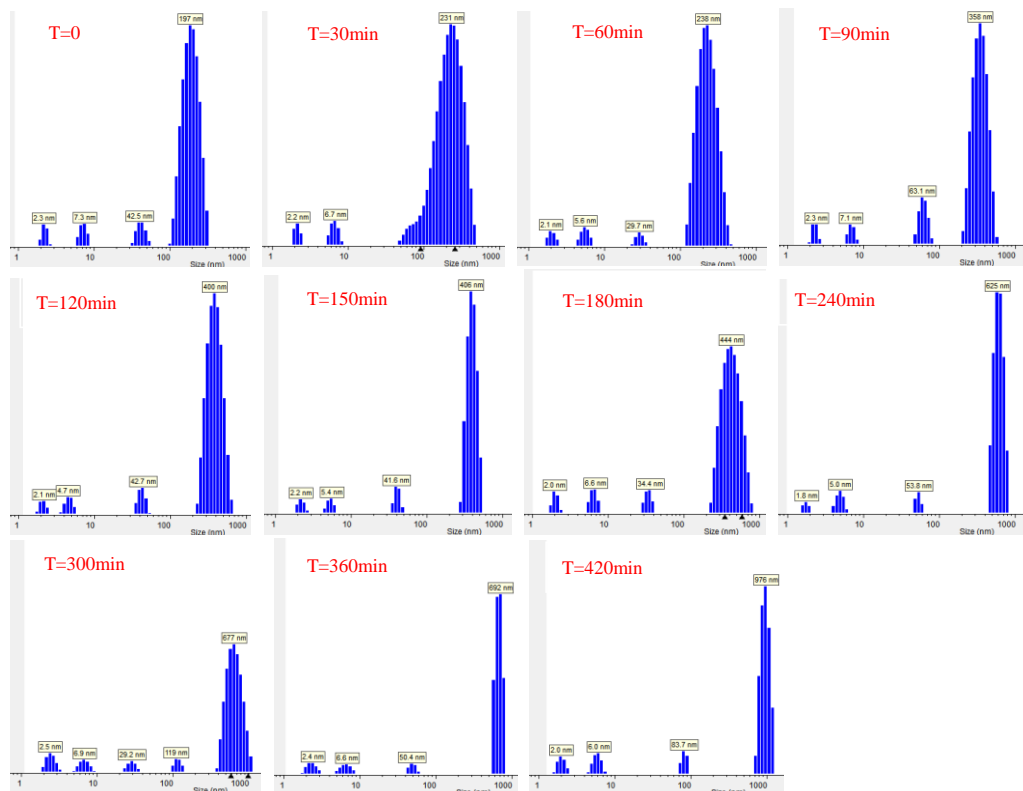


DLS analysis - HEWL+ p(PEGMA₄₇₅)

Combined correlation function

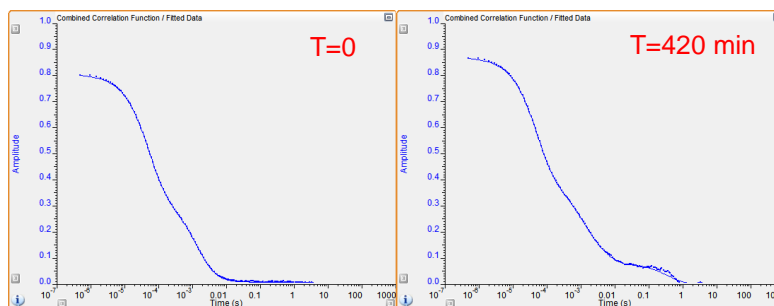


Intensity distribution

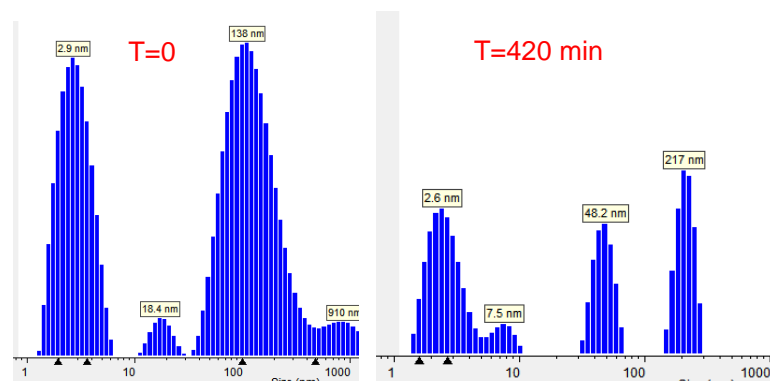


DLS analysis - HEWL+ quaternised p(DMAEMA)

Combined correlation function

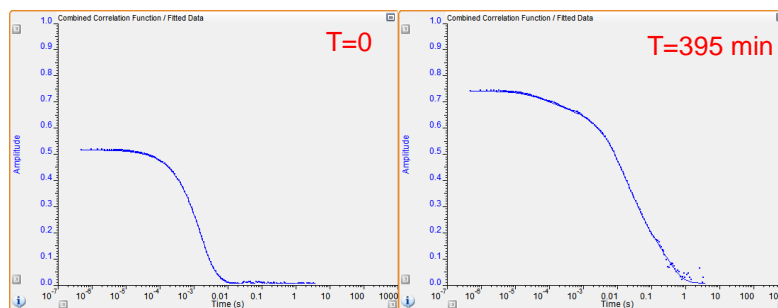


Intensity distribution

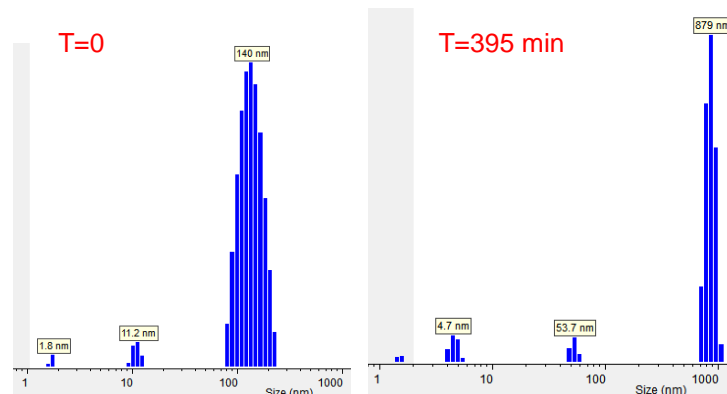


DLS analysis - HEWL+ mixed polymers of p(PEGMA₄₇₅) & p(DMAEMA)

Combined correlation function

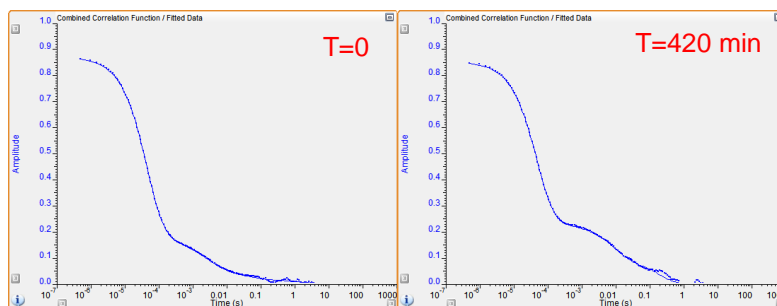


Intensity distribution

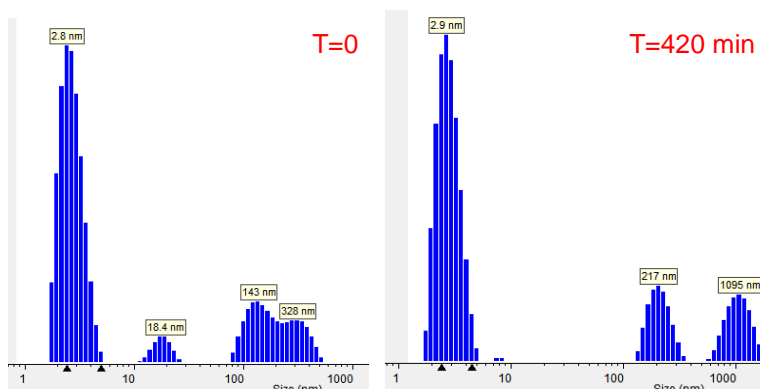


DLS analysis - HEWL + p(DMAPMAM)

Combined correlation function

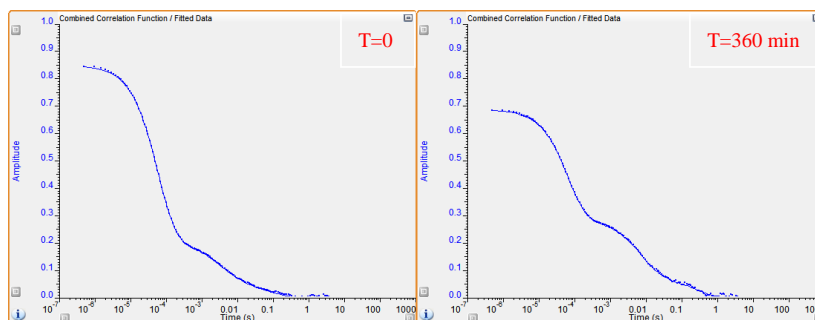


Intensity distribution

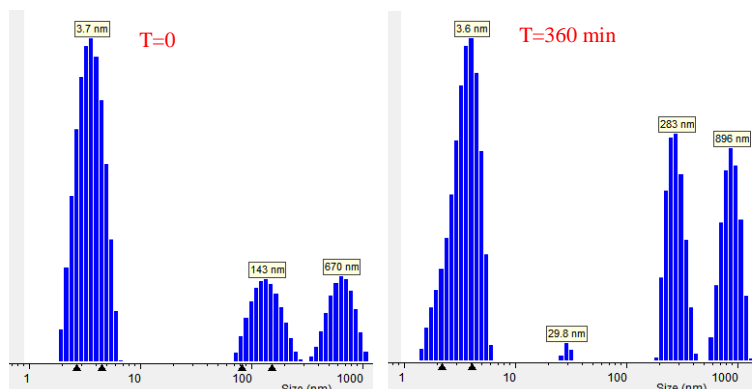


DLS analysis - HEWL + p(AMPS)

Combined correlation function

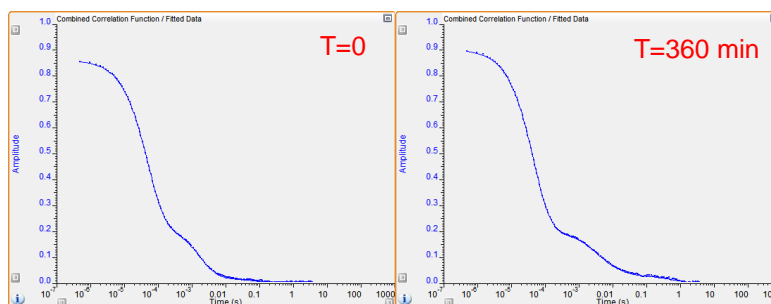


Intensity distribution

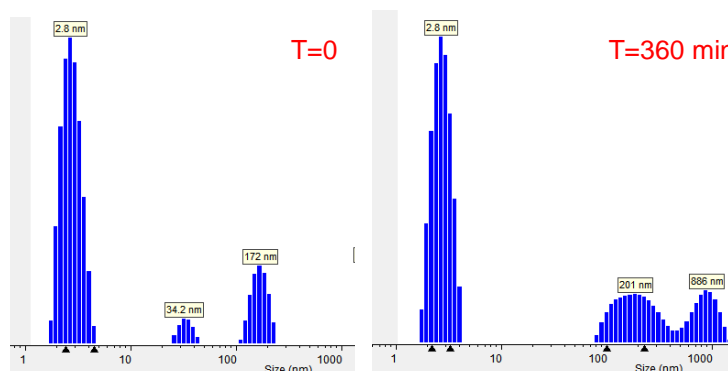


DLS analysis - HEWL+ p(2-AmAA)

Combined correlation function

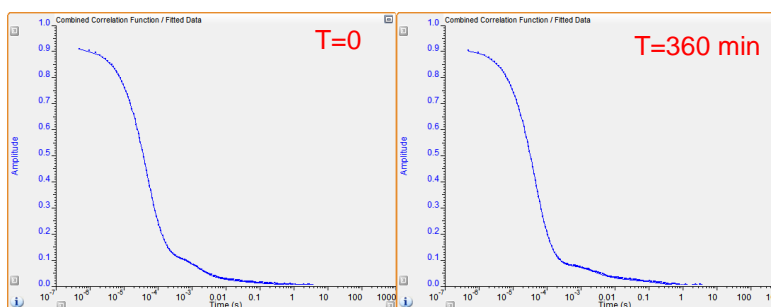


Intensity distribution

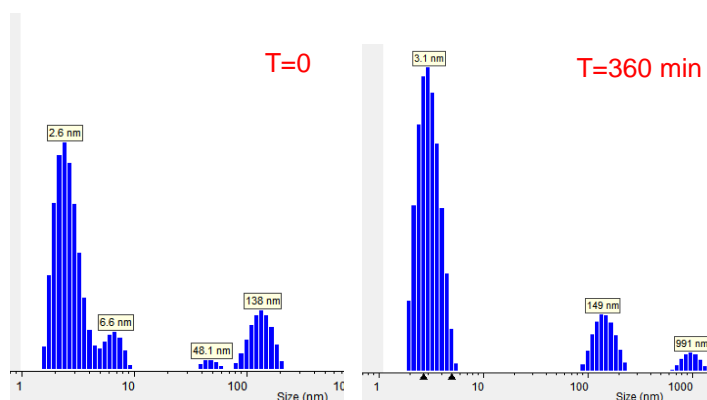


DLS analysis - HEWL+ p(4-AmBA)

Combined correlation function



Intensity distribution



References

1. Braden, C.; Tooze, J., *Introduction to Protein Structure*. Garland publishing, Inc. : New York and London, 1991.
2. Kam, Z.; Shore, H. B.; Feher, G., Crystallization of Proteins. *Journal of Molecular Biology* **1978**, *123*, 539-555.
3. McPherson, A., Macromolecular crystals. *Scientific American* **1989**, *260*, 62-69.
4. Patel, S.; Cudney, B.; McPherson, A., Polymeric precipitants for crystallization of macromolecules. *Biochemical and Biophysical Research Communications* **1995**, *207*, 819-828.
5. McPherson, A., *Crystallization of biological macromolecules*. Cold Spring Harbor Laboratory Press: Cold Spring Harbor, New York, 1999.
6. Capdeville, R.; Buchdunger, E.; Zimmermann, J.; Matter, A., Glivec (STI571, imatinib), a rationally developed, targeted anticancer drug. *Nature Reviews Drug Discovery* **2002**, *1*, 493-502.
7. Illanes, A., Stability of biocatalysts. *Electronic Journal of Biotechnology: Process Biotechnology* **1999**, *2*, 7-15.
8. Vuolanto, A.; Uotila, S.; Leisola, M.; Visuri, K., Solubility and crystallization of xylose isomerase from *Streptomyces rubiginosus*. *Journal of Crystal Growth* **2003**, *257*, 403-411.
9. Vuolanto, A.; Pastinen, O.; Schoemaker, H. E.; Leisola, M., C-2 epimer formation of tetrose, pentose and hexose sugars by xylose isomerase. *Biocatalysis and Biotransformation* **2002**, *20*, 235-240.
10. Moks, T.; Abrahmsen, L.; Osterlof, B.; Josephson, S.; Ostling, M.; Enfors, S. O.; Persson, I.; Nilsson, B.; Uhlen, M., Large-scale affinity purification of human insulin-like growth factor-I from culture medium of *Escherichia coli*. *Nature Biotechnology* **1987**, *5*, 379-382.
11. Wurm, F. M., Production of recombinant protein therapeutics in cultivated mammalian cells. *Nature Biotechnology* **2004**, *22*, 1393-1398.
12. Salmaso, S.; Bersani, S.; Semenzato, A.; Caliceti, P. J., Nanotechnologies in protein delivery. *Journal of Nanoscience and Nanotechnology* **2006**, *6*, 1-18.
13. Lu, Y.; Yang, J.; Sega, E., Issues related to targeted delivery of proteins and peptides. *American Association of Pharmaceutical Scientists* **2006**, *8*, E466-E478.
14. Solaro, R.; Chiellini, F.; Battisti, A., Targeted delivery of protein drugs by nanocarriers. *Materials* **2010**, *3*, 1928-1980.
15. Haag, R.; Kratz, F., Polymer therapeutics: concept and applications. *Angewandte Chemie International Edition* **2006**, *45*, 1198-1215.
16. Cleland, J. L.; Duenas, E.; Daugherty, A.; Marian, M.; Yang, J.; Wilson, M.; Celniker, A. C.; Shahzamani, A.; Quarmby, V.; Chu, H.; Mukku, V.; Mac, A.; Roussakis, M.; Gillette, N.; Boyd, B.; Yeung, D.; Brooks, D.; Maa, Y. F.; Hsu, C.; Jones, A. J. S., Recombinant human growth hormone poly(lactic-co-glycolic acid) (PLGA) microspheres provide a long lasting effect. *Journal of Controlled Release* **1997**, *49*, 193-205.
17. Sanders, L. M.; Kell, B. A.; McRae, G. I.; Whitehead, G. W., Prolonged controlled-release of nafarelin, a luteinizing hormone-releasing hormone analogue, from biodegradable polymeric implants: Influence of composition and molecular weight of polymer. *Journal of Pharmaceutical Sciences* **1986**, *75*, 356-360.
18. Ogawa, Y. M.; Okada, H.; Yashiki, T.; Shimamoto, T., A new technique to efficiently

- entrap leuprolide acetate into microcapsules of polylactic acid or copoly(lactic/glycolic) acid. *Chemical & pharmaceutical bulletin* **1988**, *36*, 1095-1103.
19. Johnson, O. L.; Jaworowicz, W.; Cleland, J. L.; Bailey, L.; Charnis, M.; Duenas, E.; Wu, C.; Shepard, D.; Magil, S.; Last, T.; Jones, A. J. S.; Putney, S. D., The Stabilization and Encapsulation of Human Growth Hormone into Biodegradable Microspheres. *Pharmaceutical Research* **1997**, *14*, 730-735.
20. Cleland, J. L.; Duenas, E. T.; Park, A.; Daugherty, A.; Kahn, J.; Kowalski, J.; Cuthbertson, A., Development of poly-(d,l-lactideoglycolide) microsphere formulations containing recombinant human vascular endothelial growth factor to promote local angiogenesis. *Journal of Controlled Release* **2001**, *72*, 13-24.
21. Magnusson, J. P.; Saeed, A. M.; Fernández-Trillo, F.; Alexander, C., Synthetic polymers for biopharmaceutical delivery. *Polymer Chemistry* **2011**, *2*, 48-59.
22. Culajay, J. F.; Blaber, S. I.; Khurana, A.; Blaber, M., Thermodynamic characterization of mutants of human fibroblast growth factor 1 with an increased physiological half-life. *Biochemistry* **2000**, *39*, 7153-7158.
23. Luo, P.; Hayes, R. J.; Chan, C.; Stark, D. M.; Hwang, M. Y.; Jacinto, J. M.; Juvvadi, P.; Chung, H. S.; Kundu, A.; Ary, M. L.; Dahiyat, B. I., Development of a cytokine analog with enhanced stability using computational ultrahigh throughput screening. *Protein science : a publication of the Protein Society* **2002**, *11* (5), 1218-26.
24. Veronese, F. M.; Pasut, G., PEGylation, successful approach to drug delivery. *Drug Discovery Today* **2005**, *10*, 1451-1458.
25. Basu, S. K.; Govardhan, C. P.; Jung, C. W.; Marqolin, A. L., Protein crystals for the delivery of biopharmaceuticals. *Expert Opinion on Biological Therapy* **2004**, *4*, 301-317.
26. Jen, A.; Merkle, H. P., Diamonds in the rough: protein crystals from a formulation perspective. *Pharmaceutical Research* **2001**, *18*, 1483-1488.
27. Simonelli, A. P.; Mehta, S. C.; Higuchi, W. I., Inhibition of sulfathiazole crystal growth by polyvinylpyrrolidone. *Journal of Pharmaceutical Science* **1970**, *59*, 633-638.
28. Shekunov, B. Y.; York, P., Crystallization processes in pharmaceutical technology and drug delivery design. *Journal of Crystal Growth* **2000**, *211*, 122-136.
29. Lima-de-Faria, J., *Historical Atlas of Crystallography*. Kluwer Academic Publishers: Dordrecht, 1990.
30. Weber, P. C., Physical principles of protein crystallization. *Advance in Protein Chemistry* **1991**, *41*, 1-36.
31. Buckley, H. E., *Crystal growth*. John Wiley & Son: New York, 1951.
32. Asherie, N., Protein crystallization and phase diagrams. *Methods* **2004**, *34*, 266-272.
33. Drenth, J.; Haas, C., Protein crystals and their stability. *Journal of Crystal Growth* **1992**, *122*, 107-109.
34. Rhodes, G., *Crystallography Made Crystal Clear*. Academic Press: San Diego, 1993.
35. Feher, G.; Kam, Z., Nucleation and growth of protein crystals: general principles and assays. *Methods in Enzymology* **1985**, *114*, 77-111.
36. Boistelle, R.; Astier, J. P., Crystallization mechanisms in solution. *Journal of Crystal Growth* **1985**, *90*, 14-30.
37. Koszelak, S.; Martin, D.; Ng, J.; McPherson, A., Protein crystal growth rates determined by time lapse microphotography. *Journal of Crystal Growth* **1991**, *110*, 177-181.

38. Abraham, F. F., *Homogeneous Nucleation Theory*. Academic Press: New York, 1974.
39. DeLucas, L. J.; Suddath, F. L.; Snyder, R.; Naumann, R.; Broom, M. B.; Pusey, M.; Yost, V.; Herren, B.; Carter, D.; Nelson, B.; Meechan, E. J.; McPherson, A.; Bugg, C. E., Preliminary investigations of protein crystal growth using the space shuttle. *Journal of Crystal Growth* **1986**, *76*, 681-693.
40. Luft, J. R.; DeTitta, G. T., Kinetic aspects of macromolecular crystallization. *Methods in Enzymology* **1997**, *276*, 110-131.
41. Bugg, C. E., The future of protein crystal growth. *Journal of Crystal Growth* **1986**, *76*, 535-544.
42. Frey, M., Water structure associated with proteins and its role in crystallization. *Acta crystallographica. Section D, Biological crystallography* **1994**, *50* (Pt 4), 663-6.
43. Pjura, P. E.; Lenhoff, A. M.; Leonard, S. A.; Gittis, A. G., Protein crystallization by design: chymotrypsinogen without precipitants. *Journal of Molecular Biology* **2000**, *300* (2), 235-9.
44. Salemme, F. R.; Genieser, L.; Finzel, B. C.; Hilmer, R. M.; Wendolowski, J. J., Molecular factors stabilizing protein crystals. *Journal of Crystal Growth* **1988**, *90*, 273-282.
45. Kierzek, A. M.; Zielenkiewicz, P., Models of protein crystal growth. *Biophysical chemistry* **2001**, *91* (1), 1-20.
46. McPherson, A., Introduction to protein crystallization. *Methods* **2004**, *34* (3), 254-65.
47. Hunefeld, F. L., *Der Chemismus in der tierescher Organization*: Leipsig: Brockhaus, 1840.
48. Kendrew, J. C.; Parrish, R. G.; Marrack, J. R.; Orlans, E. S., The species specificity of myoglobin. *Nature* **1954**, *174* (4438), 946-9.
49. Beichert, K. E., *Archiv für Anatomie, Physiologie und Wissenschaftliche Medizin* **1849**.
50. Funke, O., *Atlas der physiologischen Chemie*. Leipzig: W. Englemann, 1853.
51. Osborne, T. B., The proteins of the kidney bean. *Journal of the American Chemical Society* **1894**, *16* (9), 633-643.
52. Sumner, J. B., The Isolation and Crystallization of the Enzyme Urease. *Journal of Biological Chemistry* **1926**, *69*, 435-441.
53. Abel, J. J., Chemistry in Relation to Biology and Medicine With Especial Reference to Insulin and Other Hormones. *Science* **1927**, *66*, 307-319, 337-346.
54. Berman, H. M.; Westbrook, J.; Feng, Z.; Gilliland, G.; Bhat, T. N.; Weissig, H.; Shindyalov, I. N.; Bourne, P. E., The Protein Data Bank. *Nucleic Acids Research* **2000**, *28*, 235-242.
55. Chernov, A. A., Crystal growth and crystallography. *Acta Crystallographica, Section A: Foundations of Crystallography* **1998**, *54*, 859-872.
56. Garcia-Ruiz, J. M., Nucleation of protein crystals. *Journal of Structural Biology* **2003**, *142*, 22-31.
57. Ducruix, A.; Giege, R., *Crystallization of Nucleic Acids and Proteins. . A Practical Approach*. Oxford University Press: New York, 1992.
58. Saridakis, E.; Chayen, N. E., Towards a 'universal' nucleant for protein crystallization. *Trends in Biotechnology* **2008**, *27*, 99-106.
59. McPherson, A., Review: current approaches to macromolecular crystallization. *European journal of biochemistry / FEBS* **1990**, *189* (1), 1-23.

60. McPherson, A., *Preparation and analysis of protein crystals* J. Wiley & Sons: New York, 1982.
61. Christopher, G. K.; Phipps, A. G.; Gray, R. J., Temperature-dependent solubility of selected proteins. *Journal of Crystal Growth* **1998**, *191*, 820-826.
62. Green, A. A., The solubility of hemoglobin in solutions of chlorides and sulfates of varying concentrations. *The Journal of Biological Chemistry* **1932**, *95*, 47-66.
63. Guilloteau, J. P.; Ries-Kautt, M. M.; Ducruix, A. F., Variation of lysozyme solubility as a function of temperature in the presence of organic and inorganic salts. *Journal of Crystal Growth* **1992**, *122*, 223-230.
64. Eerden, J. P. v. d.; Bruinsma, O. S. L., *Science and Technology of Crystal Growth*. Kluwer Academic Publishers: Dordrecht, 1995.
65. Osborne, T. B., *The Vegetable Proteins*. 2nd ed.; Longmans, Green: New York, 1924.
66. King, M. V., a low-resolution structural model for cubic glucagon based on packing of cylinders. *Journal of Molecular Biology* **1965**, *11*, 549-561.
67. Branden, C.; Tooze, J., *Introduction to Protein Structure*. 2nd ed.; Garland: New York, 1999.
68. Choi, S. H.; Kwon, J. H.; Kim, C. W., Microencapsulation of insulin microcrystals. *Bioscience, Biotechnology and Biochemistry* **2004**, *68*, 749-752.
69. Chayen, N. E.; Stewart, P. D. S.; Blow, D. M., Microbatch crystallization under oil - a new technique allowing many small-volume crystallization trials. *Journal of Crystal Growth* **1992**, *122* (1-4), 176-180.
70. Hamada, H.; Arakawa, T.; Shiraki, K., Effect of Additives on Protein Aggregation. *Current Pharmaceutical Biotechnology* **2009**, *10*, 400-407.
71. Song, R. Q.; Cölfen, H., Additive controlled crystallization. *CrystEngComm* **2011**, *13*, 1249-1276.
72. McPherson, A.; Cudney, B., Searching for silver bullets: an alternative strategy for crystallizing macromolecules. *Journal of Structural Biology* **2006**, *156* (3), 387-406.
73. McPherson, A.; Nguyen, C.; Cudney, R.; Larson, S. B., The role of small molecule additives and chemical modification in protein crystallization. *Crystal Growth & Design* **2011**, *11*, 1469-1474.
74. Timasheff, S. N.; Arakawa, T., Mechanism of protein precipitation and stabilization by co-solvents. *Journal of Crystal Growth* **1988**, *90*, 39-46.
75. Collins, K. D., Ions from the Hofmeister series and osmolytes: effects on proteins in solution and in the crystallization process. *Methods* **2004**, *34*, 300-311.
76. Zulauf, M., *Crystallization of Membrane Proteins*. CRC Press: Boca Raton, Florida, 1990.
77. Trakhanov, S.; Quioco, F. A., Influence of divalent cations in protein crystallization. *Protein science : a publication of the Protein Society* **1995**, *4* (9), 1914-9.
78. Bolen, D. W., Effects of naturally occurring osmolytes on protein stability and solubility: issues important in protein crystallization. *Methods* **2004**, *34* (3), 312-22.
79. Hofmeister, T., Zur Lehre von der Wirkung der Saltz. *Naunyn Schmiedebergs Arch Exp Pathol Pharmacol* **1888**, *24*, 247-260.
80. Cohn, E. J.; Ferry, J. D., *The Interactions of Proteins with Ions and Dipolar Ions*. . Van Nostrand-Reinhold: Princeton, New Jersey, 1943.

81. Collins, K. D.; Washabaugh, M. W., The Hofmeister effect and the behaviour of water at interfaces. *Quarterly reviews of biophysics* **1985**, *18* (4), 323-422.
82. Carbonnaux, C.; Ries-Kautt, M.; Ducruix, A., Relative effectiveness of various anions on the solubility of acidic Hypoderma lineatum collagenase at pH 7.2. *Protein science : a publication of the Protein Society* **1995**, *4* (10), 2123-8.
83. England, S.; Seifter, S., Precipitation Techniques. *Methods in Enzymology* **1990**, *182*, 301-306.
84. Cohn, E. J.; Hughes, W. L., Jr.; Weare, J. H., Preparation and properties of serum and plasma proteins; crystallization of serum albumins from ethanol water mixtures. *Journal of the American Chemical Society* **1947**, *69* (7), 1753-61.
85. King, M. V.; Bello, J.; Pagnatano, E. H.; Harker, D., Crystalline forms of bovine pancreatic ribonuclease. Some new modifications. *Acta Crystallographica* **1962**, *15*, 144-147.
86. McPherson, A.; Shlichta, P. J., Facilitation of the growth of protein crystals by heterogeneous epitaxial nucleation. *Journal of Crystal Growth* **1987**, *85*, 206-214.
87. McPherson, A.; Shlichta, P. J., Heterogeneous and epitaxial nucleation of protein crystals on mineral surfaces. *Science* **1988**, *239*, 385-387.
88. Kimble, W. L.; Paxton, T. E.; Rousseau, R. W.; Sambanis, A., The effect of mineral substrates on the crystallization of lysozyme. *Journal of Crystal Growth* **1998**, *187*, 268-276.
89. Leung, C. J.; Nall, B. T.; Brayer, G. D., Crystallization of yeast iso-2-cytochrome c using a novel hair seeding technique. *Journal of Molecular Biology* **1989**, *206*, 783-785.
90. Pham, T.; Lai, D.; Ji, D.; Tuntiwechapakul, W.; Friedman, J. M.; Lee, T. R., Well-ordered self-assembled monolayer surfaces can be used to enhance the growth of protein crystals. *Colloids and Surfaces B: Biointerfaces* **2004**, *34*, 191-196.
91. Chayen, N. E.; Saridakis, E.; Sear, R. P., Experiment and theory for heterogeneous nucleation of protein crystals in a porous medium. *Proceedings of the National Academy of Sciences of the United States of America* **2006**, *103*, 597-601.
92. Stolyarova, S.; Saridakis, E.; Chayen, N. E.; Nemirovsky, Y., A model for enhanced nucleation of protein crystals on a fractal porous substrate. *Biophysical Journal* **2006**, *91*, 3857-3863.
93. Sanjoh, A.; Tsukihara, T.; Gorti, S., Surface-potential controlled Si-microarray devices for heterogeneous protein crystallization screening. *Journal of Crystal Growth* **2001**, *232*, 618-628.
94. Tsekova, D.; Dimitrova, S.; Naney, C. N., Heterogeneous nucleation (and adhesion) of lysozyme crystals. *Journal of Crystal Growth* **1999**, *196*, 226-233.
95. Falini, G.; Fermani, S.; Conforti, G.; Ripamonti, A., Protein crystallisation on chemically modified mica surfaces. *Acta crystallographica. Section D, Biological crystallography* **2002**, *58* (Pt 10 Pt 1), 1649-52.
96. Chayen, N. E.; Saridakis, E.; El-Bahar, R.; Nemirovsky, Y., Porous silicon: an effective nucleation-inducing material for protein crystallization. *Journal of Molecular Biology* **2001**, *312* (4), 591-5.
97. Page, A. J.; Sear, R. P., Heterogeneous nucleation in and out of pores. *Physical review letters* **2006**, *97* (6), 065701.
98. Takehara, M.; Ino, K.; Takakusaqi, Y.; Oshikane, H.; Nureki, O.; Ebina, T.; Mizukami, F.; Sakaquchi, K., Use of layer silicate for protein crystallization: effects of micromica and

- chlorite powders in hanging drops. *Analytical Biochemistry* **2008**, *373*, 322-329.
99. Foroughi, L. M.; Kang, Y. N.; Matzger, A. J., Polymer-induced heteronucleation for protein single crystal growth: structural elucidation of bovine liver catalase and concanavalin A forms. *Crystal Growth & Design* **2011**, *11*, 1294-1298.
100. Colfen, H., Polymer-mediated growth of crystals and mesocrystals. *Methods Enzymol* **2013**, *532*, 277-304.
101. Lang, M.; Grzesiak, A. L.; Matzger, A. J., The use of polymer heteronuclei for crystalline polymorph selection. *Journal of the American Chemical Society* **2002**, *124* (50), 14834-5.
102. Cha, J. N.; Stucky, G. D.; Morse, D. E.; Deming, T. J., Biomimetic synthesis of ordered silica structures mediated by block copolypeptides. *Nature* **2000**, *403* (6767), 289-92.
103. Price, C. P.; Grzesiak, A. L.; Matzger, A. J., Crystalline polymorph selection and discovery with polymer heteronuclei. *Journal of the American Chemical Society* **2005**, *127* (15), 5512-7.
104. Grzesiak, A. L.; Matzger, A. J., New form discovery for the analgesics flurbiprofen and sulindac facilitated by polymer-induced heteronucleation. *Journal of Pharmaceutical Sciences* **2007**, *96* (11), 2978-86.
105. Liberski, A. R.; Tizzard, G. J.; Diaz-Mochon, J. J.; Hursthouse, M. B.; Milnes, P.; Bradley, M., Screening for polymorphs on polymer microarrays. *Journal of combinatorial chemistry* **2008**, *10* (1), 24-7.
106. Capes, J. S.; Cameron, R. E., Effect of polymer addition on the contact line crystallisation of paracetamol. *CrystEngComm* **2007**, *9*, 84-90.
107. Porter, W. W., 3rd; Elie, S. C.; Matzger, A. J., Polymorphism in Carbamazepine Cocrystals. *Crystal Growth & Design* **2008**, *8* (1), 14-16.
108. Yao, Y.; Hu, H. M.; Xue, Y. L.; Ma, S. S.; Feng, X. Z., Morphology control of lysozyme crystal shapes by different block copolymers. *CrystEngComm* **2008**, *10*, 166-169.
109. Boistelle, R.; Astier, J. P., Crystallization mechanisms in solution. *Journal of Crystal Growth* **1988**, *90*, 14-30.
110. G, W.; A, S.; K., Z., Enzyme analogue built Polymers and their use for theresolution of racemates. *Tetrahedron Letters* **1973**, *14* (44), 4329-4332.
111. Alexander, C.; Andersson, H. S.; Andersson, L. I.; Ansell, R. J.; Kirsch, N.; Nicholls, I. A.; O'Mahony, J.; Whitcombe, M. J., Molecular imprinting science and technology: a survey of the literature for the years up to and including 2003. *Journal of Molecular Recognition* **2006**, *19* (2), 106-80.
112. Arshady, R.; Mosbach, K., Synthesis of substrate-selective polymers by host-guest polymerization. *Makromolekulare Chemie* **1985**, *182*, 687-692.
113. Sellergren, B., Imprinted Polymers with Memory for Small Molecules, Proteins, or Crystals The author is grateful to Dr. Andrew Hall and Dr. Gunter Buchel for linguistic advice. *Angewandte Chemie (International ed. in English)* **2000**, *39* (6), 1031-1037.
114. Saridakis, E.; Khurshid, S.; Govada, L.; Phan, Q.; Hawkins, D.; Crichlow, G. V.; Lolis, E.; Reddy, S. M.; Chayen, N. E., Protein crystallization facilitated by molecularly imprinted polymers. *Proceedings of the National Academy of Sciences of the United States of America* **2011**, *108* (27), 11081-6.
115. D'Souza, S. M.; Alexander, C.; Carr, S. W.; Waller, A. M.; Whitcombe, M. J.; Vulfson, E. N., Directed nucleation of calcite at a crystal-imprinted polymer surface. *Nature* **1999**, *398*,

- 312-316.
116. Takeuchi, T.; Goto, D.; Shinmori, H., Protein profiling by protein imprinted polymer array. *The Analyst* **2007**, *132* (2), 101-3.
117. Gallagher, W. H.; Croker, K. M., Identification of a molecular switch that selects between two crystals forms of bovine pancreatic trypsin inhibitor. *Protein science : a publication of the Protein Society* **1994**, *3* (9), 1602-4.
118. Durbin, S. D.; Feher, G., Protein crystallization. *Annual review of physical chemistry* **1996**, *47*, 171-204.
119. Gebauer, D.; Voelkel, A.; Coelfen, H., Stable prenucleation calcium carbonate clusters. *Science* **2008**, *322* (5909), 1819-1822.
120. Gebauer, D.; Coelfen, H.; Verch, A.; Antonietti, M., The multiple roles of additives in CaCO₃ crystallization: A quantitative case study. *Advanced Materials* **2009**, *21* (4), 435-439.
121. Qi, L.; Colfen, H.; Antonietti, M., Crystal Design of Barium Sulfate using Double-Hydrophilic Block Copolymers. *Angewandte Chemie (International ed. in English)* **2000**, *39* (3), 604-607.
122. Qi, L.; Cölfen, H.; Antonietti, M., Control of Barite Morphology by Double-Hydrophilic Block Copolymers. *Chemistry of Materials* **2000**, *12*, 2392-2403.
123. Rosenberger, F., Inorganic and protein crystal growth--similarities and differences. *Journal of Crystal Growth* **1986**, *76*, 618-636.
124. Polson, A.; Potgieter, G. M.; Largier, J. F.; Mears, G. E.; Joubert, F. J., Fractionation of protein mixtures by linear polymers of high molecular weight. *Biochimica et biophysica acta* **1964**, *82*, 463-75.
125. McPherson, A., Jr., Crystallization of proteins from polyethylene glycol. *The Journal of Biological Chemistry* **1976**, *251* (20), 6300-3.
126. Sperling, L. H., *Introduction to physical polymer science*. Wiley-Interscience: Hoboken, New Jersey, 2006.
127. Cowie, J. M. G.; Arrighi, V., *Polymers: Chemistry and Physics of Modern Materials*. 3rd ed.; CRC Press: New York, 2008.
128. Wang, J. S.; Matyjaszewski, K., Controlled living radical polymerization-atom transfer radical polymerization in the presence of transition-metal complexes. *Journal of the American Chemical Society* **1995**, *117*, 5614-5615.
129. Matyjaszewski, K.; Tsarevsky, N. V., Nanostructured functional materials prepared by atom transfer radical polymerization. *Nature chemistry* **2009**, *1* (4), 276-88.
130. Tsarevsky, N. V.; Matyjaszewski, K., "Green" atom transfer radical polymerization: from process design to preparation of well-defined environmentally friendly polymeric materials. *Chemical reviews* **2007**, *107* (6), 2270-99.
131. Kamigaito, M.; Ando, T.; Sawamoto, M., Metal-catalyzed living radical polymerization. *Chemical reviews* **2001**, *101* (12), 3689-746.
132. Tang, W.; Tsarevsky, N. V.; Matyjaszewski, K., Determination of equilibrium constants for atom transfer radical polymerization. *Journal of the American Chemical Society* **2006**, *128* (5), 1598-604.
133. Matyjaszewski, K.; Xia, J., Atom transfer radical polymerization. *Chemical reviews* **2001**, *101* (9), 2921-90.
134. Odian, G., *Principles of Polymerization*. Wiley-Interscience: Staten Island, New York,

2004.

135. Matyjaszewski, K.; Nakagawa, Y.; Jasieczek, C. B., Polymerization of n-Butyl Acrylate by Atom Transfer Radical Polymerization. Remarkable Effect of Ethylene Carbonate and Other Solvents. *Macromolecules* **1998**, *31*, 1535-1541.

136. Wang, J. S.; Matyjaszewski, K., Controlled/"Living" Radical Polymerization. Atom Transfer Radical Polymerization in the Presence of Transition Metal Complexes. *Journal of the American Chemical Society* **1995**, *117*, 5614-5615.

137. Wang, J. S.; Matyjaszewski, K., Controlled/"Living" Radical Polymerization. Halogen Atom Transfer Radical Polymerization Promoted by Cu(I)/Cu(II) Redox Process. *Macromolecules* **1995**, *28*, 7901-7910.

138. Grimaud, T.; Matyjaszewski, K., Controlled/"Living" Radical Polymerization of Methyl Methacrylate by Atom Transfer Radical Polymerization. *Macromolecules*, **1997**, *30*, 2216-2218.

139. Zhang, X.; Xia, J.; Matyjaszewski, K., Controlled/"Living" Radical Polymerization of 2-(Dimethylamino)ethyl Methacrylate. *Macromolecules* **1998**, *31* (15), 5167-9.

140. Matyjaszewski, K.; Jo, S.; Paik, H.; Gaynor, S. G., Synthesis of Well-Defined Polyacrylonitrile by Atom Transfer Radical Polymerization. *Macromolecules* **1997**, *30*, 6398-6400.

141. Matyjaszewski, K.; Davis, T. P., *Handbook of Radical Polymerization*. Wiley Interscience: Hoboken, 2002.

142. Matyjaszewski, K.; Gnanou, Y.; Leibler, L., *Macromolecular Engineering: Precise Synthesis, Materials Properties, Applications*. Wiley-VCH: Weinheim, 2007.

143. Ma, Y.; Tang, Y.; Billingham, N. C.; Armes, S. P.; Lewis, A. L., Synthesis of biocompatible, stimuli-responsive, physical gels based on ABA triblock copolymers. *Biomacromolecules* **2003**, *4* (4), 864-8.

144. Xue, X.; Pasparkis, G.; Halliday, N.; Winzer, K.; Howdle, S. M.; Cramphorn, C. J.; Cameron, N. R.; Gardner, P. M.; Davis, B. G.; Fernández-Trillo, F.; Alexander, C., Synthetic polymers for simultaneous bacterial sequestration and quorum sense interference. *Angewandte Chemie (International ed. in English)* **2011**, *50*, 9852-9856.

145. Chiefari, J.; Chong, Y. K.; Ercole, F.; Krstina, J.; Jeffery, J.; Le, T. P. T.; Mayadunne, R. T. A.; Meijs, G. F.; Moad, C. L.; Moad, G.; Rizzardo, E.; Thang, S. H., Living free-radical polymerization by reversible addition-fragmentation chain transfer: the RAFT process. *Macromolecules* **1998**, *31*, 5559-5562.

146. Yeole, N., Thiocarbonylthio Compounds. *Synlett* **2010**, *10*, 1572-1573.

147. Moad, G.; Chiefari, J.; Chong, Y.; Krstina, J.; Mayadunne, R. T.; Postma, A.; Rizzardo, E.; Thang, S. H., Living free radical polymerization with reversible addition-fragmentation chain transfer (the life of RAFT). *Polymer International* **2000**, *49*, 993-1001.

148. Hansen, N. M. L.; Jankova, K.; Hvilsted, S., Fluoropolymer materials and architectures prepared by controlled radical polymerizations. *European Polymer Journal* **2007**, *43*, 255-293.

149. McCormick, C. L.; Lowe, A. B., Aqueous RAFT polymerization: recent developments in synthesis of functional water-soluble (co)polymers with controlled structures. *Accounts of chemical research* **2004**, *37* (5), 312-25.

150. Moad, G.; Rizzardo, E.; Thang, S. H., Toward living radical polymerization. *Accounts of chemical research* **2008**, *41* (9), 1133-42.

151. Postma, A.; Davis, T. P.; Li, G.; Moad, G.; O'Shea, M. S., RAFT polymerization with phthalimidomethyl trithiocarbonates or xanthates. On the origin of bimodal molecular weight distributions in living radical polymerization. *Macromolecules* **2006**, *39*, 5307-5318.
152. Carlsson, F.; Hyltner, E.; Arnebrant, T.; Malmsten, M.; Linse, P., Lysozyme absorption to charged surfaces. A monte carlo study. *Journal of Physical Chemistry B* **2004**, *108*, 9871-9881.
153. Entlicher, G.; Kost í, J. V.; Kocourek, J., Studies on phytohemagglutinins. 8. isoelectric point and multiplicity of purified concanavalin A. *Biochimica Biophysica Acta* **1971**, *236*, 795-797.
154. Samejima, T.; Kamata, M.; Shibata, K., Dissociation of bovine liver catalase at low pH. *Journal of biochemistry* **1962**, *51*, 181-7.
155. Jolles, P., Lysozymes: a chapter of molecular biology. *Angewandte Chemie (International ed. in English)* **1969**, *8* (4), 227-39.
156. A, F., On a remarkable bacteriolytic substance found in secretions and tissues. *Proceedings of the Royal Society B: Biological Sciences* **1922**, *93*, 306-317.
157. Fleming, A.; Allison, V. D., Observations on a bacteriolytic substance ("lysozyme") found in secretions and tissues. *British Journal of Experimental Pathology* **1922**, *13*, 252-260.
158. Schutte, H.; Kula, M. R., Pilot- and process-scale techniques for cell disruption. *Biotechnology and applied biochemistry* **1990**, *12* (6), 599-620.
159. Grzesiak, A. L.; Matzger, A. J., Selection of protein crystal forms facilitated by polymer-induced heteronucleation. *Crystal Growth & Design* **2008**, *8*, 347-350.
160. Alderton, G.; Fevold, H. L., Direct crystallization of lysozyme from egg white and some crystalline salts of lysozyme. *The Journal of Biological Chemistry* **1946**, *164*, 1-5.
161. Blake, C. C.; Koenig, D. F.; Mair, G. A.; North, A. C.; Phillips, D. C.; Sarma, V. R., Structure of hen egg-white lysozyme. A three-dimensional Fourier synthesis at 2 Angstrom resolution. *Nature* **1965**, *206* (4986), 757-61.
162. Johnson, L. N.; Phillips, D. C., Structure of some crystalline lysozyme-inhibitor complexes determined by X-ray analysis at 6 Angstrom resolution. *Nature* **1965**, *206* (4986), 761-3.
163. Rypniewski, W. R.; Holden, H. M.; Rayment, I., Structural consequences of reductive methylation of lysine residues in hen egg white lysozyme: an X-ray analysis at 1.8-A resolution. *Biochemistry* **1993**, *32* (37), 9851-8.
164. Sumner, J. B.; Gral ń, N.; Eriksson-Quensel, I. B., The molecular weights of canavalin, concanavalin A, and concanavalin B. *The Journal of Biological Chemistry* **1938**, *125*, 45-48.
165. Min, W.; Dunn, A. J.; Jones, D. H., Non-glycosylated recombinant pro-concanavalin A is active without polypeptide cleavage. *The EMBO journal* **1992**, *11* (4), 1303-7.
166. Schiefer, H. G.; Krauss, H.; Brunner, H.; Gerhardt, U., Ultrastructural visualization of surface carbohydrate structures on mycoplasma membranes by concanavalin A. *Journal of bacteriology* **1975**, *124* (3), 1598-600.
167. Shoham, J.; Inbar, M.; Sachs, L., Differential toxicity on normal and transformed cells in vitro and inhibition of tumour development in vivo by concanavalin A. *Nature* **1970**, *227* (5264), 1244-6.
168. Sumner, J. B., The globulins of the jack bean, *Canavalia ensiformis*. *Journal of Biological Chemistry* **1919**, *37*, 137-142.
169. Sumner, J. B.; Howell, S. F., Identification of Hemagglutinin of Jack Bean with

- Concanavalin A. *Journal of bacteriology* **1936**, *32* (2), 227-37.
170. Greer, J.; Kaufman, H. W.; Kalb, A. J., An x-ray crystallographic study of concanavalin A. *Journal of Molecular Biology* **1970**, *48* (2), 365-6.
171. Deacon, A.; Gleichmann, T.; Kalb, A. J.; Price, H.; Raftery, J.; Bradbrook, G.; Yariv, J.; Helliwell, J. R., The structure of concanavalin A and its bound solvent determined with small-molecule accuracy at 0.94 Å resolution. *Journal of the Chemical Society, Faraday Transactions* **1997**, *93* (24), 4305-4312.
172. Kantardjiev, K. A.; Hochtl, P.; Segelke, B. W.; Tao, F. M.; Rupp, B., Concanavalin A in a dimeric crystal form: revisiting structural accuracy and molecular flexibility. *Acta Crystallographica Section D: Biological Crystallography* **2002**, *58* (Pt 5), 735-43.
173. Loris, R.; Maes, D.; Poortmans, F.; Wyns, L.; Bouckaert, J., A structure of the complex between concanavalin A and methyl-3,6-di-O-(alpha-D-mannopyranosyl)-alpha-D-mannopyranoside reveals two binding modes. *The Journal of Biological Chemistry* **1996**, *271* (48), 30614-8.
174. Hamodrakas, S. J.; Kanellopoulos, P. N.; Pavlou, K.; Tucker, P. A., The crystal structure of the complex of concanavalin A with 4'-methylumbelliferyl-alpha-D-glucopyranoside. *Journal of Structural Biology* **1997**, *118* (1), 23-30.
175. Jain, D.; Kaur, K. J.; Salunke, D. M., Plasticity in protein-peptide recognition: crystal structures of two different peptides bound to concanavalin A. *Biophysical Journal* **2001**, *80* (6), 2912-21.
176. Kadirvelraj, R.; Foley, B. L.; Dyekjaer, J. D.; Woods, R. J., Involvement of water in carbohydrate-protein binding: concanavalin A revisited. *Journal of the American Chemical Society* **2008**, *130* (50), 16933-42.
177. Shoham, M.; Yonath, A.; Sussman, J. L.; Moulton, J.; Traub, W.; Kalb, A. J., Crystal structure of demetallized concanavalin A: the metal-binding region. *Journal of Molecular Biology* **1979**, *131* (2), 137-55.
178. Bouckaert, J.; Loris, R.; Poortmans, F.; Wyns, L., Crystallographic structure of metal-free concanavalin A at 2.5 Å resolution. *Proteins* **1995**, *23* (4), 510-24.
179. Emmerich, C.; Helliwell, J. R.; Redshaw, M.; Naismith, J. H.; Harrop, S. J.; Raftery, J.; Kalb, A. J.; Yariv, J.; Dauter, Z.; Wilson, K. S., High-resolution structures of single-metal-substituted concanavalin A: the Co,Ca-protein at 1.6 Å and the Ni,Ca-protein at 2.0 Å. *Acta crystallographica. Section D, Biological crystallography* **1994**, *50* (Pt 5), 749-56.
180. Bouckaert, J.; Dewallef, Y.; Poortmans, F.; Wyns, L.; Loris, R., The structural features of concanavalin A governing non-proline peptide isomerization. *The Journal of Biological Chemistry* **2000**, *275* (26), 19778-87.
181. Kanellopoulos, P. N.; Tucker, P. A.; Pavlou, K.; Agianian, B.; Hamodrakas, S. J., A Triclinic Crystal Form of the Lectin Concanavalin A. *Journal of Structural Biology* **1996**, *117* (1), 16-23.
182. Hardman, K. D.; Ainsworth, C. F., Structure of concanavalin A at 2.4-Å resolution. *Biochemistry* **1972**, *11* (26), 4910-9.
183. Chelikani, P.; Fita, I.; Loewen, P. C., Diversity of structures and properties among catalases. *Cellular and molecular life sciences : CMLS* **2004**, *61* (2), 192-208.
184. Boon, E. M.; Downs, A.; Marcey, D., Catalase: H₂O₂: H₂O₂ oxidoreductase. *Catalase Structural Tutorial Text*.

185. Sumner, J. B.; Dounce, A. L., Crystalline catalase. *Science* **1937**, *85* (2206), 366-7.
186. Murthy, M. R.; Reid, T. J., 3rd; Sicignano, A.; Tanaka, N.; Rossmann, M. G., Structure of beef liver catalase. *Journal of Molecular Biology* **1981**, *152* (2), 465-99.
187. McPherson, A., Jr.; Rich, A., Crystallographic study of beef liver catalase. *Archives of biochemistry and biophysics* **1973**, *157* (1), 23-7.
188. Foroughi, L. M.; Kang, Y. N.; Matzger, A. J., Sixty years from discovery to solution: crystal structure of bovine liver catalase form III. *Acta crystallographica. Section D, Biological crystallography* **2011**, *67* (Pt 9), 756-62.
189. Hamada, H.; Arakawa, T.; Shiraki, K., Effect of additives on protein aggregation. *Curr Pharm Biotechnol* **2009**, *10* (4), 400-7.
190. Wang, X. S.; Winnik, M. A.; Manners, I., Synthesis and self-assembly of poly(ferrocenyldimethylsilane-*b*-dimethylaminoethyl methacrylate): toward water-soluble cylinders with an organometallic core. *Macromolecules* **2005**, *38*, 1928-1935.
191. Roy, D.; Cambre, J. N.; Sumerlin, B. S., Sugar-responsive block copolymers by direct RAFT polymerization of unprotected boronic acid monomers. *Chemical communications (Cambridge, England)* **2008**, (21), 2477-9.
192. Moya, A.; Gil, R.; Latorre, A.; Pereto, J.; Pilar Garcillan-Barcia, M.; de la Cruz, F., Toward minimal bacterial cells: evolution vs. design. *FEMS microbiology reviews* **2009**, *33* (1), 225-35.
193. Hussain, H.; Mya, K. Y.; He, C., Self-assembly of brush-like poly[poly(ethylene glycol) methyl ether methacrylate] synthesized via aqueous atom transfer radical polymerization. *Langmuir : the ACS journal of surfaces and colloids* **2008**, *24* (23), 13279-86.
194. Ali, M. M.; Stover, H. D. H., Well-defined amphiphilic thermosensitive copolymers based on poly(ethylene glycol monomethacrylate) and methyl methacrylate prepared by atom transfer radical polymerization. *Macromolecules* **2004**, *37*, 5219-5227.
195. Lutz, J. F.; A. Hoth, Preparation of ideal PEG analogues with a tunable thermosensitivity by controlled radical copolymerization of 2-(2-methoxyethoxy)ethyl methacrylate and oligo(ethylene glycol) methacrylate. *Macromolecules* **2006**, 893-896.
196. Zeng, F.; Shen, Y.; Zhu, S.; Pelton, R., Synthesis and characterization of comb-branched polyelectrolytes 1, preparation of cationic macromonomer of 2-(dimethylamino)ethyl methacrylate by atom transfer radical polymerization. *Macromolecules* **2000**, *33*, 1628-1635.
197. Xiong, Q.; Ni, P.; Zhang, F.; Yu, Z., Synthesis and characterization of 2-(dimethylamino)ethyl methacrylate homopolymers via aqueous RAFT polymerization and their application in miniemulsion polymerization. *Polymer Bulletin* **2004**, *53*, 1-8.
198. Zhang, Z.; Liu, G.; Bell, S., Synthesis of poly(solketal methacrylate)-block-poly(2-(dimethylamino)ethyl methacrylate) and preparation of nanospheres with cross-linked shells. *Macromolecules* **2000**, *33*, 7877-7883.
199. Creutz, S.; Teyssié P.; Jôme, R., Living Anionic Homopolymerization and Block Copolymerization of (Dimethylamino)ethyl Methacrylate. *Macromolecules* **1997**, *30* (1), 6-9.
200. Baines, F. L.; Billingham, N. C.; Armes, S. P., Synthesis and Solution Properties of Water-Soluble Hydrophilic-Hydrophobic Block Copolymers. *Macromolecules* **1996**, *29* (10), 3416-3420.
201. Roy, D.; Cambre, J. N.; Sumerlin, B. S., Triply-responsive boronic acid block copolymers: solution self-assembly induced by changes in temperature, pH, or sugar concentration.

- Chemical Communications* **2009**, *16*, 2106-2108.
202. Albertin, L.; Stenzel, M. H.; Barner-Kowollik, C.; Davis, T. P., Effect of an added base on (4-cyanopentanoic acid)-4-dithiobenzoate mediated RAFT polymerization in water. *Polymer* **2006**, *47* (01), 1011-1019.
203. Bailon, P.; Palleroni, A.; Schaffer, C. A.; Spence, C. L.; Fung, W. J.; Porter, J. E.; Ehrlich, G. K.; Pan, W.; Xu, Z. X.; Modi, M. W.; Farid, A.; Berthold, W., Rational design of a potent, long-lasting form of interferon: A 40 kDa branched polyethylene glycol-conjugated interferon alpha-2a for the treatment of hepatitis C. *Bioconjugate Chemistry* **2001**, *12* (2), 195-202.
204. Greenwald, R. B., PEG drugs: an overview. *Journal of Controlled Release* **2001**, *74* (1-3), 159-171.
205. Xue, X.; Pasparakis, G.; Halliday, N.; Winzer, K.; Howdle, S. M.; Cramphorn, C. J.; Cameron, N. R.; Gardner, P. M.; Davis, B. G.; Fernández-Trillo, F.; Alexander, C., Synthetic Polymers for Simultaneous Bacterial Sequestration and Quorum Sense Interference. *Angewandte Chemie International Edition* **2011**, *50* (42), 9852-9856.
206. Yasayan, G.; Redhead, M.; Magnusson, J. P.; Spain, S. G.; Allen, S.; Davies, M.; Alexander, C.; Fernandez-Trillo, F., Well-defined polymeric vesicles with high stability and modulation of cell uptake by a simple coating protocol. *Polymer Chemistry* **2012**, *3* (9), 2596-2604.
207. Schwartz, A. M.; Berglund, K. A., In situ monitoring and control of lysozyme concentration during crystallization in a hanging drop. *Journal of Crystal Growth* **2000**, *210*, 753-760.
208. Steinrauf, L. K., Preliminary X-ray data for some new crystalline forms of β -lactoglobulin and hen-egg-white lysozyme. *Acta Crystallographica* **1959**, *12*, 77-79.
209. Jeruzalmi, D., First analysis of macromolecular crystals: biochemistry and x-ray diffraction. *Methods in molecular biology (Clifton, N.J.)* **2007**, *364*, 43-62.
210. Ko, T. P.; Day, J.; Malkin, A. J.; McPherson, A., Structure of orthorhombic crystals of beef liver catalase. *Acta crystallographica. Section D, Biological crystallography* **1999**, *55* (Pt 8), 1383-94.
211. Helliwell, J. R., Protein crystal perfection and its application. *Acta crystallographica. Section D, Biological crystallography* **2005**, *61* (Pt 6), 793-8.
212. ten Wolde, P. R.; Frenkel, D., Enhancement of protein crystal nucleation by critical density fluctuations. *Science* **1997**, *277* (5334), 1975-8.
213. Chodankar, S.; Aswal, V. K.; Kohlbrecher, J.; Hassan, P. A.; Wagh, A. G., Time evolution of crystallization phase of lysozyme protein in aqueous salt solution as studied by scattering techniques. *Physica B: Condensed Matter* **2007**, *398*, 164-171.
214. Dierks, K.; Meyer, A.; Einspahr, H.; Betzel, C., Dynamic light scattering in protein crystallization droplets: adaptations for analysis and optimization of crystallization processes. *Crystal Growth & Design* **2008**, *8*, 1628-1634.
215. Muschol, M.; Rosenberger, F., Interactions in undersaturated and supersaturated lysozyme solutions: static and dynamic light scattering results. *Journal of Chemical Physics* **1995**, *103*, 10424-10432.
216. Thomas, B. R.; Vekilov, P. G.; Rosenberger, F., Effects of microheterogeneity in hen egg-white lysozyme crystallization. *Acta crystallographica. Section D, Biological crystallography* **1998**, *54* (Pt 2), 226-36.

217. Veessler, S.; Marcq, S.; Lafont, S.; Astier, J. P.; Boistelle, R., Influence of polydispersity on protein crystallization: a quasi-elastic light-scattering study applied to alpha-amylase. *Acta crystallographica. Section D, Biological crystallography* **1994**, 50 (Pt 4), 355-60.
218. Wilson, W. W., Light scattering as a diagnostic for protein crystal growth--a practical approach. *Journal of Structural Biology* **2003**, 142 (1), 56-65.
219. Slayter, E. M.; Slayter, H. S., *Light and electron microscopy*. Cambridge University Press: Cambridge, UK, 1992.
220. Gavira, J. A.; Alexander, E. S.; Driessche, V.; Garcia-Ruiz, J. M., Growth of ultrastable protein-silica composite crystals. *Crystal Growth & Design* **2013**, 13, 2522-2529.
221. Falkner, J. C.; Al-Somali, A. M.; Jamison, J. A.; Zhang, J.; Adrianse, S. L.; Simpson, R. L.; Calabretta, M. K.; Radding, W.; Phillips, G. N.; Colvin, V. L., Generation of size-controlled, submicrometer protein crystals. *Chemistry of Materials* **2005**, 17, 2679-2686.
222. Bhamidi, V.; Skrzypczak-Jankun, E.; Schall, C. A., Dependence of nucleation kinetics and crystal morphology of a model protein system on ionic strength. *Journal of Crystal Growth* **2001**, 232, 77-85.
223. Falkner, J. C.; Al-Somali, A. M.; Jamison, J. A.; Zhang, J. Y.; Adrianse, S. L.; Simpson, R. L.; Calabretta, M. K.; Radding, W.; Phillips, G. N. J.; Colvin, V. L., Generation of size-controlled, submicrometer protein crystals. *Chemistry of Materials* **2005**, 17, 2679-2686.
224. Hermans, J., Excluded-volume theory of polymer-protein interactions based on polymer chain statistics. *The Journal of Chemical Physics* **1982**, 77, 2193-2204.
225. Lee, J. C.; Lee, L. L., Preferential solvent interactions between proteins and polyethylene glycols. *The Journal of Biological Chemistry* **1981**, 256 (2), 625-31.
226. Hoogeveen, N. G.; Stuart, M. A. C.; Fleer, G. J., Can charged (block co)polymers act as stabilizers and flocculants of oxides. *Colloids and surfaces. A, Physicochemical and engineering aspects* **1996**, 117, 77-88.
227. Sauter, C.; Ng, J. D.; Lorber, B.; Keith, G.; Brion, P.; Hosseini, M. W.; Lehn, J. M.; Giege, R., Additives for the crystallization of proteins and nucleic acids. *Journal of Crystal Growth* **1999**, 196 (2-4), 365-376.
228. Collins, K. D., Sticky ions in biological-systems. *Proceedings of the National Academy of Sciences of the United States of America* **1995**, 92 (12), 5553-5557.
229. Rieskautt, M. M.; Ducruix, A. F., Crystallization of basic-proteins by ion-pairing. *Journal of Crystal Growth* **1991**, 110 (1-2), 20-25.
230. Hall, C. E., Electron microscopy of crystalline catalase. *Journal of Biological Chemistry* **1950**, 185 (2), 749-754.
231. Unwin, P. N. T., Beef liver catalase structure: interpretation of electron micrographs. *Journal of Molecular Biology* **1975**, 98 (1), 235-242.
232. Wrigley, N. G., Lattice spacing of crystalline catalase as an internal standard of length in electron microscopy. *Journal of Ultrastructure Research* **1968**, 24 (5-6), 454-&.
233. Dorset, D. L.; Gilmore, C. J., Direct methods in protein electron crystallography - beef liver catalase in its fully hydrated form at room temperature. *Acta Crystallographica Section A* **1999**, 55, 448-456.
234. Vanderleeden, M. C.; Kashchiev, D.; Vanrosmalen, G. M., Effect of additives on nucleation rate, crystal growth rate and induction time in precipitation. *Journal of Crystal Growth* **1993**, 130 (1-2), 221-232.